

Synthesis of Charged Polystyrene Colloids and Polymer Hydrogel Photonic Crystal Mercury Sensor

A Thesis Submitted for the degree of

DOCTOR OF PHILOSOPHY



BY

Dhamodaran Arunbabu

**School of Chemistry
University of Hyderabad
Hyderabad- 500 046
INDIA**

November 2010

**Dedicated
To my
Appa and
Amma**

DECLARATION

I hereby declare that the matter embodied in the thesis entitled **“Synthesis of Charged Polystyrene Colloids and Polymer Hydrogel Photonic Crystal Mercury Sensor”** is the result of investigations carried out by me in the School of Chemistry, University of Hyderabad, Hyderabad, India under the supervision of **Dr. Tushar Jana** and it has not been submitted elsewhere for the award of any degree or diploma or membership, etc.

In keeping with the general practice of reporting scientific investigations, due acknowledgements have been made wherever the work described is based on the findings of other investigators. Any omission or error that might have crept in is regretted.

November 2010

Dhamodaran Arunbabu

UNIVERSITY OF HYDERABAD

Central University (P.O.), Hyderabad-500046, INDIA

Dr. Tushar Jana
Associate Professor
School of Chemistry



Tel: 91-40-23134808 (Office)

91-9440127016 (Mobile)

Fax: 91-40-23012460

E-mail: tjsc@uohyd.ernet.in

tjscuoh@gmail.com

Web: <http://chemistry.uohyd.ernet.in/~tj/>

CERTIFICATE

This is to certify that the work described in this thesis entitled **“Synthesis of Charged Polystyrene Colloids and Polymer Hydrogel Photonic Crystal Mercury Sensor”** has been carried out by Mr. Dhamodaran Arunbabu under my supervision and the same has not been submitted elsewhere for any degree.

Dean
School of Chemistry
University of Hyderabad
Hyderabad- 500 046
India

Dr. Tushar Jana
(Thesis supervisor)

PREFACE

The present thesis entitled “*Synthesis of Charged Polystyrene Colloids and Polymer Hydrogel Photonic Crystal Mercury Sensor*” has been divided into seven chapters. **Chapter 1** provides an insight on polymer colloids, emulsion polymerization, polymer hydrogel materials, PCCA sensing materials and enzymatic kinetics and inhibition. **Chapter 2** describes the synthesis of charged spherical poly [S-co-DVB-co-2-PSA] particles of various sizes (50nm-400nm). Effects of emulsifier and initiator concentration on polymer properties are discussed. In **Chapter 3** study has been carried out for the development of series of recipes for the synthesis of 24–102 nm sized highly charged poly (S-co-DVB-co-SPM) particles by emulsion polymerization. **Chapter 4** investigates the effect of sodium styrene sulfonate (NaSS) in the emulsion copolymerization of Poly(S-co-NaSS). Monomer reactivity ratio, copolymerization kinetics, particle size, shift in the loci of polymerization and thermal properties are examined. **Chapter 5** deals with study on the effect of ionic comonomer structure on the particle size, polymerization kinetics and other copolymer properties in the emulsion copolymerization of styrene with various other ionic comonomers. **Chapter 6** demonstrates development of urease enzyme coupled novel polymer hydrogel based photonic crystal sensor material for the inhibitive determination of toxic mercury ion (Hg^{+2}) concentration in water. **Chapter 7** summarizes the findings of the present investigations, presents concluding remarks, and the future scopes and upcoming challenges.

November, 2010

School of chemistry,

University of Hyderabad

Hyderabad 500 046, India

Dhamodaran Arunbabu

Acknowledgement

It is my immense pleasure to express my sincere heartfelt gratitude to my research supervisor Dr. Tushar Jana, for his constant cooperation, encouragement, inspiration and a kind guidance. He has been quite a force to reckon with in both academic and personal fronts for me. It has been great pleasure and fortune to work with him who introduced me to the field of Polymer Chemistry. His disciplined working style and honesty for the research has paved a new path in my career. I am also indebted to him for the work freedom he has given me during the last five years.

I would like to thank the former Deans and present Dean, School of Chemistry, for their constant support and for allowing me to avail the available facilities. I am extremely thankful individually to all the faculty members of the school of chemistry for their inspiration kind help and cooperation at various stages of my stay in the campus. I am also grateful to all my former teachers for their help.

I am very grateful to Prof. Anunay Samanta for his inspiration and support throughout my research career. I would like to express my sincere gratitude to Prof. T. P. Radhakrishnan for his inspiration support and valuable suggestions.

Financial assistance from UGC, New Delhi in the form of junior and senior research fellowship and various instrumental facilities, are sincerely acknowledged.

I would also like to express my sincere gratitude to Dr. S.M. Ahmed, Dr. Manjunath, Mr. Nageshwar Rao and Mr. C.S.Murthy of central Instrumental Laboratory (CIL), UoH for their help with SEM and ultracentrifugation experiments. I sincerely acknowledge Dr. R. Banerjee and Dr. A. Choudhury of IICT, Hyderabad for helping with Zetasizer experiments. I also sincerely thank centre for Nanotechnology, UoH for allowing me to use the TEM facility.

I am indebted to all my teachers starting from the school, to the college and to the University for teaching me all the discipline, values and education throughout my academic career.

I am really blessed to have colleagues like Arindam, Murali, Sandip, Mousumi, Sudhangshu, Malkappa and Shuvra during my Ph.d life. Arindam and Murali are as thick as my brothers, who stood by me in my highs and lows and they played a crucial role in my Ph. D. career. I am thankful to Sandip for his support and caring. I am really thankful to mousumi for her backing up and help. I acknowledge my junior brothers and sisters, Sudhangshu, Malkappa, and Shuvra for maintaining the friendly atmosphere in the lab. My special thanks to M.Sc project students Venkatesh, Somshankar, Josheph, Sanga, Bidhan, Seenimeera, Shubadeep, Ashok, Apparao, Muthupandi, Niranjana, Swamy, Chandrasekhar, Ajay Krishnan, chandrakala, abhishek and srikanth.

I thank all the non-teaching staff members for their support and help, particularly Mr. Mallaiah Shetty.

I thank my senior “annas” for showing me the way to live a calm disciplined and honorable life. I still have within me those fond moments that I have spent with them which I can cherish in my

whole future life. Thanks to all my lovable annas Senthil kumar (vaanga Boss), Padmanaban Madhu, Sundharam, Venkatesan, Vairaprakash, Muthu, Balaraman, Prakash, Saravanan, Arumuganathan, Selva, Francis, Gnanavel, Vijayan and Kannapiran. Also my sincere thanks to Bharathi, Muthu, Saravanan, Satish, and Venkat saravanan. My special thanks to bhuvaneshwari akka.

I am blessed with good friends like (Kabali) Vijayan, Navinkumar, Sakthivel and Senthil kumar who have supported and cared me when mattered. I am really lucky to have bunch of younger brothers like Viji, Vignesh, Santhanam, Prabu, Ganesh, Ramesh, Shanmugarajan, suresh, Manoj, Sudalai, Venkatachalam and Prakash. Also I am thankful to my dear sisters Sakthidevi, Sarfunisha, Manasa, Manasi, Saipriya, and Subha.

I must thank my seniors like Phavan, Sharath, Prasun, Moloy, Manab, Biju, Tanmay Abhijeet, Anirudha, Prasanth, Raji, Bhaswati, Pradip, and Phani pavan. I also thank friends like Tatpta, Vikram, Ramu, Kishore, Ramkumar, Sivarankan, Naren, Ramesh, Chaitanya, Rumpa, Narayana, Sanjib, Naba, Ranjit, Susruta, Dinesh, Rishi, Kishore, Vikranth and Anoop.

I am privileged to have lovely friends like Atazo, Poornima, Machun, and Akum. I am thankful to them for their love, support and prayers. I thank chandrani for her support and well wishes.

Back in my home town I must thank my best pals Loghu, Jayagopal, Saravanan, and Sekhar for their selfless love and support in my tough times.

Deep from my heart, I express my gratitude and earnest emotions to my best friend Anitha Jerin for her unconditional caring, moral support and understanding.

My father and my mother...mean the world to me!... whatever I have achieved would not have been possible without their endless love and sacrifice. I attribute my success to my skills, simplicity, strength and my good virtues which I have received from them. I owe them a debt which, I believe, I cannot payback. I thank my sweet brothers Harikishan, Nesam, Ram and Lakshmanan who were my strength in all walk my life and they have stood by me in my difficult times. I thank all my paatti, thaathaa, periamma, periappa, akka, anna, thambi, thangai, uncle, aunty, cousins and my cousins. I thank my "little rabbits" sweetest ever, Gladis and Gladson for their endless love and prayers. I thank my pup Lolly for his incomparable love and affection. I thank almighty god for his blessings, guidance, wisdom and knowledge.

"God has not given the spirit of fear; but of power, love and sound mind"

-Timothy II 1:7

November 2010

Dhamodaran Arunbabu

University of Hyderabad,

Hyderabad-500 046

India

Common Abbreviations

SDS	Sodium dodecyl sulphate
APS	Ammonium per sulphate
S	Styrene
DVB	Divinylbenzene
CMC	Critical micellar concentration
SPM	Sulphopropylmethacrylate
SEM	Scanning electron microscope
AFM	Atomic force microscopy
TEM	Transmission electron microscopy
N_p	Number of particles
\overline{M}_v	Viscosity-average molecular weight
\overline{M}_w	Weight average molecular weight
CCA	Crystalline colloidal array
PCCA	Polymerized crystalline colloidal arrays
Z	Charges per particle
σ	Surface charge density
Q	Total charge on the particle
T_g	Glass transition temperature
AAc	Acrylic acid
MAA	Methacrylic acid
HEMA	2-Hydroxyethylmethacrylate
NaSS	Sodium styrene sulphonate
MCL	Maximum contamination limit
UPCCA	Urease coupled polymerized crystalline colloidal arrays
L-B plot	Lineweaver-Burk plot
K_M	Michaelis-Menten constant

CONTENTS

Declaration	i
Certificate	ii
Preface	iii
Acknowledgement	iv-v
Common Abbreviations	vi
Chapter 1 Introduction	1- 54
1.1. Colloids	2
1.2. Monodisperse Colloids	4
1.3. Polymer Colloids	8
1.4. Polystyrene colloids	14
1.5. Synthesis of Polymer Colloids	17
1.6. Emulsion Polymerization	18
1.6.1. Overview	18
1.6.2. Basic ingredients	19
1.6.3. Underlying Features and Principles	21
1.6.4. Other types of Emulsion Polymerization	25
1.7. Application of Polystyrene Colloids	27
1.8. Hydrogel	28
1.9. Polymerized Crystalline Colloidal Array Materials	34
1.10. Enzymatic Reaction	40
1.10.1. Michaelis-Menten Kinetics	41
1.10.2. Lineweaver-Burk Plot	42
1.10.3. Inhibition Mechanism of Enzymes	43
1.11. Scope of the thesis	46
References	48

Chapter 2	Tuning the Particle Size and Charge Density of the Crosslinked Polystyrene Particles	55- 76
2.1.	Introduction	56
2.2.	Experimental section	58
2.2.1.	Materials	58
2.2.2.	Synthesis and purification of colloidal Particles	58
2.2.3.	Characterization of colloidal particles	59
2.3.	Results and Discussion	60
2.3.1.	Particle size versus emulsifier concentration	60
2.3.2.	Particle size versus initiator concentration	66
2.3.3.	Surface charge density of the colloidal particles	70
2.4.	Conclusions	72
	References	74
Chapter 3	Synthesis of Crosslinked Poly(Styrene-co-DVB-co-SPM) Nanoparticles by Emulsion Copolymerization	77- 97
3.1.	Introduction	78
3.2.	Experimental section	79
3.2.1.	Materials	79
3.2.2.	Synthesis Poly(S-co-DVB-SPM) colloidal particles	79
3.2.3.	Purification of Colloids Particles	81
3.2.4.	Characterization of Colloidal Particles	81
3.2.5.	Preparation of PCCA and diffraction studies	82
3.3.	Results and Discussion	82
3.3.1.	Particle Size	84
3.3.2.	Number of Particles (N_p)	87
3.3.3.	Surface charge density	89
3.3.4.	Charges per Particle	91
3.3.4.	Diffraction Studies of PCCA	93

3.4. Conclusion	94
References	96
Chapter 4 Emulsion copolymerization of Styrene and Sodium Styrene Sulfonate	98 -126
4.1. Introduction	99
4.2. Experimental section	101
4.2.1. Materials	101
4.2.2. Synthesis and Purification of Poly(S-co-NaSS) Colloidal Particles	101
4.2.3. Characterization of Poly(S-co-NaSS) Particles	103
4. 3. Results and Discussion	104
4.3.1. Studies of Copolymerization Kinetics	104
4.3.2. FTIR Analysis	107
4.3.3. NMR Studies and Reactivity Ratios	109
4.3.4. Particle Size	116
4.3.5. Thermal studies of the copolymers	118
4. 4. Conclusions	122
References	124
Chapter 5 Emulsion Copolymerization of Styrene: Effect of ionic Comonomer Structure	127- 163
5.1. Introduction	128
5.2. Experimental section	131
5.2.1. Materials and Reagents	131
5.2.2. Synthesis Styrene Copolymer Colloidal Particles	131

5.2.3. Purification of Polystyrene copolymer Colloidal Particles	133
5.2.4. Characterization of Colloidal Particles	133
5.3. Results and Discussion	135
5.3.1. FTIR Spectroscopy	135
5.3.2. Particle Size	137
5.3.3. Copolymerization Kinetics	147
5.3.4. N_p vs. Emulsifier concentration	149
5.3.5. Surface charge density	152
5.3.6. Thermal studies of the copolymers	154
5.3.7. Diffraction Studies of Self-assembled latexes	157
5.4. Conclusion	158
References	160

Chapter 6 Photonic Crystal Hydrogel Material for the Sensing of Toxic Mercury Ion (Hg^{+2}) in Water

164- 198

6.1. Introduction	165
6.2. Experimental section	168
6.2.1. Preparation of PCCA	169
6.2.2. Preparation of ionic strength responsive PCCA (carboxylated PCCA)	170
6.2.3. Preparation of Urease Coupled PCCA (UPCCA) Sensor for Mercury	170
6.2.4. Preparation of CCA Free Urease Coupled Hydrogel	170
6.2.5. Determination of Coupled Enzyme Concentration and Free Carboxylate Concentrations	171
6.2.6. Measurement of UPCCA mercury sensor response	171
6.2.7. Enzyme kinetics studies	172
6.3. Results and Discussion	172
6.3.1. Coupling of urease in the ionic strength	

Responsive PCCA	174
6.3.2. Dependence of UPCCA diffraction on urea Concentration	176
6.3.3. Dependence of UPCCA diffraction on Mercury concentration	178
6.3.4. Studies of inhibition mechanism	181
6.3.5. Responses towards various inhibitors	191
6.3.6. Reversible nature of the UPCCA sensor	193
6.4. Conclusion	194
References	196
 Chapter 7 Summary and conclusion	 199-208
 Publications & Presentation	 209-212

Chapter 1

Introduction

1.1. Colloids

Alchemists were succeeded in preparing colloidal gold called portable gold (an elixir of life) or purple of cassius which was used to manufacture ruby glass. Macquer in his dictionary of chemistry (1774) speculated the presence of finely divided form of gold in the alchemist's material. Selmi synthesized colloidal sulphur and silver halides which were named "demulsions"¹. Michael Faraday mentioned that the purple gold solution contains "very minute in dimension" gold particles². In 1861 T. H. Graham³ named these minute particles as "colloids" in his paper which deals with unique diffusion properties of these particles. Oswald (1914) called colloids "*as materials of neglected dimensions*" in his book *the world of neglected dimensions*. Faraday's detailed account of work and systematic interpretation on these particle dispersions paved the way to modern colloidal chemistry. Modern literature describes colloids as follows: *colloids are the microscopic substances dispersed evenly and thoroughly in another medium known as continuous phase, wherein the size of the each colloidal grain is bigger than that of continuous phase molecules*. Each type of colloid is given a different name depending upon the state and the medium of dispersion or continuous phase whether they are solid, liquid and gas (Table 1.1). The size of colloidal particles covers the spectrum of 1nm to 1000nm falls in the interphase of microscopic world of atoms and molecules and macroscopic world of biological and technological systems (Figure 1.1). Hence colloids are now referred as mesoscopic materials and have drawn decade old scientific attention by the dawn of nanotechnology⁴⁻⁷. Colloids have become a subject of extensive research in the context of chemistry, biology, materials science, condensed matter physics, applied optics, and fluid dynamics.

Examples of colloidal materials we use in day to day life and the systems in which colloidal phenomenon is involved are given in Table 1.2. The table self-explanatory describes the importance of colloids in our daily life. The above list gives an idea how extensively the colloidal materials and more importantly how the colloidal state provides a helping hand in day to day life. In view of the above table one can clearly observe the rapport the colloidal state and the modern living facilities share and

they are simply inseparable. Colloidal science is the interface where the major divisions of science such as biology physics and chemistry meet⁵.

Table 1.1. *Types of colloids (adapted from reference 7)*

Phase	Gas	Liquid	Solid
Gas	Molecular solution	Liquid aerosol (mist)	Solid aerosol (smoke)
Liquid	Liquid Foam (shampoo)	Emulsion (mayonnaise)	Sol (ink)
Solid	Solid foam (packaging)	Solid emulsion (Butter)	Solid sol (stained Glass)

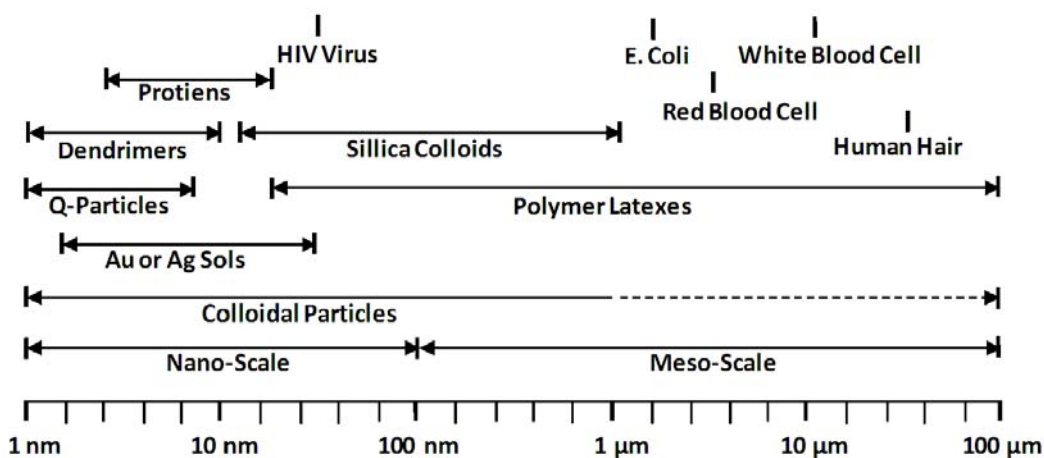


Figure 1.1. *The colloidal domain: the dimensions and typical examples of materials that fall in the colloidal size range (Adapted from reference 14).*

Table 1.2. *Colloidal systems and processes involving colloidal materials and their phenomenon.*

Colloidal systems	Processes which involve colloidal phenomenon	Colloidal systems	Processes which involve colloidal phenomenon
Aerosols	Adhesion	Soil	Ion exchange
Agrochemicals	Chromatography	Rubber	Grinding Water
Cement	Detergency	Plastics	clarification
Cosmetics	Ore flotation	Pharmaceuticals	Catalysis
Dyestuffs	Precipitation	Foams	Water repellency
Emulsions	Sewage disposal	Foodstuffs	Lubrication
Fabrics	Polymerization	Ink	Wetting
Paint	Food processing	Pigmented plastics	Oil-well drilling
Paper	Electrophoresis	Insecticides	Road surfacing

1.2. Monodisperse Colloids

A colloidal system in which particles are uniform in shape and size is monodisperse whereas when it lacks size and shape uniformity then it is known as polydisperse⁸ (Figure 1.2). Initial attempts made by scientists to synthesize monodisperse particles were essentially considered as a challenge and as a subject of curiosity^{9, 10}. After the invention of electron microscopy the fascination towards the synthesis of monodisperse colloids had increased significantly. Monodisperse colloids were used to quantitatively interpret the physical properties and surface interactions of colloidal dispersion as a function of particle size, number, shape and other characteristics¹¹⁻¹³. Morphology and various other physical characteristics along with chemical composition determines the physical properties of colloids such as magnetic, optical, electric, adsorptive, catalytic, and other properties. Also in principle, the

intrinsic properties of monodisperse colloidal particles can be tightly controlled by changing the parameters such as diameter, chemical composition, the bulk substructure, crystallinity (polycrystalline, single crystalline, or amorphous) and the surface functional groups (thus the interfacial free energy and surface charge density). The spherical shape is the simplest and less energetic form that a colloidal particle can easily adopt during the nucleation or growth process, due to the minimization of interfacial energy¹⁴.

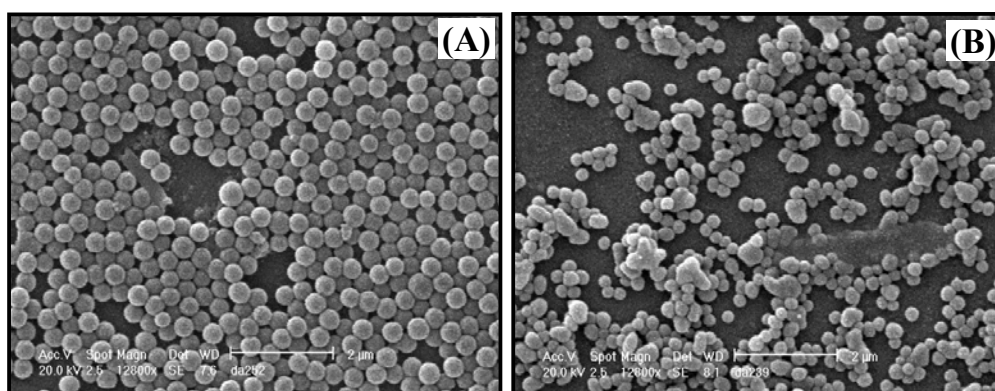


Figure 1.2. Microscopic images of (A). monodisperse (B). polydisperse polystyrene particles. These images are obtained from the polystyrene particles synthesized in our laboratory.

Recent years it has been realized that these materials are essential in numerous technological and medical applications, such as in ceramics, pigments, paints, adhesive materials, recording materials, electronics, catalysis, medical diagnostics, drug delivery systems, chromatographic supports and countless others^{12,13}. Matejevic has extensively carried out research for synthesizing colloids of various inorganic, organic, and polymeric materials of different shapes and sizes⁹⁻¹³. Hard metallic monodisperse particles pack themselves in a less energetic FCC, BCC or HCP close packed structures. These self assembled structures are known as photonic crystals which are used in photonic band gap materials and optical devices^{15, 16, 17}.

Mostly inorganic monodisperse colloids were prepared using precipitation technique which involves two sequential processes namely nucleation and growth of a nuclei. LaMer formulated important criteria of maintaining a clear boundary for both the nucleation and growth of the monomer (a solid precursor or complex) in their LaMer diagram in which the feed or release of monomers in a closed system is controlled in such a way that it does not exceed the supercritical concentration. LaMer have synthesized sulphur colloids by acidifying thiosuphate solutions and have drawn the above conclusion from it^{18, 19, 20}. Stober and Pink²¹ have utilized LaMer graph to synthesize silica colloids by hydrolyzing tetraethylorthosilicate (TEOS) at high pH. Matijevic further developed this method and applied this strategy to the synthesis of monodispersed colloidal spheres, cubes, rods, and ellipsoids from a broad range of materials such as metal oxides and carbonates⁹⁻¹³. Silica colloids are extensively studied systems because of their unique properties. Iler has contributed a lot to silicon chemistry²². Silica colloids prepared using TEOS contain silanol (-Si-OH) group which can be ionized above pH 7 to generate negative charges²². The surface properties of silica colloids can be enhanced using siloxane chemistry to form self-assembled monolayers (SAMs) with the silanol groups²³. Monodisperse gold colloids have a long history²⁴ and were extensively studied system since Faraday's painstaking research by his gold fluid² and the breakthrough invention of slit ultra microscope by German colloidal chemist Zsigmondy²⁵. Zsigmondy had synthesized monodisperse colloidal gold reducing chloroauric acid by formaldehyde^{26, 27}. Takiyama²⁸ and Turkevich^{29, 30} have modified the Zsigmondy's method by replacing formaldehyde with citric acid. Matijevic applied versatile precipitation method to synthesize monodisperse gold colloidal spheres from aqueous auric chloride solution and iso-ascorbic acid as a reducing agent³¹. Colloidal gold has been used in many applications such as catalysis³² biology³³, in non linear optics³⁴ and medical diagnosis. Also monodisperse iron oxide especially hematite particles of ellipsoidal³⁵, spindle, ³⁶spherical³⁷ and cubic³⁸ shapes were prepared, and utilized extensively in various applications. Matijevic has pioneered the synthesis of several uniform shape particles of chromium hydroxide, α -AlOOH, amorphous alumina,

palladium, ZnS, PbS, silver, and many other metals, metal oxides, hydroxides, carbonates and sulphates^{9-13, 39}.

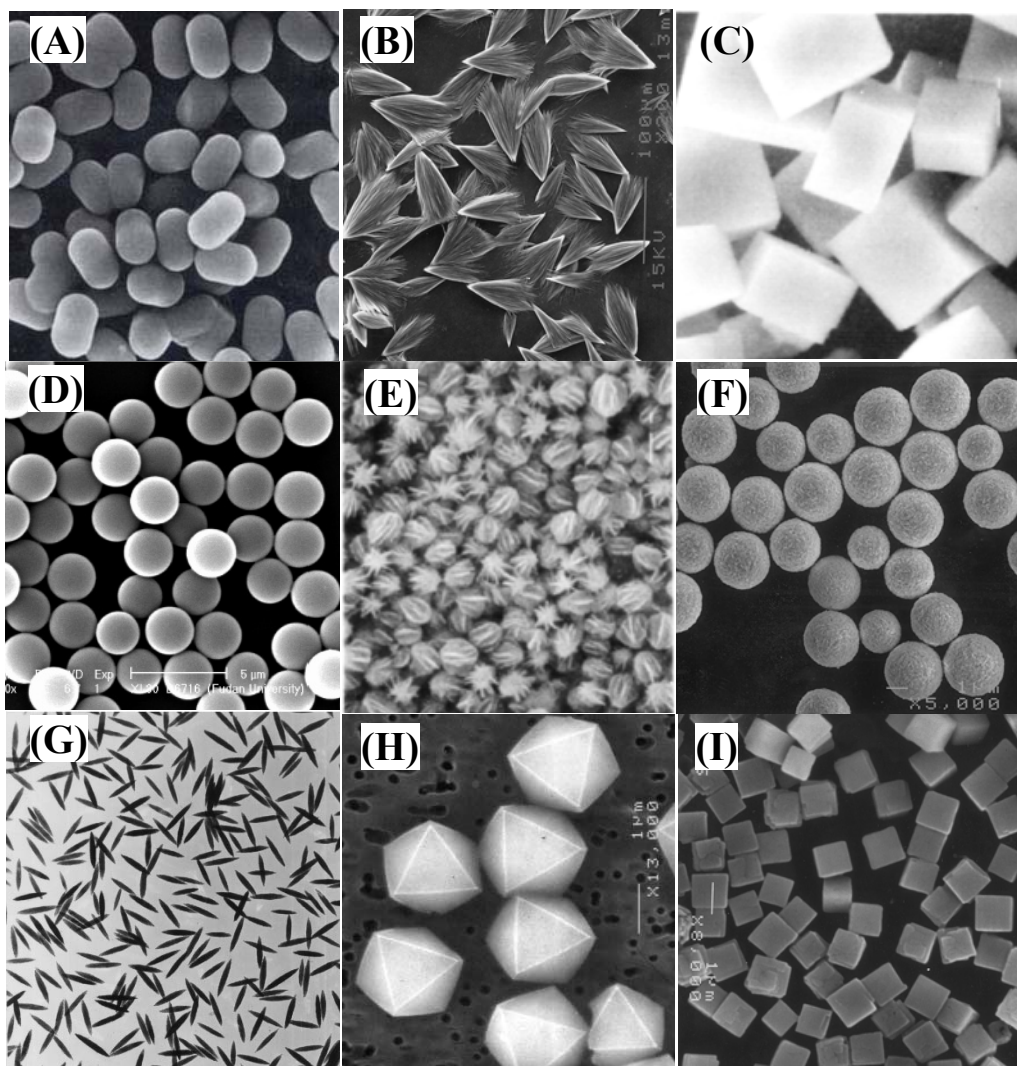


Figure 1.3. Monodisperse particles of different shapes and sizes (A) Hematite (Elipse)³⁵, (B) Calcium naproxonate⁴³, (C) PbS⁹⁻¹³, (D) Titanium⁴⁴, (E) Bohemite (α -AlOOH)⁹⁻¹³, (F) Gold³¹, (G) α -Fe₂O₃ (Spindle)³⁶, (H) Sodium Jarosite⁴⁵, (I) Sodium magnesium fluoride (NaMgF₃)⁴⁶

Monodisperse particles of different shapes and sizes are shown Figure 1.3. Monodisperse colloid sphere surfaces can be modified by coating with other materials of different thickness and this type of structures called core-shell structures⁴⁰. The structure, size, and composition of core shell materials could be modified to tune their optical, electro optical, thermal, electrical, Magnetic and catalytic properties^{14, 40}. Monodisperse inorganic and hybrid inorganic-organic hollow spheres have been prepared by coating colloidal core templates with alternating layers of oppositely charged inorganic or inorganic-hybrid nano particles and polymer thereafter removing core templates by either heat, radiation or chemical treatment⁴¹. Properties of hollow spheres can be changed by changing the thickness of the core and shell. Monodisperse hollow particles have found a wide spectrum of applications in encapsulation of drugs, cosmetics, ink and dye for a controlled release, the protective layer for air sensitive components, catalysis, fillers, coatings and composites⁴².

1.3. Polymer Colloids

1.3.1. History of Polymer Colloids

The term “polymer colloids” defines subdivided state in which polymolecular particles dispersed in a continuous liquid medium as individual particles and should have at least in one direction dimension of roughly between 1 nm and 1000 nm. But there should be clear distinction for polymer colloids since both organic (e.g. polystyrene, PMMA) and inorganic (e.g. Silica) colloids exist. Our focus mainly will be on organic polymer dispersions or colloids. Polymer colloidal dispersion can be called as either latex or polymer dispersion as per the recommendation of IUPAC. They are also known as emulsion of polymers or emulsions since the majority of these product polymers are derived from emulsion polymerization. Latex is defined as “a colloidal dispersion of polymer particles in an aqueous medium. The polymer may be organic or inorganic.”⁴⁷ The pioneering work of the first synthetic latex particles occurred in Leverkusen, Germany. In 1912, Kurt Gottlob at Friedrich Bayer & Co., invented a method to manufacture the synthetic rubber by polymerization of isoprene in aqueous

viscous solutions⁴⁸. In the following decades significant progress have been made in heterophase synthetic techniques when natural rubber is replaced by oleates, alkyl aryl sulphates as stabilizers, water phase polymerizations and water soluble peroxides were employed as an initiators which lead to faster and easier synthetic pathways⁴⁹.

1.3.2. Stability and Classification of Polymer Colloids

Polymer stability can be correlated with constancy in number of particle per unit volume and time. Polymer dispersion is unstable and prone to either coagulation or phase separation driven by impurities in the dispersion. Generally 1mL of a polymer dispersions contains approximately 10^5 number of polymer particles whereas 1particle contains 1 to 10000 polymer chains or macromolecule and 1macromolecule contains 10^2 to 10^6 monomer units (Figure 1.4)⁴⁷.

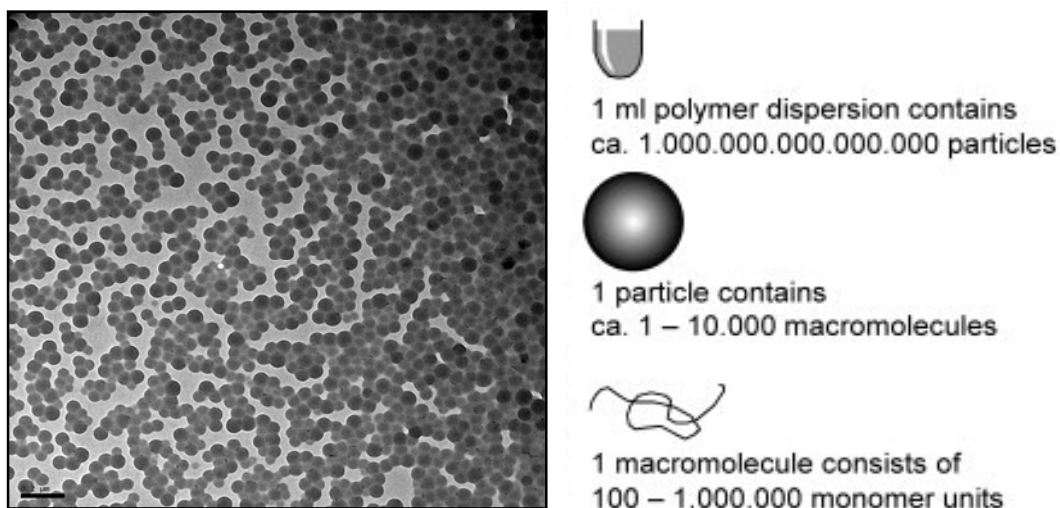


Figure 1.4. An example of polymeric colloidal dispersions and physical meaning of terms associated with latex particles ⁴⁷. Poly(styrene-co-NaSS) copolymer particles produced from our laboratory.

Three important parameters; aggregation (coagulation or flocculation), sedimentation and chemical reactions play the vital role in decreasing the constancy in

the number of particles. There is no clear cut definition available to define and differentiate coagulation and flocculation. Flocculation can be defined as reversible aggregation of particles in which particles can be redispersed whereas coagulation is permanent association of particles. Some authors describe flocculation as an event occurs in case of polymer particles and polyelectrolytes whereas coagulation takes place in case of lower molecular weight electrolytes. Chemical reagents known as flocculants when added to colloidal solution may induce flocculation by destabilizing the colloidal dispersion accelerating aggregation of particles. Flocculation is an important phenomenon of colloids which have found application in water purification, in paper industries and bacteriology. In waste water treatment plants a sludge feed and polymer solution is mixed to flocculate the sludge. Flocculated sludge is moved to dewatering units where excess water is squeezed through belt filter process. Coagulants are chemicals which cause destabilization of colloidal dispersions or coagulation by charge neutralization. High molecular weight polymers are very well known flocculants which are used extensively in industrial processes⁵². Sedimentation is another colloidal phenomenon which means the settling of dispersions using gravitational or centrifugal forces which is useful in analytical and theoretical studies.

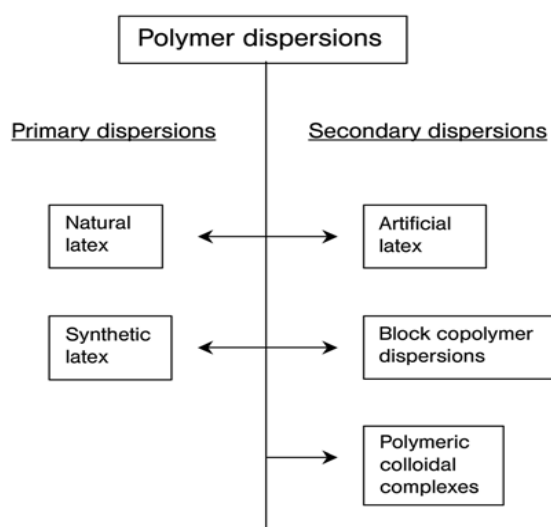


Figure 1. 5. *Classification of colloidal polymer dispersions*⁴⁸

Polymer dispersions can be mainly classified as primary dispersions and secondary dispersions. Primary dispersions include natural latex dispersions produced in living organisms and manmade dispersions (synthetic latexes). Secondary latexes are prepared by dispersing solid polymer or emulsifying them in a proper solvent medium. Block copolymers form micelles in solvents selective for only one set of block, which produces sterically stabilized polymer particles and thus belong to the class of polymer dispersions⁵⁰. Polymeric colloidal complexes result from triggering polymer solutions by inducing either hydrophobic or electrostatic interactions in the system. The formation of hollow spheres via layer-by-layer assembly of oppositely charged polyelectrolytes on the surface of various templates is an example for polymer colloidal complexes^{45, 51}. A schematic representation of various types of polymer dispersion is given in Figure 1.5.

1.3.3. Monodisperse Polymer Colloids

Generally metallic colloids adopt different shapes such as ellipsoidal, spherical, cubic etc, but in the case of polymer particles spherical shape is thermodynamically stable. Even though it is possible to make polymer colloids with nonspherical shape, but they are often in a thermodynamic metastable state, which leads to a progressive evolution toward a spherical form depending on the diffusion capability of the polymers. The control of particle size and particle size distribution (monodispersity) is very important requirement since it regulates the bulk polymer chemical and physical properties. The size monodispersity should be obeyed for several reasons; for the sake of reproducibility of immunoassays used in diagnostics, in drug delivery systems in which particle size should not overcome a limit, in transport in micrometer-sized channels, for the preparation of two or three dimensional organization of particles on a surface or in a volume, and for other uses. Polymer colloidal solution is generally white in color but appears iridescent blue when the latex particles are highly monodisperse and highly charged on the surface (Figure 1.6).

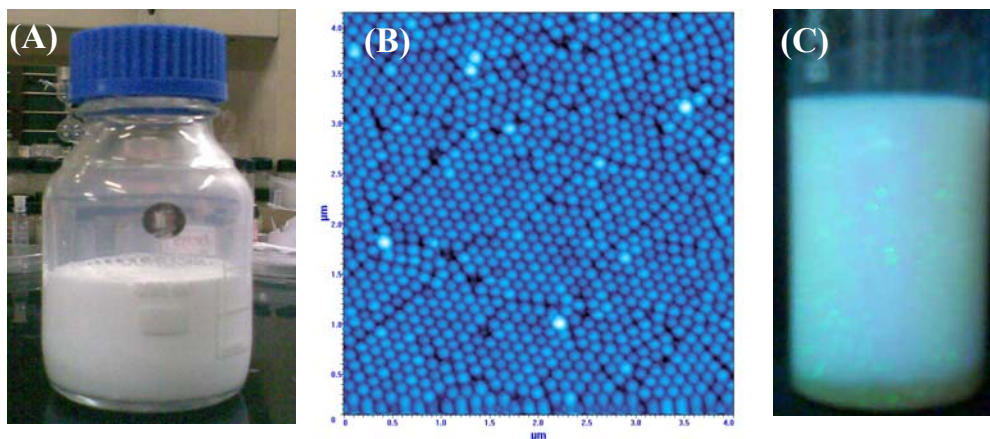


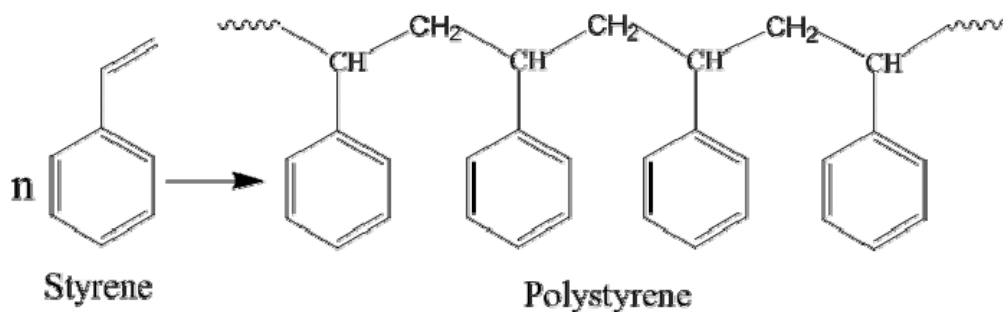
Figure 1.6. (A) Polymer colloidal solution (B) AFM image of monodisperse polymer colloid and (C) self-assembled particles diffract visible light. The images presented here are obtained from our laboratory samples.

1.3.4. Application of Polymer Colloids

Latex particles are a force to reckon in the worldwide commerce and as well as in scientific studies. It is not an exaggeration to say that they are important in our day to day life mainly because of their versatile characteristics and applications. The main application of polymer colloids are in paper making, all kinds of paints and coatings, the construction industry, adhesives, the textile and leather industries, optical devices, chemo and biosensing, and also in medicine in and pharmaceutical industries^{47, 48, 52}. When the latex particles are narrow in size shape and carry an electrostatic charge they tend to repel each other which cause the system instability. To reduce the force of repulsion they are aligned in certain positions keeping an equal distance from each other particle counterparts which results in self assembly of these particles into non close packed structures such as FCC and BCC or HCP which Bragg diffracts visible light⁵³. The packing unlike in metals is different in this case where the inter particle distance is more than the particle diameter. This three dimensional arrays which are popularly known as crystalline colloidal array (CCA) in the literature.⁵⁴

The Bragg diffracting phenomenon of these colloidal crystalline arrays has found vast applications in the fields of optics, spectroscopic instrumentation. Asher et al developed a smart sensing materials by immobilizing the CCA inside a three dimensional hydrogel network to produce polymerized crystalline colloidal array (PCCA) which can be functionalized with certain ligands, enzymes to sense and quantify biologically important molecules, toxic metal ions etc⁵⁵. Latex paint emulsions are easily formulated using latex particles and dispersed pigments of desired colors. The polymer particles in emulsion paint have a very low T_g which causes these particles coalesce to form a continuous film once dries⁵². Latex paints revolutionized the paint and coating industry when they were introduced in 1950s. Latex paints also extended their magical touch to floor coatings ('polishes'), printing inks, adhesives, paper overprint varnishes, carpet backing and paper making. In some applications polymer colloids are used as admixes with another material to enhance the properties. Rubberized concrete is one such a kind where rubbery polymer latex like poly(styrene-co-Butadiene) is mixed with cement and sand to make a flexible, thermally expandable and strong reinforced cement concrete which is used in airport runways and highways⁵². Another important property of colloidal particle is their specific surface area which is inversely proportional to size and depends upon the shape also. Smaller the size larger the surface area of a spherical polymer particle. The large surface area of a polymer particle has several advantages like adsorption, desorption, chemical reaction, light scattering and etc.,⁵ Polymer supported catalysts systems are very useful in industrial production of materials where the surface area of the catalyst play a vital role. The porosity and permeability of polymeric supports are important properties which makes the polymer supports an ideal one. To attach metal catalysts such as Zn, Ti, Pd functionalization of polymer particle with appropriate reactive groups is important. Polymer particles bearing amino, carboxyl, hydroxyl or thiol groups can be coupled with biologically important molecules to be used in medical immunological studies. In other cases they are used in DNA, antibody and drug delivery applications⁵⁶⁻⁵⁸. Particles surfaces can be engineered with other functionalities depending on the application technique and on the type of detection (optical, electric, dielectric, and magnetism)

involved for the analysis. The applications of polymer latexes are numerous, we have tried to mention some of the important applications in this thesis.



Scheme 1.1. *Polystyrene polymerized from styrene monomer*

1.4. Polystyrene Colloids

1.4.1. Polystyrene classification and Properties

Polystyrene (Scheme 1.1) based on the arrangement of phenyl ring can be classified as isotactic, atactic and syndiotactic polystyrene. Syndiotactic polystyrene shows a crystalline behavior due to which it has a high melting point of 270°C. Syndiotactic polystyrene was first claimed as engineering plastic due to its high melting point. Commercially available polystyrene is atactic and hence amorphous. Polystyrene is chemically inert and resists alkali, halide acids, oxidizing and reducing agents. But it can be subjected to nitration, chlorination, and sulphonation. The high refractive index (1.60) of polystyrene makes it useful as polymer based optical components. Polystyrene is a good electrical insulator and has a low dielectric loss factor at moderate frequencies. Its tensile strength reaches about 8000 psi. Polystyrene has a thermal stability of 380°C is highly brittle and light polymer which is the reason for its low or non biodegradability. Polystyrene disposal has become a major environmental problem due to its low biodegradability. Polystyrene properties are listed in Table 1.3. The rubbery domains allow distribution of the stress concentration over a larger volume, toughening

the material. Styrene is one of the few monomers which can be polymerized via free radical, anionic, cationic and metal catalyzed conditions. Polystyrene particles in the range within the colloidal domain are polystyrene colloids since polystyrene particles of several microns exist. Commercially polystyrene particles are prepared via bulk, suspension and emulsion polymerizations. It yields spherical particles of sizes from 10 nm to 1000 micrometer if it is synthesized from emulsion polymerization⁵⁹.

Table 1.2. *Properties of Atactic Polystyrene (obtained from reference 60)*

Physical Property	Magnitude	Physical Property	Magnitude
Density	1.05 g/cm ³	Notch test	2 –5 kJ/m ²
Density of EPS	16–640 kg/m ³ [4]	Glass transition temperature (T _g)	95°C
Dielectric constant	2.4–2.7	Melting point	240°C
Electrical conductivity (s)	10 ⁻¹⁶ S/m	Vicat B	90°C
Thermal conductivity (k)	0.08W/(m·K)	Linear expansion coefficient (α)	8×10 ⁻⁵ /K
Young's modulus(<i>E</i>)	3000–3600 MPa	Specific heat (<i>c</i>)	1.3 kJ/(kg·K)
Tensile strength (s _t)	46–60 MPa	Water absorption	(ASTM) 0.03–0.1
Elongation at break	3–4%	Decomposition	Unknown

1.4.2. Polystyrene Copolymers and Applications

Any given monomer is copolymerized with another monomers either to tune, improve, and modify the chemical and physical properties or to functionalize the resultant polymer with desired functionalities for various applications.

1.4.2.1. Ion Exchange Resins

Cationic exchange resins are synthesized by the polymerization of styrene with divinylbenzene which yields spherical particles and followed by sulphonating in such a way that each benzene moiety contains $-\text{SO}_3\text{H}$ group. Whereas anionic benzene is prepared by copolymerizing benzene with divinylbenzene and vinyl ethylbenzene and later on treated with chloromethylether to functionalise benzene ring with chloromethyl group for ion exchange⁵⁹.

1.4.2.2. Polymers of Styrene Derivatives

Poly(ortho-methyl styrene), even though has better heat resistance than polystyrene, however it has failed to survive because of brittleness and difficulty in fabrication due to a low ceiling temperature of 61°C . Poly (p-tert-butylstyrene) is used as a viscosity improver in motor oils, and polychlorostyrene is valuable because of its self extinguishing characteristics⁵⁹. Poly (sodium styrene sulfonate) is useful as a water soluble flocculating agent, and used in medical diagnosis. Poly (p-methyl styrene) may become of commercial interest because of a new monomer synthesis from toluene and ethylene that could result in lower prices; some key properties of the polymer are improved over those of polystyrene.

1.4.2.3. Copolymers of polystyrene

To improve the properties of polystyrene it is copolymerized with other monomers depending upon the property desired. For example it is polymerized with butadiene rubber to produce strong and more flexible copolymer. High-impact polystyrene (HIPS), which has an impact strength 5–10 times than the neat polystyrene, is a multiphase material in which polybutadiene rubbery domains are distributed within the polystyrene matrix⁵⁹. Styrene is copolymerized with monomers such as acrylic acid, methacrylic acid, itaconic acid to functionalize the particles with carboxyl group, particle nucleation studies and impart hydrophilic character⁶¹. Poly (styrene-co-sodium

styrene sulphonate) has found applications in biological system studies, PEM fuel cell membranes, ion exchange resins, water purification systems etc.⁶².

1.5. Synthesis of Polymer Colloids

Mostly free radical polymerization is utilized in different heterogeneous polymerization techniques to synthesize polymers in exclusively in particulate form. Free radical polymerization techniques based on the solubility of monomer, initiator other ingredients in continuous medium are classified into homogeneous and heterogeneous polymerization. Generally heterogeneous polymerization techniques has a tendency to yield polymers in particle form and generalized as particle forming polymerizations^{47, 63}. Very rarely polymer obtained from homogeneous polymerization technique posses particle morphology. The possible explanation is as follows; the classification of homogeneous and heterogeneous polymerizations arises from the initial polymerization reaction mixture, but we cannot neglect the possibility of polymer particle formation in the later stage of the polymerization, where it becomes heterogeneous from homogeneous polymerization due to insolubility of polymer which transforms into particle. Homogeneous system includes bulk, solution, and gas phase polymerization techniques which are used extensively in industrial processes. Heterogeneous polymerizations are two phase systems in which monomer(s), or the resultant polymer are in the form of fine dispersion in an immiscible liquid. The principal heterogeneous or particle forming polymerization techniques can be subdivided into precipitation, dispersion, suspension, micro suspension, miniemulsion, conventional emulsion and microemulsion polymerization. Each of these techniques has branches or sub classes of their own. Figure 1.7 gives an account of resultant characteristic particle size for different particle forming polymerization or heterogeneous polymerization. The terms emulsion, suspension, precipitation, and dispersion are defined and differentiated based on the following criteria; initiation of the polymerization mixture, kinetics of polymerization, mechanism of particle formation, and size and shape of the final particle size.⁶³ There are numerous amount of literature

available for heterogeneous techniques which produce particles of sizes covering the whole spectrum of colloidal domain and beyond that⁶³.

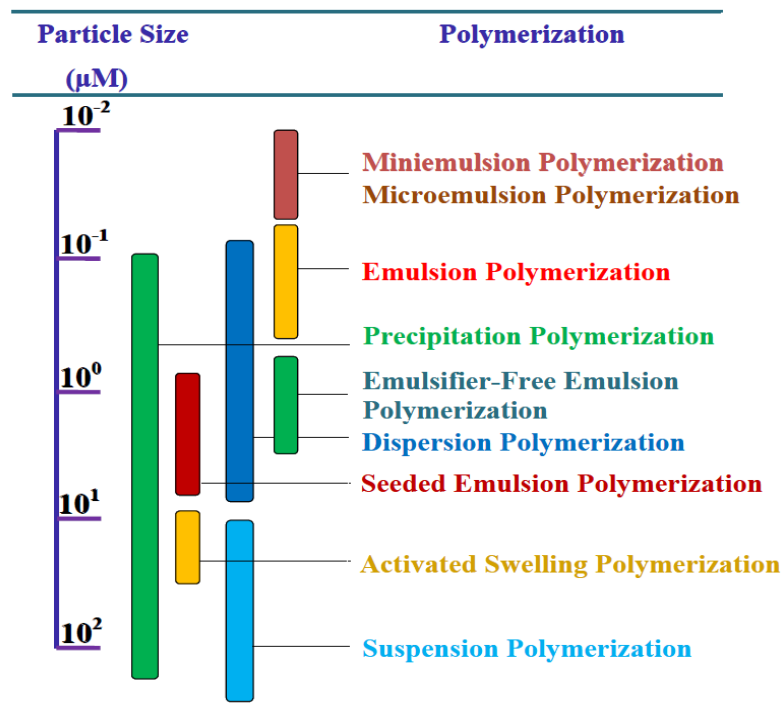


Figure 1.7. Particle size of polymers from different heterogeneous particle forming polymerization techniques⁶³.

1.6. Emulsion Polymerization

1.6.1. Overview

Emulsion polymerization involves polymerization of hydrophobic monomers dispersed in the continuous aqueous phase with the help of emulsifiers and subsequent

initiation by water soluble initiators. Emulsion technique yields spherical particles with a size range of 30 nm to 1000 nm but more commonly 80 nm-300 nm. Emulsion polymerization encompasses several related processes like conventional emulsion, miniemulsion, microemulsion, and emulsifier free emulsion polymerization. Emulsion polymerization is commercially innovative and important technique to obtain polymers as colloidal particles dispersed in water (latex dispersions). Emulsion polymerization has several advantages. These are (1) colloidal state makes it easy to control (2) less thermal and viscosity problems compared to bulk processes and (3) latexes can be used without separations^{64, 65}. Apart from these physical differences the distinctive feature of emulsion polymerization is the molecular weight of polymer can be increased without decreasing polymerization kinetics which is not possible for other polymerization processes. The mechanism of emulsion technique affords it to obtain the high molecular weight polymerization without decreasing the rate^{64, 65}.

Synthetic polymer dispersions are produced via emulsion technique and half of these are commercialized as waterborne dispersions. Carboxylated styrene-butadiene copolymers, acrylic, styrene-acrylic copolymer latexes, vinyl acetate homopolymer and copolymer are main classes of emulsion polymers. Emulsion polymerization is commonly utilized for the commercial polymerizations of vinyl acetate, chloroprene, various acrylate copolymerizations, and copolymerizations of butadiene with styrene and acrylonitrile. The main uses of these latex dispersions are paints and coatings, paper coating, adhesives, carpet making etc. This type of polymer dispersion has also found wide variety of applications in fields of medicine, which includes diagnosis drug delivery and treatment, optics, bio and chemo sensing⁴⁷. Another half of the polymer dispersions are commercialized as solid dry materials which include styrene-butadiene rubber (SBR) for tires, nitrile rubbers, about 10% of the total poly(vinyl chloride) production, 75% of the total acrylonitrile-butadiene-styrene (ABS) an elastomer modified thermoplastic which is used in electrical appliances, home and office appliances and redispersed powders as construction materials^{64, 65}.

1.6.2. Conventional Emulsion Polymerization- Basic Ingredients

1.6.2.1. Water

In the emulsion polymerization water is the main ingredient in which monomers are dispersed with the help of emulsifier molecules and free radical polymerization are carried out using a water soluble initiator to form latex dispersions. Water, as a continuous phase, apart from serving as an inert medium also lowers the reaction viscosity and heat. Most importantly it isolates the reaction loci. Water serves as a medium of transfer of monomer from droplets to particle, as a locus of initiator decomposition and oligomer formation and as a medium of exchange of emulsifier molecules between phases. The ratio of water to monomers is usually from 70/30 to 60/40⁶⁴⁻⁶⁶.

1.6.2.2. Surfactant or Emulsifier

Surfactant or emulsifier molecule consists of a hydrophilic head and an hydrophobic tail which reduces the surface tension of medium enormously. Surfactants at high concentration tend to form molecular aggregates which are known as micelles and the concentration above which the micelles are formed is known as *critical micelle concentration* (CMC) which is a characteristic of surfactant molecule. In micelles hydrophilic or ionic end of a surfactant is pointed outwards and the hydrophobic ends towards the core or inside. Micelles known to exist in different structures like sphere, rod etc; of which sphere is energetically stable. Micelles typically are in size of 2-10 nm and each micelle consists of 50-150 emulsifier molecules. Number of micelles and their size is a function of emulsifier concentration, and the large amount of surfactant molecules yields huge number of smaller sized micelles. In emulsion polymerization technique surfactant (emulsifier) performs dual role as a site of particle nucleation (i.e., monomer swollen micelles) as well as stabilizing agent for the growing particle after being adsorbed on the particle-water interface. Although anionic surfactants (e.g., sodium dodecylsulphate) are generally used, other surfactants that include cationic emulsifiers to prepare cationic latexes and non-ionic surfactants for controlling the

morphology and enhancing the stability of yield polymer spheres from mechanical shear, freezing and added electrolytes are also used. Polymerizable surfactants are surface active molecules which have reactive vinyl groups adsorbed on particle surfaces which prevents surfactant desorption during film formation and reduce the water sensitivity^{65, 66}.

1.6.2.3. Initiator

Water soluble persulphate salts are the most common initiators which dissociates on heating into two sulphate anions and initiate the polymerization. Redox initiators a mixture of reducing and an oxidizing agent, whose reaction generate radicals, can also be used as an initiator. Oil soluble azo compounds such as AIBN (azobisisobutyronitril) are also used to control the particle morphology and the grafting inside the particles, and to reduce the residual monomers at the end of the polymerization reaction^{65, 66}.

1.6.2.4. Monomer

Monomer employed in emulsion polymerization is either water-insoluble or sparingly water soluble and when the monomer is added to the medium it dissolves and diffuses to the hydrophobic core of the spherical micelle. The monomer swollen micelles are confirmed by X-ray and light scattering experiments. The amount of monomer present in micellar core is always high when compared to the aqueous medium for water insoluble, non-polar monomers. A large amount of monomer is dispersed as droplets which are stabilized by surfactant molecules adsorbed on the surface whose size range is 1- 100nm. Thus in an emulsion polymerization systems monomer droplets are more in size than monomer swollen micelles. The concentration of the micelle is 10^{19} to 10^{21} per liter and the monomer droplet concentration is 10^{12} to 10^{14} L^{-1} . Monomer inside the micelle is initiated by the diffusing initiator molecules and the polymerization proceeds until all the monomer is converted into polymer and the final particle obtained is spherical in shape stabilized by surfactant molecules adsorbed on the surface^{65, 66}.

1.6.3. Emulsion Polymerization – Underlying Features and Principles

1.6.3.1. Locus of Polymerization

Locus of polymerization is not the monomer droplets because the initiator employed here is water soluble and if an oil soluble initiator is employed the polymerization will occur at monomer droplet which is known as suspension polymerization. Initiator is an important factor which differentiates emulsion polymerization from suspension polymerization. Polymerization in solution cannot be ruled out but insignificant due to the facts; (i) the presence of small amount of monomer (ii) oligomer produced precipitates out quickly. Hence the monomer swollen micellar core is the main locus of the polymerization. As the polymerization proceeds the size of the micelle increases with the regular supply of monomer from aqueous medium whose monomer concentration is enhanced with the dissolution of monomer droplets which act as a reservoir. When all monomers present inside the micellar core is polymerized then it is no more considered as a micelle but are referred as polymer particles. All the particles formed will have uniform shape and size⁶⁵⁻⁶⁷.

1.6.3.2. Particle Nucleation Mechanisms

Three mechanisms were proposed for the particle formation in emulsion polymerization namely micellar or heterogeneous nucleation, homogeneous nucleation and droplet nucleation.

1.6.3.2.1. Micellar or Heterogeneous Nucleation

An initiator or oligomeric radical enters into monomer swollen micelles and polymerizes the monomer to form monomer polymeric particles which grow in size by propagation. Generally nucleation is active until all the micelles are utilized after which the number of particles remain constant but in some other cases nucleation decreases due to lack of sufficient surfactant molecules to maintain colloidal stability or in the later stages of the polymerization nucleation may increase because of desorption of surfactant molecules from well grown particles which causes secondary particle

generation. Monomer droplets act as a reservoir and supply the monomer molecules constantly to growing particles until their disappearance. Micellar nucleation is dominant for highly hydrophobic water insoluble non polar monomers such as styrene, methyl methacrylate etc. Figure 1.8 gives an overall description of the heterogeneous nucleation process.

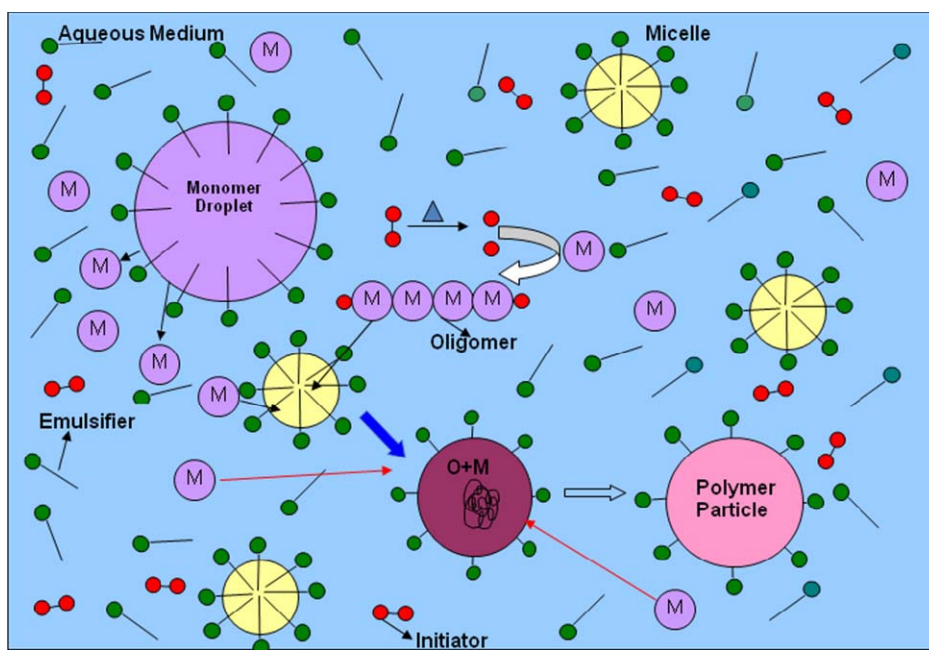


Figure 1.8. Description of heterogeneous or micellar nucleation mechanism. The schematic presentation is drawn by us to represent the micellar mechanism using references 65-68.

1.6.3.2.2. Homogeneous Nucleation

If the amount of surfactant is not enough to produce micelles then this kind of nucleation occurs. Solution polymerized oligomeric radicals grow in size until they reach a critical chain length and precipitates due to its hydrophobicity. The precipitated oligomeric radical is stabilized by surfactants. This precursor particle absorbs monomer

allowing further propagation and growth. The process is known as homogeneous nucleation mechanism. A sibling of homogeneous nucleation is known as coagulative nucleation where a small sized precursor particles are formed by homogeneous nucleation and they grow in size by rapid aggregation or coagulation to form stable and mature particles. Figure 1.11 represents an overall picture of homogeneous nucleation process⁶⁵⁻⁶⁹.

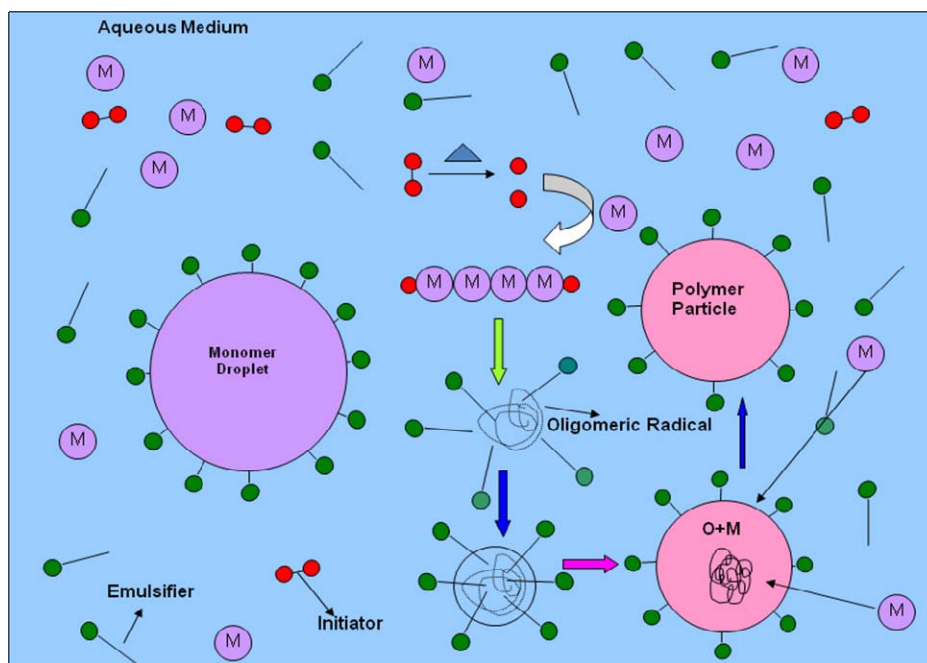


Figure 1.9. Description of homogeneous nucleation mechanism. The schematic presentation drawn by us to represent the homogeneous mechanism using references 65-68.

1.6.3.2.3. Droplet Nucleation

Droplet nucleation occurs when an oligoradical or initiator radical enter into droplet and starts nucleating. The surfactant molecules adsorbed on the growing particle and monomer droplet gives the colloidal stability. This mechanism is predominant in

miniemulsion and microemulsion polymerization. For this mechanism usually a co-surfactant (e.g. hexadecane) along with main surfactant is employed⁶⁶.

1.6.3.2.4. Proportion of each Particle Nucleation in Overall Particle Formation

In conventional emulsion technique all the three mechanisms operate simultaneously but the proportion varies considerably. Depending upon the surfactant concentration, monomer solubility in aqueous medium any one of the nucleation processes predominates. For highly water insoluble monomers micellar or heterogeneous nucleation is primary nucleation process. For emulsion polymerization systems at above CMC regions micellar nucleation dominates. On the other hand homogeneous nucleation mechanism is a major nucleation process for high water soluble monomers. Homogeneous nucleation is dominant mechanism when the surfactant concentration is below the CMC region and in emulsifier-free emulsion polymerization techniques. In emulsion technique droplet nucleation is considered as insignificant but becomes significant in case of mini- or micro- emulsion processes where the droplet size is in submicron range. When the monomer is highly water insoluble then the droplet nucleation dominates in miniemulsion techniques.

1.6.4. Other Types of Emulsion Polymerization

1.6.4.1. Emulsifier free Polymerization

Pure latexes free of surfactant are needed in instrumentation techniques such as microscopy calibration and pore size determination. Removal of emulsifier molecules either by directly or desorption may lead to particle collapse by coagulation or aggregation. Surfactant free emulsion polymerization is a useful approach to overcome this problem. In this technique initiator radical (for example persulphate radical) imparts stability to the formed latex which is chemically bound and removal of unreacted monomer from the polymer particle can be done without loss of stability. A

characteristic feature of emulsifier free emulsion polymerization is the particle number is usually less than the conventional emulsion polymerization i.e. 10^{12} mL⁻¹ for surfactant free technique compared to 10^{14} per mL of emulsion polymerization. Due to the sole stabilization contribution from initiator radical in the absence of surfactant leads to lower total particle surface area which decreases the total particle number but particle sizes will be relatively higher^{62, 65, 70}.

1.6.4.2. Inverse Emulsion Polymerization

Instead of emulsifying the hydrophobic monomer by the means of emulsifier and initiating with water soluble initiator (conventional emulsion polymerization) an aqueous solution of hydrophilic monomer can be emulsified in non-polar solvents such as xylene or paraffin oil using excess surfactant and polymerized by oil soluble initiator. Reverse micelles were formed. The process is known as inverse emulsion polymerization where the former technique is known as *oil-in-water* and the latter is called *water-in-oil* emulsions. Inverse emulsion process is used in commercial polymerization of acrylamide as well as other water soluble monomers. The product latex is prone to flocculation and the product polymer readily dissolves in water. The aqueous polymer solution is used in secondary oil recovery and flocculation⁶⁴⁻⁶⁶.

1.6.4.3. Miniemulsion polymerization

In miniemulsion polymerization the droplet size is decreased substantially (50-1000 nm) compared to droplets in conventional emulsion technique (1-100 μ m) with suitable emulsifier and a smart emulsifying apparatus. The resultant miniemulsion droplet is stabilized against diffusional degradation or oswald ripening or coagulation by a cosurfactant. In this technique surfactant concentration is well below CMC and all the available emulsifier molecules were absorbed on the surface of the monomer droplet hence there are no micelles in the system. Both water and oil soluble initiators were employed in the system. When added to the system initiator nucleates the droplets and the final particle size is similar to initial monomer droplet size^{65-67, 71}.

1.6.4.4. Microemulsion Polymerization

The droplet size much smaller (1-100 nm) compared to miniemulsion (50-1000nm) and macroemulsion (1-100 μ m). Micelles are present in the system because surfactant concentration is above CMC. Generally the initiator employed in this system is water soluble but in some cases oil soluble initiator was employed. In many aspects microemulsion resembles emulsion polymerization but both are not exactly same. Particle size of the final polymer particle is in the range of 10 to 50 nm^{64-67, 72}.

1.7. Application of Polystyrene Colloidal Spheres

Polystyrene microspheres have found applications in catalysis and ion exchange resins, chromatographic and microscopic calibration standards, biomedical applications which include diagnosis and drug delivery, polymer template assisted nano particle synthesis, photonic crystal devices, sensing applications, paper, carpet, and leather industries, and emulsion and paint technology and etc. Polystyrene crosslinked with divinylbenzene is polymerized with (vinylbenzyl)trimethylammonium chloride and resultant microspheres with quaternary ammonium functionalized group is used as phase transfer catalysts⁷³. Also microspheres containing triarylphosphonium group were utilized for Wittig reaction⁷³. Submicron size polystyrene copolymer particles functionalized with -COOH, -OH, -CHO, and -NH₂ groups are coupled with antibodies, drug molecules, DNA, proteins and utilized in targeted drug delivery applications and immunological studies^{56, 57, 74}. Polystyrene colloidal spheres were coated with several silica multi layers and the polystyrene core was removed by calcination to prepare hollow silica particles⁵¹. Polystyrene colloidal spheres tend to self assemble upon drying into certain non close packed forms such as BCC, FCC, or HCP. The gaps can be filled with metal nanoparticles followed by the removal of polystyrene core using calcination form metal nanostructures which can be used in photonic band gap applications¹⁴. Monodisperse TiO₂ spheres were prepared by templating sol-gel precursor against 3D crystalline array of polystyrene after which the polystyrene was removed by selective etching using toluene¹⁴. Ibuprofen, indomethacin loaded polystyrene

particles were used in clinical pain treatments⁷⁵. Some of the leading polymer microsphere suppliers⁷⁶ produce mostly $-\text{COOH}$, $-\text{NH}_2$, $-\text{CHO}$, and $-\text{OH}$ functionalized polystyrene, for coating antibodies, DNA, proteins, antigens, peptides or nucleic acid probes for applications in life sciences. Dye loaded fluorescent polystyrene microspheres and plain polystyrene particles are utilized as microscopy calibration standards⁷⁶. Polystyrene based superparamagnetic microspheres have found huge applications in bioseparation, immunoassays, biosensors, chemosensors and biopanning⁷⁷. In solution highly charged monodispersed polystyrene copolymer particles at an appropriate volume fraction of polymer solution tend to self assemble into long range ordered non close packed structures which diffract visible light obeying Bragg's law ($n\lambda=2d\sin\theta$)⁵⁴. These self assembled structures are known as crystalline colloidal array (CCA) which has very interesting optical properties. Asher et al. immobilized this CCA inside polymer hydrogel which they name as polymerized CCA (PCCA) and use this PCCA for sensing applications⁵⁵.

1.8. Hydrogel

Hydrogel is three dimensional cross linked network structure containing cavities filled with water. Hydrogels is hydrophilic three dimensional chemical or physical network swollen in water^{78, 79}. It is capable of absorbing 10-1000 times of its dry volume of water without dissolution. Hydrogel tend to contract, expand and bend in response to external chemical and physical stimuli like pH, ionic strength, irradiation, electric field, magnetism etc. Hydrogel play an important role in water- borne polymer technologies such as cosmetics, coatings, food and industrial process. Hydrogel revolutionized the field of medicine as a drug cargo which delivers the drug with controlled smartness and sharpness. Hydrogel is like a magical tissue which has found huge application in tissue engineering due to its resemblance to human tissues. Hydrogel is ideal materials in controlled drug delivery and tissue engineering because of their high biocompatibility and low toxicity⁷⁸⁻⁸¹.

1.8.1. Volume Phase Transition of Hydrogel

Stimuli responsive hydrogel is important for drug delivery and tissue engineering applications, and it changes in volume depending upon the environment. There are numerous amount of literature on hydrogel swelling phenomenon^{81, 83}. Neutral hydrogel swells well in good solvents but the swelling is restricted by crosslinks which controls the elastic restoring forces. Hydrogel containing ionic groups responds chemically due to the change in pH and ionic strength of the environment. Based on the theories of Flory⁸² and Tanaka⁸³ swelling phenomenon can be well understood. Equilibrium hydrogel volume swelling or total free energy of a gel swelling can be written as follows,

$$\Delta G_{\text{Total}} = \Delta G_{\text{Mix}} + \Delta G_{\text{Ion}} + \Delta G_{\text{Elas}} \quad (1.1)$$

Where the total free energy (ΔG_{total}) is a combination of three free energies and these are

1. free energy of ionic electrostatic energy resulting from Donnan membrane potential and electrostatic repulsion between charged ionic groups of the polymer backbone (ΔG_{ionic}),
2. free energy of mixing of polymer chains and solvent medium (ΔG_{mix}), and
3. free energy of elasticity of crosslinked networks (ΔG_{elas}).

For the ionic hydrogel all the above three free energies contributions come to the total free energy. Whereas in the case of non ionic gels, ΔG_{ionic} contribution will be absent. Hence by varying the three free energies one can increase the total free energy. When a particular free energy increases inside the gel in an effort to bring it to normal the gel, responds by either swelling or collapsing. Depending upon the magnitude of the alteration of a particular free energy the total free energy changes. Free energy of polymer- solvent mixing and network elasticity according to Flory and Tanaka can be written as equation 1.2 and 1.3, respectively

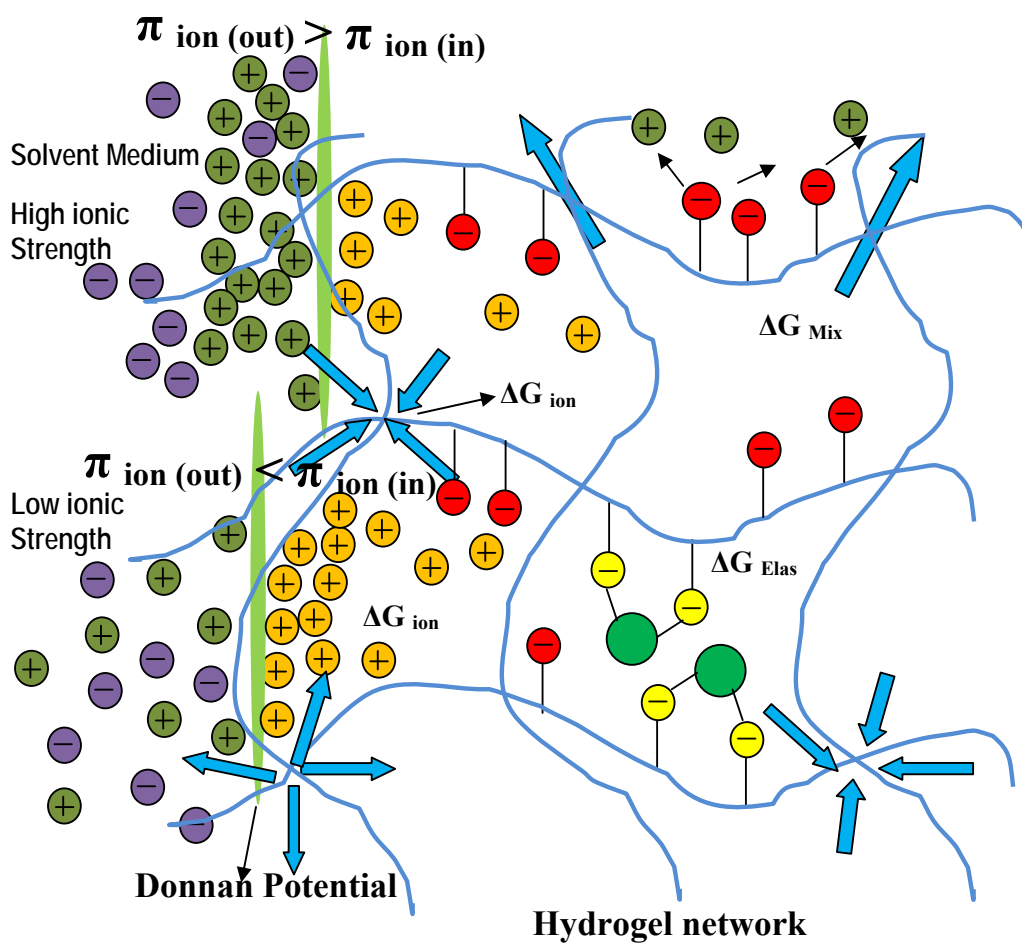
$$\Delta F_{\text{mix}} = K_B T \frac{V}{v_{\text{Site}}} (1 - \phi) [\ln(1 - \phi) + \chi \phi] \quad (1.2)$$





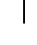
$$\Delta F_{mix} = \frac{3K_B T}{2} v_e \left[\left(\frac{V}{V_0} \right)^{\frac{2}{3}} - 1 - \frac{1}{3} \ln \left(\frac{V}{V_0} \right) \right] \quad (1.3)$$

Where k_B is the Boltzmann constant, T is the temperature, and v_{site} is the volume of a single lattice element in the Flory model⁸²⁻⁸⁴. ϕ is the polymer volume fraction in the swollen network, and χ is the Flory-Huggins polymer/solvent mixing parameter. V_e is the effective number of polymer chains in the network, and V is the volume of the hydrogel in the presence of the analyte. Let us assume that V_0 is the volume of the hydrogel in pure water.

ΔG_{Mixing} changes when the mixing between polymer and solvent increases because the gel backbone is modified due to the interaction of attached molecule and an analyte whereas the mixing is zero or negligible in case of unmodified hydrogel⁸⁴. Enhanced polymer/solvent interaction increases the Flory-Huggins solvent-polymer mixing parameter χ which increases the magnitude of ΔG_{mixing} and in response to that gel expands. If the medium is a good solvent for a complex formed between a coupled molecule and an analyte then we should consider another sources of contributions it brings to the total free energy. If polymer chain mixes more with the solvent then the complex formed which is bound to the gel backbone should ionize. ΔG_{ionic} changes when there is a change in osmotic pressure due to ionic strength gradient inside and outside the gel caused by mobilized counter ions which results in Donnan membrane potential. To reduce the inner increased potential gel swells whereas if an inner potential is smaller than outer potential then shrinkage occurs. Gel volume increases and reaches maximum when the gel crosslinks that keep the gel together resists further elongation.

The restoring force is known as elastostatic free energy which can be increased only when some or all crosslinks were broken or a new crosslinks were added to the polymer⁸⁵. The above equation 1.1 can be rewritten in terms of Donnan membrane potential as follows (equation 1.4)



-  Resultant product ions due to the reaction between attached molecule and an analyte
-  attached molecule and an analyte
-  Ionised unattached functional group of gel group
-  Ionized molecular recognition moiety
-  Analyte ion or molecule

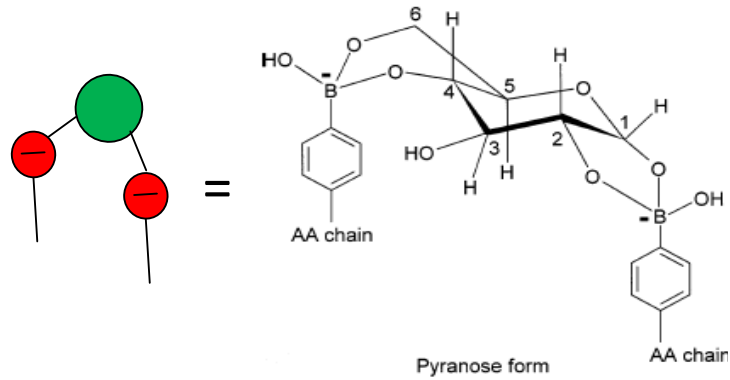


Figure 1. 10. An illustration of gel volume phase transition mechanism as a function of summation of free energy of mixing, free energy of electrostatic repulsion due to ionic groups, and free energy of elasticity. An example of change in ΔG_{Elas} is shown here which is adapted from reference 86.

$$\frac{\partial \Delta G_{total}}{\partial \Delta V} = \Delta \pi_{total} = \Delta \pi_{ion} + \Delta \pi_{mix} + \Delta \pi_{Elas} \quad (1.4)$$

Where $\Delta \pi_{total}$ is the total membrane potential, $\Delta \pi_{ionic}$ membrane potential due to ionic contribution, $\Delta \pi_{mix}$ is the membrane potential of mixing when the number of solvent molecule or medium changes or the change in Flory-Huggins solvent mixing parameter (χ) and $\Delta \pi_{elastic}$ is membrane potential change due to the induced crosslinking⁸²⁻⁸⁴. Asher developed a high ionic strength glucose sensor coupling boronic acid to the polymer backbone⁸⁶. Glucose forms 2:1 boronate complex with 2 boronic acid units which brings added crosslinks to the gel network. Due to the increase in crosslink density, ΔG_{Elas} decreases and the gel shrinks (Figure 1.10). A schematic presentation of hydrogel swelling and shrinking (volume change) due to the change in total free energy changes is presented in Figure 1.10.

1.8.1.1. pH Responsive Hydrogels

Carboxylic group ($-\text{COOH}$) containing hydrogel undergoes ionization at high pH and the resulting increase in free H^+ ion concentration inside of the gel creates a Donnan potential membrane. To minimize the potential gel swells so that it can maintain equilibrium potential inside and outside of the hydrogel. In another way swelling also occurs due to the increased repulsion between charged $-\text{COO}^-$ groups which expands the gel increasing the equilibrium distance between two $-\text{COO}^-$ groups^{87, 88}. For example hydrogels can be coupled with amoxicillin or metronidazole and administered in stomach for *Helicobacter pylori*^{87,88}. High pH of intestine ionizes the ionic groups of the gel and expands the gel due to repulsion of COO^- groups which triggers the gel collapse and drug release^{85, 87, 88}. An example of drug release by changing the hydrogel volume is quoted here from reference 87 and 88 in Figure 1.11.

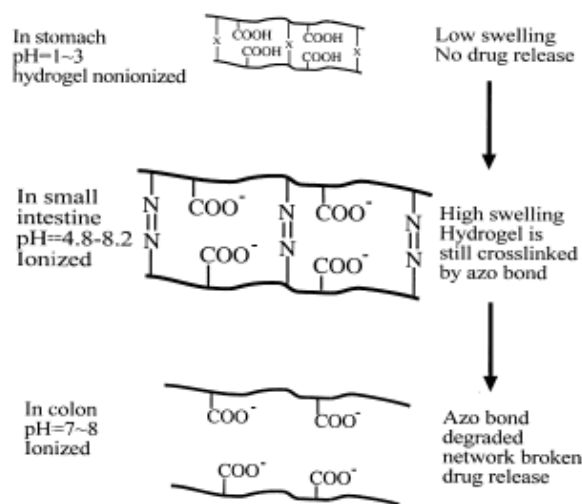


Figure 1.11. Illustration of oral specific delivery for colon by biodegradable pH sensitive hydrogel. Azoaromatic moieties are represented as $-\text{N}=\text{N}-$. (from reference 87 and 88)

1.8.1.2. Ionic Strength Responsive Hydrogels

Poly (acrylamide-co-N, N'-methylenebisacrylamide) hydrogels were coupled with enzymes, ligands and other molecular recognition agents. When in contact with specific counter ions or molecules these recognition agents coupled gels interact with them and produces ions. This creates an ionic inequilibrium inside and outside of the hydrogel which generates Donnan membrane potential across the gel membrane. To reduce the potential hydrogel swells enormously. The swelling dynamics is a function of analyte material concentration. So hydrogel material provides an excellent platform to be used as sensing materials. But the only challenge was to measure the hydrogel contraction and expansion. Asher et al.^{55, 84-86} have pioneered PCCA sensing materials which takes advantage of hydrogel volume phase transition phenomenon. Also, Lowe et al.^{89, 90} developed holographic sensor materials, which have a resemblance to Asher's PCCA smart sensing materials, also have utilized the hydrogel swelling dynamics.

1.9. Polymerized Crystalline Colloidal Array Materials

1.9.1. Crystalline Colloidal Array (CCA)

Highly monodisperse and highly charged colloidal particles at a particular particle concentrations readily self assemble into non close packed structures BCC, FCC or HCP and these self assembled structures tend to Bragg diffract visible light obeying Bragg's law⁶¹⁻⁶³ ($n\lambda=2d\sin\theta$, where λ is diffracted wavelength, n refractive index of the solvent medium, d interplanar distance and θ glancing angle). The self assembled structures are known as crystalline colloidal array (CCA) or photonic crystal (Figure 1.12) which have found numerous applications in the fields of sensing and photonic crystal devices⁵³⁻⁵⁵. Lattice spacing of CCA is greater than the particle diameter. The electrostatic force of repulsion of highly monodispersed and charged particles drives them to self assemble to minimize the energy which results in ordered packing in solvent medium. Upon dilution CCA lattice spacing increases (d) which leads to change

in diffraction red shifts (λ) of CCA91. This unique property of CCA have inspired Asher to immobilize these CCA inside hydrogel to study the hydrogel swell/shrink behaviour by measuring CCA diffraction changes⁵⁵. Immobilized CCA are called Polymerized Crystalline Colloidal Array (PCCA) have found applications as chemo and bio sensor materials^{53-55, 84-86, 91}. Highly charged monodispersed polystyrene copolymer particles synthesized by emulsion polymerization was utilized to generate CCA⁹¹.

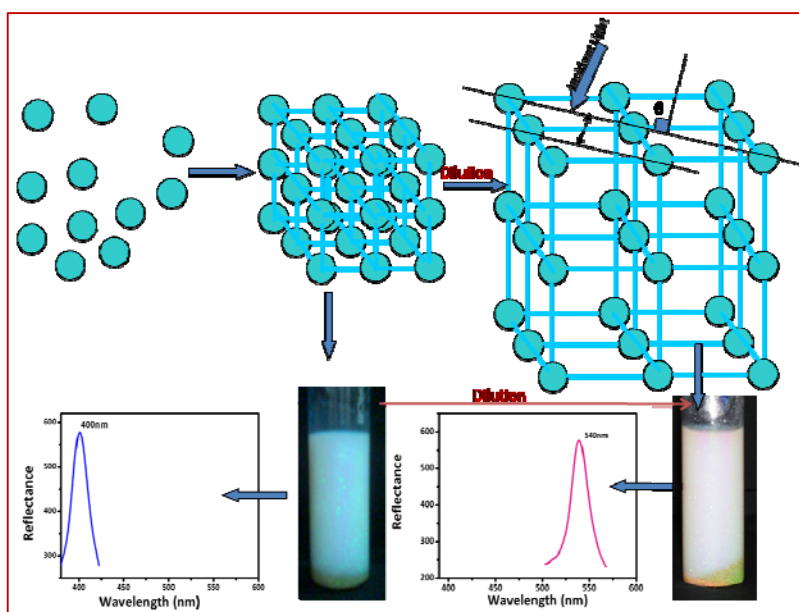


Figure 1.12. Self assembly of highly charged monodisperse polymer particles to form Crystalline Colloidal Array (CCA).The picture is drawn by utilizing the information available in the numerous literature.

1.9.2. Principle of PCCA sensing

CCA ordering in PCCA depends upon the surrounding hydrogel material. The hydrogel volume phase transitions caused by certain stimuli can be studied by measuring the diffraction changes of CCA ordering. Ligands, enzymes or recognition

molecules upon the interaction with analyte ion or molecule triggers the hydrogel volume phase transition^{53-55, 84-86, 91}. For example consider a situation where initial solution does not have any ions and the hydrogel contains unbound COO^- groups. But ions slowly come into the solution after the hydrogel bound molecule catalyzes or reacts with the analyte. Due to the ionic strength gradient inside and outside the hydrogel osmotic pressure develops inside the gel leads to Donnan membrane potential. To decrease the Donnan membrane potential, gel shrinks and, the order of the CCA spacing decreases. Due to the decrease in lattice spacing (d), wavelength blue shifts. Diffraction blue shift ($\Delta\lambda$) is proportional to the analyte concentration^{54, 55, 86}. Figure 1.13 is an illustration of this phenomenon.

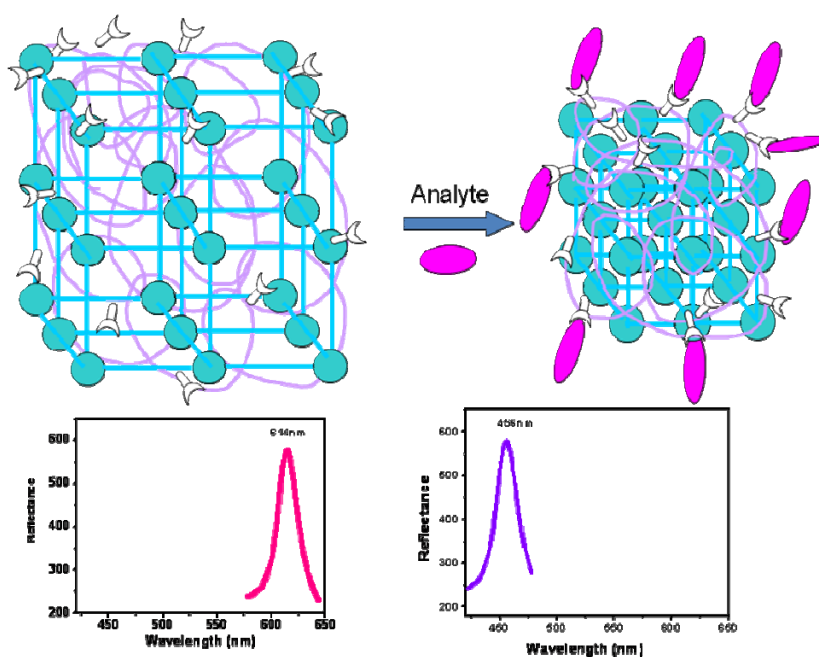


Figure 1. 13. A pictorial representation PCCA that function through changes in ΔG_{ion} .

Consider another example of PCCA sensor where the cation-sensitive PCCA coupled with 4-acryloylaminobenzo-18-crown-6 (AAB18C6) crown ether is neutral in

the absence of complexing cations and swell or shrink in response to electrolytes. But when the crown ether forms complexes with cations, they behave as ionized side chains. Now the formerly neutral gel is activated to be a polyelectrolyte gel. Because of this hydrogel expands, primarily due to an osmotic pressure that result from the mobile counterions, electrolytes, and fixed charges on the hydrogel. Also the repulsion between the crown ether-cation complexes will trigger the gel to swell, as well as due to an increased solubility of the crown ether-cation side groups compared to the neutral, uncomplexed side groups (ΔF_{mix} would increase)⁸⁴. Initial PCCA diffraction was measured and diffraction changes due to gel expansion were measured. Due to the alteration of inter planar distance (d) caused by expansion ($d \text{ in } n\lambda = 2d \sin\theta$) the ordering of CCA changes and λ changes. Diffraction wavelength ($\Delta\lambda$) changes are a magnitude of cation concentration in the medium.

1.9.3. PCCA Sensing Materials

1.9.3.1. Metal ion sensing PCCA smart sensors

4-acryloylaminobenzo-18-crown-6 (AAB18C6) crown ether coupled PCCA functions as cationic sensor and also a quantitative determination tool for metal ions Pb^{2+} , Ba^{2+} , Na^+ , K^+ and Li^+ ^{55,84}. But the crown ether coupled PCCA sensor is more specific to Pb^{2+} and detects in the range of 0.1 μM to 20mM (~ 20 ppb-4000 ppm)⁸⁴. PCCA bound to 8-hydroxyquinoline serves as efficient sensing tool for cations⁹² Cu^{2+} , Co^{2+} , Ni^{2+} , and Zn^{2+} . At low Cu^{2+} concentration, 8-hydroxyquinoline immobilized PCCA forms a bisliganded $[\text{Cu}(\text{8-hydroxyquinolate})_2]$ complex with Cu^{2+} . Due to the newly formed additional crosslinks the magnitude of ΔG_{elas} decreases^{82,83,92}, in response hydrogel contracts, which leads to decrease in CCA lattice parameter (d). Because of all these factors PCCA diffraction blue shifts in proportion to Cu^{2+} concentration. However with increasing Cu^{2+} concentration after a certain limit old bisliganded complex breaks and new monoliganded $\text{Cu}(\text{8-hydroxyquinolate})$ complex forms (Figure 1.14). After the breakage of newly formed crosslinks in the hydrogel free energy of elasticity ΔG_{Elas}

increases^{82, 83}. Because of the increase in free energy of elasticity gel expands in volume as a result PCCA diffraction starts red shifting. Other metal ions show relatively the same behavior as Cu^{2+} ⁹².

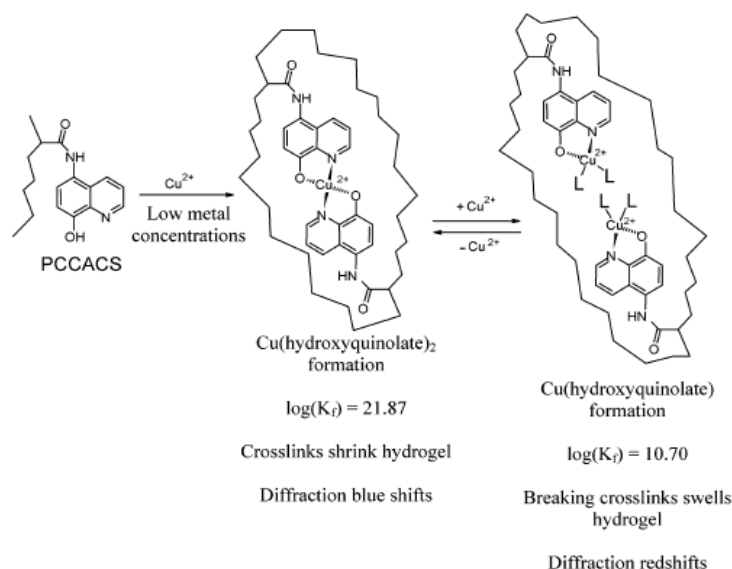


Figure 1.14. Proposed mechanism for the functioning of 8-Hydroxyquinoline PCCA sensor for Cu^{2+} (adapted from reference 92).

1.9.3.2. Carbohydrate sensors

Asher et al. developed variety of PCCA sensing materials for glucose⁹³ in high ionic strength medium⁸⁶, low ionic strength medium⁹⁴, fast responsive glucose sensor⁹⁵ and tear fluids non- invasive glucose⁹⁶. Biotinylated PCCA coupled with avidinated glucose oxidase performs glucose sensing by the enzymatic oxidization of glucose. After the oxidation process reduced glucose oxidase enzyme will be oxidized by atmospheric oxygen to its stable non ionic form. So there exists a competition between glucose oxidase oxidation of glucose and the glucose oxidase self oxidation. At low oxygen levels, the self oxidation of Glucose oxidase is suppressed. When an oxidation of a reduced enzyme is absent then at sub nano glucose concentration PCCA expands due to increased osmotic pressure resulting from donnan membrane potential which in

turn is caused by ionized glucose oxidase or mobile counterions⁹³. High ionic strength glucose sensors boronic acid is coupled to PCCA interacts with glucose. Two boronate molecules forms a complex with glucose resulting in crosslinking and due to the increase in G_{elas} gel shrinks^{82, 83, 86} (See also in section 1.8.1 and Figure 1.10). Diffraction red shifts are proportional to glucose concentration⁸⁶.

1.9.3.3. Enzymatic PCCA Sensors

Creatinine is an important molecule in the diagnosis of muscle mass and renal function. Creatinine in bodily fluids such as serum or plasma should be around 35-140 μM in healthy adults. But the creatinine level will be as high as 1mM in patients with renal dysfunction⁹⁷. Creatinine deminase enzyme coupled PCCA serves as a quantitative sensing tool to selectively determine creatinine levels in human serum. The method is accurate and fast than the available diagnosis processes. Creatinine deminase and nitrophenol coupled PCCA, when treated with creatinine solution yields OH^- as a product due to the enzymatic hydrolysis of creatinine by creatinine deminase coupled with PCCA⁹⁷. Due to the steady increase in pH as a result of OH^- production from enzymatic reaction nitrophenol molecules titrates and deprotonates. The gel swells in response to increased solubility of phenolate ions (ΔG_{mix} increases). Due this CCA lattice spacing changes which results in red shift and wavelength red shift is proportional to creatinine concentration⁹⁷. PCCA sensor coupled with an enzyme acetylcholinesterase (AChE) is a sensor for organophosphate compound parathion a nerve agent which are irreversible inhibitors for central nervous systems. It functions by the binding of AChE enzyme with the toxic parathion irreversibly which produces phosphoryl species and due to donnan potential PCCA red shifts as a function of organophosphate compound⁹⁸. PCCA coupled to organophosphorus hydrolase (OPH) functions as a sensor for methyl paraxon another nerve agent⁹⁹. It operates by PCCA blue shift due to the shrinking of a gel caused by the decreased solubility of hydrogel due to the protonation of m-aminophenolate ion coupled to hydrogel as secondary sensing element. P-Nitrophenolate, dimethyl phosphate and 2 H^+ are the byproducts from enzyme OPH catalyzed hydrolysis of paraxon at basic pH. Secondary sensing

element m- aminophenolate deprotonates due to the decrease in pH⁹⁹. Cholesterol oxidase (ChOxH) coupled PCCA oxidizes analyte cholesterol to 4-cholesten-3- one and H₂O₂. During the enzymatic oxidation a flavin in cholesterol oxidase is reduced which acts as anion immobilized to hydrogel and due to donnan potential increase PCCA red in proportion to cholesterol¹⁰⁰. Urease coupled PCCA for urea which blue shifts because of the gel contraction due to the osmotic pressure decrease inside the gel by the increased ionic strength in the bath solution. Ionic strength of outer bath increases due to the products ammonia and bicarbonate from bound urease catalyzed hydrolysis of urea at basic pH. Diffraction blue shifts are proportional to urea concentration¹⁰¹.

1.9.3.4. PCCA Sensing in Medical Diagnosis

Myocardial ischemia is an severe heart disease where the patient's heart gets reduced blood supply due to the sudden attack¹⁰². Chest pain is a common symptom of the *ischemic attack*. But among the patients complaining chest pain only 10-15% have the real problem. After the attack of *myocardial ischemia* affinity of metal ions such as Co²⁺, Ni²⁺ to bodily plasma or serum decreases which results in concentration hike of uncomplexed metal ions in serum. Also after *myocardial ischemia* increased nickel concentration close to 20 nmL⁻¹ has been found out¹⁰². By measuring the Ni²⁺ concentration in the serum employing 8- Hydroxyquinoline coupled PCCA the chest pain can be differentiated from *myocardial ischemia* on the basis of Ni²⁺ concentration¹⁰². The functioning of the PCCA is similar to the Cu²⁺ PCCA sensor⁹². Ammonia sensor¹⁰³ based on 3-aminophenol and Bertholet reaction¹⁰³ coupled PCCA was developed to sense ammonia. At first ammonia reacts with sodium hypochlorate and produce chloramines which crosslinks two 3-aminophenol to form indophenol blue¹⁰³. Due to the additional crosslinks PCCA material blue shifts linearly with ammonia concentration¹⁰².

1.10. Enzymatic Reaction

Enzymes exhibit specificity which means they catalyze only specific reaction. Specificity of enzymes is classified in to three types. One absolute specificity in which

an enzyme is specific to only one substrate. Urease exclusively catalyzes the hydrolysis of urea. The second kind of specificity is *group specificity*, where the enzyme catalyzes any of a group of reactions. Protease catalyzes the hydrolysis of different kinds of proteins, but will never catalyze the hydrolysis of fats or carbohydrates. *Stereochemical specificity* is the third kind of specificity, in which an enzyme will catalyze the reaction of one optical isomer but not its enantiomorph. Protease catalyzes the hydrolysis of polypeptides made of L-amino acids, but not the polypeptides made of D-amino acids. Hence enzymes exhibit impressive levels of stereospecificity, regioselectivity and chemoselectivity. The distinguishing feature of an enzyme-catalyzed reaction is that it takes place within the enzyme compartment known as active site. The molecule that is bound to the active site and acted upon by the enzyme is called the substrate. The surface of the active site is full of amino acid residues with substituent groups which catalyzes substrates chemical transformation. The active site can be compared to a socket into which the reactant molecule fits in, like a key in a lock¹⁰⁴⁻¹⁰⁷.

1.10.1. Enzyme Kinetics: Michaelis-Menten Kinetics

An enzymatic reaction is designed as two step process. The binding of substrate (S) by enzyme (E) for the formation of an enzyme-substrate (ES) complex followed by an irreversible breakdown of the enzyme-substrate complex to free enzyme and product (P). A simple enzymatic reaction scheme can be written as follows,



The familiar expression for the velocity of an enzyme catalyzed reaction is written as

$$v = \frac{v_{\max} [S]}{K_m + [S]} \quad (1.6)$$

Where $K_m = (k_{-1} + k_2) / k_1$ is called the *Michaelis–Menten constant* or the *Michaelis constant*. Equation 1.6 is known as *Michaelis-Menten equation*¹⁰²⁻¹⁰⁷. The equation establishes a statement of the quantitative relationship between the initial velocity v , the maximum velocity v_{\max} , and the initial substrate concentration $[S]$, with Michaelis constant K_m .

1.10.2. Lineweaver-Burk Plot

By taking reciprocal on each side of Michaelis-menten equation (equation. 1.6) one can write as

$$\frac{1}{v} = \frac{K_m + [S]}{v_{\max} [S]} \quad (1.7)$$

On rearrangement,

$$\frac{1}{v} = \frac{K_m}{v_{\max} [S]} + \frac{1}{v_{\max}} \quad (1.8)$$

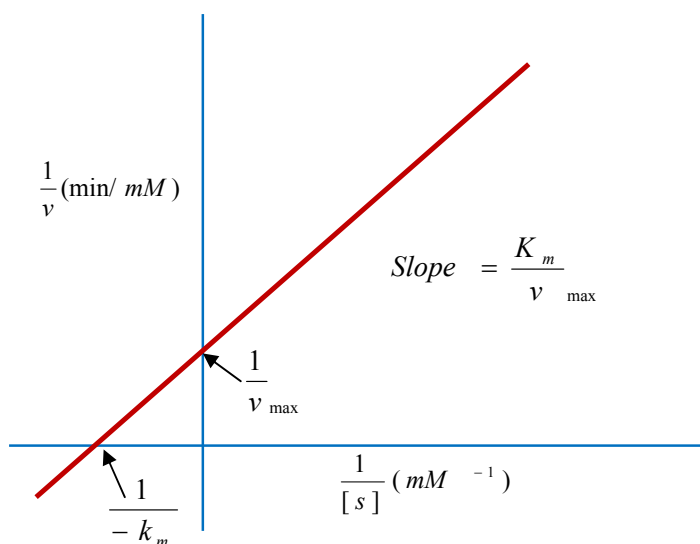
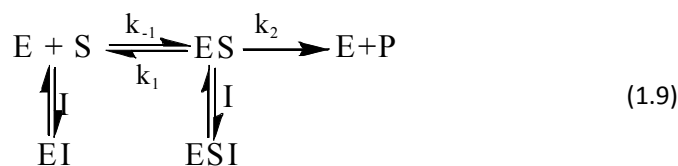


Figure 1. 15. Double reciprocal or Lineweaver-Burk (L-B) plot

The above form of the Michaelis-Menten equation is known as **Lineweaver-Burk equation**. For enzymes following the Michaelis-Menten relationship, a plot of $1/v$ versus $1/[S]$ yields a straight line (Fig. 1.15) which has a slope of K_m/v_{\max} , an intercept of $1/v_{\max}$ on the $1/v$ axis, and an intercept of $-1/K_m$ on the $1/[S]$ axis. The double-reciprocal presentation, also called a Lineweaver-Burk plot, has the great advantage of allowing a more accurate determination of v_{\max} , which can only be approximated from a simple plot of v versus $[S]$. The most important application of Lineweaver-Burk plot is to find the type of inhibition mechanism a pair of enzyme and inhibitor follows¹⁰⁴⁻¹⁰⁷.

1.10.3. Inhibition Mechanism of Enzymes

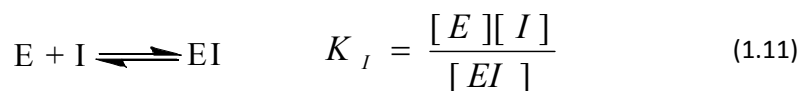
Enzyme inhibitors are molecules which interfere kinetics of the enzymatic reaction by either stopping or slowing down the rate of the reaction¹⁰⁴. In presence of inhibitor the enzyme-substrate reaction sequence presented in equation 1.5 modified as

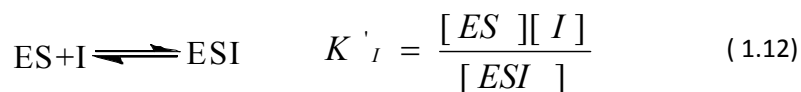


Hence inhibitor has the possibility to react either with substrate alone to produce EI or with enzyme-substrate (ES) complex to form ESI. Hence the Lineweaver-burk equation (1.8) in presence of initiator has been modified and expressed as

$$\frac{1}{v} = \frac{\alpha K_m}{v_{\max}} \frac{1}{[S]} + \frac{\alpha'}{v_{\max}} \quad (1.10)$$

Where, $\alpha = 1 + [I]/K_I$ and $\alpha' = 1 + [I]/K_I'$ in which $[I]$ is the inhibitor concentration K_I and K_I' are the stability constants for the following reaction sequences,





There are three types of inhibition mechanisms known in the literature and these are *competitive inhibition*, *uncompetitive inhibition*, *mixed or non competitive inhibition*¹⁰⁶ based on the formation of EI and ESI.

1.10.3.1. Competitive inhibition

In competitive inhibition inhibitor competes with the substrate for the active site of an enzyme¹⁰⁴⁻¹⁰⁷. While the inhibitor (I) succeeds in occupying the active site it prevents binding of the substrate molecule to the enzyme. Many competitive inhibitors are molecule that resemble the substrate and combine with the enzyme to form an EI complex, but without leading to catalysis. Since the inhibitor binds reversibly to the enzyme, the competition can be nullified simply by adding more substrate to favor the substrate. Hence in case of competitive inhibition only EI complex is formed and there is no ESI complex formation. Therefore $\alpha > 1$ and $\alpha' = 1$. So it is expected Lineweaver-Burk plot of competitive inhibition will display different slopes for inhibitive and non inhibitive processes while showing the similar intercepts. In Figure 1.15A increasing [I] results in a group of lines with a common intercept on the $1/v$ axis but with different slopes. Because the intercept on the $1/v$ axis equals $1/v_{\max}$, we can understand that the presence of a competitive inhibitor does not change V_{\max} . Also it reveals irrespective of the concentration of a competitive inhibitor, a sufficiently high substrate concentration will always displace the inhibitor from the enzyme's active site.

1.10.3.2. Uncompetitive Inhibition

In uncompetitive inhibition (Figure 1.15C) inhibitor binds at a site different from the substrate active site and, unlike a competitive inhibitor, where binding takes place only to the ES complex¹⁰⁴. In the presence of an uncompetitive inhibitor, very often binding occurs as ESI complex formation. Hence $\alpha = 1$ but $\alpha' > 1$. The intercepts and slopes of Lineweaver-Burk plots are different for inhibitive and non inhibitive processes

in uncompetitive inhibition. At high concentrations of substrate, v approaches V_{\max}/α hence an uncompetitive inhibitor decreases the measured v_{\max} . Apparent K_m also decreases, because the $[S]$ required to reach one-half v_{\max} decreases by the factor α' . In Figure 1.15C the linear fits for uncompetitive inhibition have similar slopes and different intercept values. Intercept value increases with $[I]^{104-107}$.

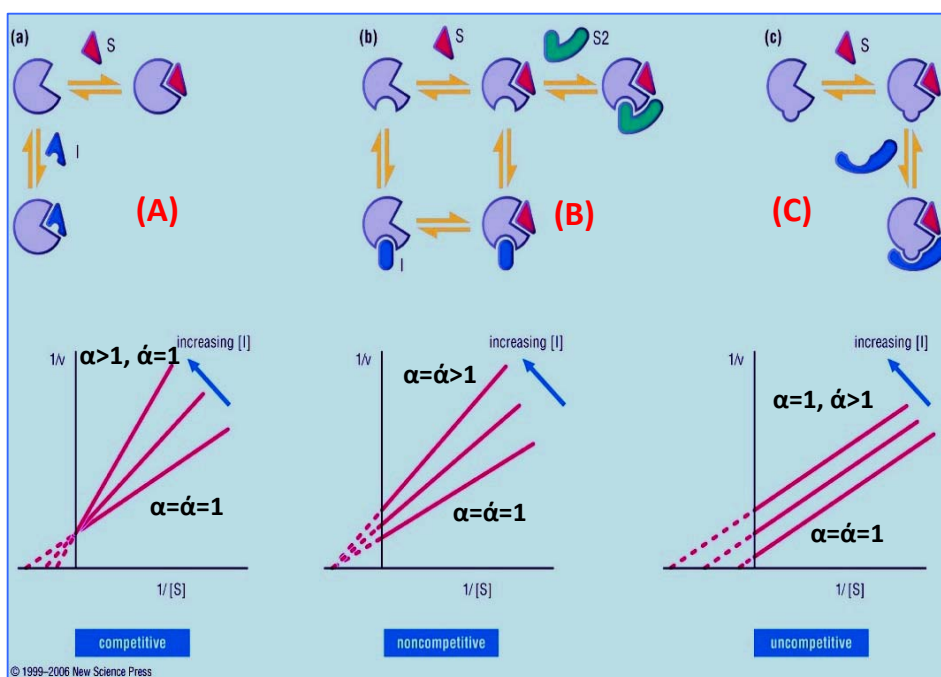


Figure 1.15. Different type of inhibition processes and respective Lineweaver-Burk plots, (A) Competitive (B) Non-competitive (C) Uncompetitive.

1.9.4.3. Noncompetitive or mixed inhibition

In mixed inhibition (Figure 1.16B) too inhibitor binds at a site distinct from the substrate active site, but it tends to bind to either E or ES. Therefore with EI and ESI formation takes place and hence α and α' are bigger than 1. Hence both slopes and intercepts of L-B plots in presence of inhibitor changes as shown in Figure 1.16B. A non competition inhibition affects V_{\max} but not K_M . For this class of inhibition intercept

at x axis ($-1/K_M$) will be same. But the slope and intercept at y axis will be different¹³⁸⁻¹⁰⁴⁻¹⁰⁷.

1.11. Scope of the Thesis

In this introduction chapter we have discussed various aspects of both metallic and polymer colloids. Synthesis of polymer colloids through different heterogeneous polymerization techniques known as dispersion, precipitation, suspension, and emulsion polymerization techniques are discussed. Among all these techniques emulsion polymerization technique proved to be the ideal to synthesize highly monodispersed polystyrene copolymer colloidal particles. Our discussion of emulsion polymerization covers some important aspects such as particle formation mechanism and different types of emulsion polymerization. Monodisperse charged polymeric colloids, especially polystyrene particles are of great interest owing to their fascinating properties particularly unusual optical property and thus these particles find innumerable applications. Despite of myriad reports on the synthesis of charged polystyrene colloids using emulsion polymerization technique there are many controversial issues concerning the dependence of particle sizes and charge densities which need to be addressed. This thesis focuses on these topics based on our recent observations cumulated from the emulsion polymerizations of styrene with variety of ionic monomers such as 2-propene sulfonic acid, sulfopropyl methacrylate, sodium styrene sulfonate, acrylic acid, hydroxyethylmethacrylate methacrylic acid etc. Chapter 2 discusses about the synthesis of highly monodispersed and charged poly(styrene-co-sodium-2-propene-1-sulphonate) copolymer particle of different sizes by varying emulsifier and initiator concentration in emulsion copolymerization. An ideal recipe to synthesize colloidal particles and CCA has been developed. Third chapter is an extension of 2nd chapter where a different comonomer (3-sulphopropylmethacrylate) is employed for the particle synthesis with almost similar results. In chapter 4 even though our initial attempts are to generate CCA from emulsion copolymerization of styrene and 4-Sodium styrene sulphonate. As time progressed our initial plan lead to different path in which we have studied the reactivity ratios of monomers in emulsion

copolymerization systems which is lacking in literature. From chapter 2, 3 and 4 we observed the trend in particle size is not similar for different structural comonomers even though the conditions are identical. The observation prompted us to study the effect of ionic comonomer structures on emulsion copolymerization of styrene and copolymer properties which is presented in chapter 5. Here also our principle aim is to identify perfect condition that yields CCA. Finally chapter 6 deals with our long standing effort in generating a *jack beans urease* coupled PCCA which senses Hg^{2+} as low as 1ppb in aqueous medium based on enzyme inhibitive sensing mechanism. Hg^{2+} sensor which can detect mercury at low ppb levels in water is completely missing in literature. Also there is a huge lack of literature for an enzyme behavior in free and bound form to substrate and inhibitor which inspired us to study the enzyme inhibition kinetics and the type of inhibition. More detailed aim of the each chapter has been discussed at the introductory part of the each individual chapter.

References

1. Everett D.H., *Basic principles of colloid science* RSC publishing Co: London, 1988.
2. Faraday, M. “*Experimental Relations of Gold (and Other Metals) to Light*”, *Philos. Trans. R. Soc. London* **1857**, 147, 145.
3. Graham, T. H. *Philos. Trans. R. Soc. London* 1861, 151, 183.
4. Norde, W. *Colloids and Interfaces in Life Sciences* Marcel Dekker, Inc: New York, 2003.
5. Shramm, L. *Emulsions, Foams and Suspensions: Fundamental and application*, WILEY-VCH Verlag GmbH & Co. KGaA, Weinheim, 2005.
6. T. Cosgrow,(Ed.,) *Colloid Science: Principles, methods and applications*, 2nd edition Wiley interscience: West Sussex, 2010.
7. Goodwin, J. W “*Colloid and interface with surfactants and polymers*” 2nd edition Wiley interscience: Sussex 2009.
8. Lyklema, H. “*Introduction colloid and interface science: Volume V. Particulate Colloids*”, Elsevier Science: Amsterdam, 2005,
9. Matijevic, E. *Acc. Chem. Res.* **1981**, 14, 22.
10. Matijevic, E. *Annu. Rev. Mater. Sci.* **1985**, 15, 483.
11. Matijevic, E. *Langmuir*, **1986**, 2, 1.
12. Matijevic, E. *Chem. Mater.* **1993**, 5, 412.
13. Matijevic, E. *Langmuir*, **1994**, 10, 1.
14. Xia Y.; Gates, B.; Yin Y.; Lu Y. *Adv. Mater.* **2000**, 12, 10
15. Pieranski, P. *Contemp. Phys.* **1983**, 24, 25.
16. Yablonovitch, E. *Phys. Rev. Lett.* **1987**, 58, 2059
17. Joannopoulos, J. D.; Villeneuve, P. R.; Fan, S. *Nature* **1997**, 386, 143.
18. Zaiser, E. M.; LaMer, V. K. *J. Colloid Interface Sci.* **1948**, 3, 571.
19. LaMer, V. K.; Dinegar, R. H. *J. Am. Chem. Soc.* **1950**, 72, 4847.
20. LaMer, V. K. *Ind. Eng. Chem.* **1952**, 44, 1270.
21. Stöber, W.; Fink, A. *J. Colloid Interface Sci.* **1968**, 26, 62.

22. Iler, R. K. “*The Chemistry of Silica*”, Wiley Interscience: New York **1979**.
23. Ueda, M.; Kim, H. B.; Ichimura, K. *J. Mater. Chem.* **1994**, 4, 883.
24. Zsigmondy, R.; “*The Chemistry of Colloids (kolloid chemie)*”, Spear E. (Transl.), John Wiley & sons: New York, 1917.
25. Zsigmondy, R. In *Colloid and Ultramicroscope* Alexander (transl.) Wiley and Sons: New York, 1909.
26. Zsigmondy, R. *Z. Phys. Chem.* **1906**, 56, 65, 77.
27. Zsigmondy, R. *Z. Anorg. Allgem. Chem.* **1917**, 99, 105.
28. Takiyama, K. *Bull. Chem. Soc. Jpn.* **1958**, 31, 944.
29. Turkevich, J.; Stevenson, P. C.; Hillier, J. *Discuss. Faraday Soc.* **1951**, 11, 55.
30. (a) Turkevich, J. *Gold. Bull.* **1985**, 18, 86. (b) Turkevich, J. *Gold. Bull.* **1985**, 18, 125.
31. Goia, D. V.; Matijevic E. *Colloids and Surfaces A: Physicochem. Eng. Aspects* **1999**, 146, 139.
32. Wilcoxon, J. P.; Martino, A.; Baughmann, R.L.; Klavetter, E.; Sylwester, A. *Mater. Res. Soc. Symp. Proc.* **1993**, 286, 131.
33. Goodman, S.L. *SEM*, **1980**, 11, 133.
34. Olsen, A.; Kafafi, Z.H. *J. Am. Chem. Soc.* **1991**, 113, 7758.
35. Sugimoto, T.; Khan, M. M. Muramatsu, A. *Colloids Surfaces A: Physicochem. Eng. Aspects* **1993**, 70, 167.
36. Ishikawa T.; Matijevic, E. *Langmuir*, **1988**, 4, 26.
37. Matijevic, E.; E.; Scheiner. P. J. *Colloid Interface Sci.* **1978**, 63, 509.
38. Hamada, S.; Matijevic. J. *Colloid Interface Sci.* **1981**, 84, 4.
39. Goia, D. V.; Matijevic, E. *New J. Chem.* **1998**, 22, 1203.
40. (a) Chang, S. Y.; Liu, L.; Asher, S. A. *J. Am. Chem. Soc.* **1994**, 116, 6739. (b) Philipse, A. P.; Van Bruggen, M. P. B.; Pathmamanoharan, C. *Langmuir* **1994**, 10, 92. (c) Walsh, D.; Mann, S. *Nature* **1995**, 377, 320. (d) Averitt, R. D.; Sarkar, D.; Halas, N. J. *Phys. Rev. Lett.* **1997**, 78, 4217. (e) Giersig, M.; Liz-Marzan, L. M.; Ung, T.; Su, D.; Mulvaney, P. *Bunsenges. Phys. Chem.* **1997**, 101, 1617. (f) Bamnolker, H.; Nitzan, B.; Gura, S.; Margelo, S. *J. Mater. Sci.*

- Lett.* **1997**, *16*, 1412. (g) Oldenburg, S. J.; Averitt, R. D.; Westcott, S. L.; Halas, N. J. *Chem. Phys. Lett.* **1998**, *288*, 243. (g). Velikov, K. P.; Blaaderen, A.V.; *Langmuir* **2001**, *17*, 4779..(h). Lu, Y.; Yin, Y.; Li, Z.Y.; Xia, Y. *Nano Lett.*, **2002**, *2*, 7.
41. Caruso, F.; Caruso, R.A.; Möhwald, H. *Chem. Mater.* **1999**, *11*, 3309.
42. *Hollow and Solid Spheres and Microspheres: Science and Technology Associated With Their Fabrication and Application*; Wilcox, D. L., Sr., Berg, M., Bernat, T., Kellerman, D., Cochran, J. K., Jr., Eds.; Materials Research Society Proceedings: Pittsburgh, 1995; Vol. 372.
43. Goia, C.; Matijevic, E. *J. Colloid Interface Sci.* **1998**, *206*, 583.
44. Cheng, X.; Chen, M.; Wu, L.; Gu, G. *Langmuir* **2006**, *22*, 3858.
45. SonDI, I.; Shi, S.; Matijevic, E. *Colloid Polym. Sci.* **2001**, *279*, 161.
46. Hsu, W.P.; Zhong, Q.; Matijevic E. *J. Colloid Interface Sci.* **1996**, *181*, 142.
47. Urban, D.; Takamura, K. *Polymer Dispersions and Their Industrial Applications*, Wiley-VCH Verlag GmbH: Weinheim, 2002.
48. Tauer, K. *Latex particles in Colloid and Colloid Assemblies*, Caruso, F.; Ed., Wiley-VCH Verlag GmbH: Weinheim, 2004.
49. (a) German Patent *DRP 558 890* (patented from January 9, **1927** on) to I.G. FarbenindustrieAkt-Ges in Frankfurt A.M. (b) US Patent 1 732 795 (patented October 22, **1929**; application filed September 13, 1927, R. P. Dinsmore. (c) H. Fikentscher, H. Gerrens, Schuller, *Angew. Chem.* **1960**, *72*, 856.
50. (a). Förster, S.; Antonietti, M. *Adv. Mater.* **1998**, *10*, 195. (b) Mortensen, K. *Polym. Adv. Technol.* **2001**, *12*, 2. (c) Milchev, A.; Bhattacharya, A.; Binder, K. *Macromolecules* **2001**, *34*, 1881.
51. (a). Caruso, F.; Caruso, R. A.; Möhwald, H. *Science* **1998**, *282*, 1111. (b). Donath, E.; Sukhorukov, G.B.; Caruso, F.; Davis, S. A.; Möhwald, H. *Angew.Chem. Int. Ed.* **1998**, *37*, 2201.
52. Fitch, R. M., *Polymer Colloids*, Academic Press: San Diego, 1997.
53. (a) Alfrey, Jr.; T., Bradford, E. B.; Vanderhoff, J. W. *J. Opt. Soc. Am.* **1954**, *44*, 603. (b) Krieger, I. M.; O'Neill, F. M. *J. Am. Chem. Soc.* **1968**, *90*, 3114. (c)

- Hiltner, P. A.; Krieger, I. M.; *J. Phys. Chem.* **1969**, 73, 2386 (d) Hiltner, P. A.; Papir, Y. S.; and Krieger, I. M.; *J. Phys. Chem.* **1971**, 75, 1881.
54. (a) Carlson, R. J.; Asher, S. A. *Appl. Spec.* **1984**, 38, 297; (b) Okubo, T., *Acc. Chem. Res.* **1988**, 21, 281. (c) Runquist, P. A.; Photinos, P.; Jagannathan, S.; Asher, S. A. *J. Chem. Phys.* **1989**, 91, 4932. (d) Asher, S. A.; Holtz, J. H.; Liu, L.; Wu, Z.; *J. Am. Chem. Soc.* **1994**, 116, 4997. (e) Weissman, J. M.; Sunkara, H. B.; Tse, A. S.; Asher, S. A., *Science* **1996**, 274, 959. (f) Pan, G.; Sood, A. K.; Asher, S. A. *J. Appl. Phys.* **1998**, 84, 83. (g) Pan, G.; Tse, A. S.; Kesavamoorthy, R.; Asher, S. A. *J. Am. Chem. Soc.* **1998**, 120, 6518.
55. Holtz J. H.; Asher, S. A. *Nature* **1997**, 389, 829.
56. Kawaguchi, H. *Prog. Polym. Sci.* **2000**, 25, 1171.
57. Pichot, C. *Current Opinion in Colloid & Interface Science* **2004**, 9, 213.
58. Elaïssari, A. (Editor), *Colloidal polymers, synthesis and characterization, Surfactant Series vol. 115*, Marcel Dekker; New York, 2003.
59. Billmeyer, F.W. *Textbook of Polymer Science, 3rd Edn.* John Wiley & sons: New York, 1984.
60. <http://en.wikipedia.org/wiki/Polystyrene>
61. Tuncel, A.; Tuncel, M. Ergun, B.; Alagoz, C.; Bahar, T. *Colloids and Surfaces A: Physicochemical and Engineering Aspects* **2002**, 197, 79.
62. Brijmohan, S. B.; Swier, S.; Weiss, R.A.; Shaw, M.T. *Ind. Eng. Chem. Res.* **2005**, 44, 8039.
63. Kawaguchi, H. *Polymer latices*, in *Fine particles: synthesis, Characterization, and Mechanism of Growth* T. Sugimoto, (Ed.), Surfactant Science Series Vol. 92, Marcel Dekker Inc: New York, 2000.
64. Barandiaran, M. J.; De la cal, J. C.; Ashua, J. M. *Emulsion polymerization*, in Ashua, J.M. (Ed.) *Polymer reaction engineering*, Blackwell Publishing Ltd: Malaysia, 2006.
65. Odian, G., *Principles of polymerization, Chapter 4: Emulsion polymerization*, John Wiley & sons: New York, 2004.

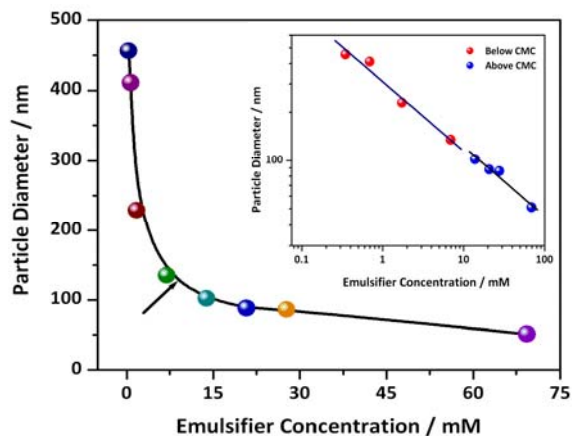
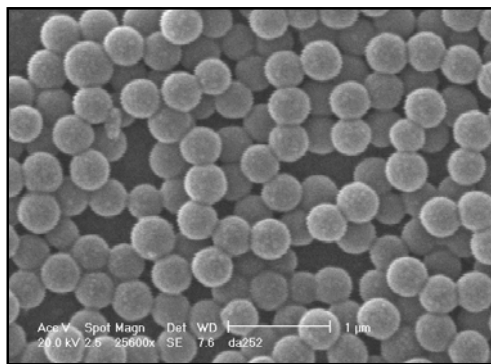
66. Lovell, P.A.; El-Aasser, M.S.; *Emulsion Polymers and emulsion Polymerization.*; Wiley: London, 1997.
67. Harkins, W.D. *J. Am. Chem. Soc.* **1947**, *69*, 1428.
68. Smith, W.V.; Ewart, R. H. *J. Chem. Phys.* **1948**, *16*, 592.
69. Hansen, F.K.; Ugelstad in *Emulsion polymerization.*; Pirma, I. (ed.,) Academic press: New York, 1982.
70. Turner, R. S, Weiss, R. A.; Robert, D. L. *J. Polym. Sci. Chem. Ed.* **1985**, *23*, 535
71. Antonietti, M.; Landfester, K. *Prog. Polym. Sci.*, **2002**, *27*, 689.
72. Candau, F. (1997) In J.M. Asua (ed.), *Polymeric Dispersions: Principles and Applications*. Kluwer Academic Publishers, Dordrecht, pp. 127–140.
73. (a) Ford, W. T.; Yu, H.; Lee, J. J.; El-Hamshary, H. *Langmuir*, **1993**, *9*, 1698. (b) Margaret, B.; Ford, W.T. *J. Org. Chem.* **1983**, *48*, 326.
74. Bolivar, J. A. M.; Gonzalez. F. G.; *J. Macromol. Sci. Part C:Polym. Rev.* **2005**, *45*, 59.
75. (a).Tamilvanan, S.; Sa, B. *J. Microencapsul.* **1999**, *16*, 411. (b). Tamilvanan, S.; Sa, B. *Int. J. Pharm.* **2000**, *201*, 187.
76. www.bangslabs.com, www.dukesci.com www.idclatex.com www.snowtex.com
www.polysciences.com, www.seradyn.com
77. (a). <http://www.bangslabs.com/files/bangs/docs/pdf/102.pdf>
(b). <http://www.bangslabs.com/files/bangs/docs/pdf/100.pdf>
78. Peppas, N.A.; Huang, Y.; Torres-lugo, M.; Ward, J.H.; Zhang, J. *Annu. Rev. Biomed. Eng.* **2000**, *2*, 9.
79. Kuru, E. A.; Orakdogan, N.; Okay O. *European Polymer Journal* **2007**, *43*, 2913.
80. Pitt, C. G.; Gu, Z.W.; Hendren, R.W.; Thompson, J.; Wani M.C. *Journal of Controlled Release*, **1985**, *2*, 363.
81. Lee K. Y.; Mooney D. J. *Chem. Rev.* **2001**, *101*, 1969.
82. Flory, P. J. *Principles of Polymer Chemistry*; Cornell University Press: New York, 1953

83. (a). Tanaka, T.; Fillmore, D.; Sun, S. T.; Nishio, I.; Swislow, G.; Shah, A. *Phys. Rev. Lett.* **1980**, *45*, 1636. (b). Annaka, M.; Tanaka, T. *Nature* **1992**, *355*, 430, (c). Li, Y.; Tanaka, T. *Annu. Rev. Mater. Sci.* **1992**, *22*, 243, (d). Mafe, S.; Manzanares, J. A.; English, A. E.; Tanaka, T. *Phys. Rev. Lett.* **1997**, *79*, 3086.
84. Holtz, J. H.; Holtz, J. S. W.; Munro, C.H.; Asher, S. A. *Anal. Chem.* **1998**, *70*, 780.
85. K. Lee and S. A. Asher, *J. Am. Chem. Soc.*, **2000**, *122*, 9534.
86. V.L. Alexeev, A.C. Sharma, A.V. Goponenko, S. Das, I.K. Lednev, C.S. Wilcox, D.N. Finegold and S.A. Asher, *Anal. Chem.*, **2003**, *75*, 2316.
87. Qiu, Y.; Park, K. *Adv. Drug Delivery Rev.* *53* (2001) 321.
88. Ghandehari, H.; Kopeckova, P.; Kopecek, J. *Biomaterials* **1997**, *18*, 861.
89. Mayes, A. G.; Blyth, J.; Millington, R. B.; Lowe, C. R. *Anal. Chem.* **2002**, *74*, 3649.
90. Marshall, A. J.; Young, D. S.; Blyth, J.; Kabilan, S.; Lowe, C. R. *Anal. Chem.* **2004**, *76*, 1518.
91. (a).Guerrero, R. C.; Weissman, J.; Lee K.; Asher, S. A. *J. Colloid and Interface Science*, **2000**, *232*, 76. (b). Reese C.; Asher, S. A.; *J. Colloid Interface Science*, **2002**, *248*, 41. (c). Pan, G.; Tse, A. S.; Kesavamoorthy, R.; S. A. Asher, *J. Am. Chem. Soc.* **1998**, *120*, 6518.
92. Asher, S.A.; Sharma, A.C.; Goponenko A.V.; Ward, M.M. *Anal. Chem.*, **2003**, *75*, 1676
93. Asher, S. A.; Holtz, J. *LEOS Newsletter* **1998**, *12*, 32-34.
94. I.K. Lednev, C. Wilcox, D. Finegold and S.A. Asher, *J. Am Chem. Soc.*, **2003**, *125*, 3322.
95. Ben-Moshe, M.; Alexeev, V.; Asher, S. *Anal. Chem.*, **2006**, *78*, 5149.
96. Baca, J. T.; Finegold, D. N.; Asher, S. A. *The Ocular Surface*, **2007**, *5*, 280.
97. Sharma, A.; Jana, T.; Kesavamoorthy, R.; Shi, L.; Virji, M.; Finegold D.; Asher, S. A. *J. Am. Chem. Soc.* **2004**, *126*, 2971.

98. Walker, J. P.; Asher, S. A. *Anal. Chem.* **2005**, 77, 1596.
99. Walker, J. P.; Kimble, K. W.; Asher, S. A. *Analytical and Bioanalytical Chemistry*, **2007**, 389, 2115.
100. Maurer, M. K.; Gould, S. E.; Scott, P. J. *Sensors and Actuators B* **2008**, 134, 736.
101. Zeng, F.; Wu, S.; Sun, Z.; Xi H.; Li, R.; Hou, Z. *Sens. Actuators, B* **2003**, 81, 273.
102. Baca, J.T.; Finegold, D. N.; Asher S. A. *Analyst*, **2008**, 133, 385.
103. Kimble, K.; Walker, J.; Finegold D.; Asher, S.A. *Anal. and Bioanal. Chem.*, **2006**, 385, 678.
104. Lehninger, A. L.; Nelson, D.L.; Fox, M.C. *Lehninger, Principles of Biochemistry*, 4thEdn., W. H. Freeman & co:
105. Atkins, P.; De Paulo, J. *Physical Chemistry*, 8th edition Oxford University Press: New York, 2006.
106. Mortimer, R. G.; *Physical Chemistry*, 3rd edition, Elsevier Academic Press: Birmingham, 2008.
107. Murray, R. K.; Granner, D. K.; Mayes, P. A.; Rodwell, V.W. *Harper's Illustrated Biochemistry*, 26th edition. McGraw-Hill Inc: New York, 2003.

Chapter 2

Tuning the Particle Size and Charge Density of the Crosslinked Polystyrene Particles



Poly [styrene-(co-2-propene sulfonic acid)] particles crosslinked with divinylbenzene of various sizes from 50 nm to 400 nm are synthesized by emulsion polymerization. Effect of emulsifier and initiator concentration on the polymerization kinetics, particle size and charge density are studied.

2.1. Introduction

For several decades, emulsion polymerization has been widely used for the synthesis of polymeric particles. This polymerization technique is a unique process for the preparation of latex polymer colloids and has several distinct advantages compared to other homogeneous radical chain polymerization^{1, 2}. Apart from the physical differences, there is one significant kinetic difference between emulsion polymerization and other polymerization processes. Although the other polymerization processes show an inverse relationship between the rate of polymerization and the molecular weight, emulsion polymerization can afford increase in molecular weight without decreasing the rate of polymerization. The mechanism and the kinetics of emulsion polymerization have been reported extensively by several authors; for example, a recent review by Chern³ has summarized various issues of emulsion polymerization developed so far.

Monodisperse polymer colloidal particles have many applications in various technologies such as paints, coatings, finishes, and floor polishes etc¹⁻⁴. Among various methods⁵⁻⁹ employed for the synthesis of monodisperse spherical colloidal particles of polymers such as polystyrene, poly (methyl methacrylate) etc., emulsion polymerization technique is found to be the most reliable one. These monodisperse colloidal particles self-assemble readily at high particle concentration and produce highly ordered close packed colloidal crystals, which exhibit bright iridescence due to Bragg diffraction of light. Also, efforts have been made to prepare highly charged, monodisperse spherical polymer colloidal particles by covalently attaching ionizing groups on the polymer backbone¹⁰⁻¹⁷. These charged particles are self-assembled in solution in a non close packed three-dimensional array, commonly known as crystalline colloidal array (CCA). As atomic crystals diffract X-rays meeting the Bragg condition, colloidal crystalline array also diffract ultraviolet, visible, and near-infrared light depending on the lattice spacing¹⁰⁻¹⁷. These colloidal crystalline arrays have been immobilized into a polymer hydrogel matrix to fabricate sensor materials based on hydrogel volume phase transition^{18, 19}. In a recent report, it has been demonstrated that colloidal array can also

be used to make proton conducting membrane for polymer electrolyte membrane fuel cell²⁰.

Since the self-assembly, phase transitions, and the optical properties of these colloidal particle dispersions depend upon the size, charge, size polydispersity, and volume fraction of the particles; it is utmost necessary to control these parameters by altering the emulsion polymerization recipe during the synthesis of polymer colloids. There are several factors in the polymerization recipe, such as emulsifier concentration, initiator concentration, monomer concentration, and the reaction temperature, which can alter the particle size and charges^{3, 13, 14, 21, 22}. Among these, the concentration of the emulsifier and initiator play the major role to optimize the particle size and charges. Emulsifier forms micelles when its concentration exceeds the critical micelle concentration (CMC) and large amount of emulsifier yields large number of smaller sized micelles. During polymerization two types of particle nucleations are possible depending on the amount of emulsifier present in the polymerization mixture. When the emulsifier concentration is around the CMC or well above the CMC, the growth of the particle takes place inside the micelle, known as micellar particle nucleation or heterogeneous particle nucleation. On the other hand, if the emulsifier concentration is well below the CMC, then the particle nucleation takes place on to the emulsifier-stabilized precipitated oligomeric radicals, which is known as homogeneous particle nucleation^{1, 23–25}. Hence, these two particle nucleation processes can be classified into two regimes as regime-I (below CMC) and regime-II (above CMC). Thorough investigations of various aspects of colloidal particles synthesis by emulsion polymerization in both the regimes have been carried out both theoretically and experimentally^{23–29}. However, studies on the crosslinked charged copolymer particles are not reported extensively in the literature^{7,13–16,30–32}. The effect of the emulsifier concentration on the charged crosslinked particle sizes as well as on the particle charges in both regime I and II have not been studied systematically. This observation prompted us to carry out emulsion polymerization for the synthesis of charged crosslinked colloidal particles by varying the emulsifier concentration in both the regime I and II.

In this chapter, we are reporting the synthesis and characterization of crosslinked charged spherical polystyrene colloidal particles. We have used sodium salt of 2-propene sulfonic acid (PSA) and sodium dodecyl sulfate (SDS) as the charged monomer and an emulsifier, respectively. Both the charged monomer and emulsifier has been extensively used before and are readily available in the commercial source compared to the others reported in the literature. We have measured the particle size, particle volume fraction, surface charge density, and determined viscosity-average molecular weight of the polystyrene colloidal particles.

2.2. Experimental Section

2.2.1. Materials

Styrene (Sisco, India) monomer, divinyl benzene (DVB, Aldrich) crosslinker were purified using the method described elsewhere³⁰ to remove the inhibitor. Sodium salt of 2-propene sulfonic acid (PSA) as an ionic comonomer (Polyscience, USA), sodium dodecyl sulfate (SDS) as surfactant (Merck), sodium bicarbonate (Sisco), and ammonium per sulfate (APS, Merck) as the buffer, and an initiator, respectively, were used as received from the suppliers. Dowex mixed bed ion-exchange resin (Sigma-Aldrich) was also used as received. Triple distilled water was used for all experiments.

2.2.2. Synthesis and purification of colloidal particles

Crosslinked charged polystyrene colloidal particles were synthesized by emulsion polymerization technique in a four-neck mercury-sealed round bottom flask fitted with a reflux condenser, a teflon stirrer attached to a high-torque overhead mechanical stirrer, nitrogen, and reagent inlet. The temperature was maintained by placing the reaction vessel in a controlled temperature oil bath. The reaction vessel was charged with 75 mL of triple distilled water containing 0.1 g of sodium bicarbonate. The water solution was deoxygenated by bubbling nitrogen for 40 min. After thorough deoxygenation, the weighted amount of SDS dissolved in 10 mL of water was added, and the temperature was increased to 50°C. Freshly deoxygenated styrene (33 g, 0.32

mol) and DVB (1.65g, 0.013 mol) were injected slowly at a constant rate of 4 mL/min. The 2-PSA sodium salt (1.98 g, 0.014mol) was dissolved in 5 mL of water and injected 10 min after the addition of styrene and DVB. The temperature was increased to 70⁰C and the stirring speed was increased to 350 rpm. After equilibration for 30 min, required amount of APS dissolved in 10 mL of water was injected into the reaction mixture. The reaction was refluxed for 3–4 hours. A nitrogen blanket and the stirring rate of 350 rpm were maintained during refluxing. We have varied both the surfactant (SDS) and initiator (APS) concentration extensively in the reaction mixture and presented in Tables 2.1 and 2.2.

A milky white colloidal solution was obtained upon the completion of the reaction. It was then allowed to cool and filtered through glass wool. The filtered solution was centrifuged for 40 min at 45,000 rpm at 15⁰ C in an ultracentrifuge. The residue (solid white mass) was thoroughly dispersed in triple distilled water with the help of sonication and mixing in a vortex motor. Centrifugation and dispersion process were repeated 3–4 times to remove all the impurities from the colloidal polystyrene particles. The particles showed bright iridescence after this purification steps. The colloidal solution was taken in a storage glass bottle and mixed bed ion-exchange resin was added and placed on a vertical rotor for the thorough mixing of the particles with resin.

2.2.3. Characterization of colloidal particles

Particle sizes were measured from the dilute solution of colloids using a Zetasizer instrument (Zetasizer 3000HS, Malvern Instruments) at 25⁰C. The instrument was operating at a wavelength of 633 nm and measurements were carried out at a detection angle of 90⁰. For each sample at least three measurements were taken to check the repeatability of the results and the analysis was done using CONTIN analysis mode. Particle sizes were also verified from images observed in scanning electron microscope (SEM, Philips- XL30ESEM). Aqueous diluted colloidal juice was dropped on a cleaned

glass piece and air dried for SEM experiments. For SEM experiments samples were gold coated and then SEM images were taken.

The polymerization (% of conversion vs. time profile) was followed by removing 2 mL of reaction mixture from the reaction vessel at different time intervals. Hydroquinone (1% by weight) was used to stop the polymerization. The aliquots with 1% hydroquinone at different time intervals were dried in an oven and the percentage of conversion was measured gravimetrically. Particle volume fractions were measured gravimetrically in triplicate considering the polystyrene density as 1.05 g/cm³.³³ Particle charge densities were measured by potentiometric titration³⁴. Since the crosslinked polymer cannot be dissolved fully in any solvent, crosslinker free linear polystyrene samples were prepared separately using the similar recipe mentioned in Tables 2.1 and 2.2 for the molecular weight measurements. All these crosslinker free samples were purified in a similar way as aforementioned for crosslinked particles. The viscosity of the freeze-dried samples was measured in butan-2-one solvent using Cannon Ubbelohde dilution viscometer at 30°C. The viscosity-average molecular weight (\overline{M}_v) of the samples were determined using the Mark-Houwink relation, $\eta = k \overline{M}_v^a$; where values of K is 3.9 X 10⁻⁴ dL/g and “a” is 0.58, respectively, for polystyrene in buta-2-one at 30°C³⁵.

2.3. Results and Discussion

2.3.1. Particle size versus emulsifier concentration

Charged, crosslinked styrene–DVB–2-PSA copolymer colloidal particles with diameter 51–456 nm were synthesized by varying emulsifier concentration in both regime I (below CMC) and II (above CMC). The detailed reaction recipes, particles, and polymers characterizations are listed in Table 2.1. In all the cases monomers, crosslinker, and initiator concentrations are kept constant. Also, the reaction conditions such as temperature, stirring speed, and reflux time etc. for all the reactions are same. The only parameter that we have varied in these reactions is the emulsifier

concentration. The CMC of SDS emulsifier is 8.1 mM. This CMC value of SDS has been well established and reported in the literature by several authors. We have used the emulsifier concentration as low as 0.348 mM (sample 1) and as high as 69.35 mM (sample 8) in the polymerization. Figure 2.1 shows representative SEM micrographs of the colloidal spheres of various sizes obtained by altering the SDS concentration in the polymerization. All the particles are spherical in shape as evident from the SEM images. Particle sizes measured by the Zetasizer for all the samples are listed in Table 2.1. We have observed a very little variation (less than 10%) between particle sizes measured by Zetasizer and microscopy. Particle sizes obtained from Zetasizer are little bigger because it measures the hydrodynamic size of the particles whereas microscopic technique gives the size of dry particles¹⁴. The variation of particle diameter with increasing emulsifier concentration is plotted in Figure 2.2. The arrow in the figure indicates the CMC of the emulsifier. The diameter decreases as the surfactant concentration increases since the lower surfactant concentration produces less number of micelles resulting in bigger particles.^{1,13,21,22,36}. Figure 2.3 demonstrates that the number of particles (N_p) follows a linear relationship with the surfactant concentration which results an inverse relationship of N_p with particle diameters^{13, 21, 22, 37}.

Table 2.1. *Polymerization recipe and particle characterization by varying emulsifier concentration*

Sample	SDS (mM)	APS (mM)	Diameter ^a (nm)	PD ^b	Charge Density ($\mu\text{C}/\text{cm}^2$)	N_p (no./ml) $\times 10^{-13}$	Measured \overline{M}_v
1	0.348	17.54	456	0.32	43.62	0.0559	2.13×10^4
2	0.693	17.54	411	0.42	27.70	0.0641	1.97×10^4
3	1.734	17.54	229	0.06	14.80	1.23	36.47×10^4
4	6.935	17.54	135	0.20	8.16	4.61	25.83×10^4
5	13.870	17.54	102	0.17	6.37	9.52	33.38×10^4
6	20.806	17.54	88	0.17	4.37	18.48	38.36×10^4
7	27.741	17.54	86	0.46	4.19	19.23	42.60×10^4
8	69.353	17.54	51	0.13	2.11	43.87	55.38×10^4

a. Diameter measured by Zetasizer

b. PD is the polydispersity; obtained from Zetasizer

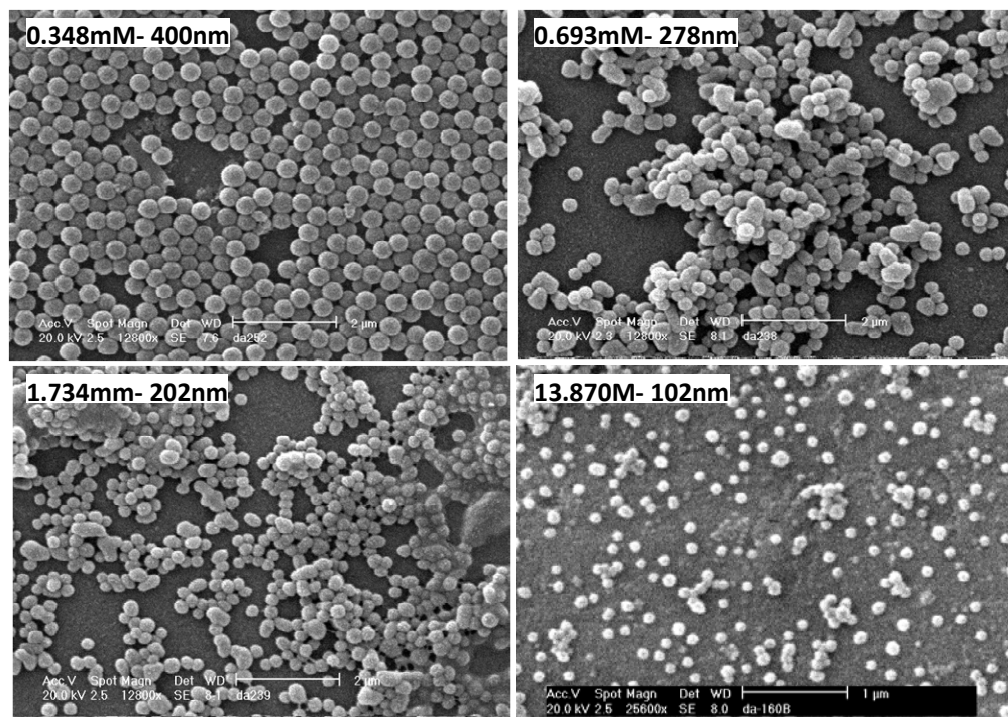


Figure 2.1. SEM images of crosslinked polystyrene colloidal spheres of various sizes. (Particle sizes were calculated from the respective SEM images)

A careful analysis of Figure 2.2 reveals that the particle size is decreasing very sharply with increasing emulsifier concentration below the CMC (regime-I) whereas the decrease in particle size is not very prominent with the change of surfactant concentration after the CMC (regime-II). Therefore, a larger tuning of particle size can be achieved within the small range of concentration in regime-I compared to regime-II, though the particle size (D) dependence on the surfactant concentration (S) in both the regime is $D \propto S^{-0.43}$, which is obtained from the slopes of the double logarithmic plot of D against S (Inset of the Figure 2.2). The dependence of the number of particles (N_p) with the surfactant concentration (S) in both the regimes is obtained from the log-log plot of N_p against S and presented in the inset of the Figure 2.3. It shows that $N_p \propto S^{1.63}$ in regime-I and $N_p \propto S^{0.89}$ in regime-II. The positive exponent of $N_p \propto S$ is in agreement

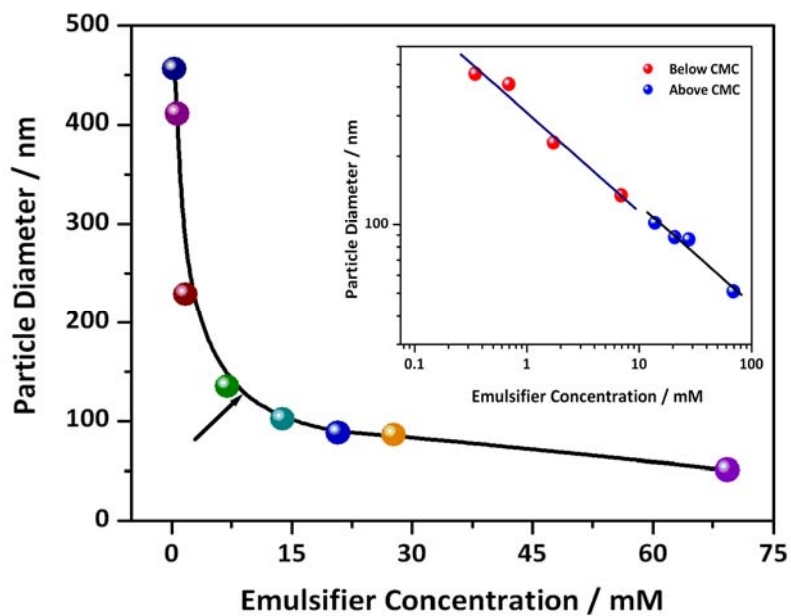


Figure 2.2. Effect of emulsifier concentration (S) on particle size (D) at a fixed initiator concentration; arrow indicates CMC of the emulsifier. Inset: A double logarithmic plot of D vs. S .

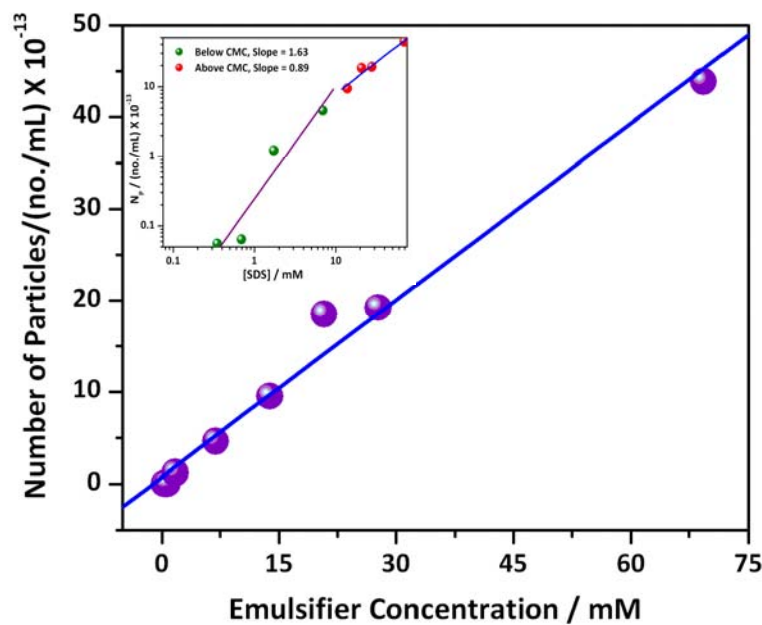


Figure 2.3. Plot of number of particles (N_p) vs. emulsifier concentration (S) at a fixed initiator concentration. Inset: A double logarithmic plot of $[SDS]$ vs. N_p .

with the basic principle of emulsion polymerization^{21, 29} and indicates that the rate of polymerization will be higher for higher surfactant concentration which is clearly visible in the conversion–time profile presented in the Figure 2.4. The exponent values of $N_p \propto S$ obtained here are similar to the reported values,^{1, 21, 29} and reveal that in the both the cases coagulative nucleation process takes place. However, different exponent values obtained from the inset of Figure 2.3 for two regimes indicate that the particle growth mechanisms in regime I and regime II are not exactly similar.

A critical analysis of the conversion–time profile (Figure 2.4) demonstrates that the polymerization rates are quite different in regime-I compared to regime II. When the emulsifier concentration is below the CMC, conversion increases slowly whereas it increases rapidly above the CMC. Also, we have observed that the yield of the polymerization is much higher in the regime II than regime I. These observations clarify that the particle growth mechanisms are different for below and above the CMC. When the emulsifier concentration is well below of its CMC as in regime I, it does not form any micelle. Therefore, polymerization starts in the aqueous medium itself and water insoluble oligomeric radicals produced are precipitating out from the aqueous medium. These oligomeric radicals become stabilized by absorbing surfactant and further particle growth proceeds on to these oligomeric radicals.³⁸ In regime II, particle nucleation occurs inside the micellar core. In case of emulsion polymerization, the rate of polymerization and molecular weight of the polymer can be increased by increasing emulsifier concentration at constant initiation rate, that is, by keeping initiator concentration unchanged. In regime I, the evolution of viscosity-average molecular weight (\bar{M}_v) with emulsifier concentration is more compared to regime II as evident from the Figure 2.5. It is clear from Figure 2.5 that the \bar{M}_v increases very sharply up to the CMC of emulsifier (as asterisk indicates in the Fig. 2.5) and then it levels up gradually. Therefore, it can be argued that molecular weight of the polymer and polymerization rate play an important role for the variation of particle diameter with emulsifier concentration in both the regimes I and II. We have cross checked the particle

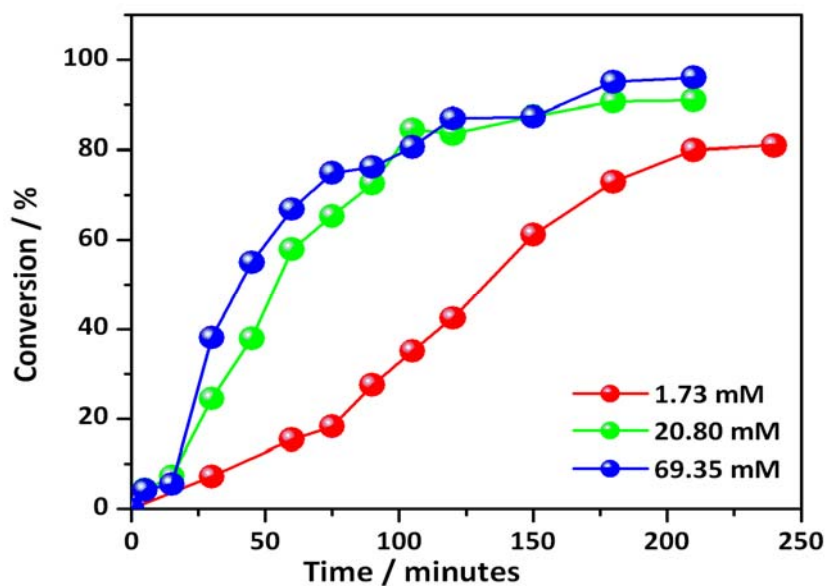


Figure 2.4. Conversion vs. time profile at the indicated emulsifier concentration

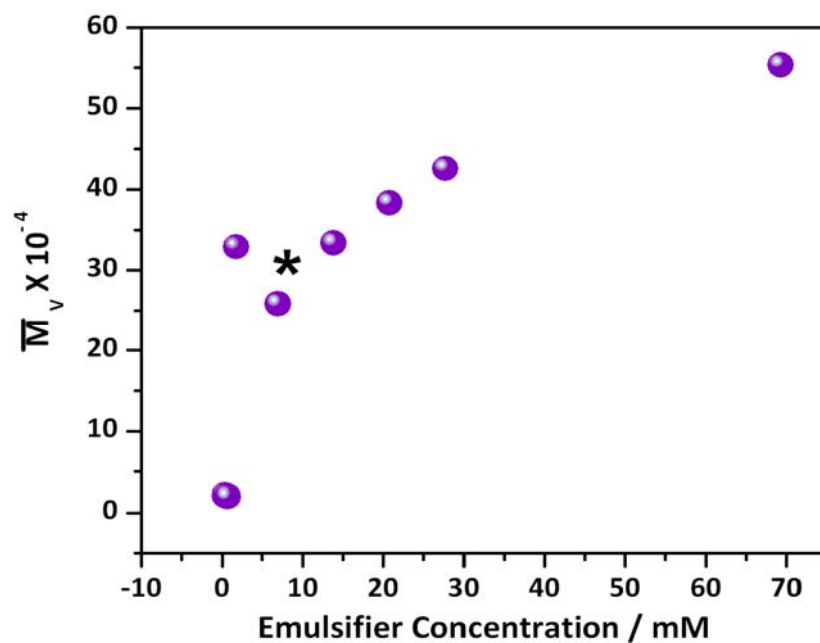


Figure 2.5. Plot of \overline{M}_v vs. emulsifier concentration at a fixed initiator concentration (Asterisk indicates CMC of SDS)

size of the crosslinker free samples with crosslinked particles. The size differences are less than 10% in most of the cases. Hence, the viscosity-average molecular weights obtained from crosslinker free samples can be utilized for crosslinked particles for comparisons.

2.3.2. Particle size versus initiator concentration

A series of charged spherical crosslinked colloidal particles of diameter varying from 99 to 108 nm have been synthesized by changing the initiator concentration in the emulsion polymerizations recipe. Figure 2.6 shows SEM micrographs of the colloidal spheres of different sizes obtained by varying the APS concentration in the polymerization. All other parameters for these reactions are kept constant. Polymerization recipe, particle, and polymer characterization are presented in Table 2.2. It is to be noted that the concentration of emulsifier used for all these polymerization is 13.87mM, which is above the CMC of the emulsifier. Therefore, all these polymerizations belong to regime II and follow the micellar particle nucleation. A log-log plot of the particle size against the initiator concentration is shown in Figure 2.7.

Table 2.2. *Polymerization recipe and particle characterization by varying initiator concentration*

Sample	SDS (mM)	APS (mM)	Diameter ^a (nm)	PD ^b	Charge Density ($\mu\text{C}/\text{cm}^2$)	N_p ((no./ml) $\times 10^{-13}$)	Measured \overline{M}_v
9	13.87	8.77	99	0.20	3.069	18.36	31.07×10^4
5	13.87	17.54	102	0.17	6.374	9.52	33.38×10^4
10	13.87	26.31	101	0.07	4.492	10.10	21.95×10^4
11	13.87	35.08	107	0.15	7.364	6.59	18.0×10^4
12	13.87	43.86	108	0.17	5.752	10.43	19.68×10^4

a. Diameter measured by Zetasizer.

b. PD is the polydispersity; obtained from Zetasizer

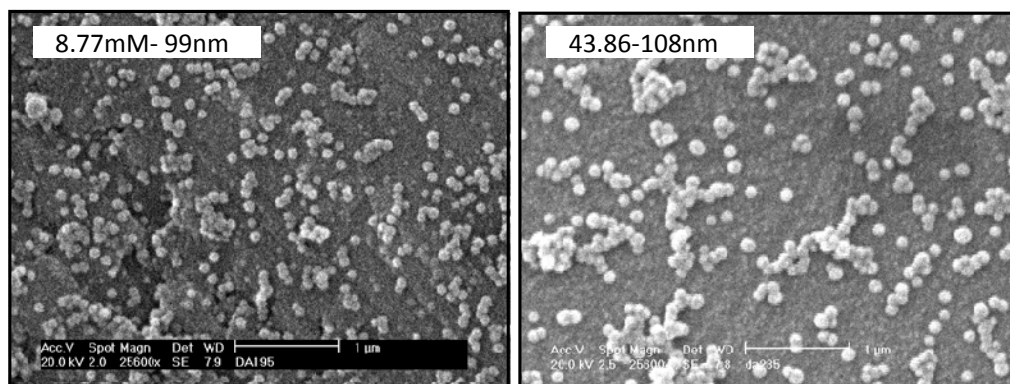


Figure 2.6. SEM images of crosslinked polystyrene colloidal spheres obtained by varying APS concentration (at fixed SDS concentration). (Particle sizes were calculated from the respective SEM images)

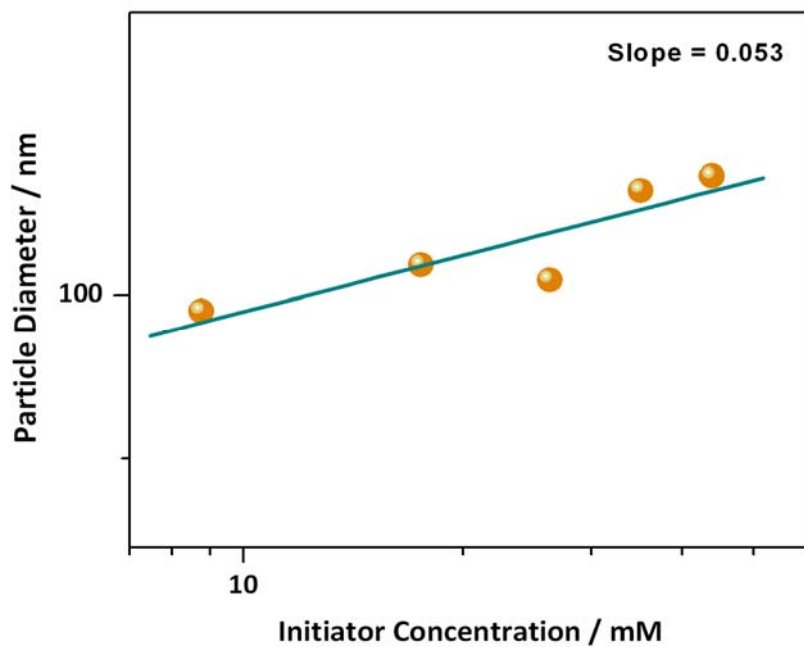


Figure 2.7. Effect of initiator concentration on particle size at a fixed emulsifier concentration.

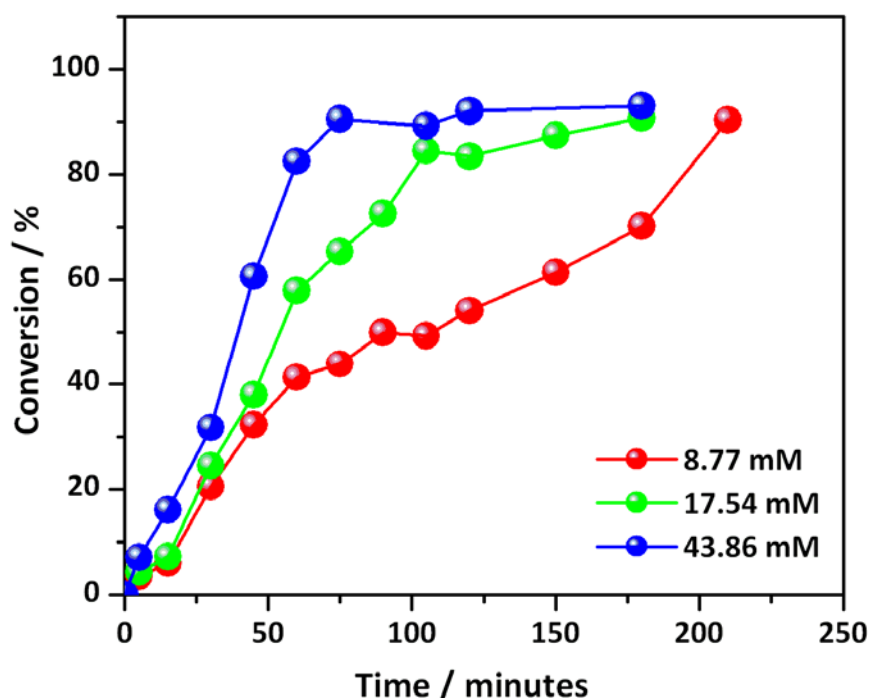


Figure 2.8. Conversion vs. time profile at the indicated initiator concentration

The particle diameter increases with increasing initiator concentration linearly; although the increase in size is very small over the initiator concentration (I) range studied here. The dependence exponent is only 0.053 i.e., $D \propto I^{0.053}$ (Figure 2.7), is very low compare to the emulsifier dependence exponent (0.43) aforementioned. A probable reason for this is that at a fixed surfactant concentration the rates of the reactions are not very much different for the different initiator concentrations in regime II. The conversion–time profile presented in Figure 2.8 clearly demonstrates that up to ~ 50% conversions, the rates are independent of initiator concentration. Therefore, from the above observations we may conclude that in the regime II, the initiator concentration does not affect the particle size and the rate significantly. This observation is not matching with the earlier observation reported in the literature for linear polystyrene. Since the particles studied here are crosslinked charged polystyrene; hence, it may not be worthy to compare this observation with the reported ones. A thorough

understanding of the crosslinker effects on the charged particles is under progress. The number of particles³⁷ as well as the molecular weights⁹ maintains an inverse relationship with the initiator concentration for a fixed surfactant concentration (above CMC) as presented in Table 2.2 and Figure 2.9, respectively. It is well known that the polymer molecular weight decreases as the initiator concentration increases. It has also to be noted that, an inverse correlation between the particle size and the molecular weight (the larger particles have the lowest molecular weight) is observed for both emulsifier and initiator concentration variation. Similar observation was noted in case of polystyrene particles prepared by the dispersion polymerization^{9, 39}.

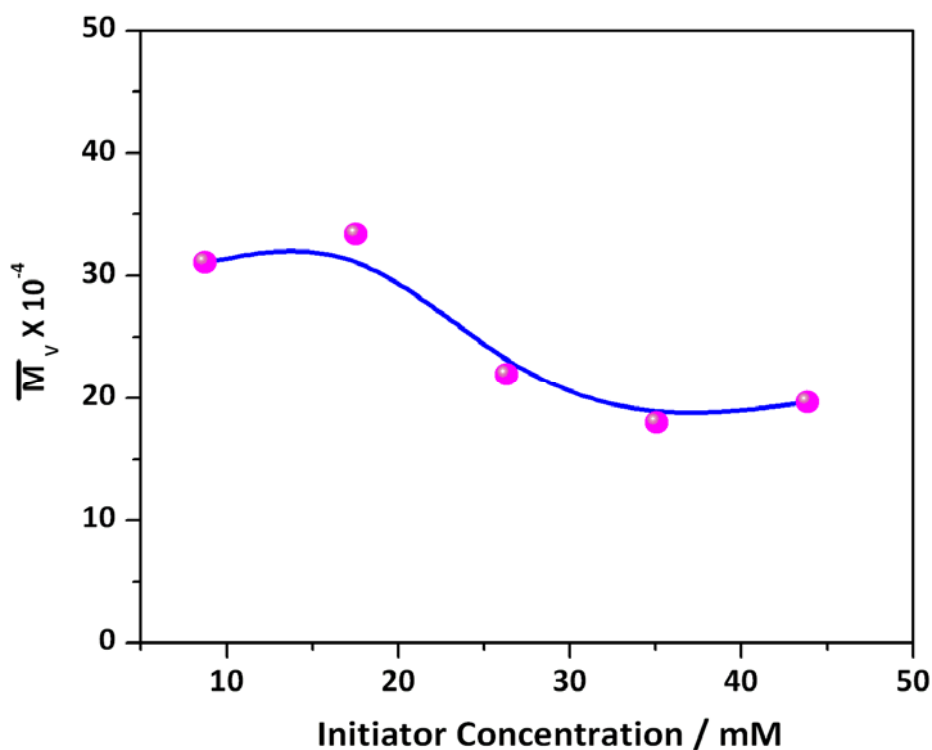


Figure 2.9. Plot of \overline{M}_v vs. initiator concentration at a fixed emulsifier concentration

2.3.3. Surface charge density of the colloidal particles

The influences of emulsifier and initiator on particle surface charge density have been studied by varying the concentration of SDS and APS, respectively, in the emulsion polymerization recipes. Figure 2.10 shows that the charge density decreases as the emulsifier concentration increases. This inverse correlation between the charge density and the emulsifier concentration is quite obvious since the charge density is directly proportional to the particle diameter⁴⁰ (Figure 2.11) and inversely proportional to the molecular weight¹⁶. Figure 2.10 shows increase of charge density as a function of particle diameter.

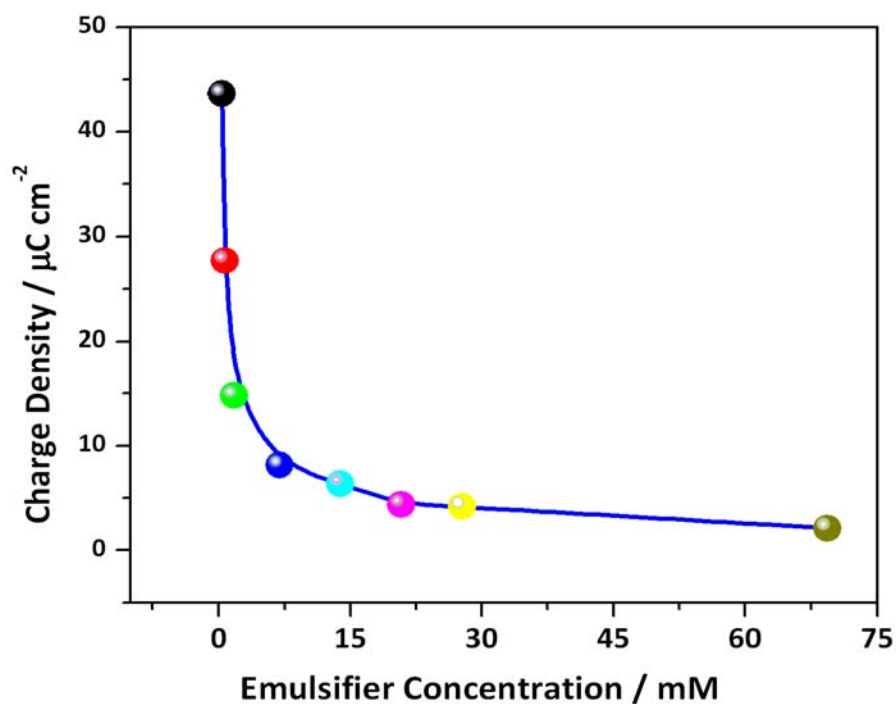


Figure 2.10. Charge density vs. SDS concentration at a fixed APS concentration

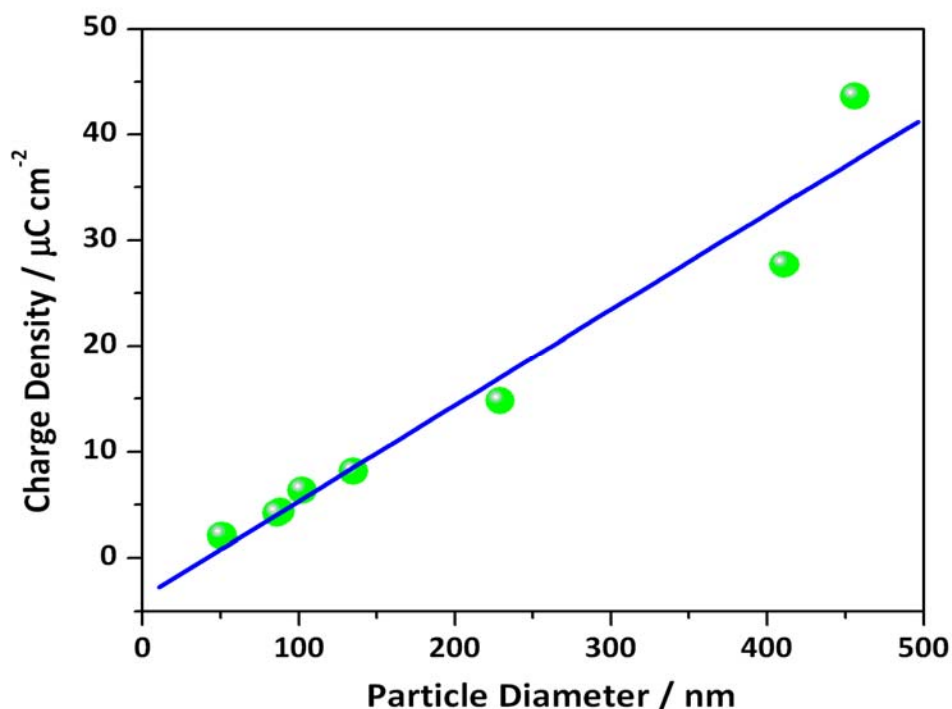


Figure 2.11. Charge density vs. particle diameter at a fixed APS concentration

A plot of charge density against the initiator concentration is presented in Figure 2.12. The line in the figure is the best fit line. Although the deviation of the data points from the best fit line is a bit higher, yet it is clear from Figure 2.12 that the surface charge density increases as the initiator concentration increases. This observation is in good agreement with the previous report in the literature¹⁶. Asher and coworkers¹⁶ showed that the charge density and molecular weight is inversely proportional. Since the molecular weight is decreasing with increasing initiator concentration (Figure 2.9 and Table 2.2), therefore, it is expected that surface charge density will increase with increasing initiator concentration. However, the charge density variation in Figure 2.12 is low compared to Figure 2.10, which indicates that the optimization of particle surface

charge can be achieved more reliably by varying emulsifier concentration than the initiator concentration.

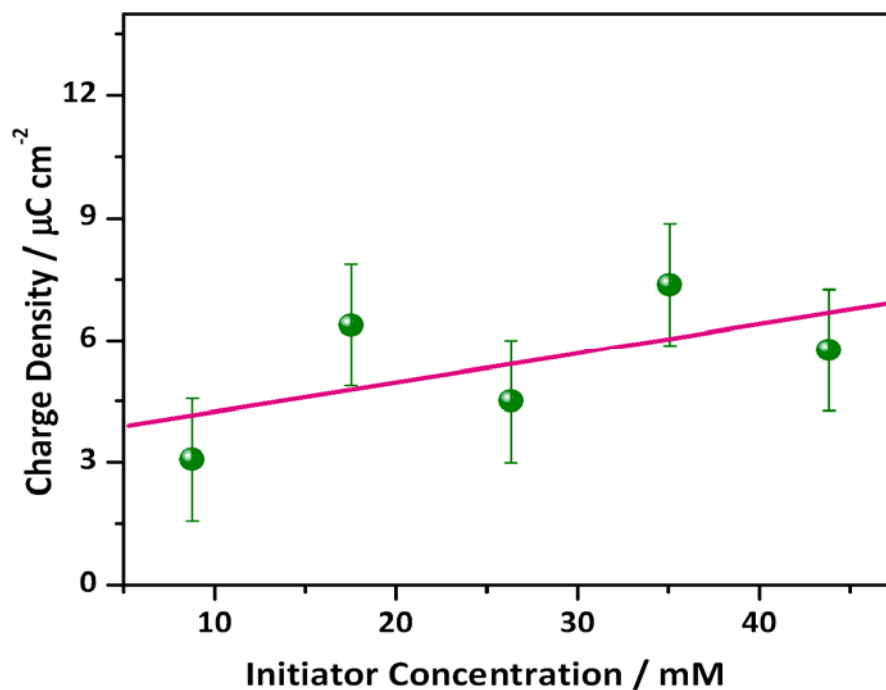


Figure 2.12. Charge density vs. APS concentration at a fixed SDS concentration

2.4. Conclusions

A series of charged crosslinked spherical polystyrene particles of different sizes have been synthesized by emulsion polymerization and characterized. The amount of emulsifier in the polymerization recipe was varied both in below the CMC region (regime-I) and above the CMC region (regime-II). The decrease in particles size with increasing emulsifier concentration in two regimes is not similar; it is more visible in the regime-I compare to regime-II. In contrast to the inverse relationship of the particle

size with the emulsifier concentration, there is a direct proportional correlation of the particle size with the initiator concentration. The exponent for particle size dependence in case of emulsifier variation is bigger (0.43) compared to initiator variation (0.053), which implies that the variation of the emulsifier concentration would be the better way to prepare particles of different sizes. The dependence of the number of particles with surfactant concentration in both the regime is different and probably this is because the polymerization rates are different in two regimes. The measured molecular weight increases with increasing emulsifier concentration and decreases with increasing initiator concentration. Particle size and molecular weight is inversely related, that is, higher molecular weight produces smaller particle and vice versa. The surface charge density of the particles also depends upon the emulsifier concentration and the initiator concentration. However, the optimization of the charge density of the colloidal particles can be done more efficiently by varying the emulsifier concentration rather than the initiator concentration.

References

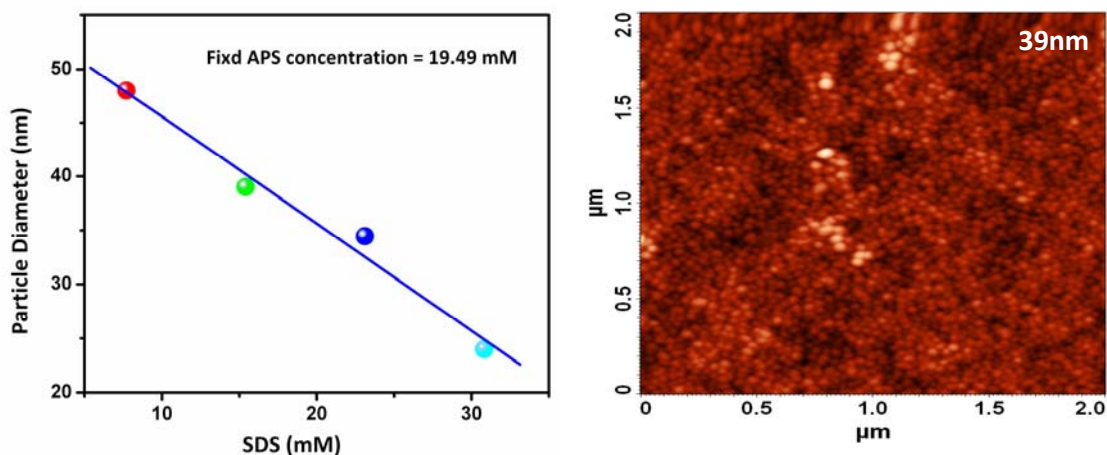
1. Odian, G. *Principles of polymerization*, 4th edn.; Wiley-Interscience: New York, 2004.
2. Gilbert, R.G. *Emulsion Polymerization: A Mechanistic Approach*; Academic Press: London, 2005.
3. Chern, C. S. *Prog. Polym. Sci.* **2006**, *31*, 443, and references there in.
4. Fitch, R. M. *Polymer Colloids: A Comprehensive Introduction*; Academic Press: San Diego, 1997.
5. Duracher, D.; Elaissari, A.; Pichot, C. *J. Polym. Sci. Part A: Polym. Chem.* **1999**, *37*, 1823.
6. Awan, M. A.; Dimone, V. L.; El-Aasser, M. S. *J. Polym. Sci. Part A: Polym. Chem.* **1996**, *34*, 2633.
7. Sunkara, H. B.; Jethmalani, J. M.; Ford, W. T. *J. Polym. Sci. Polym. Chem. Ed.* **1994**, *32*, 1431.
8. Wolfe, M. S.; Scopazzi, C. J. *J. Colloid Interface Sci.* **1989**, *133*, 265.
9. Paine, A. J.; Luymes, W.; McNulty, J. *Macromolecules* **1990**, *23*, 3104.
10. Krieger, I. M.; O'Neill, F. M. *J. Am. Chem. Soc.* **1968**, *90*, 3114.
11. Hiltner, P. A.; Papir, Y. S.; Krieger, I. M. *J. Phys. Chem.* **1971**, *75*, 1881.
12. Hiltner, P. A.; Krieger, I. M. *J. Phys. Chem.* **1969**, *73*, 2386.
13. Reese, C. E.; Guerrero, C. D.; Weissman, J. M.; Lee, K.; Asher, S. A. *J. Colloid Interface Sci.* **2000**, *232*, 76.
14. Mohanty, P. S.; Kesavamoorthy, R.; Matsumoto, K.; Matsuoka, H.; Venkatesan, K. A. *Langmuir* **2006**, *22*, 4552.
15. Reese, C. E.; Asher, S. A. *J. Colloid Interface Sci.* **2002**, *248*, 41.
16. Pan, G.; Tse, A. S.; Kesavamoorthy, R.; Asher, S. A. *J. Am. Chem. Soc.* **1998**, *120*, 6518.
17. Ito, K.; Nakamura, H.; Ise, N. *J. Chem. Phys.* **1986**, *85*, 6143.
18. Sharma, A. C.; Jana, T.; Kesavamoorthy, R.; Shi, L.; Virji, M. A.; Finegold, D. N.; Asher, S. A. *J. Am. Chem. Soc.* **2004**, *126*, 2971.

19. Asher, S. A.; Sharma, A. C.; Goponeko, A. V.; Ward, M. M. *Anal. Chem.* **2003**, *75*, 1676.
20. Gao, J.; Lee, D.; Yang, Y.; Holdcroft, S.; Frisken, B. J. *Macromolecules* **2005**, *38*, 5854.
21. Smith, W. V.; Ewart, R. H. *J. Chem. Phys.* **1948**, *16*, 592.
22. Goodwin, J. W.; Ottewill, R. H.; Pelton, R.; Vianello, G.; Yates, D. E. *Br. Polym. J.* **1978**, *10*, 173.
23. Herrera-Ordóñez, J.; Olayo, R. *J. Polym. Sci. Part A: Polym. Chem.* **2000**, *38*, 2201.
24. Herrera-Ordóñez, J.; Olayo, R. *J. Polym. Sci. Part A: Polym. Chem.* **2000**, *38*, 2219.
25. Herrera-Ordóñez, J.; Olayo, R. *J. Polym. Sci. Part A: Polym. Chem.* **2001**, *39*, 2547.
26. Chern, C.-S.; Chang, H.-T. *Euro. Polym. J.* **2003**, *39*, 1421.
27. Herrera-Ordóñez, J.; Rivera, O.; Maldonado-Textile, H.; Ramirez, J. C. *J. Polym. Sci. Part A: Polym. Chem.* **2005**, *43*, 1963.
28. Lu, Y.-Y.; Lin, C.-C. *Polym. Eng. Sci.* **1985**, *25*, 57.
29. Feeney, P. J.; Napper, D. H.; Gilbert, R. G. *Macromolecules* **1984**, *17*, 2520.
30. Brijmohan, S. B.; Swier, S.; Weiss, R. A.; Shaw, M. T. *Ind. Eng. Chem. Res.* **2005**, *44*, 8039, and references there in.
31. Matsumoto, A.; Kodama, K.; Aota, H.; Capek, I.; *Euro. Polym. J.* **1999**, *35*, 1509.
32. Ford, W. T.; Yu, H.; Lee, J.-J.; El-Hamshary, H. *Langmuir* **1993**, *9*, 1698.
33. Stecher, P. G. *The Merck Index*; Merck & Co., Inc: Rahway, New Jersey, 1968.
34. Masui, J. S.; Watillon, A. J. *Colloid Interface Sci.* **1975**, *52*, 479.
35. Collins, E. A.; Bares, J.; Billmeyer, F. W. *Experimental Polymer Science*; Wiley Interscience: New York, 1973.
36. Evans, D. F.; Wennerstrom, H. *The Colloidal Domain: Where Physics, Chemistry, Biology and Technology Meet, 2nd ed.*; Wiley-VCH: New York, 1999.

37. Tse, A. S.; Wu, Z.; Asher, S. A. *Macromolecules* **1995**, 28, 6533.
38. Fitch, R. M.; Prenosil, M. B.; Sprick, K. J. *J. Polym. Sci.* **1969**, C27, 95.
39. Ryu, J.-H.; Kim, J.-W.; Suh, K.-D. *Colloid Polym. Sci.* **1999**, 12, 1205.
40. Roberts, J. M.; Linse, P.; Osteryoung, J. G. *Langmuir* **1998**, 14, 204.

Chapter 3

Synthesis of Crosslinked Poly(Styrene-*co*-DVB-*co*-SPM) Nanoparticles by Emulsion Copolymerization



We have developed a series of recipes to synthesize 24 nm–102 nm size highly charged, crosslinked poly(styrene-co-divinylbenzene-co-sulfopropyl methacrylate) copolymer colloidal particles using emulsion polymerization. The effects of concentration of the emulsifier and the initiator on the particle size and the charge density of the colloidal particles are studied.

3.1. Introduction

Monodisperse polymer colloidal particles with narrow molecular weight distribution have unique properties which make them interesting and find applications in numerous fields^{1, 2}. Generally, emulsion polymerization technique is employed to prepare the monodisperse polymer particles with narrow molecular weight distribution^{3, 4, 5}. Functionalization of polymer particles with the desired functional groups is obtained by employing appropriate ionic or nonionic monomers as a comonomer in the polymerization recipe. Functional polymer particles are useful in various fields such as catalysis, photonics, paint technology, medicine, biotechnology etc.^{6,7,8,9} Colloidal particles which are highly functionalized by ionic monomers can readily self assemble into non-close pack structures. These particles diffract light according to Bragg's law in the near-IR, ultra-violet and visible regions depending upon the particle size and volume fraction of the particles in the medium. This class of colloidal material which is known as the crystalline colloidal arrays (CCA)¹⁰⁻¹⁷ has pioneered a new class of materials where CCA are embedded inside polymer hydrogel matrix. This CCA polymerized polymer hydrogel is known as polymerized crystalline colloidal array (PCCA). PCCA is used as smart materials¹⁸⁻¹⁹ for various applications such as in photonics,^{20, 21} the sensing of metal ions, pH sensor and sensors for biologically important analytes like glucose and creatinine etc²²⁻²⁴. The degree of self-assembly of the colloidal particles to create CCA has correlation with particle size, surface charge density and ionic strength of the particle dispersion medium⁴. Therefore, it is absolutely necessary to fine tune the particle size and the charge density of the colloidal particles as per the needs of the applications. Our aim in this paper is to synthesize copolymer colloidal particles with tunable particle size and charge density which can be utilized to develop PCCA based smart materials.

The properties of the polymer colloidal particles can be fine tuned by varying the sizes of the colloidal particles. In case of emulsion polymerization technique particle size has been shown to vary depending upon the concentration of emulsifier, initiator, monomer, stirring speed and size of the stirrer blade and temperature. Among all these

parameters emulsifier and initiator concentration variation gives rise to particles with a narrow molecular weight and higher monodispersity. Andre and Henry²⁵ employed sulfopropyl methacrylate (SPM) as an ionogenic monomer and showed that at constant ionogenic monomer concentration particle size has direct correlation with ionic strength and at constant ionic strength particle size decreases with the concentration of ionogenic monomer. In the previous chapter, we have shown that particle size can be varied very sharply by varying the surfactant concentration below the critical micellar concentration of the emulsifier (heterogeneous particle nucleation) and particle size variation can also be achieved by varying the initiator concentration²⁶.

Here, in this chapter we have studied the synthesis of highly charged cross linked poly (styrene-co-divinylbenzene-co-sulfopropyl methacrylate) colloidal particles of various sizes (~20–100 nm) using emulsion polymerization method, and in particular, we have studied the effect of emulsifier and initiator concentration on the particle size and the charge density of the colloidal particles. This report benefitted from the numerous previous works on the synthesis of functionalized monodisperse latex particles^{4, 5, 27, 28, 29, 30}.

3.2. Experimental Section

3.2.1. Materials

Divinyl benzene (DVB, Aldrich), 3-sulfopropyl methacrylate (SPM, Poly Sciences), sodium dodecyl sulfate (SDS, Merck), sodium bicarbonate (Sisco) and ammonium persulfate (APS, Merck) were used as received.

3.2.2. Synthesis of poly (styrene-co-divinylbenzene-co-sulfopropylmethacrylate) colloidal particles

Poly(styrene-co-divinylbenzene-co-sulfopropylmethacrylate), hereafter poly (S-co-DVB-co-SPM), colloidal particles were synthesized by emulsion polymerization

technique in four neck mercury sealed round bottom flask fitted with a reflux condenser, teflon stirrer powered by a high-torque mechanical stirrer, nitrogen and reagent inlet. The temperature was maintained by placing the reaction vessel in a controlled temperature oil bath. The reaction vessel was charged with previously deoxygenated 75 ml of double distilled water and 0.1 g of sodium bicarbonate was added. A stirring rate of 360 rpm and a nitrogen blanket were maintained throughout the course of the reaction. The buffer solution was deoxygenated by bubbling with nitrogen for 40 min. After thorough de-oxygenation, the required amount of SDS dissolved in 5 ml of water was added and the temperature was increased to 50°C. Freshly deoxygenated styrene (33 g, 0.32 mol) and DVB (1.65 g, 13 mmol) were added at a rate of 4 ml/min using pressure equalizer. The 3-sulfopropylmethacrylate (2 g, 8 mmol) was dissolved in 5 ml of water and injected 10 min after the addition of styrene and DVB. The temperature was increased to 70°C. After equilibration for 30 min, required amount of ammonium persulfate dissolved in 5 ml of water was injected into the reaction mixture. The reaction was refluxed for 3–4 hours. We have varied both the emulsifier/surfactant (SDS) and initiator (APS) concentration keeping all other reaction parameters constant in the polymerization mixture and various reactions recipe are presented in Table 3.1.

Table 3.1. *Variation of emulsifier and initiator concentration in the reaction.*

Sample No.	SDS (% Wt.)	SDS (mmol)	APS (% Wt.)	APS (mmol)
VS129	0.16	0.69	0.32	1.75
VS14	0.32	1.39	0.32	1.75
VS117	0.48	2.08	0.32	1.75
VS128	0.64	2.77	0.32	1.75
VS131	0.32	1.39	0.8	4.39
VS138	0.32	1.39	2.4	13.16
VS141	0.32	1.39	4.8	26.32

3.2.3. Purification of poly(S-co-DVB-co-SPM) colloidal particles

The polymer formed at the end of the reaction appeared milky white colloidal solution which was filtered through a glass wool. The filtered solution was centrifuged for 40 min at 45000 rpm at 15°C in an ultra centrifuge. The residue (solid white mass) was thoroughly dispersed in double distilled water with the help of sonication and mixing in a vortex motor. Centrifugation and dispersion process were repeated 3–4 times to remove all impurities from the colloidal particles.³⁰ The colloidal solution was taken in a culture tube and ion-exchange resin (Bio Rad mixed bed; AG501-X8 used as received) was added and placed on a vertical rotor. After 1–2 days of stirring the colloidal solutions were exhibiting bluish violet colours indicating the formation of self assembled array of colloidal particles.

3.2.4. Characterization of poly(S-co-DVB-co-SPM) colloidal particles

The sizes of the colloidal copolymer particles were measured from the microscopic images obtained from the atomic force microscopy (AFM, model: Solver Pro M of NT-MDT) working in semi-contact mode. A micro cantilever with a spring constant of 10 N/m was used to scan the samples. The colloidal juice was diluted with water and a drop was placed on a glass substrate and then imaged in AFM. Particle size was measured from the images obtained from the AFM study. The particle charge density and charges per particle were calculated by measuring the volume fraction and H^+ concentration of the colloidal solution. Volume fraction of colloidal solution was measured gravimetrically in triplicate. The amount of H^+ ion in the colloidal juice was measured by potentiometric acid-base titration using an Auto– Titrator (Titrino 701) instrument^{31, 32}. The colloidal juice was titrated against the 0.1 (N) NaOH solution and H^+ ion concentration was calculated from the potentiometric titration curve.

3.2.5. Preparation of PCCA and diffraction studies

A polymerization mixture consisting of acrylamide (0.1 g, 1.39 mmol, Sigma Aldrich), N,N'-methylenebisacrylamide (0.005 g, 0.032 mmol, Sigma Aldrich), CCA [2.00 g, 102 nm particle of poly(S-co-DVB-co-SPM)] latex spheres and 0.1 g mixed bed resin was prepared. 10% w/v diethoxyacetophenone (DEAP, 8 drops, 100 μ L, 4.96 mmol, Sigma Aldrich) in dimethylsulfoxide was added to the mixture and mixed thoroughly. The polymerization solution from this mixture was withdrawn in syringe carefully using a needle to remove the ion-exchange resin. The reaction mixture was then injected into a cell consisting of two quartz disks, separated by \sim 125 μ m thick para films spacer. An UV lamp (Mercury source spot bulb, Sigma Aldrich) operating at 365 nm was focused on the polymerization cell for 4 h. After polymerization, the cell was opened in Millipore water and the PCCA was washed thoroughly with water. A diffracting PCCA was obtained. All diffraction measurements were carried out in reflectance mode using an Ocean Optics fibre optic spectrometer (USB4000-VIS-NIR).

3.3. Results and Discussion

All the copolymers are characterized by using FT-IR spectroscopy. A representative FT-IR spectrum along with the polymer structure and the peaks assignments is shown in Figure 3.1. The spectrum clearly indicates the presence of stretching frequencies for all the monomers (styrene, divinyl benzene and sulfopropyl methacrylate) and therefore, we can conclude that the synthesized copolymers consist of all the monomers. In Table 3.2, we have summarized all the characterization results obtained from the emulsion polymerization reactions (Table 3.1) for various concentrations of surfactant and initiator.

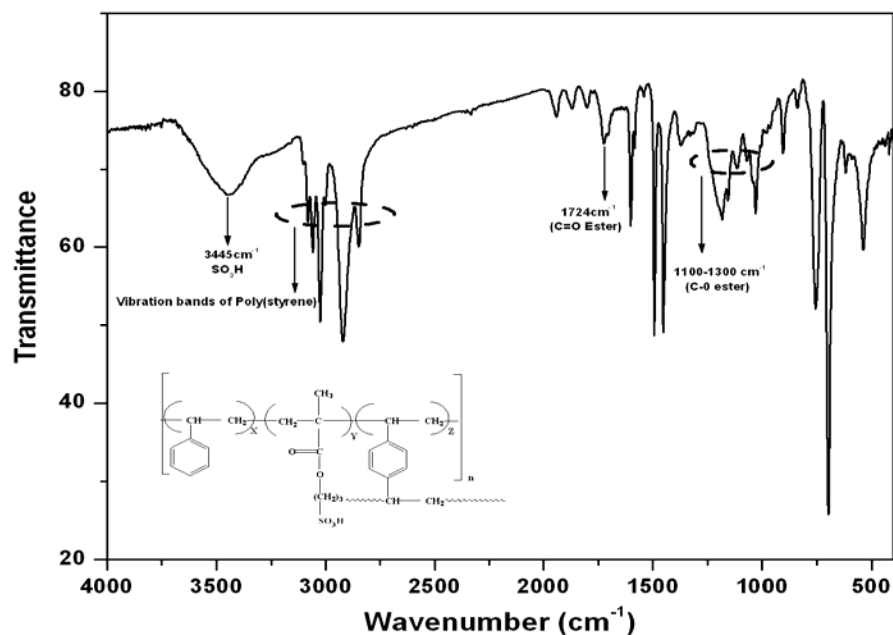


Figure 3.1. Representative FT-IR spectrum of poly(S-co-DVB-co-SPM) copolymer along with copolymer backbone structure and the peak assignments.

Table 3.2. Characteristic data such as particle size and charge density of all synthesized copolymer colloidal particles

Sample No.	SDS (mM)	APS (mM)	Particle diameter (nm)	Surface Charge density ($\mu\text{C}/\text{cm}^2$)	<u>Charges</u> Spheres (Z) (\bar{e} /sphere)	No of particles (N_p) (no./mL) $\times 10^{-15}$
VS129	7.71	19.49	48	19.20	8675	1.019
VS 14	15.41	19.49	39	11.32	3376	1.674
VS 117	23.12	19.49	34	1.057	239	4.76
VS128	30.82	19.49	24	0.837	95	8.94
VS 131	15.41	48.72	68	2.69	2439	1.269
VS 138	15.41	146.19	79	16.89	20680	0.739
VS 141	15.41	292.40	102	6.024	12290	0.558

3.3.1. Particle size

3.3.1.1. Emulsifier concentration vs. particle diameter.

The particle size decreases from 48 nm to 24 nm with an increasing concentration of emulsifier (SDS) in solution and is highly dependent upon the concentration of SDS in the reaction mixture (Table 3.2). The representative AFM images of the poly(Sty-co-DVB- o-SPM) colloids prepared from different surfactant

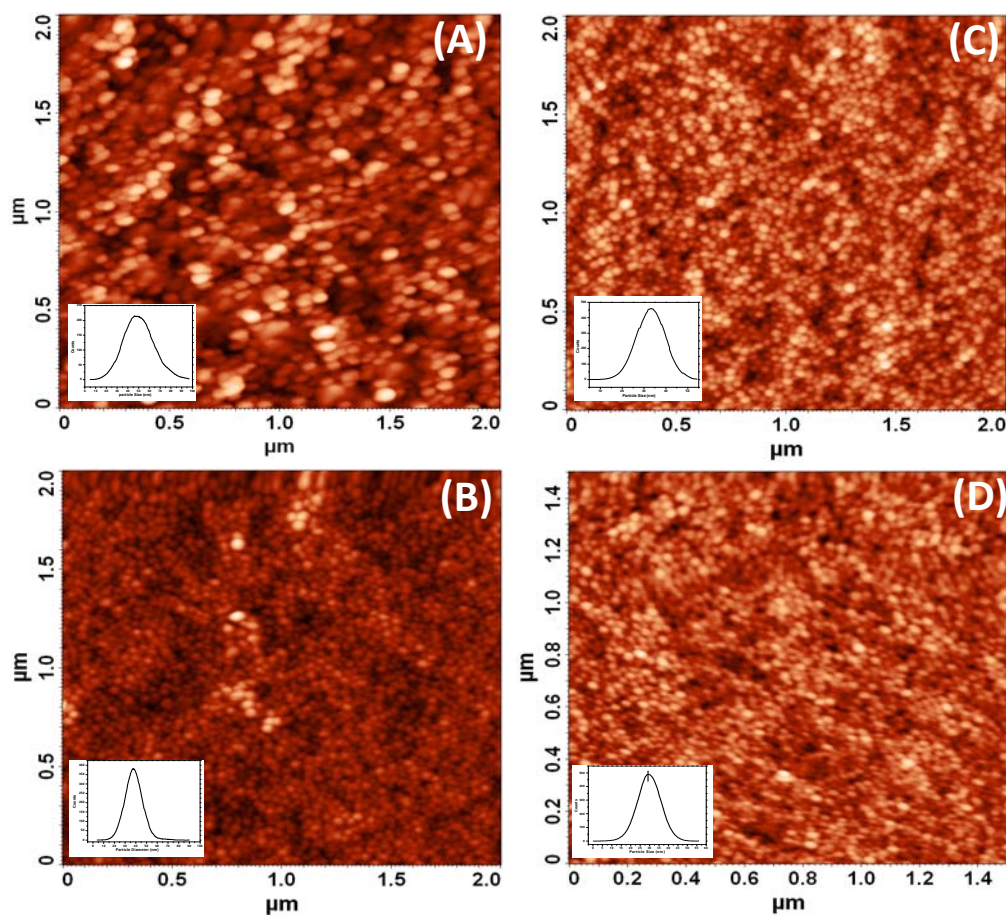


Figure 3.2. AFM images of colloidal particles prepared by varying SDS concentration: (A) 48 nm, SDS = 7.71 mM (VS129), (B) 39 nm, SDS = 15.41 mM (VS14), (C) 34 nm, SDS = 23.12 mM (VS117) and (D) 24 nm, SDS = 30.82 mM (VS128). Particle size distributions are shown in the insets of each micrograph.

concentrations are presented in Figure 3.2. We have measured particle sizes of the colloids from the AFM images. A plot of particle diameter vs surfactant concentration for a fixed initiator concentration (19.49 mM) is presented in Figure 3.3. The particle diameter decreases as the surfactant concentration increases. Lower emulsifier concentration produces very less number of micelles which consequently results in larger colloidal polymer particles³³. A large number of smaller size micelles are found at high emulsifier concentration. Therefore, with increasing emulsifier concentration the particle size decreases (Figures 3.2 and 3.3). Also, we have observed that as the emulsifier concentration decreases particles size distribution becomes broad (insets of Figure 3.2). This is due to the agglomeration of the colloidal particles because of the decreased stability of the colloids.

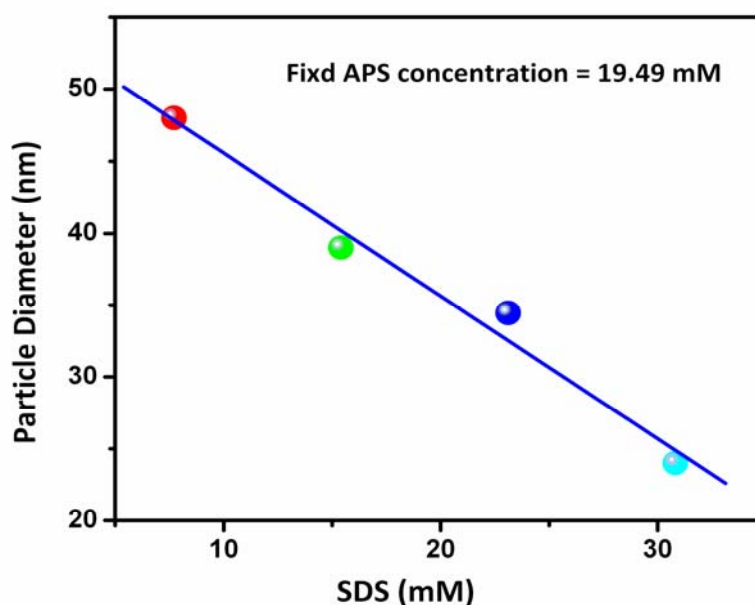


Figure 3.3. Dependence of particle diameter on SDS (emulsifier) concentration at a fixed APS (initiator) concentration.

3.3.1.2. Initiator concentration vs. particle diameter.

Particle size can also be tuned by varying the initiator concentration in the polymerization mixture. Figure 3.4 shows the AFM images of different size particles

obtained by changing the initiator concentration in the reaction mixture by keeping emulsifier concentration constant. A plot of particle diameter against the initiator concentration for a fixed surfactant concentration is presented in Figure 3.5. It is clear that particle size increases with increasing initiator concentration. Due to the formation of a large number of free radicals at high initiator concentration the possibility of polymerization termination is very high. In an emulsion polymerization system, the probability of monomer swollen micelle maturing into a particle depends upon several factors including the initiator concentration. For a fixed concentration of emulsifier the number of micelles formed is constant but due to the variance in the initiator concentration the portion of these monomer swollen micelles becoming as a particle depends upon the initiator concentration. Higher initiator concentration leads to higher probability of termination so lesser proportions of micelles are converted into particles which results in bigger particles and a less number of particles. A closer observation of AFM images (Figure 3.4) reveal that particles are not monodisperse and they are agglomerated. These are due to the decreased electrostatic stability which increases

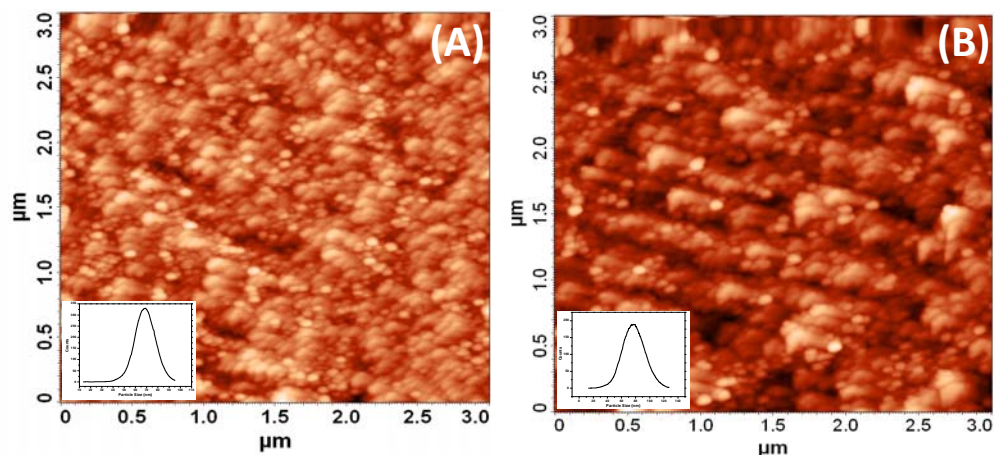


Figure 3.4. AFM images of poly (S-co-DVB-co-SPM) colloidal particles prepared by varying initiator (APS) concentration for fixed emulsifier concentration (15.41 mM); (A) 68 nm, APS = 48.72 mM (VS131) and (B) 79 nm, APS = 146.19 mM (VS138). Particle size distributions are shown in the insets of each micrograph.

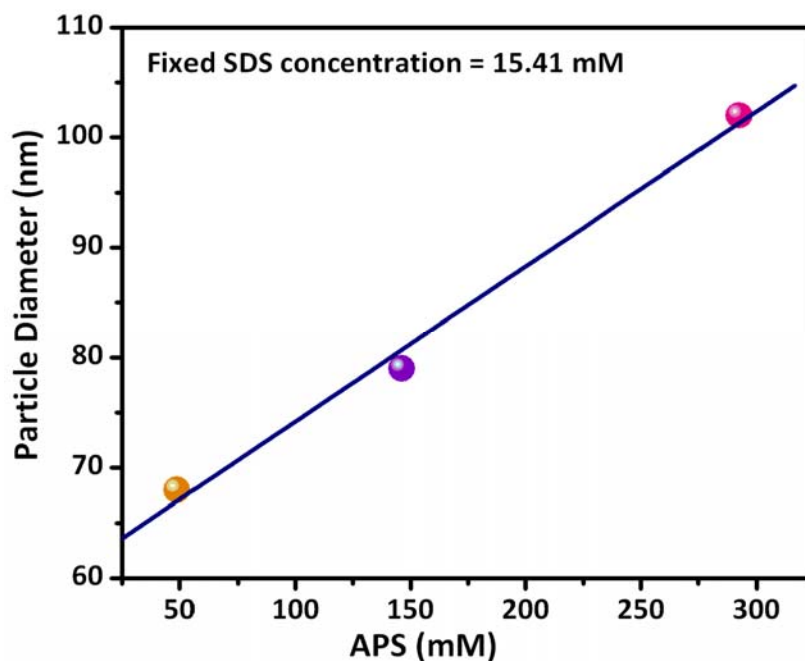


Figure 3.5. Variation of particle diameter as a function of initiator (APS) concentration at a fixed emulsifier (SDS) concentration.

with the increase in particle size. Hence particle size has a direct relationship with initiator concentration which is in agreement with our previous report (chapter 2) for similar type of colloids²⁶ but not in agreement with the results reported previously by Asher and coworkers³⁴ for the fluorinated colloidal particles.

3.3.2. Number of particles

3.3.2.1. Number of particles vs surfactant concentration.

Harkins' in his classical paper on mechanism of emulsion polymerization³⁵ proposed that micelles act as a polymerization locus where polymer chain tends to grow in a micelle compartment. Number of particles formed in the yield per unit volume is a function of number of micelles which is a function of concentration of emulsifier

molecules. Higher surfactant concentration leads to more number of micelles which consequently mature into smaller polymer particles. From Figure 3.6 it is evident that the number of particles increases with the emulsifier concentration. Hence an inverse relationship between number of particles and particle diameter is expected as presented in the inset of Figure 3.6. The dependence of the number of particles (N_p) with the emulsifier/ surfactant concentration (S) is obtained from the slope of the straight line in the log–log plot of N_p vs S (Figure 3.7) and it is 1.57. Therefore, the N_p is proportional to $S^{1.57}$. The exponent value is very similar to our earlier observation for the similar kinds of colloids²⁶. The positive exponent of $N_p \propto S$ indicates that coagulative nucleation process takes place during particle formation.

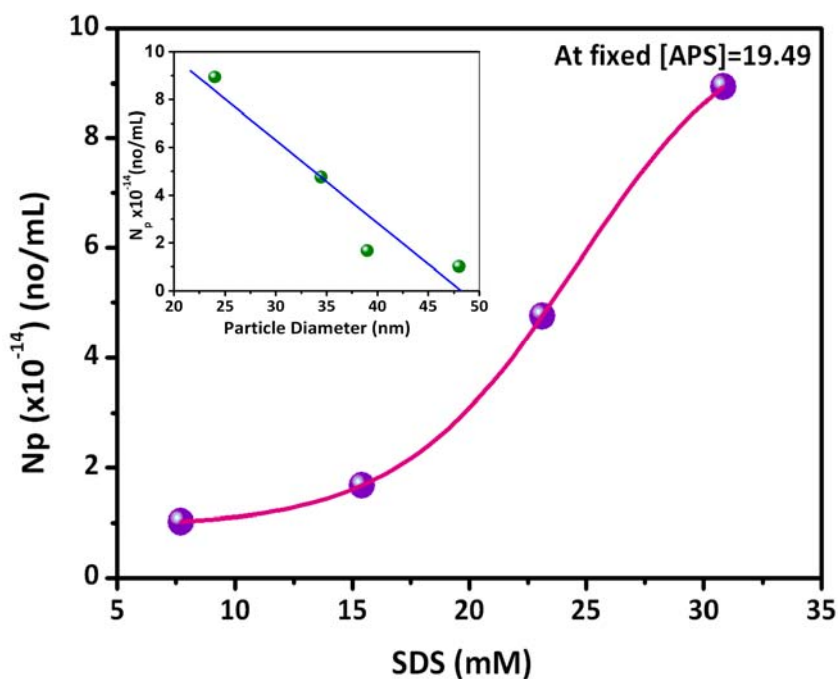


Figure 3.6. Plot of number of particles vs emulsifier concentration. Inset: N_p vs particle diameter.

3.3.2.2. Number of particles vs. initiator concentration.

The number of particles decreases with increasing initiator concentration (Table 3.2). The number of micelles is constant for a fixed SDS concentration but polymer particles formed at the end after reaction decides the N_p . All the monomer swollen micelles cannot mature as a polymer particle; only a proportion of them transforms to polymer and this transformation depends upon different parameters such as initiator concentration. The lower initiator concentration increases the probability of transformation of monomer swollen micelles into polymer particles and yields smaller and more number of particles. Thus N_p is inversely proportional to both particle size and initiator concentration³⁶.

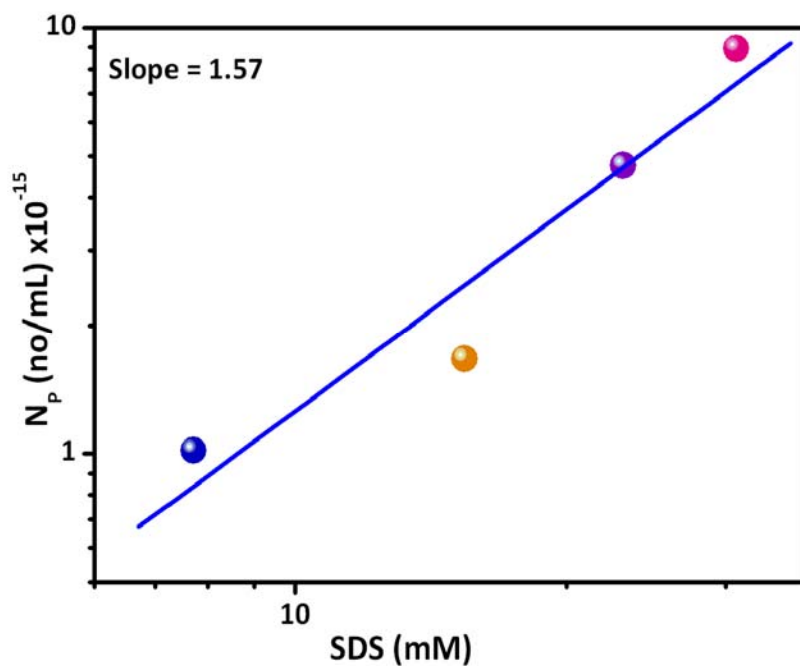


Figure 3.7. Log-log plot of N_p vs. S ; slope of the solid line is 1.57.

3.3.3. Surface charge density

Charge on the surface of the particle plays a vital role in designing PCCA based sensor materials. Monodisperse particles with charges on the surface tend to self assemble into non-close packed structures like bcc or fcc in solution. The self assembly is essential in the designing of PCCA based sensing materials. The optimization of the surface charges of the colloidal particles is absolutely necessary because higher charges

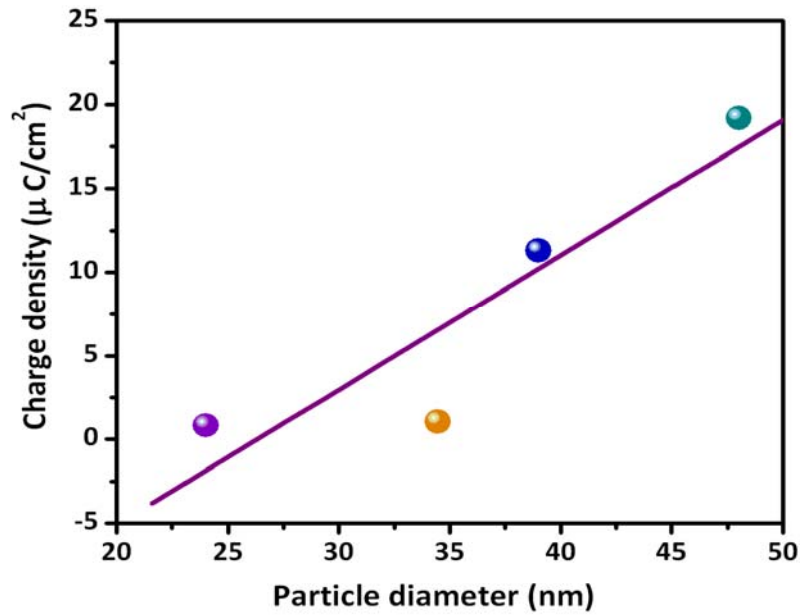


Figure 3.8. Plot of charge density vs particle diameter (at constant APS concentration).

yield coalescence particles and on the other hand, lower charges result in agglomerated particles. The role of 3-sulfopropyl methacrylate as an ionic co-monomer is to generate charge on the surface of the spherical particles. The surface charge density i.e. charges per unit area on the surface of a spherical colloidal particle, can be calculated using (Equation 3.1)

$$\sigma = \frac{FaC_{H^+}(1-\phi)}{3\phi} \quad (3.1)$$

where σ is surface charge density, F the Faraday's constant, C_{H^+} the concentration of H^+ ions, a the particle radius and ϕ the volume fraction of colloidal juice. Therefore, from (equation 3.1, one would expect that the charge density of particle would increase with particle diameter. Our results are in agreement with (equation 3.1), as observed in Figure 3.8. The charge density of the particle increases with particle diameter as is evident in Figure 3.8.

Figure 3.9 shows that charge density decreases with SDS concentration which is obvious since particle size has an inverse relationship with the SDS concentration. Therefore, it is proved that the surface charge of the colloidal particle is not the contribution from the sulfate groups of SDS; it is due to the sulfate group of ionic co-monomer which is incorporated in the polymer chain. If the surface charge contribution would have come from the SDS then the charge density should have been increased with increasing SDS concentration instead of decreasing with increasing SDS concentration (Figure 3.9). Hence, from the above results it is clearly demonstrated that the origin of the charges on the colloidal particles is the contribution of the ionic co-monomer (sulfopropyl methacrylate) present in the copolymer.

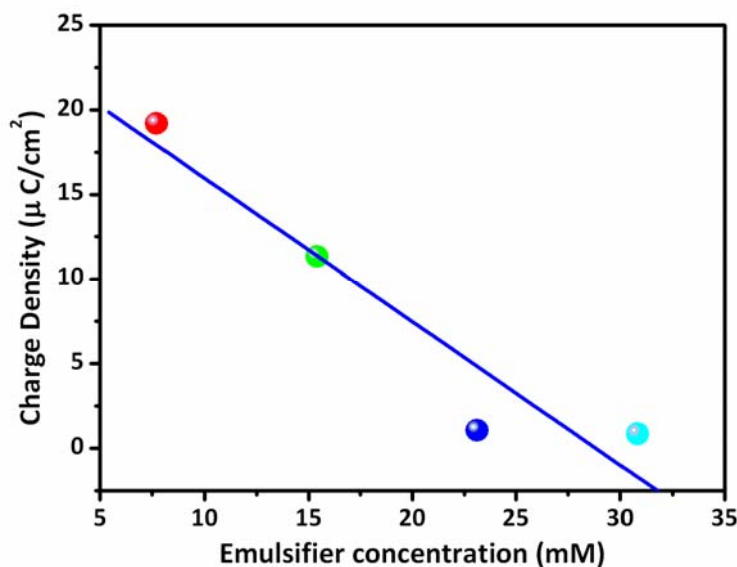


Figure 3.9. Plot of charge density vs emulsifier concentration (at constant APS concentration).

3.3.4. Charges per particle

The number of charges per particle (Z) can be calculated dividing total charge (Q) on the surface of the particle by the electronic charge. The total charge (Q) of the particle is the summation of electron charges on the surface of the sphere. Total charge (Q) on the sphere can be calculated by

$$Q = \sigma \times 4\pi a^2 \quad (3.2)$$

where σ is the charge density and 'a' is the particle radius. Since the particle is spherical the surface area will be $4\pi a^2$. Therefore, the number of charges per particle (Z) is expressed by equation 3.3

$$z = \frac{\sigma \times 4\pi a^2}{1.602 \times 10^{-19}} \quad (3.3)$$

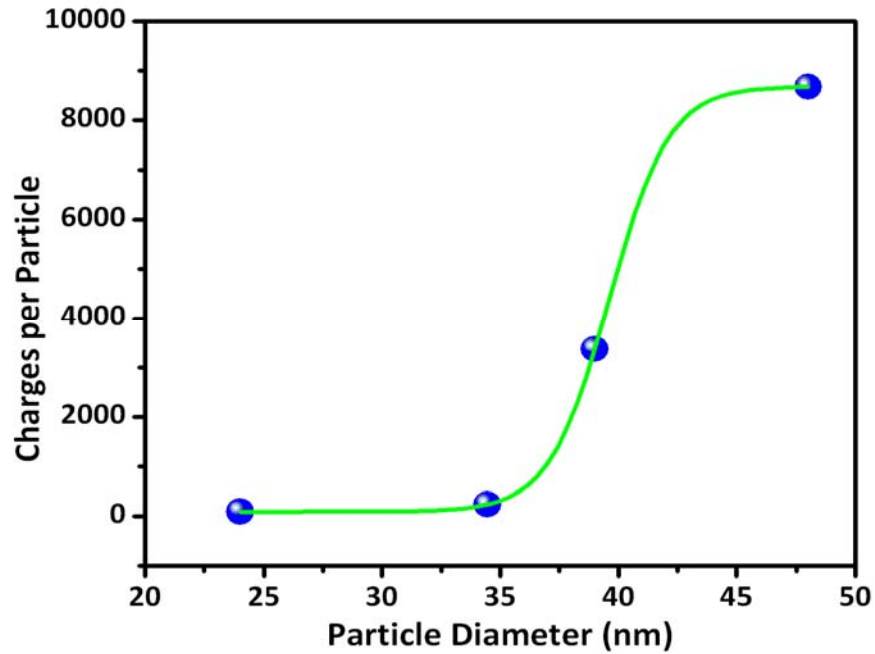


Figure 3.10. Plot of charges per particle vs particle diameter (at constant initiator concentration).

Where 1.602×10^{-19} Coulomb is the electronic charge. From (equation.3.3) one would expect a direct correlation between particle diameter and the charges per particle. Charges per particle increases slowly followed by a sudden jump after a certain diameter and attain saturation with the particle diameter as seen in Figure 3.10. Since particle size has an inverse relationship with emulsifier concentration charges per particle rapidly decreases with emulsifier concentration as observed in Figure 3.11. Therefore, one can tune the charges on the particle surface sharply varying the emulsifier concentration.

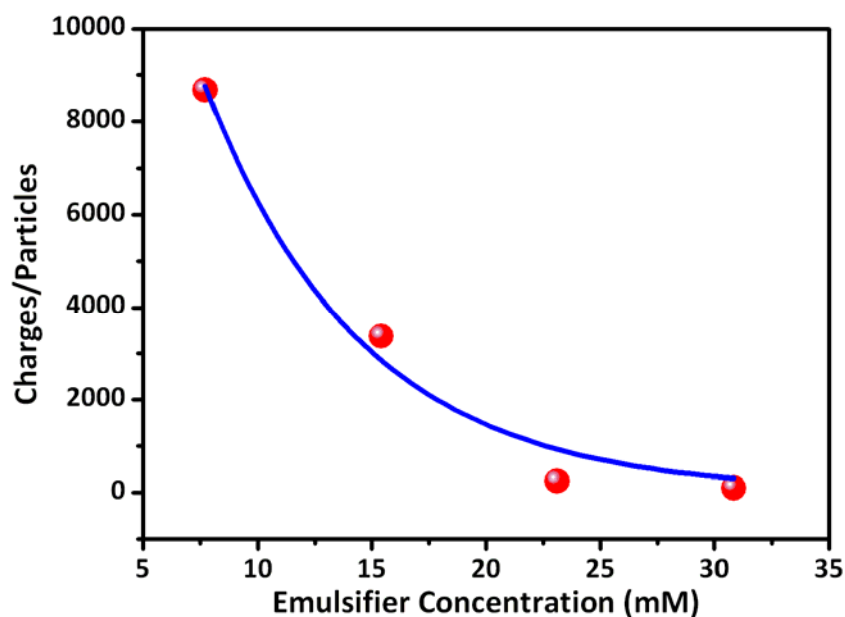


Figure 3.11. Plot of charges per particle vs emulsifier concentration (at constant initiator concentration).

3.3.5. Diffraction studies of PCCA

After the purification of the poly(S-co-DVB-co-SPM) copolymer colloidal particles we have observed a bright diffracting colour. This indicates that the colloids are self assembled and resulting in the crystalline colloidal array (CCA) ¹⁰⁻¹⁷. We have imbibed this CCA inside the polymer hydrogel matrix by photo polymerizing this

copolymer colloidal particles (CCA) with acrylamide and N,N' -methylenebisacrylamide. This CCA imbibed hydrogel is known in the literature as polymerized crystalline colloidal array (PCCA)^{18,19}. The diffraction spectrum (reflectance spectrum) of the PCCA is presented in Figure 3.12. Two diffraction peaks are observed from the PCCA (Figure 3.12). The sharp peak at higher wavelength (920 nm) is the primary diffraction peak of the CCA and the broad peak (460 nm) at the half wavelength of the primary diffraction peak is due to second order diffraction of the CCA.

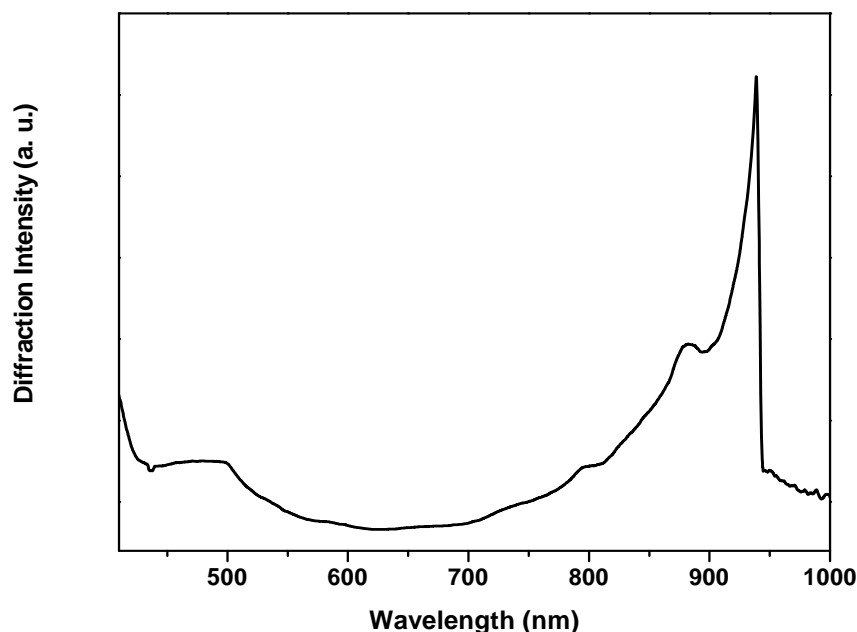


Figure 3.12. *Diffraction spectrum (reflectance spectrum) of the PCCA obtained from the poly(*S-co-DVB-co-SPM*) colloidal particles.*

3.4. Conclusion

We have synthesized highly charged colloidal poly (styrene-co-divinylbenzene-co-sulfopropyl methacrylate) copolymer particles using emulsion polymerization. A series of recipes have been developed for the synthesis of 24–102 nm size colloidal particles. Particle size is highly dependent upon the concentration of both the emulsifier

and the initiator. The particle diameter decreases with increasing concentration of emulsifier and increases with increasing concentration of initiator in the reaction mixture. Number of particles increases with the increase in emulsifier concentration whereas decreases with initiator concentration. Number of particles has an inverse correlation with the particle size. Charge density can be varied sharply by varying the emulsifier concentration. The number of charges per sphere increases with the particle diameter. Polymer hydrogel imbided with these copolymer colloidal particles diffracts the light.

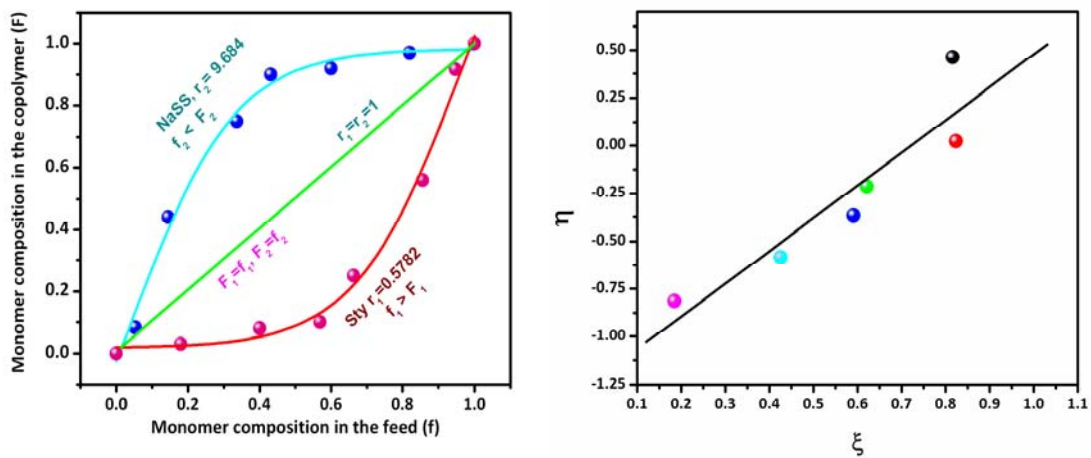
References

1. Fitch, R. M. *Polymer colloids*, Academic Press: San Diego, 1997.
2. Xia, Y.; Gates, B.; Yin, Y.; Lu, Y. *Adv. Mater.* **2000**, *12*, 10.
3. Odian, G. *Principles of polymerization* 4th edn, Wiley-Interscience: New York, 2004, Chapter 4.
4. Reese, C. E.; Guerrero, C. D.; Weissman, J. M.; Lee, K.; Asher, S. A. *J. Colloid Interface Sci.* **2000**, *232*, 76.
5. Reese, C. E.; Asher, S.A. *J. Colloid Interface Sci.* **2002**, *248*, 41.
6. Luck, V. W.; Kleir, M.; Wesslau, H. *Ber. Bunsenger. Phys.Chem.* **1963**, *67*, 75.
7. Joannopoulos, J. D.; Meade, R. D.; Winn, J. N. *Photonic crystals: molding the flow of light* Princeton University Press: Princeton, 1995.
8. Soukoulis, C. M. (ed.) *Photonic Bandgap materials*, Kluwer: Dordrecht, 1996.
9. Soukoulis, C. M. *J. Lightwave Technol.* **1999**, *17*.
10. Krieger, I. M.; O'Neil, F. M. *J. Am. Chem. Soc.* **1968**, *90*, 3114.
11. Hiltner, P. A.; Krieger, I. M. *J. Phys. Chem.* **1969**, *73*, 2386.
12. Hiltner, P. A.; Papir, Y. S.; Krieger, I. M. *J. Phys. Chem.* **1971**, *75*, 1881.
13. Carlson, R. J.; Asher, S. A. *Appl. Spectrosc.* **1984**, *38*, 297.
14. Aastuen, D. J. W.; Clark, N. A.; Cotter, L. K.; Ackerson, B. J.; *Phys. Rev. Lett.* **1986**, *57*, 1733.
15. Rundquist, P. A.; Photinos, P.; Jagannathan, S.; Asher, S. A. *J. Chem. Phys.* **1989**, *9*, 4932.
16. Rundquist P. A.; Kesavamoorthy, R.; Jagannathan, S.; Asher, S.A.; *J. Chem. Phys.* **1991**, *95*, 1249.
17. Asher, S. A.; Holtz, J.; Liu, L.; Wu, Z. *J. Am. Chem. Soc.* **1994**, *116*, 4497.
18. Holtz, J. H.; Asher, S. A. *Nature* **1997**, *389*, 829.
19. Holtz, J. H.; Holtz, J. S.W.; Munro, C. H.; Asher, S. A. *Anal.Chem.* **1998**, *70*, 780.
20. Lee, K.; Asher, S. A. *J. Am. Chem. Soc.* **2000**, *122*, 9534.

21. Reese, C. E.; Mikhonin, A. V.; Kamenjicki, M.; Tikhonov, A.; Asher, S. A. *J. Am. Chem. Soc.* **2004**, *126*, 1493.
22. Reese, C. E.; Baltusavich, M. E.; Keim, J. P.; Asher, S. A. *Anal. Chem.* **2001**, *73*, 5038.
23. Alexeev, V. L.; Sharma, A. C.; Goponenko, A. V.; Das, S.; Lednev, I. K.; Wilcox, C. S.; Finegold, D. N.; Asher, S. A. *Anal. Chem.* **2003**, *75*, 2316.
24. Sharma, A. C.; Jana, T.; Kesavamoorthy, R.; Shi, L.; Virji, M. A.; Finegold, D. N.; Asher, S. A. *J. Am. Chem. Soc.* **2004**, *126*, 2971.
25. Andre, A.; Henry, F. *Colloid Polym. Sci.* **1998**, *276*, 1061.
26. Arunbabu, D.; Sannigrahi, A.; Jana, T. *J. Appl. Polym. Sci.* **2008**, *108*, 2718.
27. Juang, M. S. D.; Krieger, I. M. *J. Polym. Sci.: Polym. Chem. Ed.* **1976**, *14*, 2089.
28. Kim, J. H.; Chainey, M.; El-Aasser, M. S.; Vanderhoff, J. W. *J. Polym. Sci. Part A: Polym. Chem.*, **1989**, *27*, 3187.
29. Kim, J. H.; Chainey, M.; El-Aasser, M. S.; Vanderhoff, J. W. *J. Polym. Sci. Part A: Polym. Chem.* **1992**, *30*, 171.
30. Sunkara, H. B.; Jethmalani, J. M.; Ford, W. T. *J. Polym. Sci. Part A: Polym. Chem.* **1994**, *32*, 1431.
31. Masui, J. S.; Watillon, A. *J. Colloid. Interface Sci.* **1975**, *52*, 479.
32. Roberts, J. M.; Linse, P.; Osteryoung, J. G. *Langmuir*, **1998**, *14*, 204.
33. Evans, D. F.; Wennerstrom, H.; *The colloidal domain: where physics, chemistry, biology and technology meet*, 2nd edn., Wiley-VCH: New York, 1999.
34. Pan, G.; Kesavamoorthy, R.; Asher, S. A. *Phys. Rev. Lett.* **1997**, *78*, 20.
35. Harkins, W. D. *J. Am. Chem. Soc.* **1947**, *69*, 1428.
36. Smith, W. V.; Ewart, R. *J. Chem. Phys.* **1948**, *16*, 592.

Chapter 4

Emulsion copolymerization of Styrene and Sodium Styrene Sulfonate



Emulsion copolymerization of sparingly water soluble monomer (styrene) and a water soluble monomer (NaSS) in various compositions (100/0 to 0/100) are carried out to study the reaction kinetics, monomer reactivity ratios and copolymer properties.

4.1. Introduction

Poly[styrene-*co*-(sodium styrene sulfonate)], poly(S-*co*-NaSS), copolymer particles with high sulfonate loads can be used as ion-exchange resins which have a large number of applications in numerous fields. These include catalysis,¹⁻⁴ water purification systems, synthesis of magnetic particles,⁵ chromatography techniques, etc.^{6,7}. Recently, a poly(S- *o*-NaSS) copolymer membrane has been used as a proton-conducting component in a composite polymer electrolyte membrane fuel cell (PEMFC)⁸⁻¹². This copolymer is also used as a polymerizable surfactant. Poly(sodium styrene sulfonate) has been found to be effective in the prevention of sexually transmitted diseases¹³⁻¹⁶. Poly(S-*co*-NaSS) copolymer has very unique structural features to serve as a model system for studying ionomeric behaviour¹⁷⁻¹⁹ at very low NaSS levels (10–15%) as well as polyelectrolyte behavior^{20,21} at a very high NaSS content. Poly(S-*co*-NaSS) copolymers containing moderate amounts of NaSS monomer in the backbone, which fall between polyelectrolytes and ionomers, are called ‘hydrophobic polyelectrolytes’. These are considered as model systems to study biomolecules²²⁻²⁴.

Sulfonation of preformed polystyrene has been the principal synthetic route for the preparation of poly(S-*co*-NaSS)²⁵⁻²⁷. This method has some advantages over the copolymerization of styrene and NaSS, especially if the preformed polystyrene employed for sulfonation has a narrow molecular weight distribution. In this case, it becomes easy to control the molecular weight and also the prediction of the final copolymer properties is simplified. Owing to these advantages, the sulfonation of preformed polystyrene is preferred over emulsion copolymerization of styrene and NaSS. Polyelectrolytes with well-defined charge content have attracted much interest recently because of their numerous applications²⁶. This is why it has proved necessary to fine tune the sulfonation method. Perhaps the copolymerization of styrene and NaSS can address this problem efficiently. Therefore, there is a challenge to prepare poly(S-*co*-NaSS) with various degrees of sulfonation. Emulsion copolymerizations of styrene and NaSS have been reported previously in the literature.^{25, 28} In those reports, the

copolymerizations were carried out with up to 40 mol% of NaSS in the feed. Emulsion polymerization is a unique polymerization technique employed in the preparation of polymers with a very high yield and narrow molecular weight distribution²⁹.

Emulsion copolymerization is a technique where two or more monomers are employed to synthesize copolymers with desired functional groups. In emulsion copolymerization the solubility of the two monomers plays a vital role in the synthesis of copolymers, copolymer properties and kinetics of the reaction^{28–30}. If we employ two monomers, one of which is water soluble and the other is very sparingly soluble, then a change in the site of polymerization nucleation is possible. In the work reported in this chapter we employed styrene as a sparingly soluble monomer and NaSS as a highly soluble monomer in water. We attempted to study the shift of the locus of particle nucleation in the polymerization. A typical emulsion polymerization recipe consists of a water dispersion medium; water-insoluble, partially soluble or completely soluble organic monomer; cationic, anionic or non-ionic emulsifier; and a water-soluble initiator²⁹. Particle nucleation in emulsion polymerization can have two different types of mechanisms: micellar or heterogeneous nucleation and homogeneous nucleation³¹. The former occurs if the emulsifier concentration is above the critical micellar concentration (CMC) and the latter is possible when the emulsifier concentration is below the CMC. However, homogeneous nucleation is possible even above the CMC if the monomer is highly soluble in the aqueous medium^{29, 31}.

In chapter 2, we have reported the variation of particle size and charge density of crosslinked polystyrene particles in both homogeneous and heterogeneous particle nucleation regimes³². In the present chapter, we copolymerized a sparingly water soluble monomer (styrene) and a water-soluble monomer (NaSS) in various compositions (100/0 to 0/100) by emulsion copolymerization. We studied the reaction kinetics, monomer reactivity ratios and copolymer properties using the techniques of Fourier transform infrared (FTIR) and ¹H NMR spectroscopies, atomic force microscopy (AFM), thermogravimetric analysis (TGA), dynamic light scattering (DLS) and differential scanning calorimetry (DSC).

4.2. Experimental Section

4.2.1. Materials

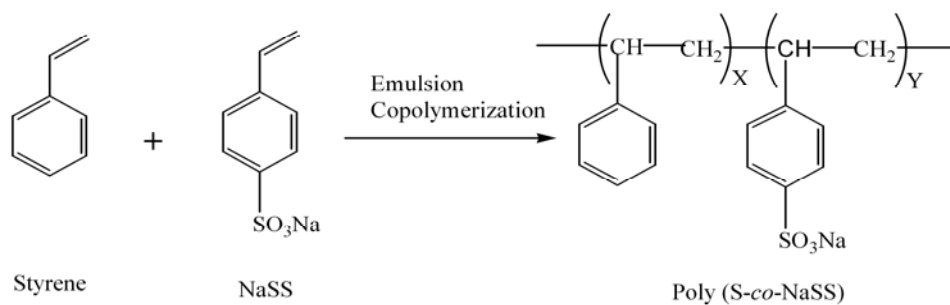
Styrene (Sisco, India) was washed with 10% sodium hydroxide solution and deionized water repeatedly to remove the inhibitor. Then it was freshly distilled prior to use. NaSS was obtained from Sigma-Aldrich and used without further purification. Sodium dodecyl sulfate (SDS) and ammonium persulfate (APS) were obtained from Merck, India. All NMR solvents (CDCl_3 , $\text{DMSO}-d_6$ and D_2O) were also purchased from Merck.

4.2.2. Synthesis and purification of poly(S-co-NaSS) colloidal particles

Poly(S-co-NaSS) colloidal particles were synthesized using the emulsion polymerization technique in a four-neck mercury-sealed round-bottom flask fitted with a reflux condenser, Teflon stirrer powered by a high-torque mechanical stirrer and nitrogen and reagent inlets. The temperature was maintained by placing the reaction vessel in a controlled-temperature oil bath. The reaction vessel was charged with 20 mL of double-distilled water containing 0.04 g (4.76 mmol) of sodium bicarbonate. A nitrogen blanket and stirring rate of 350 rpm were maintained throughout the reaction. The bicarbonate solution was deoxygenated by bubbling with nitrogen for 40 min. After a thorough deoxygenation, 0.12 g (4.16 mmol) of SDS dissolved in 5 mL of water was added and the temperature was increased to 50°C. Freshly deoxygenated styrene was added drop wise. A required amount of NaSS was dissolved in 10 mL of water and injected 5 min after the addition of styrene. The temperature was increased to 70°C. After equilibration for 30 min, 0.12 g (5.26 mmol) of APS dissolved in 5 mL of water was injected into the reaction mixture. Immediately after this addition, 1 mL of the solution was withdrawn from the reaction mixture and terminated using hydroquinone solution (2% w/v). At intervals of 15 min solutions were withdrawn and terminated. After 2 hours of polymerization, the same withdrawal and termination process was

continued at 30 min time intervals until the completion of the total 4 hours of polymerization. After that the polymer was collected and purified by dialysis for further analysis.

The terminated polymers were dried in an oven at 100 °C for 24 h. The weights of dried polymers were recorded and the percentage conversions calculated. The calculated percentage conversions were plotted against time. A simplified reaction scheme of the copolymerization is shown in Scheme 4.1. We varied the relative concentrations of styrene and ionic comonomer (NaSS) in the reaction mixture, as presented in Table 4.1. Upon completion of the reaction, the product appeared as a milky white colloidal solution. It was then allowed to cool and filtered through previously heated glass wool. The colloidal solution was poured inside a dialysis tube (Spectra/Por cellulose ester membrane, molecular weight cut-off of 50,000 g mol⁻¹ and kept inside a 500 mL beaker containing deionized water up to brim and stirred for 7 days using a magnetic stirrer with constant changing of the deionized water. After this the colloidal solution was placed in a culture tube and mixed bed ion exchange resin (Bio Rad mixed bed; AG501-X8 used as received) was added and placed on a vertical rotor. After 1–2 weeks of stirring, the colloidal solution was taken out of the culture tube using a syringe, and then placed into a Petri dish and oven dried at 100°C. Dried polymer was collected and used for further studies.



Scheme 4. 1. *Emulsion copolymerization of styrene and sodium styrene sulfonate.*

Table 4. 1. Copolymerization recipes showing the variation of monomer concentration

Styrene (% wt.)	Styrene (mmol)	NaSS (% wt.)	NaSS (mmol)	Styrene/NaSS (mol frac./mol frac.)
100	126.0	0	0.0	1/0
90	114.0	10	6.4	0.95/0.05
75	95.0	25	16.0	0.86/0.14
60	76.0	40	26.0	0.74/0.26
50	63.0	50	32.0	0.66/0.34
40	50.5	60	38.3	0.57/0.43
25	32.0	75	48.0	0.40/0.60
10	12.6	90	57.4	0.18/0.82
0	0.0	100	64.0	0/1

4.2.3. Characterization of poly(S-co-NaSS) particles

Kinetics studies were done by periodic withdrawal of polymer solution from the reaction mixture with the reaction being terminated by the addition of hydroquinone (2% w/v) solution. Conversion was calculated gravimetrically in triplicate.

FTIR spectra of polymer samples were recorded with a Nicolet 4700 FTIR spectrometer. Polymer powders were mixed with KBr and pressed into pellets. All the spectra were recorded in the wavelength range 4000–400 cm^{-1} with 32 scans. NMR spectra of the copolymer samples were recorded with a Bruker 400 MHz NMR spectrometer. NMR spectra of styrene and NaSS homo polymers were recorded in CDCl_3 and D_2O , respectively. Copolymer spectra were recorded using $\text{DMSO}-d_6$ as solvent. Copolymer compositions were estimated from the NMR spectra. Copolymers were precipitated using methanol as non solvent in ice-cold conditions for reactivity ratio determination. Monomer reactivity ratios were determined at less than 10% conversion using the linear graphical method of Fineman–Ross^{33, 34} and Kelen–Tüdös.³⁵

The particle size of colloidal copolymer particles was measured using a DLS (precision MALS) instrument using dilute colloidal dispersions in ethanol medium in a glass cuvette. Particle sizes were obtained as hydrodynamic radius (R_h). The measurements were repeated three times to ensure reproducibility. The particle size was also measured from AFM images. AFM images of dried samples in glass plates were captured using an AFM apparatus (Solver P20M of NT-MDT) working in semi-contact mode. A micro cantilever with a spring constant of 10 Nm^{-1} was used to scan the samples.

Thermo gravimetric and differential thermal analyses (TG-DTA) were carried out with a TG-DTA instrument (Netzsch STA 409PC) from room temperature to 900°C with a scanning rate of $10^\circ\text{C min}^{-1}$ in the presence of nitrogen gas flow. A DSC instrument (Pyris Diamond DSC, Perkin Elmer) was used to measure the glass transition temperature of the samples. The DSC instrument was calibrated using indium and zinc standards before the copolymer samples were scanned. All the samples were kept at 300°C for 20 min, cooled to 30°C at a cooling rate of $200^\circ\text{C min}^{-1}$, equilibrated for 30 min at 30°C and then heated from 30 to 300°C with heating rate of 10°Cmin^{-1} .

4.3. Results and Discussion

4.3.1. Studies of copolymerization kinetics

We studied the copolymerization kinetics of the poly(S-co-NaSS) copolymers with various feed ratios of styrene and NaSS. The percentage conversion *versus* time profiles of the poly(S-co-NaSS) copolymers are shown in Figure 4.1. The conversion *versus* time profile of the polymerization (rate of polymerization) is greatly influenced by the relative feed composition of the monomers (styrene/NaSS). A sharp rise and early saturation of the polymerization rate are observed for higher NaSS concentration in the feed. For example, the conversion increases sharply and saturates in *ca* 45min in the case of the 25/75 (styrene/NaSS) composition, whereas the styrene

homopolymerization (100/0) conversion slowly increases even after 150 min. The rate of copolymerization increases dramatically as the NaSS concentration increases or styrene concentration decreases in the feed. Previously, Turner *et al.*³⁶ also observed the enhancement of the copolymerization rate with increasing NaSS concentration in the feed of a similar copolymerization system. But their study was limited to about 40 mol% NaSS in the feed, whereas we have studied the kinetics for the entire range of compositions from 100/0 to 0/100 (Table 4.1). In contrast to the very high conversion reported by Turner *et al.*³⁶ our kinetics data (Figure 4.1) show low conversion at higher NaSS content. The earlier report did not address the reason behind the high conversion at higher NaSS content. In a recent report³² (chapter 2) we have shown that in case of homogeneous particle nucleation the percentage conversion is low. Since at higher NaSS feed homogeneous particle nucleation takes place (discussed later), low conversion is expected. It is important to note that a quick rise and very early saturation of the conversion with time is observed for the higher NaSS content (Figure 4. 1). This indicates a faster rate of polymerization for the higher NaSS content.

There are three possible reasons for the marked influence of NaSS concentration on the copolymerization kinetics: (i) the gel effect; (ii) the shift of the particle nucleation locus; and (iii) the number of polymer particles (N_p). The gel or Trommsdorff effect arises from the association or crosslinking between polymer chains through sulfur atoms of the sulfonate groups present in the polymer backbone. The incorporation of NaSS in the polymer backbone catalyses the gel effect. The early entry of the polymer particles into the gel state significantly delays the termination process which results in the enhancement of the rate of polymerization²⁹. The quick onset of the gel effect at the initial stage of the copolymerization leads to a very large increase in the polymerization rate^{36, 37}. Although the occurrence of the gel effect in this copolymerization system has been discussed previously,³⁶ the discussion was not supported by experimental evidence. In the next section we prove the association of the polymer chains, which is responsible for the gel effect, using FTIR spectroscopy.

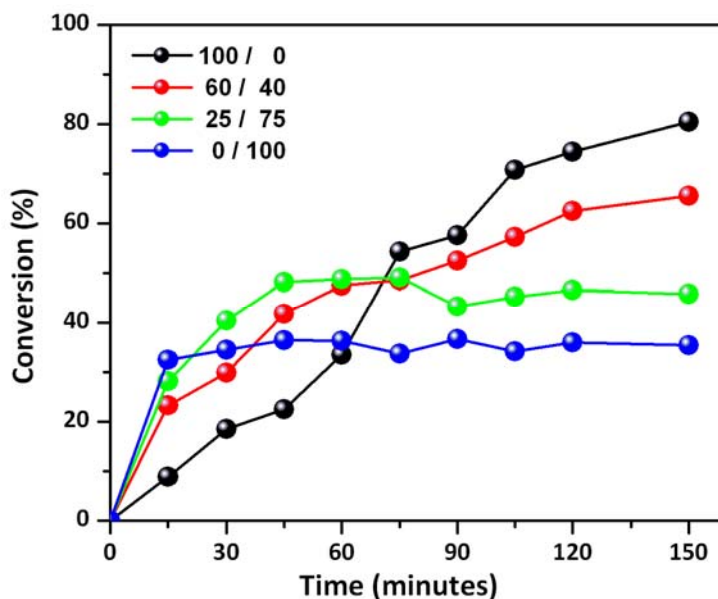


Figure 4.1. Kinetics of emulsion copolymerization of styrene and NaSS for various feed ratios (styrene/NaSS) as indicated.

The second possible explanation for the enhancement of the polymerization rate is the shifting of the locus of particle nucleation. The locus of the polymerization quickly shifts from hydrophobic micellar core (micellar or heterogeneous particle nucleation) to aqueous medium (homogeneous particle nucleation) with decreasing styrene concentration or increasing NaSS concentration in the feed owing to the increased water solubility of the monomers. The rate of homogeneous particle nucleation is always found to be faster than the micellar particle nucleation,^{31, 38} hence the rate of copolymerization increases with increasing NaSS concentration in the feed.

In the case of emulsion polymerization, a faster reaction rate can be achieved by increasing the number of polymer particles formed (N_p).^{29, 32} In this copolymerization system, N_p increases with increasing NaSS content in the feed. For example the N_p value for the 100/0 (styrene/NaSS) sample is $2.27 \times 10^{14} \text{ mL}^{-1}$, whereas it is $15.5 \times 10^{14} \text{ mL}^{-1}$ for the 0/100 (styrene/NaSS) sample. This result clearly indicates that an increase of the polymerization rate with NaSS content is expected. Turner *et al.*³⁶ also

mentioned N_p , but they did not measure N_p values. In a later section we calculate the monomer reactivity ratio of both styrene and NaSS using NMR spectroscopy. We obtained a higher reactivity ratio for NaSS compared to styrene. This suggests that the growing NaSS radical (NaSS*) reacts rapidly with the NaSS in the aqueous phase compared to styrene radicals in the micellar core since styrene has a low reactivity ratio. Because of this micellar nucleation is slower than homogeneous nucleation.

4.3.2. FTIR analysis

The FTIR spectra of the poly(S-*co*-NaSS) particles prepared with various feed compositions are shown in Figure 4.2. The broad peak at 3450 cm^{-1} [Figure 4.2(A)] is due to the O–H stretching vibration of residual water and the SO_3H group.³⁹ This peak becomes stronger and sharper with increasing NaSS content indicating the incorporation of the NaSS monomer in the polymer backbone. The peaks covering the region $2800\text{--}3100\text{ cm}^{-1}$ [dotted ellipse in Figure 4.2(A)] represent various characteristic vibration bands of polystyrene⁴⁰. As the styrene concentration in the feed decreases from 100 to 0%, the vibration bands characteristic of polystyrene gradually disappear. This once again indicates the efficient incorporation of NaSS in the polymer backbone.

The sharp peak around 698 cm^{-1} [Figure 4.2(B)] is due to the out-of plane bending vibration of the aromatic rings. A careful inspection of all the spectra [(Figure 4.2(B))] reveals that this peak disappears gradually with increasing NaSS content in the copolymerization from 100/0 to 0/100. This observation suggests that the out-of-plane bending vibration of the phenyl rings is arrested or suppressed. The gel effect or the association between the sulfonate groups of the polymer chains arises at higher NaSS content which prevents the out-of-plane bending vibration of the phenyl rings. The polymer chains become more rigid due to the association of the sulfonate groups and restrict the true vibrations of the aromatic rings. Yang *et al.*⁴¹ reported that the peak around 756 cm^{-1} is the characteristic peak of the out-of-plane bending vibration of C–H groups in the mono-substituted benzene ring. The peak at 756 cm^{-1} gradually decreases

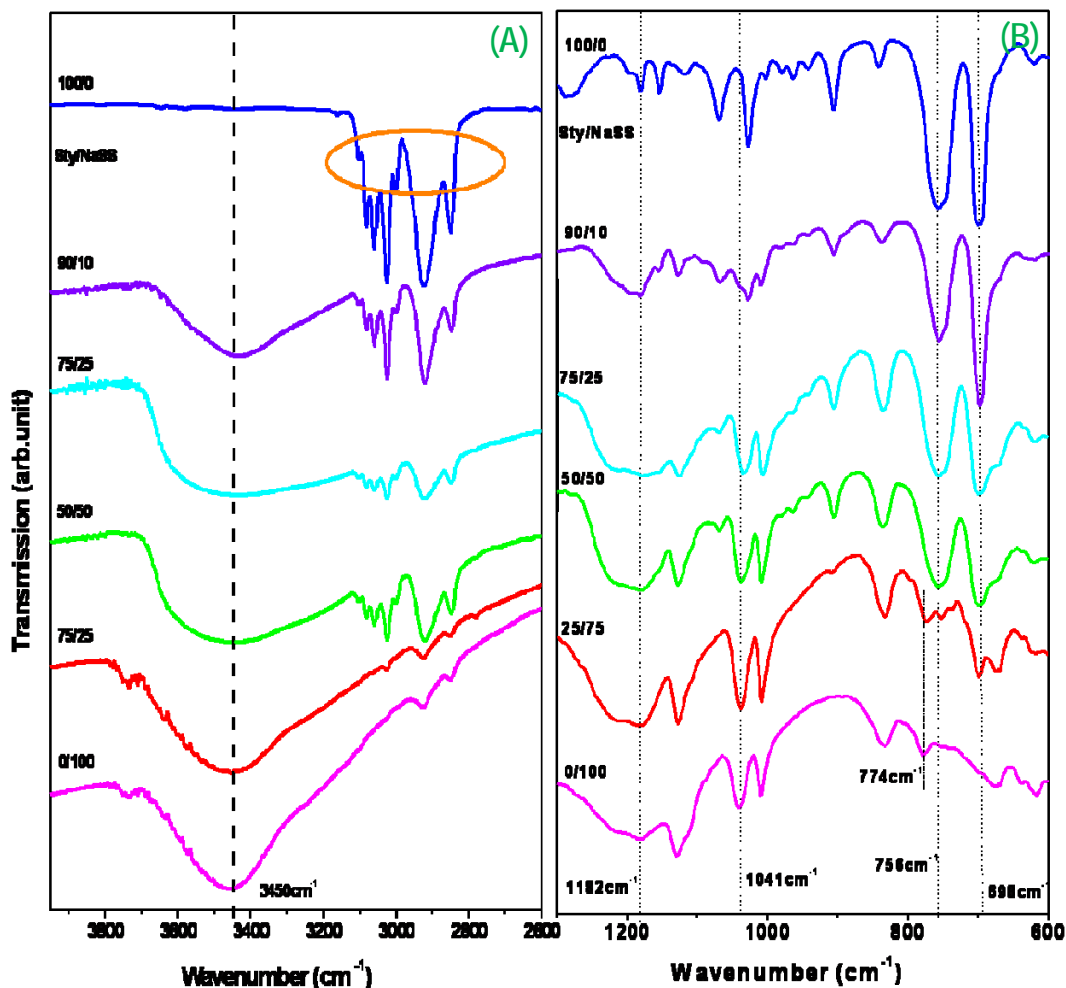


Figure 4.2. FTIR spectra for (A) 4000–2600 cm^{-1} and (B) 1300–600 cm^{-1} of poly(S-co-NaSS) copolymers for various feed ratios (styrene/NaSS) as indicated.

in intensity with increasing NaSS content and finally disappears for 100% NaSS. A new peak starts appearing at 774 cm^{-1} from 25/75 feed ratio onwards. This observation once again supports our argument of sulfonate group association. Because of this association the C–H vibrations lose their freedom and are not allowed to vibrate as freely as they do in the case of styrene. The peak at 756 cm^{-1} is shifted to 774 cm^{-1} in

case of 100% NaSS due to the maximum gel effect which makes C–H bonds shorter and stronger and so they vibrate at higher frequency. The peak around 1041 cm^{-1} represents the symmetric stretching vibration of the SO_3 groups which increases in intensity with NaSS content. The relatively broad peak around 1182 cm^{-1} represents the asymmetric vibration of the SO_3 group which increases gradually with NaSS content.

4.3.3. NMR studies and reactivity ratios

The copolymer composition in the polymer backbone has a great influence on the copolymer properties. The monomer feed ratio and the reactivity of the monomers predict the copolymer composition⁴². Therefore it is absolutely necessary to estimate the monomer reactivity parameters to get a clear picture of the polymerization behaviour and the composition of the resulting copolymer. The determination of reactivity ratios in emulsion copolymerization for various monomer pairs have been reported in the literature by several authors^{43, 44}. The reactivity ratios for the styrene–NaSS pair were obtained below 10% conversion. Aromatic-region ^1H NMR spectra of all copolymers are shown in Figure 4. 3 along with the copolymer structure (inset) and the peak assignments. Figure 4.3 shows that the intensity of peak C increases with increasing NaSS content in the copolymerization and peak B slowly disappears. The effect of NaSS incorporation into the polymer backbone can be clearly seen from the NMR spectra. Analysis of the relative peak intensities of the NMR spectra of the copolymers gives an idea about the reactivity of the monomers in the copolymerization. The intensity of peak B (I_B) decreases and that of peak C (I_C) increases as NaSS in the feed increases. The ratio of I_C to I_B is proportional to the NaSS composition in the copolymer backbone. Let us consider X as the mole fraction of NaSS monomer in the polymer backbone. Different peak intensities of poly(S-co- NaSS) can be related to the NaSS mole fraction: $I_B = 3(1 - X)$ and $I_C = 2X$. If β is the ratio of peak C to peak B ($\beta = I_C/I_B$), the NaSS composition (X) in the backbone can be determined from the NMR results by employing the equation $X = 3\beta / (3\beta + 2)$ ²⁶. The peak intensities of peaks B and C are

obtained from the integrated areas of peaks B and C in Figure 4. 3, and are given in Table 4.2.

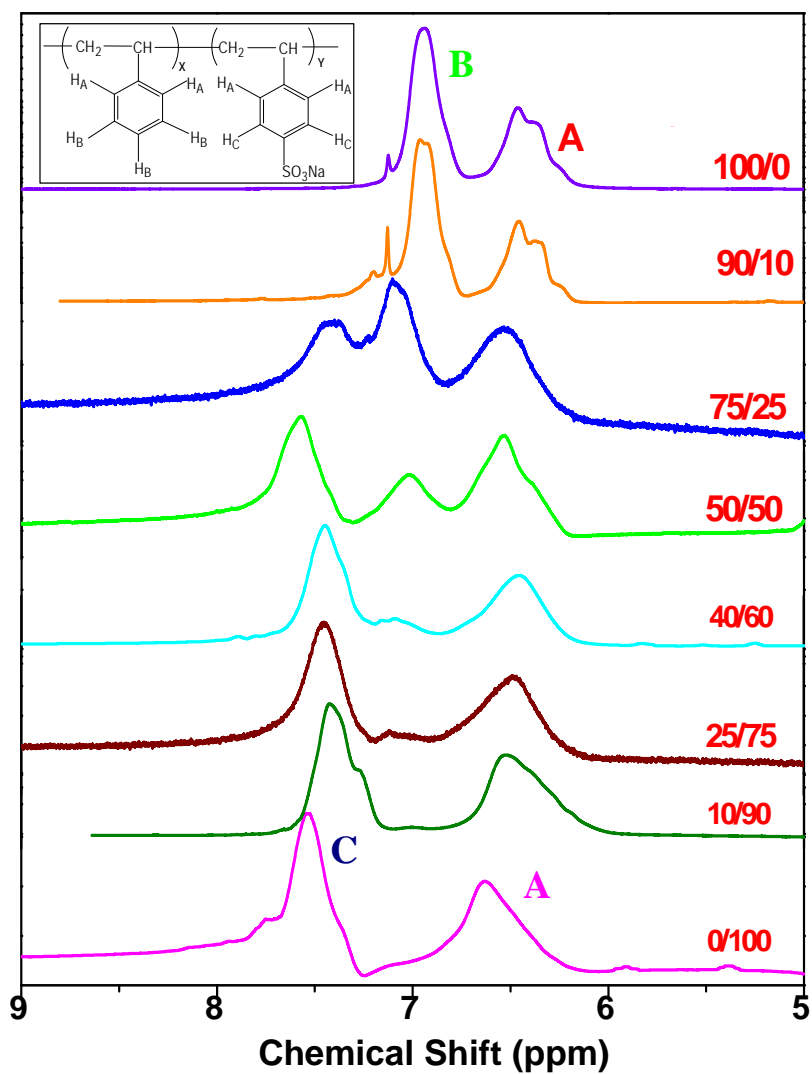


Figure 4.3. NMR spectra of poly(S-co-NaSS) copolymers for various monomer feed ratios (styrene/NaSS) as indicated. The inset shows the chemical structure of the poly(S-co-NaSS) along with the peak assignments.

Table 4.2: NMR peak intensities of copolymer protons H_B , H_c and the mole fraction of NaSS monomer in the copolymer.

Feed ratio Sty/NaSS (% w/w)	I_B	I_c	$\beta = I_c/I_B$	$X = 3\beta/(3\beta+2)$
90/10	0.71	0.04	0.056	0.078
75/25	0.32	0.18	0.5625	0.46
50/50	0.31	0.62	2.000	0.75
40/60	0.18	0.67	3.63	0.85
25/75	0.09	0.65	7.222	0.92
10/90	0.03	0.67	22.33	0.97

Monomer compositions in the feed and in the copolymer (estimated from NMR data) are presented in Table 4.3, in which f_1 , f_2 , F_1 and F_2 are the mole fractions of styrene and NaSS, respectively, in the feed and in the copolymer, respectively. The data of Table 4.3 are plotted in Figure 4.4 to investigate the deviation in the copolymer composition from the feed. The dotted line in the Figure 4.4 is the ideal situation where copolymer compositions are exactly identical to those of the monomers in the feed. In the present copolymerization system, NaSS monomer shows positive deviation (Figure 4.4) and styrene monomer exhibits negative deviation (Table 4.3) from the ideal situation.

Table 4.3. Compositions of the feed and actual composition in the copolymer.

Feed ratio S/NaSS (% w/w)	S, f_1	NaSS, f_2	S, F_1	NaSS, F_2
90/10	0.95	0.053	0.922	0.078
75/25	0.86	0.14	0.54	0.46
50/50	0.66	0.34	0.25	0.75
40/60	0.57	0.43	0.15	0.85
25/75	0.40	0.60	0.08	0.92
10/90	0.18	0.82	0.03	0.97

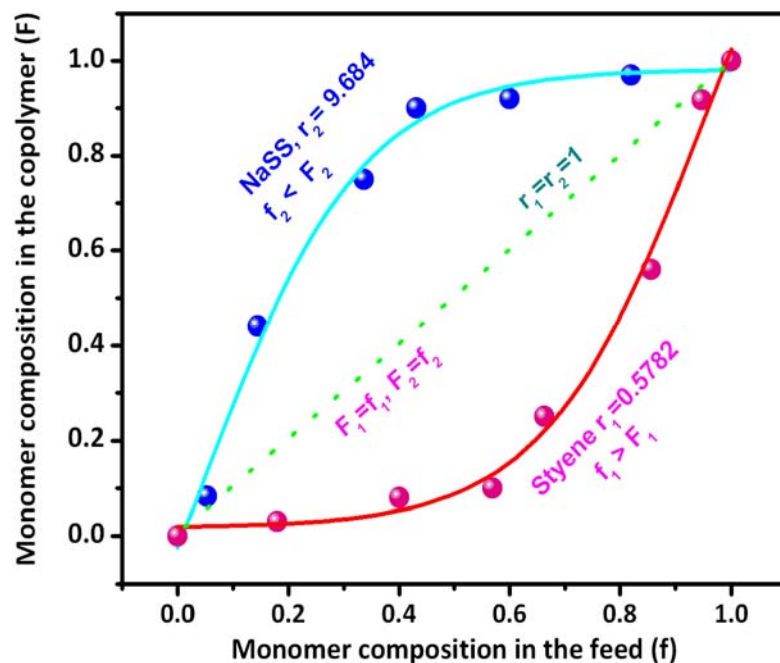
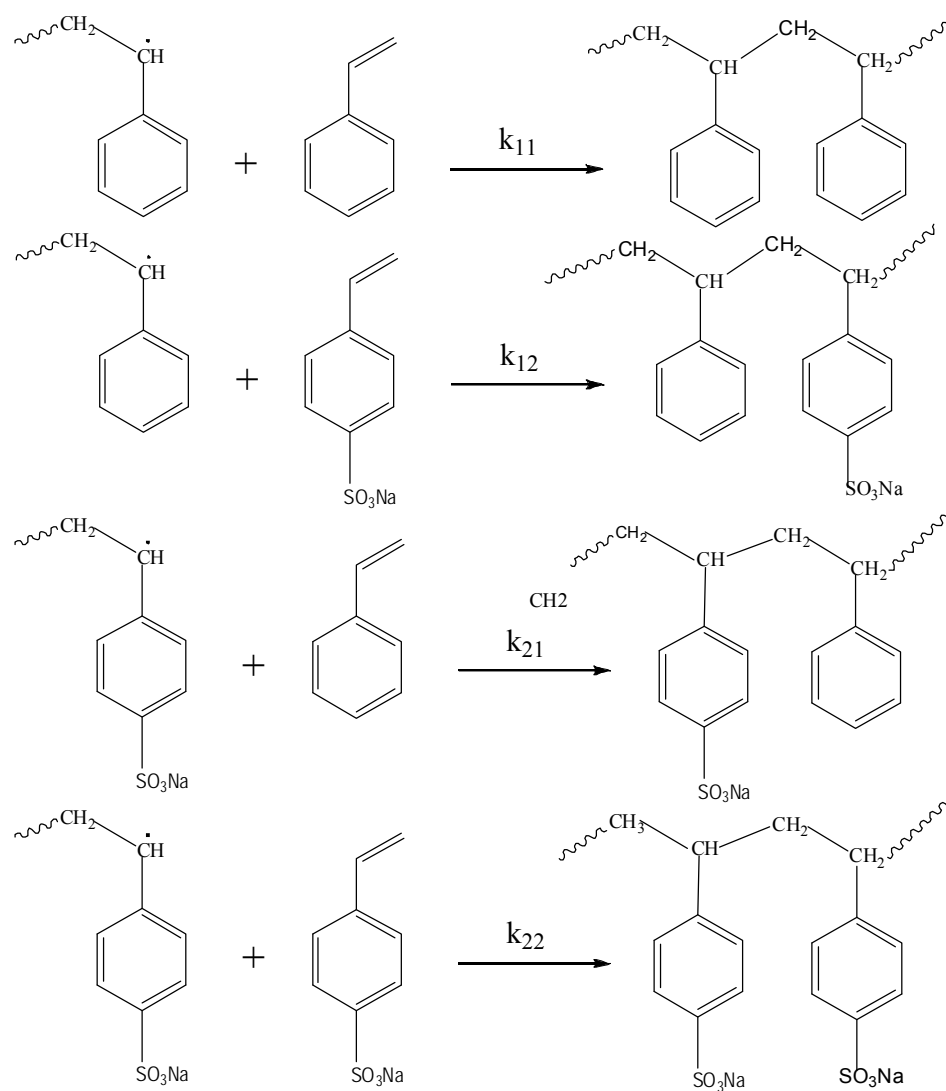


Figure 4.4. Deviation of comonomer (NaSS) composition from the feed in poly(S-co-NaSS) copolymers measured by ^1H NMR spectroscopy.

It is evident from the above analysis (Figure 4.4 and Table 4.3) that the mole fraction of styrene in the copolymers is less than that of styrene in the feed ($f_1 > F_1$); the reverse is true for NaSS ($f_2 < F_2$). These deviations hint that there is large difference in the reactivity ratios between styrene (r_1) and NaSS (r_2). If the two monomers have equal reactivity towards both the propagating radicals ($r_1 = r_2 = 1$) then the composition of the copolymer would always be equal to the composition of the feed ($F_1 = f_1$, $F_2 = f_2$) and the dotted line in Figure 4.4 results²⁹. The deviations mentioned above once again strengthen our argument for the enhancement in the reaction rate and thus the shift in the locus of the polymerization after the introduction of NaSS in the polymerization medium.

We used the Fineman–Ross^{33, 34} and Kelen–Tüdös³⁵ methods to determine the monomer reactivity ratios. In the copolymerization, two homo-propagations (where a

propagating radical adds to its own monomer) and two cross-propagations (where a propagating monomer radical adds to another monomer) are possible (Scheme 4.2).



Scheme 4.2. Possible propagation kinetics that take place during the copolymerization of styrene and NaSS.

Parameters k_{11} and k_{22} are the rate constants for homo propagations of styrene and NaSS radicals, respectively; k_{12} and k_{21} are the rate constants for cross-propagations

of styrene and NaSS propagating radicals with NaSS and styrene, respectively (Scheme 4.2). These rate constants, the copolymer composition and the monomer reactivity ratios are related to each other and can be represented using various well-known equations such as the Fineman–Ross equation [equation (4.1)] and the Kelen–Tüdös equation [equation (4.2)]. The former is written as

$$\frac{f_1(F_1 - F_2)}{f_2 F_1} = \left(\frac{F_2 f_1^2}{F_1 f_2^2} \right) r_1 - r_2 \quad (4.1)$$

$$\text{or, } G = r_1 H - r_2$$

$$\text{where, } G = \frac{f_1(F_1 - F_2)}{f_2 F_1} \text{ and } H = \left(\frac{F_2 f_1^2}{F_1 f_2^2} \right)$$

In the Fineman–Ross equation, r_1 and r_2 represent the monomer reactivity ratios of styrene and NaSS, respectively. Kinetically, $r_1 = k_{11}/k_{12}$ and $r_2 = k_{22}/k_{21}$. Hence a plot of G versus H gives the values of r_1 and r_2 from the slope and intercept, respectively (Figure 4.5). The values of r_1 and r_2 are listed in Table 4.4. In Figure 4.6 we plot η versus ξ according to the Kelen–Tüdös equation [equation (4.2)], where the linearization method has been rearranged and an arbitrary positive constant ‘ α ’ is introduced to obtain the form,

$$\eta = \left(r_1 + \frac{r_2}{\alpha} \right) \xi - \frac{r_2}{\alpha} \quad (4.2)$$

where $\eta = G/(\alpha + H)$, $\xi = H/(\alpha + H)$ and $\alpha = (F_m F_M)^{1/2}$, in which F_m and F_M are the lowest and highest values of F , respectively. A plot of η versus ξ yields the values of r_2 and r_1 . The values of r_2 and r_1 obtained from Figure 4.6 are listed in Table 4.4.

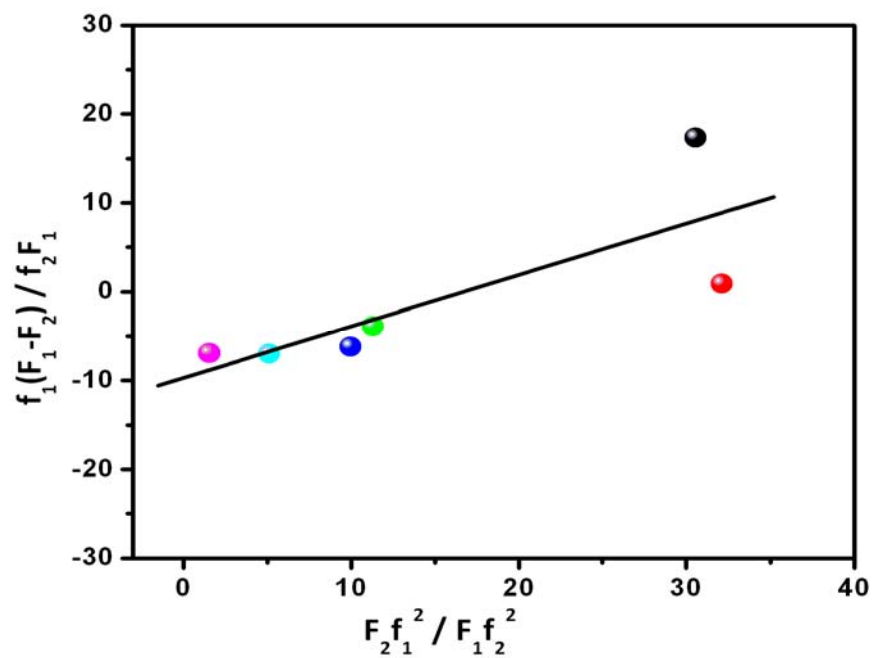


Figure 4.5. Fineman–Ross plot for styrene and NaSS copolymerization.

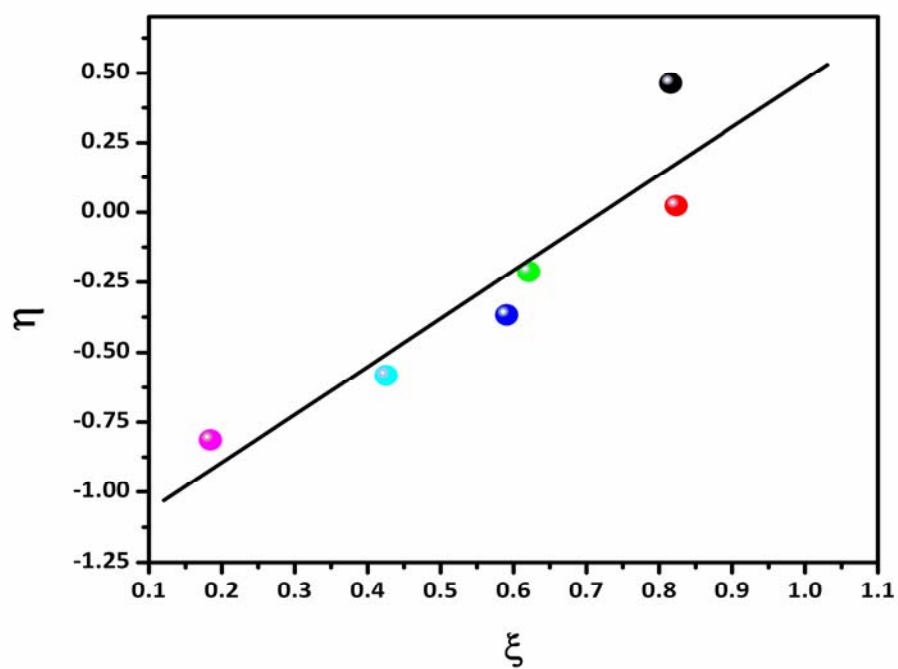


Figure 4.6. Kelen–Tüdös plot of styrene and NaSS copolymerization

Table 4.4. Monomer reactivity ratios r_1 and r_2 , obtained from two different well known methods

Method	r_1	r_2	$1/r_1 = k_{12}/k_{11}$	$1/r_2 = k_{21}/k_{22}$
Fineman-Ross Method	0.58	9.68	1.72	0.10
Kelen-Tudos Method	0.49	8.54	2.04	0.12

The larger reactivity ratio of NaSS (r_2) over that of styrene reveals that propagating NaSS radicals preferentially add to NaSS monomer rather than styrene monomer. In comparison, the reactivity ratio of styrene (r_1) is less than unity and largely lower than r_2 . This indicates that styrene homopolymerization is not preferred compared to styrene and NaSS copolymerization. In other words, the rate of styrene homopolymerization is slower than that of styrene and NaSS copolymerization. These observations explain the negative deviation in Table 4.3 in case of styrene. The value of r_2 is 16.69 ($r_2/r_1 = 16.69$, according to the Fineman–Ross method) and 17.43 ($r_2/r_1 = 17.43$, according to the Kelen–Tüdös method) times bigger than r_1 . Therefore we can state that in this copolymerization system NaSS is *ca* 17 times more reactive than styrene. The $1/r_1$ values in Table 4.4 indicate that styrene prefers to undergo copolymerization with NaSS rather than homopolymerization. On the other hand, the $1/r_2$ values in Table 4.4 indicate that NaSS prefers to undergo homopolymerization rather than copolymerization. Hence NaSS homopolymerization is *ca* 10 times faster than copolymerization and styrene copolymerization is only *ca* 2 times faster than homopolymerization.

4.3.4. Particle size

The dependence of particle size on the NaSS mole fraction (feed) in the copolymer obtained from the DLS study is shown in Figure 4.7. Initially (up to 0.14 mol

fraction) the particle size decreases with increasing NaSS concentration and then it suddenly increases with increasing NaSS (up to 0.34 mol fraction). Further increase of NaSS concentration in the feed decreases the particle size (Figure 4.7). The initial decrease of particle size with increasing NaSS concentration (up to 0.14 mol fraction, i.e. 75/25 feed composition) is due to the smaller number of monomers entering the micellar core because of the enhanced solubility of monomers in water. The sudden shift of the particle size in the composition range 0.14–0.34 (Figure 4.7) is quite interesting and can be explained in the light of particle nucleation (locus of polymerization) mechanism. Our kinetics studies reveal that the locus of the polymerization shifts from the micellar core to the aqueous medium (homogeneous particle nucleation), where particles grow on the emulsifier-stabilized oligomeric species, after 75/25 (0.14 mol fraction) composition. Since the size of the oligomeric

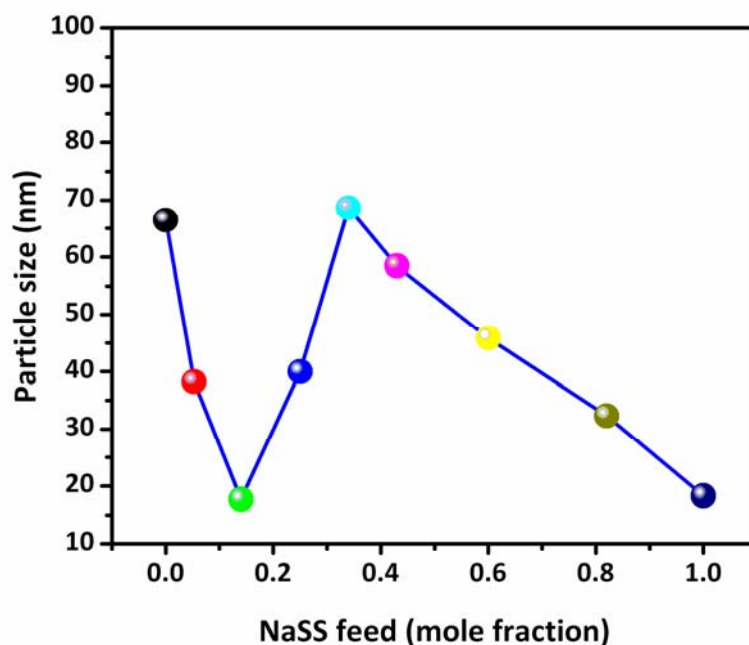


Figure 4.7. Variation of particle size as a function of NaSS mole fraction in the copolymers.

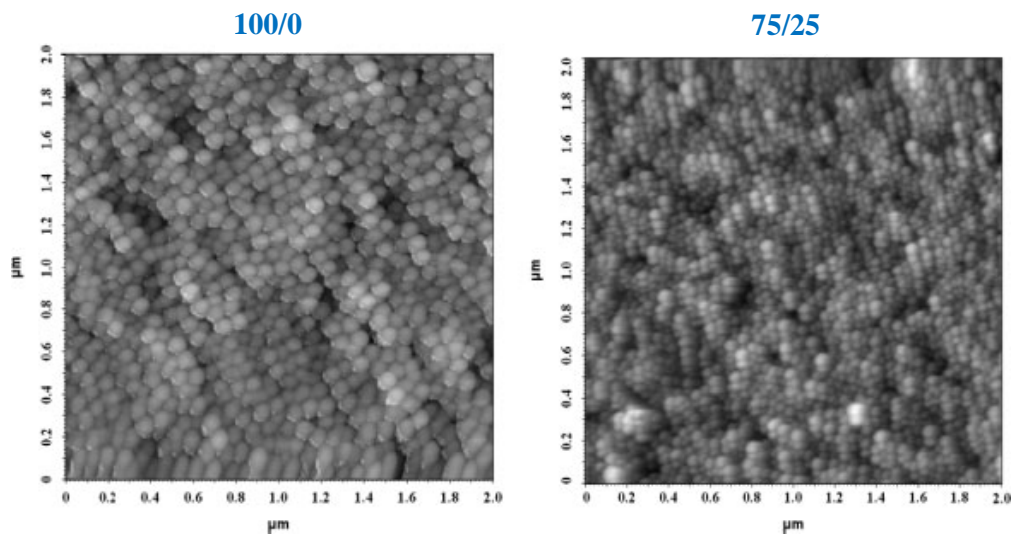


Figure 4.8. *AFM micrographs of copolymers with various monomer feed ratios (styrene/NaSS) as indicated.*

spheres is bigger than the micelle, the particle size increases after 75/25 composition. Again after 50/50 (0.34 mol fraction) composition particle size gradually decreases (Figure 4.7) because a greater number of smaller size emulsifier-stabilized oligomeric particles are formed. Figure 4.8 shows AFM images of the copolymer particles. All the particles are spherical in nature as evident from the images.

4.3.5. Thermal studies of the copolymers

The thermal stability of the copolymer particles was determined using TG-DTA in nitrogen atmosphere. The determination of thermal stability is important because of the potential application of the system under study as thermally stable materials in various areas. The TGA thermograms of the copolymers are shown in Figure 4.9. The derivatives of these thermograms are shown in Figure 4.10. Two weight losses are observed for all samples (Figure 4.9): one around 100°C and the second above 400°C. The first weight loss is associated with absorbed moisture and the second with the decomposition of the polymers. Larger weight losses are observed at 100°C for a higher

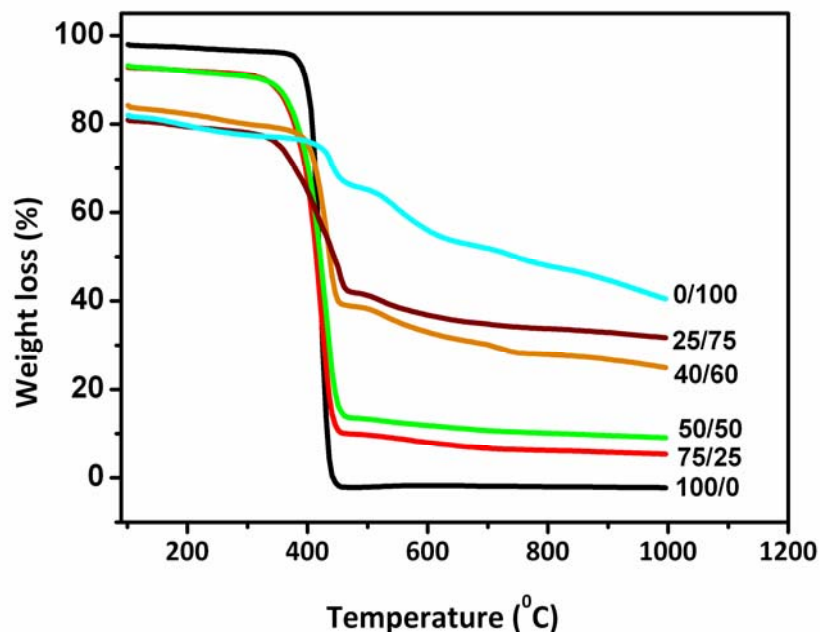


Figure 4.9. TGA thermograms of copolymers for various compositions (styrene/NaSS) as indicated.

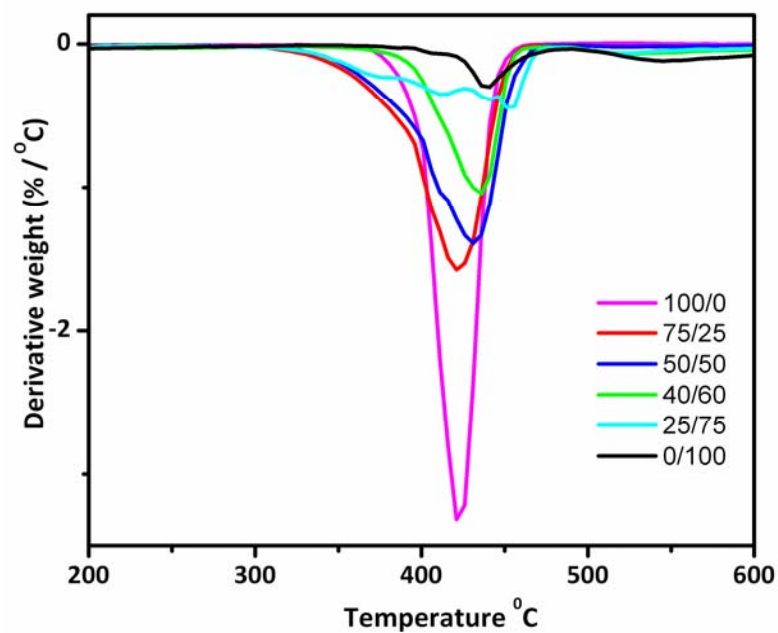


Figure 4.10. TG-DTA curves of copolymers for various compositions (styrene/NaSS) as indicated.

NaSS content in the copolymer, although the drying procedures for all samples were similar (Figure 4.9). This proves that the copolymer becomes more hygroscopic with increasing NaSS content. The derivative curves of the TGA thermograms presented in Figure 4.10 show that the polymer degradation temperature increases with increasing NaSS content in the copolymer. These observations mean that there is a significant enhancement of thermal stability of the copolymer with higher NaSS content.

The glass transition temperature (T_g) of all copolymer samples were determined using DSC. Figure 4.11 shows representative DSC thermograms of various copolymer samples. The measured T_g of 100% (100/0) polystyrene and 100% (0/100) poly(NaSS) are 104 and 220 °C, respectively. The higher T_g of poly(NaSS) is expected because of its lower flexibility owing to $-\text{SO}_3\text{H}$ groups. T_g of the copolymers increases with the increasing NaSS content in the copolymer, as shown in Figure 4.12. The segmental mobility of the polymer chains are reduced with increasing NaSS content in the copolymer because of ionic interactions. Therefore, T_g increases with increasing NaSS content. However, at very low mole fraction of NaSS, T_g is lower than T_g of 100% polystyrene. This result is consistent with previous reports^{25, 45} where authors explained this observation as a result of competing influences of the sulfonate pendent groups. Weiss *et al.*²⁵ suggested a two-phase material consisting of a styrene-rich phase and a NaSS-rich phase based on their observation of the constancy of T_g with composition and a second T_g at higher temperature for the NaSS-rich phase. In contrast to the previous report,²⁵ our DSC studies show a gradual increase of T_g with composition (Figure 4.12) and we have not observed any second T_g at higher temperature for our copolymer samples (Figure 4.11).

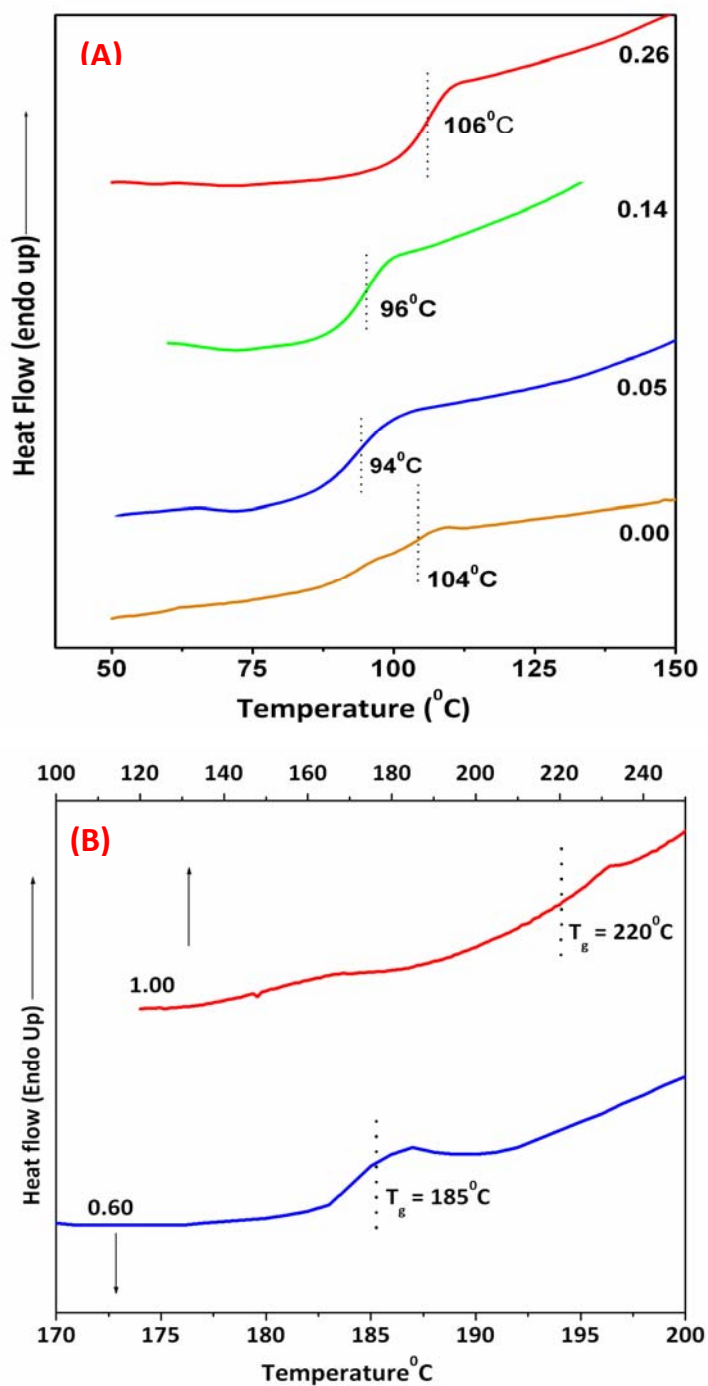


Figure 4.11. DSC thermograms of poly(S-co-NaSS) for the indicated NaSS content in the feed (mole fraction) (A) 0.00–0.26, and (B) 0.6–1.00

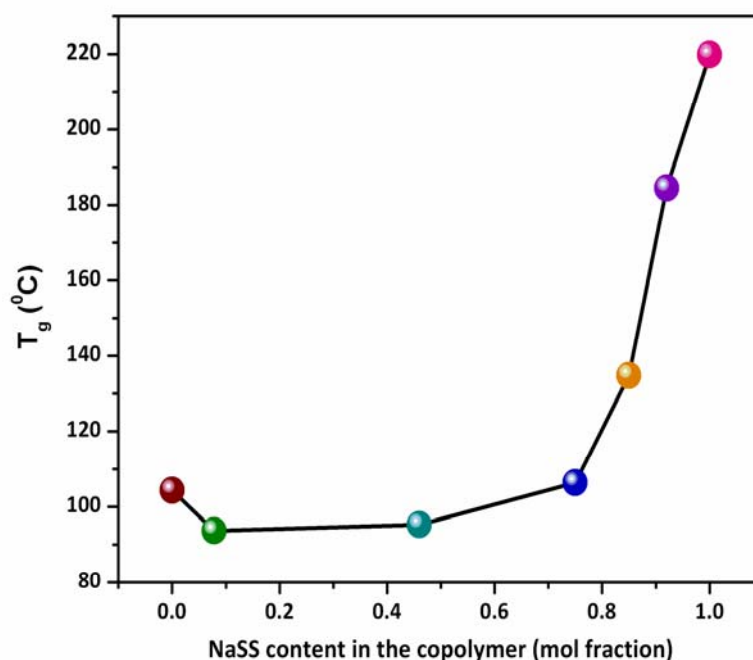


Figure 4.12. Variation of glass transition temperature (T_g) with NaSS content in the poly(S-co-NaSS) copolymers.

4.4. Conclusion

A series of poly(S-co-NaSS) copolymers containing various NaSS loadings have been synthesized using emulsion polymerization. The copolymerization kinetics are significantly influenced by the monomer feed ratio and are greatly enhanced with increasing NaSS content in the reaction. The gel effect, the shift of particle nucleation locus and the increase in the number of particles are found to be the driving force for the enhancement of the polymerization kinetics. FTIR studies demonstrate the occurrence of association of the polymer chains due to $-\text{SO}_3\text{H}$ groups which results in the gel effect. NMR spectroscopy has been used to determine the monomer composition in the copolymers and the monomer reactivity ratios. Styrene monomer reactivity ratio is less than unity, whereas that of NaSS is very high. The monomer reactivity ratio values

suggest that the NaSS selectively adds to NaSS rather than styrene, whereas styrene prefers to react with NaSS over its own monomer. Monomer reactivity ratios demonstrated that the styrene copolymerization is nearly twice as fast as the homopolymerization, whereas NaSS homopolymerization is nearly ten times faster than copolymerization with styrene. The particle size varies with the NaSS content in the copolymer. The variations of particle size have been explained in the light of the particle nucleation mechanism. TGA studies showed that the thermal stability increases markedly for higher NaSS content. The glass transition temperature depends upon the copolymer composition.

References

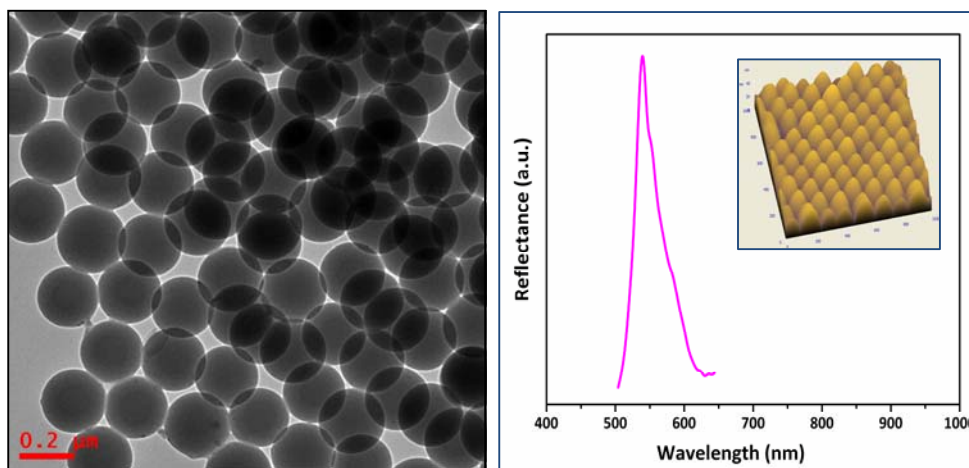
1. Koyama, K.; Otsu, T.J. *Macromol. Sci. Chem.A.* **1974**, 8, 1295.
2. Aoki, S.; Otsu, T.; Imoto, M. *Makromol. Chem.* **1966**, 99, 133.
3. Kim, J. H.; El-Aasser, M. S.; Klein, A.; Vanderhoff, J.W. *J. Appl. Polym. Sci.* **1988**, 35, 2117.
4. Djinoovic, V. M.; Antic, V. V.; Djonlagic, J.; Govedarica, M. N. *React. Funct. Polym.* **2000**, 44, 299.
5. Malini, K. A.; Anantharaman, M. R.; Sindhu, S.; Chinnasamy, C.N.; Ponpandian, N.; Narayanasamy, A. *J. Mater. Sci.* **2001**, 36, 821.
6. Boardman, N. K. *J. Chromatogr. A.* **1959**, 2, 398.
7. Hanai, T.; Walton, H.F. *Anal. Chem.* **1977**, 49, 764.
8. Hong, L.; Chen, N. *J. Polym. Sci. Part B. Polym. Phys.* **2000**, 38, 1530.
9. Chen, N.; Hong, L. *Solid State Ionics* **2002**, 146, 377.
10. Chen, N.; Hong, L. *Polymer* **2004**, 45, 2403.
11. Chen, S. L.; Krishnan, L.; Srinivasan, S.; Benziger, J.; Bocarsly, A. B. *J. Membr. Sci.* **2004**, 243, 327.
12. Oren, Y.; Fregen, V.; Linder, C. *J. Membr. Sci.* **2004**, 239, 17.
13. Foldes, R. G.; Himm, R. E.; Levinson, S. L.; Hand, D. W. *Fertil. Steril.* **1986**, 45, 550.
14. Himm, R. E.; Foldes, R. G.; Hand, D.W. *Contraception* **1985**, 32, 267.
15. Zeitlin, L.; Whaley, K. J.; Hegarty, T. A.; Moench, T. R.; Cone, R. A.; *Contraception* **1997**, 56, 329.
16. Herold, B. C.; Nigel, B.; Marcellin, D.; Kirkpatrick, R.; Strauss D. M.; Zaneveld L. J. D. *J. Infect. Dis.* **2000**, 181, 770.
17. Kim, J. S.; Eisenberg, A. *Ionomers* Wiley Interscience: New York, 1998.
18. Tant, M. R.; Mauritz, K. Aand Wilkes, G.L.(eds), *Ionomers: Synthesis, Structure, Properties and Applications.*; Chapman & Hall: London, 1997.
19. Bazuin, C.G.; Eisenberg, A. *Ind. Eng. Chem. Prod. Res. Dev.* **1981**, 20, 271.
20. Förster, S.; Schmidt, M. *Adv. Polym. Sci.* **1995**, 120L, 51.

21. Williams, C. E.; *Highly charged polyelectrolytes: experimental aspects, in Electrostatic Effects in Soft Matter and Biophysics*, Holm, C.; Kékicheff, P.; Podgornik, R. (eds.,) Kluwer: Dordrecht, 2001.
22. Schmitt-Kopplin, P.; Garrison, A. W.; Perdue, E. M.; Freitag, D.; Kettrup, A. *J. Chromatogr. A* **1998**, 807, 101.
23. Schmitt-Kopplin, P.; Garmash, A. V.; Kudryatsev, A. V.; Perminova, I.; Hertkorn, N.; Freitag, D. *J. AOAC. Int.* **1999**, 82, 1594.
24. Radlinska, E. Z.; Gulik-Krzywicki, T.; Lafuma, F.; Langevin, D.; Urbach, W.; Williams, C. E.; in *Short and Long Chains at Interfaces*, Daillant, J.; Guenoun, P.; Marques, C.; Muller, P.; Trần Thanh Văn, J.(eds.), Editions Frontières: Gif-sur-Yvette-Cedex, France, 1995, pp. 251–256.
25. Weiss, R. A.; Lundberg, R. D.; Turner, S. R. *J. Polym. Sci. Polym. Chem. Ed.* **1985**, 23, 549.
26. Baigl, D.; Seery, T. A. P.; Williams, C.E. *Macromolecules*, **2002**, 35, 2318.
27. Tran, Y.; Auroy, P.; *J. Am. Chem. Soc.* **2001**, 123, 3644.
28. Weiss, R. A.; Turner, S. R.; Lundberg, R. D. *J. Polym. Sci. Polym. Chem. Ed.*, **1985**, 23, 525.
29. Odian, G. *Principles of Polymerization*, 4th edn. John Wiley: New York, 2004.
30. Andre, A.; Henry, F.; *Colloid Polym.Sci.* **1998**, 276, 1061.
31. Chern, C.S.; *Prog. Polym.Sci.* **2006**, 31, 443; and references therein.
32. Arunbabu, D.; Sannigrahi, A.; Jana, T. *J App. Polym. Sci.* **2008**, 108, 2718.
33. Mayo, F. R.; Lewis, F. M. *J. Am. Chem. Soc.* **1944**, 66, 1594.
34. Fineman, M.; Ross, S. D. *J. Polym.Sci.* **1950**, 2, 259.
35. Kelen, T.; Tüdös, F. *J. Macromol. Sci. Chem.* **1975**, 1, 1.
36. Turner, S. R.; Weiss, R. A.; Lundberg, R. D. *J. Polym. Sci. Polym. Chem. Ed.* **1985**, 23, 535.
37. Kim, J.H.; Chainey, M.; El-Aasser, M. S.; Vanderhoff, J. W. *J. Polym. Sci. Polym. Chem.* **1992**, 30, 171.
38. Yeliseyeva, V. I. *Polymerization of polar solvents*, in *Emulsion Polymerization*, Piirma I, (ed.,) Academic Press: New York (1982).

39. Brijmohan, S. B.; Swier, S.; Weiss, R. A.; Shaw, M. T. *Ind. Eng. Chem. Res.* **2005**, *44*, 8039.
40. Bhutto, A. A.; Vesely, D.; Gabrys, B. J. *Polymer* **2003**, *44*, 6627.
41. Yang, J. C.; Jablonsky, M. J.; Mays, J. W.; *Polymer* **2002**, *43*, 5125.
42. Sannigrahi, A.; Arunbabu, D.; Sankar, R. M.; Jana, T. *J. Phys. Chem. B* **2007**, *111*, 12124.
43. Reddy, G. V. R.; Devi, N. G.; Panda, J. J. *J. Appl. Polym. Sci.* **2007**, *105*, 3391.
44. Sanghvi, P. G.; Patel, A. C.; Gopalkrishnan, K. S.; Devi, S. *Eur. Polym. J.* **2000**, *36*, 2275.
45. Weiss, R. A.; Lenz, R. W.; MacKnight, W. J. *J. Polym. Sci. Polym. Phys. Ed.* **1978**, *16*, 1101.

Chapter 5

Emulsion Copolymerization of Styrene: Effect of Ionic Comonomer Structure



A series of emulsion copolymerizations of styrene with variety of ionic comonomers are carried out by varying surfactant concentration. The effect monomer structure on copolymerization kinetics and copolymer properties are studied.

5.1. Introduction

Synthesis of charged highly monodisperse polymer colloidal particles have drawn huge attention in recent years due to their wide range of applications in various fields such as paint technology, drug and DNA delivery, microscopy and optics and have been a fascinating field of research^{1,2}. Functionalized particles with desirable functional groups on the surface of the particles have found huge applications in immunoassays^{3,4} protein separation⁵ and drug delivery systems⁶. Carboxylated micro and nanospheres prepared by polymerizing styrene with acrylic acid (AAc) and methacrylic acid (MAA) have been immobilized with Pd and Rh metal nanoparticles and are used in industrial hydrogenation⁷. Sulfonated polystyrene colloids have found application in medicinal fields^{8,9}, catalysis^{10,11}, water purification systems, PEM fuel cell membranes^{12,13} and polymeric template assisted metal nanoparticle synthesis¹⁴. Highly surface charged monodisperse particles tend to self assemble into non close packed structures such as FCC and BCC which diffract visible light according to Bragg's law¹⁵. In literature these self assembled structures are well known as crystalline colloidal array (CCA). Strong electrostatic repulsions drive the highly charged monodispersed particles to arrange in less energetic non close packed structures such as body centered cubic (BCC) and face centered cubic (FCC)^{16,17,18,19,20}. The driving force of this self assembly is high surface charge of particles, high dielectric constant of medium, and low concentration of ionic impurities. Asher et. al. showed that this CCA can be embedded in three dimensional hydrogel networks which is called polymerized crystalline colloidal array (PCCA)²¹. These PCCA materials upon hydrolysis and coupling with certain ligands, enzymes, have found huge applications in chemo and biosensing²². These smart sensing materials when treated with certain analytes undergo volume phase transition which changes the distance between the colloidal particles (d) in the lattice. Hence the diffraction change is measured and correlated with the concentration of analyte metal ion or enzyme substrate. The diffraction changes are triggered by hydrogel swelling or shrinking by external stimuli such as pH, ionic strength, and change in the solvent medium resulting through the interaction of coupled ligand or enzyme with the analyte²¹⁻²³. Asher et. al.

engineered a large variety of smart sensing PCCA materials which can sense and detect various biologically important analytes such as glucose²⁴ and creatinine²⁵ and has developed chemosensing materials for the sensing of Cu^{2+} ²⁶, Pb^{2+} ²⁷ and ammonia²⁸. Therefore, it remains a challenge to prepare robust particles with high surface charge by incorporating appropriate amount of ionic comonomer. If the charge is more it may destabilize the particle and lead to agglomeration whereas low surface charge leads to coagulation.

Monodisperse polymer particles are typically prepared by various heterogeneous polymerization procedures including emulsion^{29, 30}, suspension³¹, precipitation³², and dispersion³³ polymerizations. Among these techniques, the emulsion polymerization process has several advantages which make it a fascinating field in the synthesis of polymers of narrow particle size and narrow molecular weight with desirable physical and chemical properties. Conventional emulsion polymerization involves polymerization in an emulsion generated by emulsifying hydrophobic monomers such as styrene with the help of surfactants, after which the initiation is triggered with an addition either water soluble initiator like ammonium persulphate (APS) or oil soluble initiator like (AIBN)³⁴. In these systems particle formation is mainly through two mechanistic pathways (1). micellar nucleation which takes place in monomer swollen micelles (2). homogenous nucleation and a minor pathway is coagulative nucleation. Homogeneous nucleation requires sufficient amounts of surfactant and it becomes negligible if the polymerization occurs above the critical micellar concentration (CMC). Micellar nucleation involves processes which includes the formation of seed latex or precursor particle by diffusion of oligomeric radicals and polymerization of monomer inside the micelle. Nucleation of seed particle occurs through the absorption of monomer from reservoir droplets and the stabilization of particles by surfactant^{35, 36}. Since all the initial seed particles share equal amount of monomer the particles obtained will be similar in size and number. If other parameters such as monomer concentration, initiator temperature and the amount of water are fixed then particle size increases with

the decrease in emulsifier concentration since the number of micelles formed is the function of the later^{29, 37}.

In the preceding chapters (chapter 2 & 3) we have studied the effect of surfactant concentration on particle size, polymerization kinetics and charge density above and below the CMC region^{38, 39}. We have observed the dependence of polymer properties upon surfactant concentration is more below CMC whereas comparatively it is insignificant above the CMC of surfactant. In case of emulsion copolymerization particle size and polymer properties have been found to vary as a function of comonomer concentration, initiator concentration, stirring speed and temperature apart from emulsifier concentration. Among these the chemical incorporation of ionic comonomer offered versatility to emulsion copolymerization yielding particles with surface charged groups with desirable properties dramatically enhancing the polymerization reaction and providing stability to the product particles. When introduced a trace amount of water soluble ionogenic comonomers such as acrylic acid and methacrylic acid alters the kinetics of emulsion copolymerization alters dramatically^{40, 41}. The water soluble hydrophilic comonomer shifts the locus of the polymerization from micellar core to aqueous medium and the proportion of these two nucleations is proportional to the extend solubility quantity and the structure of the ionic comonomer^{35, 36, 42}. In chapter 4, we have studied the emulsion polymerization of sparingly water soluble monomer (styrene) and a water-soluble monomer (NaSS) in various compositions (100/0 to 0/100) where we have found out the reaction kinetics, monomer reactivity ratios, particle size, number of particles, and thermal properties change dramatically when the composition of ionic comonomer (NaSS, sodium styrene sulphonate) in the copolymer mixture changes⁴³. The dramatic change in properties can be attributed to the change in the locus of polymerization from homogeneous nucleation to micellar nucleation with the increase in NaSS content.

Thus the effect of comonomer structure on polymer properties needs a complete study to understand the effects of ionic comonomers on polymerization and the property changes it brings to the latex particles obtained. Monomeric structure plays a vital role

in monomer solubility, rate of free radical formation, free radical stability and viscosity of the polymerization mixture which dictates the incorporation of monomer in the copolymer backbone. There are good number of literature available for the copolymerization of styrene with ionic comonomers such as acrylic acid (AAc)^{42, 44-46} methacrylic acid(MAA)^{47,48}, 2-hydroxyethylmethacrylate (HEMA)^{49,50,51} and sodium styrene sulphonate (NaSS).^{43, 52-56} In the present work the structural effect of those ionic comonomer on particle size, reaction behaviour and polymer properties have been studied in detail by varying the surfactant concentration below and above the CMC regions.

5.2. Experimental section

5.2.1. Materials and reagents

Styrene (Sisco, India) was washed with 10% sodium hydroxide solution and deionized water repeatedly to remove the inhibitor before it was freshly distilled prior to use. Sodium dodecyl sulphate (SDS), initiator ammoniumperoxodisulphate (APS) and buffer NaHCO_3 were obtained from Merck, India and used as recieved. Acrylic acid (AAc, Sisco, India), methacrylic acid (MAA, Fischer, India), 2-hydroxyethylmethacrylate (HEMA, Sisco, India), and sodium styrene sulphonate (NaSS, Sigma-Aldrich) were used as ionic comonomers without further purification.

5.2.2. Synthesis of styrene copolymer colloidal particles

Polystyrene copolymer colloidal particles were synthesized by emulsion polymerization^{29, 30,38, 39, 43} technique in a four neck mercury sealed round bottom flask which contains a reflux condenser, a teflon stirrer powered by a high torque mechanical stirrer, nitrogen and reagent inlet. The temperature was maintained by placing the reaction vessel in a control temperature oil bath. The reaction vessel containing 0.1g (1.2mmol) of sodium bicarbonate was charged with 75 mL of millipore water. A nitrogen blanket and stirring rate of 360 rpm were maintained throughout the reaction.

The water solution was deoxygenated by bubbling with nitrogen for 40 minutes. After thorough de-oxygenation, required amount of SDS dissolved in 10 mL of water was added and the temperature was increased to 50⁰C. Freshly deoxygenated and 33g (317 mmol) styrene was added drop wise to the reaction flask. 0.536 g (7.44 mmol) acrylic acid was injected 5 minutes after the addition of styrene. The temperature was increased to 70⁰C. After equilibration for 30 minutes, 0.4g (1.75mmol) of APS dissolved in 15 mL of water was injected into the reaction mixture. Immediately after this addition 1mL of the solution was withdrawn from the reaction mixture and the reaction was terminated using hydroquinone solution. At every 10 minutes of interval this process was repeated, until the completion of the reaction. After the completion of 4 hours the polymer was collected and purified by dialysis for further analysis. The terminated polymer samples were dried in an oven at 100⁰C for 24 hours. The yield and the percentage of conversion of polymerization were calculated gravimetrically. SDS concentration in the polymerization mixture was varied from 0.1734 mM to 69.34 mM to prepare different sized particles and all the recipes were summarized at Table 5.1. In all the cases monomers and initiator (APS) concentrations were kept constant. The concentration of APS in all the cases was 17.53mM.

Also, the reaction conditions such as temperature, stirring speed, and reflux time etc. for all reactions were exactly identical. Similar experimental procedure and stoichiometry were employed for the emulsion copolymerizations of styrene with all other ionic comonomers and these are 2-hydroxyethylmethacrylate (HEMA), methacrylic acid and NaSS. The weight of ionic comonomer taken in all the cases were 0.536g throughout this study. This is 1.62% by weight with respect to styrene monomer weight.

Table 5.1. *Typical recipe of emulsion copolymerization of styrene with various comonomers.*

Reagent	Weight (g)	mmol
Water	100	-
NaHCO ₃	0.2	1.2
SDS	0.005- 2	0.01734 - 6.9
Styrene	33	317
Ionic Comonomer	0.536	-
Ammoniumpersulphate	0.4	1.75

5.2.3. Purification of polystyrene copolymer colloidal particles

Upon completion of the reaction, milky white colloidal solution. was purified by dialysis using a dialysis membrane (15000MW cut-off) and dialyzed against deionized water for 1 week with continuous stirring and changing the deionized water at every 12 hours interval. Colloidal solution after dialysis process was taken in a culture tube and ion-exchange resin (Bio Rad mixed Bed ion Exchange resin: AG501-X8 used as received) was added. The colloidal solution was rotated on a vertical rotor for two to three weeks. The ion exchanged purified colloidal juice was used for all the characterization techniques. After one week of stirring the colloidal solutions were taken out from culture tube using syringe and poured into petri dish which was kept on the top of the oven for 24 hours for drying. Finally the dried solid material was collected and stored for further studies.

5.2.4. Characterization of colloidal particles

The polymerization kinetics (% of conversion vs. time profile) was followed by removing 2 mL of reaction mixture from the reaction vessel at different time intervals. Hydroquinone (1% by weight) was used to stop the polymerization. The aliquots with

1% hydroquinone at different time intervals were dried in an oven and the percentage of conversion was measured gravimetrically.

Particle sizes of the resultant latexes were analyzed using various microscopic techniques. Three types of microscopic techniques were used and these are scanning electron microscope (SEM), atomic force microscopy (AFM) and transmission electron microscope (TEM). Aqueous diluted colloidal juice was dropped on a cleaned glass piece and air dried for SEM experiments. For SEM experiments samples were gold coated and then SEM images were taken in Philips- XL30ESEM. AFM images of dried samples in glass plates were captured using an AFM apparatus (Solver P20M of NT-MDT) working in semi-contact mode. A microcantilever with a spring constant of 10 Nm^{-1} was used to scan the samples. For TEM experiments the sample was prepared by dropping a latex particle solution on carbon coated copper grids and dried in vacuum for 12 hours at room temperature. TEM measurements were carried out using Philips (FEI Tecnai Model No. 2083) instrument operating at 120kV. Particle size reported here is an average of large number of similar sized particles measured from SEM, AFM, and TEM micrographs.

Thermo gravimetric and differential thermal analyses (TG-DTA) were carried out with a TG-DTA instrument (Netzsch STA 409PC) from room temperature to 800°C with a scanning rate of $10^{\circ}\text{C min}^{-1}$ in the presence of nitrogen gas flow. A differential scanning calorimeter (DSC) instrument (Pyris Diamond DSC, Perkin Elmer) was used to measure the glass transition temperature of the samples. The DSC instrument was calibrated using indium and zinc standards before the copolymer samples were scanned.

Surface charge density and charge per particle of the colloids were calculated by estimating charge on the surface of the colloidal particle utilizing potentiometric titration⁵⁷ of colloidal solution against 0.1N NaOH using SM702 Titrino (Metrohm, Switzerland) auto titrator instrument. Particle volume fractions were measured gravimetrically in triplicate considering the polystyrene density as 1.05 g/cm^3 .

The reflectance studies of the colloid particles were done as follows: colloidal solution was taken in beaker and the colloidal particles were allowed to sediment on the glass slide through vertical deposition method. All the diffraction measurements were carried out in reflection mode with Ocean Optics (USB4000-UV-VIS-NIR, Ocean Optics Inc., USA) spectrophotometer.

5.3. Results and Discussion

5.3.1. FTIR spectroscopy

The backbone structures of all polystyrene copolymers are shown in Figure 5.1. Monomer incorporation in all the copolymer samples are examined by IR spectroscopy. IR spectra of all the copolymers are shown in Figure 5.1. Table 5.2. gives a list of important peaks for functional groups present in the copolymers. Spectra reveal well defined characteristic spectral bands of polystyrene (Table 5.2). In Figure 5.2A, the broad peak at $3440\text{--}3450\text{ cm}^{-1}$ for all the copolymers results from --OH stretching vibrations due to incorporation of --COOH (in case of AAc and MAA), SO_3H (NaSS), --OH (HEMA) groups from their ionic comonomers AAc, MMA, NaSS and HEMA, respectively^{43,56}. The peaks from 2800 to 3100 cm^{-1} [marked by ellipse in Figure 5.2(A)] exhibit various characteristic vibration bands of polystyrene^{43, 56}. A very small peaks at 1705 cm^{-1} for P(S-co-AAc) and P(S-co-MAA) copolymers corresponds to C=O stretching in carboxylic groups of their respective monomers, acrylic and methacrylic acid which clearly indicates the incorporation of these vinyl acids in the polymer^{45, 46}. The very small intensity of peaks denotes a small amount of incorporation due to the small amount of co monomer feed (1.6%) incase of acrylic monomers. In case of NaSS monomer --S=O symmetric (1041 cm^{-1}) and asymmetric stretching (1182 cm^{-1}) peaks were overshadowed by polystyrene peaks or possibly by unreacted ammonium per sulphate initiator's --SO_3 group. HEMA copolymer has got its characteristic --OH stretching band at 3450 cm^{-1} . In Figure 5.2B, the sharp peak at 697 cm^{-1} is the out-of-plane bending vibration of the styrene ring. Another sharp and intense

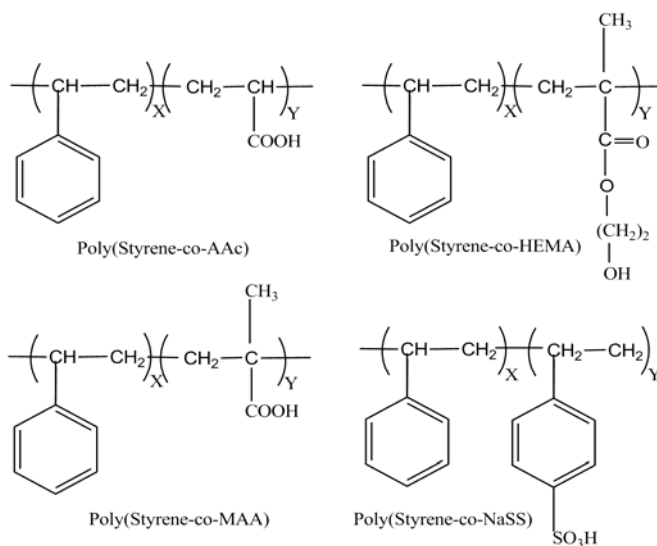


Figure 5.1. Schematic illustration of copolymer backbone structures.

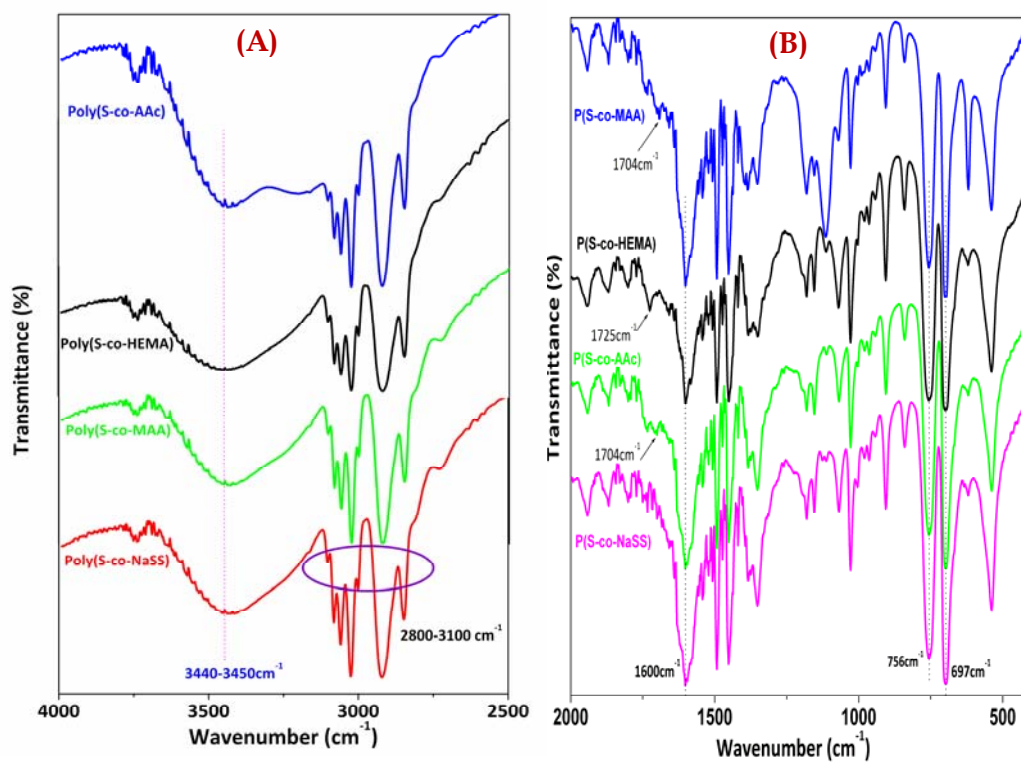


Figure 5.2. FTIR spectra (A) 4000–2500 cm⁻¹ and (B) 2000–400 cm⁻¹ of copolymers.

Table 5.2. *Infrared absorption peak assignments for polystyrene and its copolymers with AAc, MAA, HEMA, NaSS.*

Peak position (cm^{-1})	Functional group
3450	O-H stretching in $-\text{COOH}$, SO_3H , R-OH, groups
2900-2950	CH_2 stretchings
2800-3100	polystyrene stretching bands
1704	$-\text{C}=\text{O}$ stretching in the $-\text{COOH}$ group
1600	C-C in-plane stretching of benzene ring
834	C-H out-of-plane vibration for para position
756	C-H out-of-plane bending
697	Phenyl out-of-plane bending

peak at 756 cm^{-1} is a characteristic of the out-of-plane bending vibration of C-H groups in the monosubstituted benzene ring^{43,56} [Figure 5.2(B)].

5.3.2. Particle Size

SEM and TEM micrographs of styrene copolymer colloidal particles obtained from emulsion copolymerization of styrene with different ionic monomers; AAc, MAA, HEMA, and NaSS; by varying surfactant (SDS) concentration are shown in Figures 5.3-5.6. All the colloidal particles obtained from the copolymerization of styrene are highly monodisperse and robust in nature. In some cases the close packing of particles are also observed. Particle sizes measured from these micrographs are tabulated in Table 5.3. A plot of particle size against surfactant concentration (SDS) for all the copolymer samples is shown in Figure 5.7. In emulsion polymerization, it is well known that the particle size decreases with increasing surfactant concentration due to the fact that the higher surfactant concentration yields large number of smaller size micelles^{29, 30, 37, 38}.

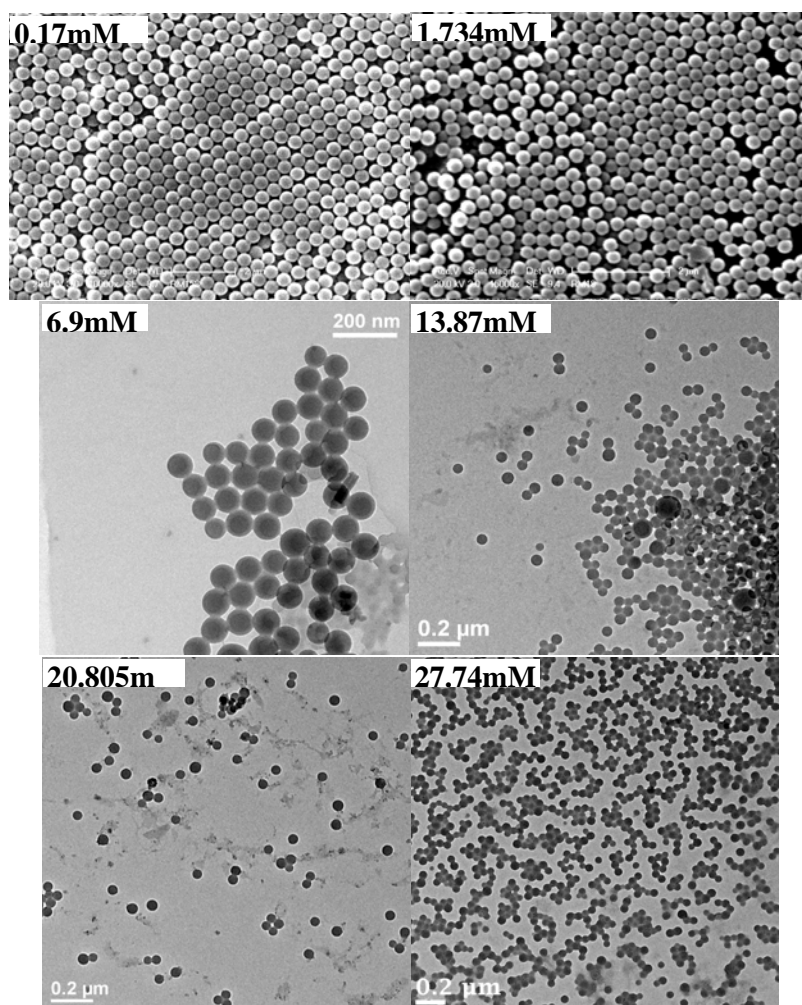


Figure 5.3. SEM and TEM micrographs of poly (styrene-co-acrylic acid); Poly(S-co-AAc), copolymer particles. The SDS concentration of the polymerization by which these particles are obtained is indicated in the figure.

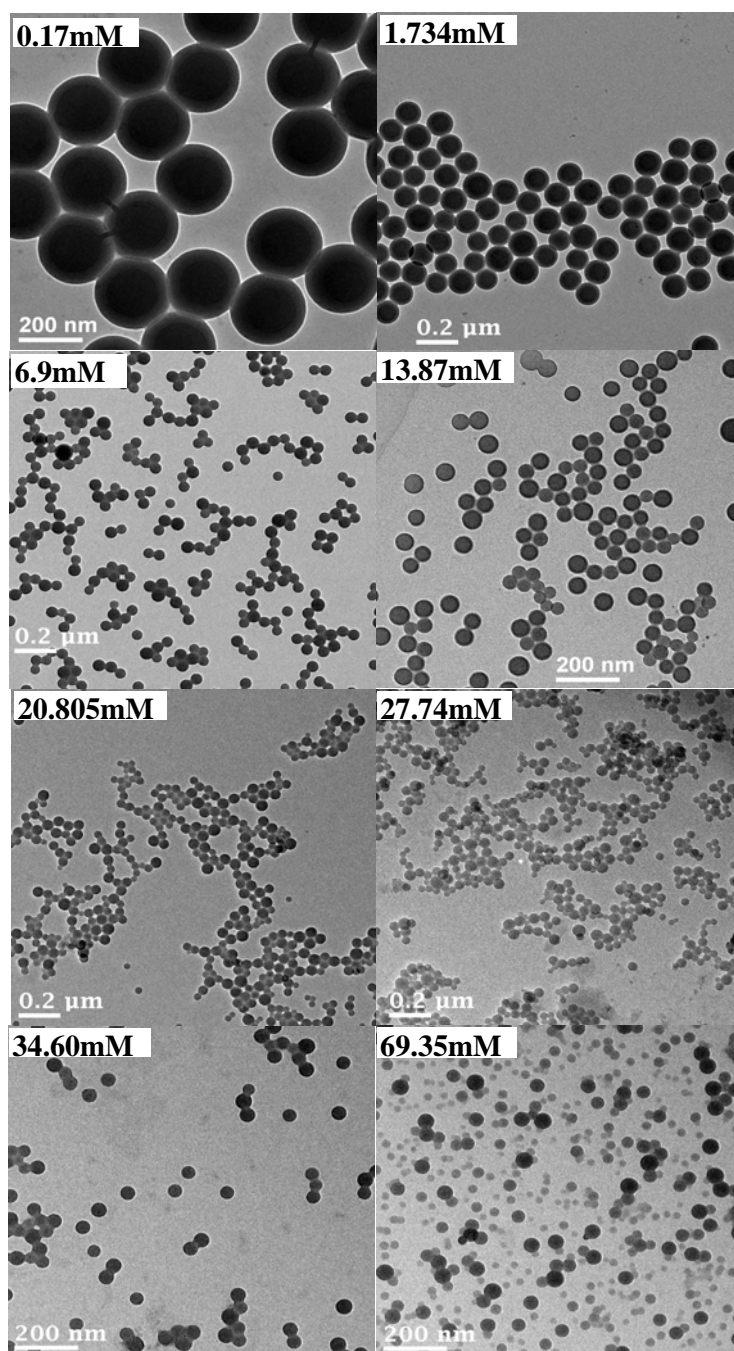


Figure 5.4. TEM micrographs of poly (styrene-co-methacrylic acid); Poly (S-co-MAA) copolymer particles. The surfactant concentration of the polymerization is indicated in the figure.

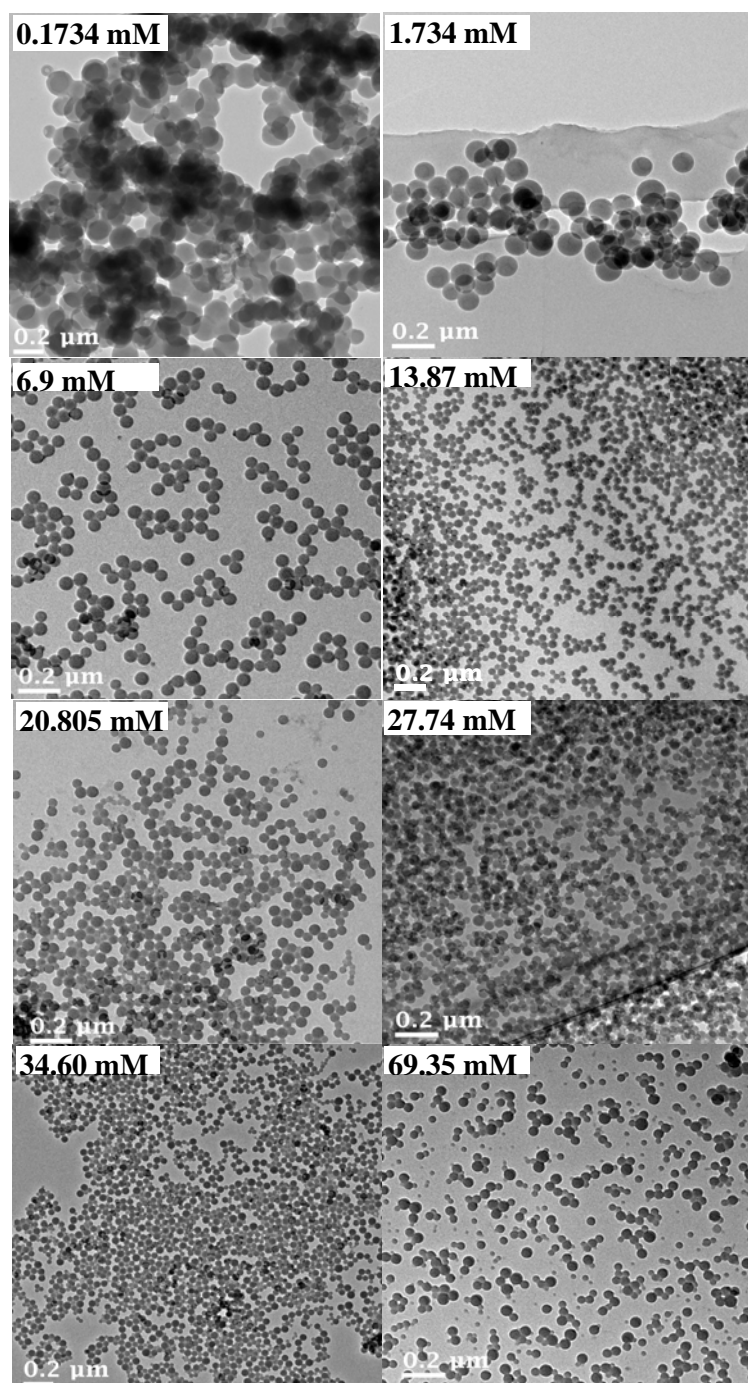


Figure 5.5. TEM micrographs of poly (styrene-co-2-hydroxymethacrylate); Poly (S-co-HEMA) copolymer particles. The surfactant concentration of the polymerization is indicated in the figure.

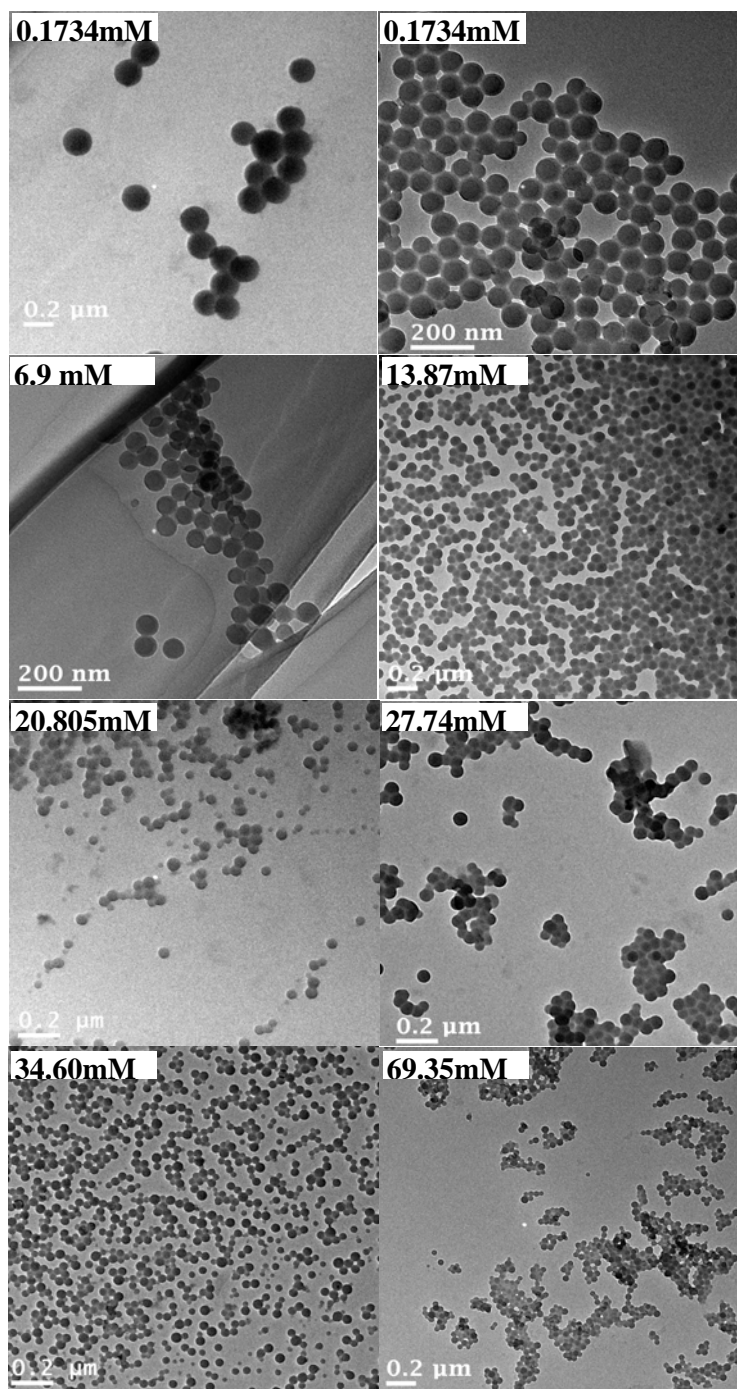


Figure 5.6: TEM micrographs of poly (styrene-co-sodium styrene sulfonate); Poly (S-co-NaSS) copolymer particles. The surfactant concentration of the polymerization is indicated in the figure.

Our current results for all sets of copolymer are in agreement with the general observation of emulsion polymerization as stated above. In the current study we have widely varied the SDS concentration from 0.1734mM to 69.35mM. The critical micellar concentration (CMC) of SDS is ~ 8.1 mM, hence we have made the colloidal particles with below CMC region and above CMC region.

It must be noted from Figure 5.7 that the change in particle size with SDS concentration is not identical for all the copolymers and also the dependence of particle size on SDS below CMC region and above CMC region are different. To get a better picture we have made a log-log plot of particle size (D) with SDS concentration (S) and presented in Figure 5.8. It is clear from the Figure 5.8. that the dependence of D on S is different below and above CMC and also it depends upon the structure of the ionic comonomer. Table 5.4 shows the values of slopes in both the regions for all comonomers obtained from Figure 5.8. Table 5.4 and Figure 5.8 indicate that the dependence of particle size on SDS concentration varies from monomer to monomer and as well with the surfactant concentration region (below and above CMC). It must be noted that except NaSS in all other cases the decrease of particle size with SDS concentration; the slopes of the $\log D$ vs $\log S$, higher below CMC region indicating that a sharp dependence of particle size with SDS concentration below CMC than above CMC region. The dependence of particle size with SDS concentration below CMC follows the order as AAc (0.4460) > MAA (0.3956) > NaSS (0.2524) > HEMA (0.2408) (Table 5.4). However, the dependency is altogether different above the CMC region where the dependency order is NaSS (0.4061) > HEMA (0.2281) > AAc (0.2062) > NaSS (0.172) (Table 5.4).

The unusual size dependency of SDS concentration below and above CMC can be justified by considering the hydrophobicity of the oligomeric particles produced at the beginning stage of the polymerization^{45, 58, 59}. It is well known that the homogeneous particle nucleation is the predominant particle formation process in the below CMC region. In this process the oligomeric radicals produced at the beginning of the

Table 5.3. Particle sizes of copolymer particles calculated from TEM micrographs. The values reported here are average values calculated at least from 25 number of particles.

SDS (mM)	Particle size (nm) of copolymer			
	AAc	MAA	HEMA	NaSS
0.1734	480	251	186	185
1.734	204	126	120	83
6.900	90	58	75	76
13.87	54	58	60	70
20.805	48	48	55	66
27.74	47	45	46	58
34.60		42	46	48
69.35		38	42	38

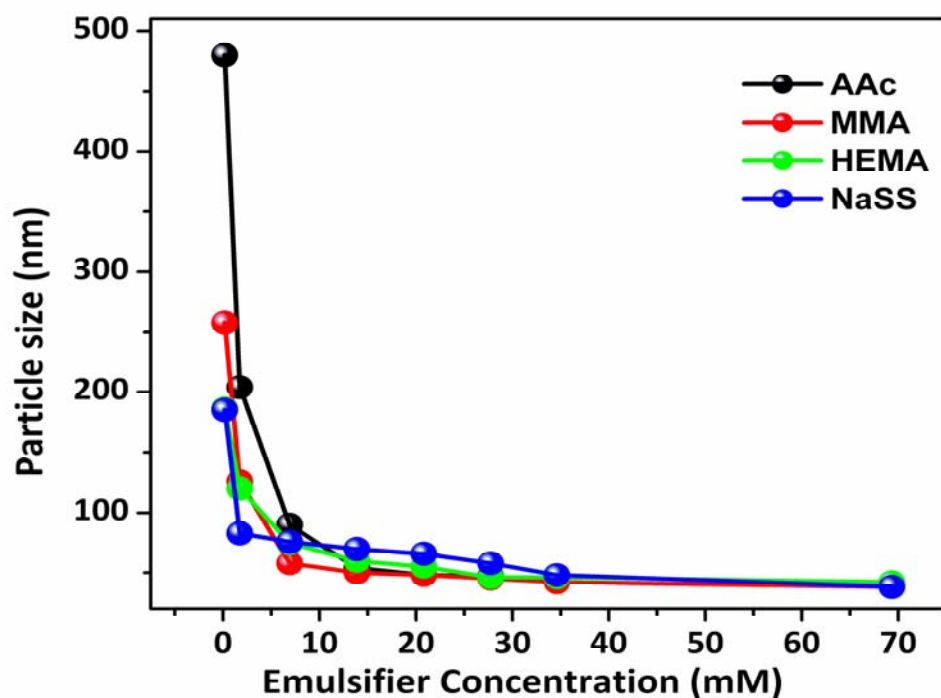


Figure 5.7. A plot of particle size vs. emulsifier concentration for various comonomers. The initiator concentration (17.54mM) is constant for all the cases.

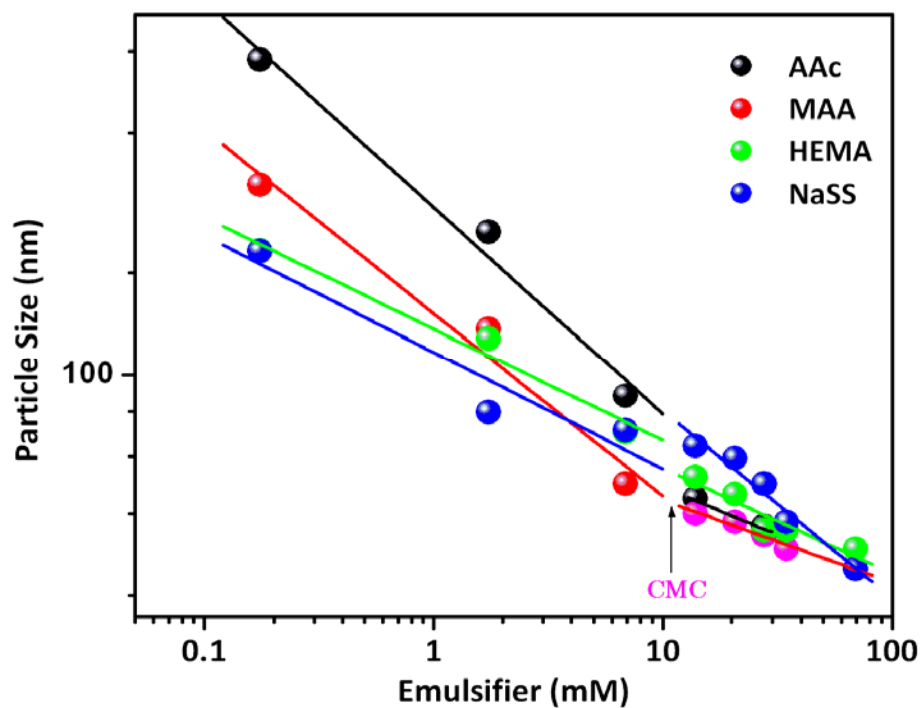


Figure 5.8: A log-log plot of particle size vs. emulsifier concentration

Table 5.4. Slope values obtained from log-log plot of (Figure 5.8) particle size vs. emulsifier concentration.

Monomer	Below CMC	Above CMC
AAc	-0.4460	-0.2062
MAA	-0.3956	-0.172
HEMA	-0.2408	-0.2281
NaSS	-0.2524	-0.4061

polymerization are precipitated out from the reaction mixture and stabilized by the free surfactant molecules in the medium. This surfactant stabilized oligomers further grow into the colloidal particles. Therefore it is expected that the size and number of oligomer particles will dictate the size of the resulting colloids. Further the size of the oligomer particles varies with the hydrophobic nature of the oligomer; more the hydrophobic nature size will be smaller since size it will precipitate out from the aqueous reaction phase easily. Hence the above argument concludes that higher the hydrophobicity of the oligomer produced at the early stage of the polymerization smaller size particles will be obtained.^{45, 58, 59} The hydrophobicity order of the oligomers produced from the monomers studied here is as follows NaSS~HEMA>MAA>AA. Hence the critical length of an oligomer to precipitate in the medium is smaller for HEMA or NaSS copolymer compared to other systems. Or in other words the HEMA or NaSS oligomer precipitates easily compared to MAA, and more hydrophilic AAc oligomers. Due to the rapid precipitation and stabilization more number of HEMA or NaSS precursor particles are formed followed by MAA, and AAc^{45, 58, 59}. Since the monomer concentration is constant, smaller size particles are obtained when the number of precursor particles is large^{45, 48, 59, 29, 30, 37}. Therefore it is expected that for a similar SDS concentration below CMC the order of particle size should be AAc>MAA>HEMA>NaSS. Table 5.3 data proves the above statement.

Now the question still remains why the dependence of D with S below CMC follows the order as AAc>MAA>NaSS>HEMA. In fact Table 5.4 suggests that the dependence in case of AAc and MAA are almost twice than NaSS and HEMA. This results attributes that below CMC region the change in particle size with SDS concentration is highly depends on SDS concentration for AAc and MAA but it is not largely dependent on SDS concentration in case of NaSS and HEMA. The sharp dependence for less hydrophobic oligomer (AAc and MAA) is probably due to the fact that stabilization of oligomer particles becomes easier with increasing SDS concentration and hence large number of smaller particles formed readily. Whereas in case of HEMA and NaSS the large number of smaller particles are already formed and

hence SDS concentration does not affect much. Above CMC the dependency of D with S is reversed compared to below the CMC. Here NaSS shows the sharpest change, followed by HEMA, AAc, and MAA.

Above CMC the reversal of dependence of D on S is observed which can be explained by micellar nucleation; a dominant particle forming mechanism in the above CMC region. Above CMC when the precursor oligomer is precipitated it diffuses into the core of the micelle and starts polymerizing the monomers inside the micelles. Precursor oligomer should be hydrophobic enough to enter in the hydrophobic micellar core. In the above CMC regime NaSS radicals due to its crosslinking arising from “gel effect”^{52,53} and hydrophobic nature is stabilized easily once the precursor particles are formed and diffuse easily into the hydrophobic micellar cores to polymerize the monomer present in it than the other monomers studied here. HEMA too produces more hydrophobic smaller particles with increasing surfactant concentration and diffuses in to the core of the micelle but not as effectively as NaSS. So NaSS and HEMA are more hydrophobic and they strictly involve in micellar nucleation rather than homogeneous mechanism hence particle size decreases sharply with the increase in surfactant^{45, 48, 59}. Whereas acrylic comonomers due to their high hydrophilicity tend to precipitate slowly. The above justification explains the dependency of D on S for all the monomers studies here.

In case of AAc and MAA the significant amount of particle formation takes place either on the surface of the micellar particle through homogeneous nucleation⁴⁶ owing to their high hydrophobic character. As a result the colloidal particles yielded for AAc and MAA displays a core shell morphology in which the core is hydrophobic styrene and the shell is hydrophilic acrylic monomers. The TEM micrographs shown in Figure 5.3 and 5.4 display the core shell morphology justifies our claim. In contrast the core shell morphology is not observed for NaSS and HEMA (Figure 5.5 and 5.6) indicating the fact that in these two cases the particle nucleation takes place inside micellar core and the highly hydrophobic nature of NaSS and HEMA oligomeric radicals is the driving force for this behavior.

5.3.3. Copolymerization Kinetics

Figure 5.9 shows the conversion (%) vs. time profile (rate of the reaction) of emulsion copolymerization of styrene with all four monomers studied here for wide range of SDS concentrations. The rate of the polymerization increases with increasing surfactant concentration, which is in agreement with the theory of emulsion polymerization^{35-37, 59}. In all the systems rate increases slowly in the below CMC region with increasing emulsifier concentration. For lower emulsifier concentration (below CMC region) in all the cases the rate is slow except NaSS. As the emulsifier concentration increases the number of reaction sites are also increases which leads to enhancement of polymerization kinetics. For NaSS the kinetics profile is entirely different because of “gel effect” which enhances the rate dramatically.^{43, 53, 54} We have reported the similar observation previously (chapter 4)⁴³. Above CMC the rate of polymerization does not influence much by the change of SDS concentration for all the system. This is also observed and reported by our group previously (chapter 2)³⁸ and is due to the fact that in this region of SDS concentration the polymerization occurs inside the micellar core.

For the comparison of comonomer structural effect on the rate copolymerization, kinetic profiles of different monomeric systems for a fixed concentration of emulsifier are represented in Figure 5.10. It is observed that the HEMA copolymerization has very low rate followed by methacrylic acid, acrylic acid and NaSS when emulsifier concentration is below CMC (0.1734mM) (Figure 5.10A). NaSS copolymerization rate is more due to gel effect which enhances the rate significantly as observed by several authors previously^{53, 54}. In the above CMC emulsifier (27.04mM) concentration region (Figure 5.10B) the rate of AAc, MAA and NaSS are comparable but HEMA conversion is quite slow compared to others. This observation clearly demonstrates the effect of ionic comonomer structure on the emulsion copolymerization of styrene. The slower polymerization rate of HEMA compared to other monomers can be attributed to the high hydrophobicity and sterical hinderence of HEMA oligomeric radicals which leads to slow incorporation of the monomer in the polymer backbone. In comparison

hydrophilic ionic comonomers like AAc and MAA enhances the rate of formation of primary oligomeric radicals in the aqueous phase which leads to the enhancement of polymerization rate^{45, 46}. In case of NaSS because of gel effect the rate is faster. Also it is well known that in case of emulsion polymerization a faster reaction rate can be achieved by increasing the number of polymer particles (N_p) formed³⁴⁻³⁶. We have measured the N_p values for all the monomeric systems at all the SDS concentration and we have observed that N_p for HEMA is always much lower than all other monomers. A detailed discussion will be followed in the next section.

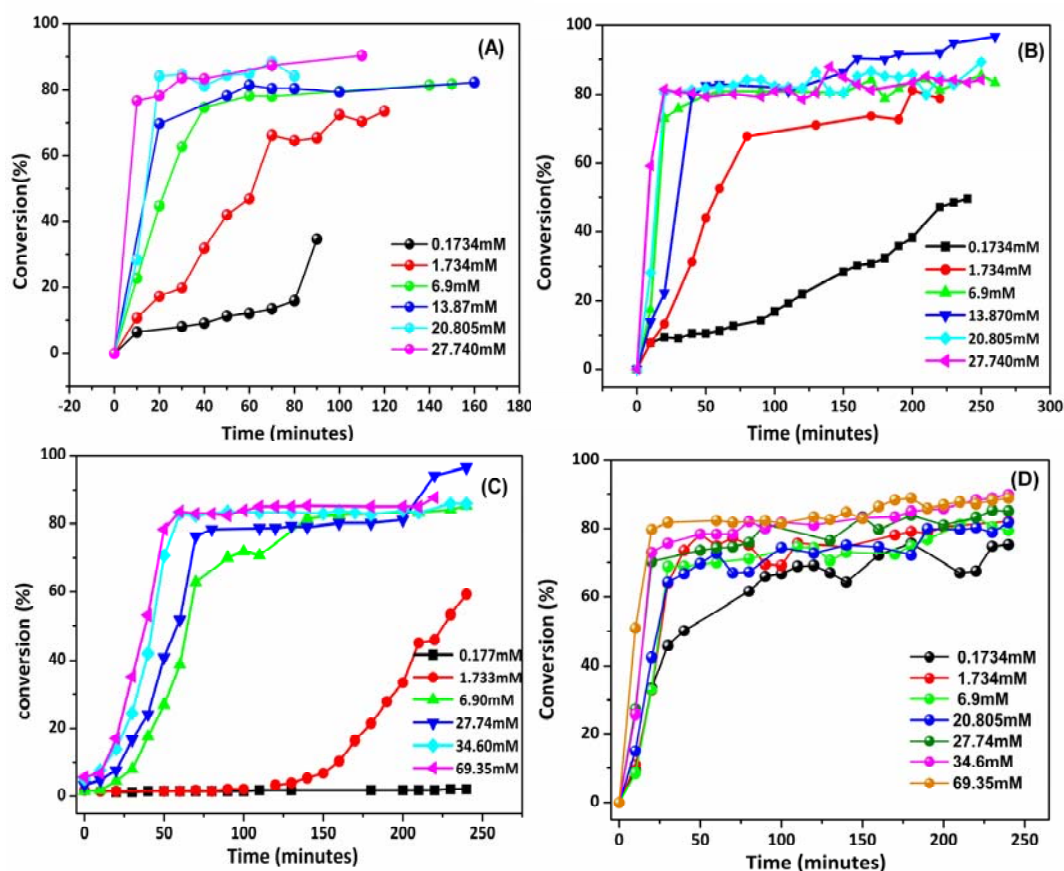


Figure 5.9. Conversion vs. time profiles of copolymerization of styrene with (A) Acrylic acid, (B) Methacrylic acid, (C) HEMA and (D) NaSS.

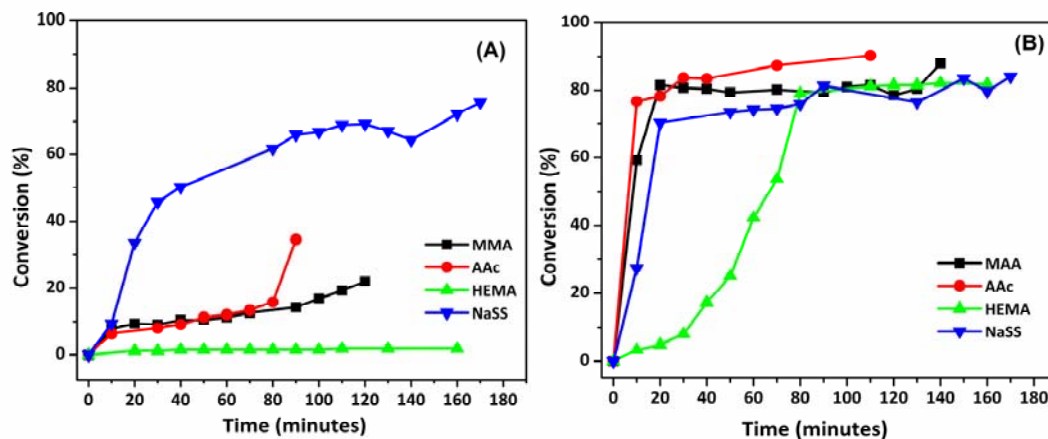


Figure 5.10. Copolymerization kinetics curves of various monomer for fixed emulsifier concentration (A) Below CMC region (SDS concentration is 0.1734mM) and (B) Above CMC region (SDS concentration is 27.704mM).

5.3.4. Number of particle vs. emulsifier concentration

Number of particles (N_p) is a function of number of micelles which is a function of emulsifier concentration in the polymerization^{34-37, 59}. Figure 5.11 presents the effect of emulsifier concentration on number particles for all the ionic comonomers. N_p increases with increasing emulsifier concentration owing to the fact that large numbers of smaller size micelles are formed for higher emulsifier concentration^{34-37, 59}. Hence it is expected that N_p should be inversely related to the size of the particles indicating that N_p will decrease with increasing particle size (Figure 5.12). It must be noted from both Figures 5.11 and 5.12 that the dependence of N_p on emulsifier concentration and particle size is not identical for the all ionic monomer systems. N_p of HEMA is always much lower than all other three comonomers (Table 5.5). Also N_p values among the rest three comonomers (AAc, MAA and NaSS) varies significantly throughout all emulsifier concentration as evident from Figure 5.11, Figure 5.12 and Table 5.5. All these results

clearly demonstrate the fact that the structure of the ionic comonomers plays an important role in the emulsion copolymerization.

Table 5.5. Number of particles(N_p) of copolymer particles with emulsifier concentration

Number of particles (no/mL) $\times 10^{-14}$				
SDS(mM)	AAc	MAA	HEMA	NaSS
0.1734	0.17	0.85	0.00593	0.55
1.734	0.36	1.54	0.198	3.6
6.900	4.2	15.3	0.626	9.9
13.87	18.3	22.5	6.18	12.4
20.805	20.0	30.0	12.0	16.0
27.74	36.0	54.9	23.7	22.7
34.60		67.0	21.5	33.33
69.35		83.5	30.4	53.9

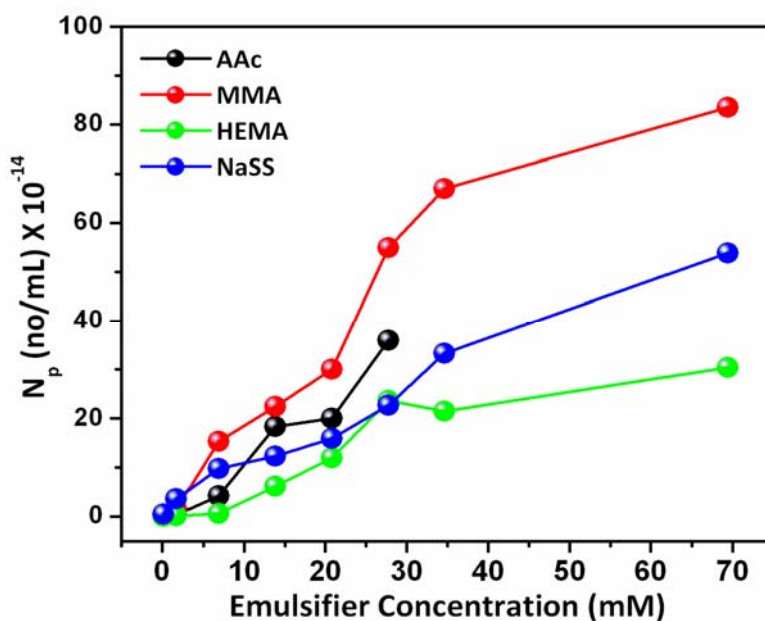


Figure 5.11. Number of particles (N_p) vs. emulsifier concentration for all polystyrene copolymer colloidal particles synthesized using different ionic comonomers.

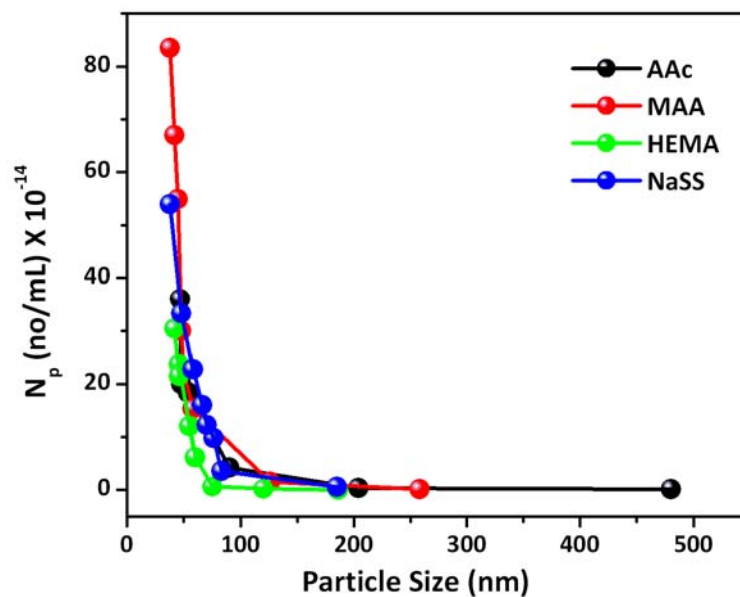


Figure 5.12. N_p vs. particle size of polystyrene copolymer colloidal particles synthesized using different ionic comonomers.

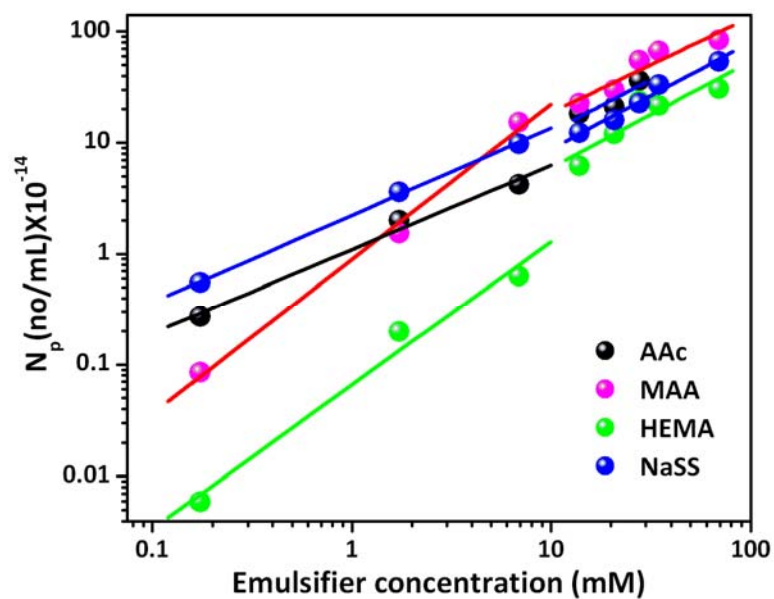


Figure 5.13. Log-log plot of number of particles (N_p) vs. emulsifier concentration

Table 5.6. Slope values obtained from log-log plot of number of particles vs. emulsifier concentration from the Figure 5.13.

Monomer	Below CMC	Above CMC
AAc	0.7556	0.9344
MAA	1.3943	0.8325
HEMA	1.2913	0.9626
NaSS	0.7843	0.9632

A log-log plot of number of particles vs. emulsifier concentration (Figure 5.13) shows the dependence of emulsifier concentration on N_p for various comonomers. The slopes of the plots below and above CMC are tabulated in Table 5.6. It is clear from the Figure 5.13 and Table 5.6 that all the slopes are positive which is in agreement with our previous studies. Also the different slope values before and after CMC regions indicates that the nucleation mechanisms are different in two regions^{35-37, 59}. However the most important observation for Table 5.6 is that the slope values vary from monomer system to system attributing the effect of ionic comonomer structure on the emulsion copolymerization of styrene.

5.3.5. Surface charge density

Surface charge density of the colloidal particle is an important quantity to understand and tune the self assembly of the particles. The surface charge density of the latex particles has a direct correlation with the size of the particles and here it has an inverse relationship with emulsifier concentration^{19, 20, 29, 30, 38}. Therefore it is expected

that the surface charge density will increase with increasing particle size and decrease with increasing emulsifier concentration. Figure 5.14 matches well with the above statement. However it must be noted here that the variation of surface charge density presented in Figure 5.14 is highly dependent upon the ionic comonomer structure, reinforcing our observation that the structure of the monomer plays an important role for the emulsion polymerization of styrene.

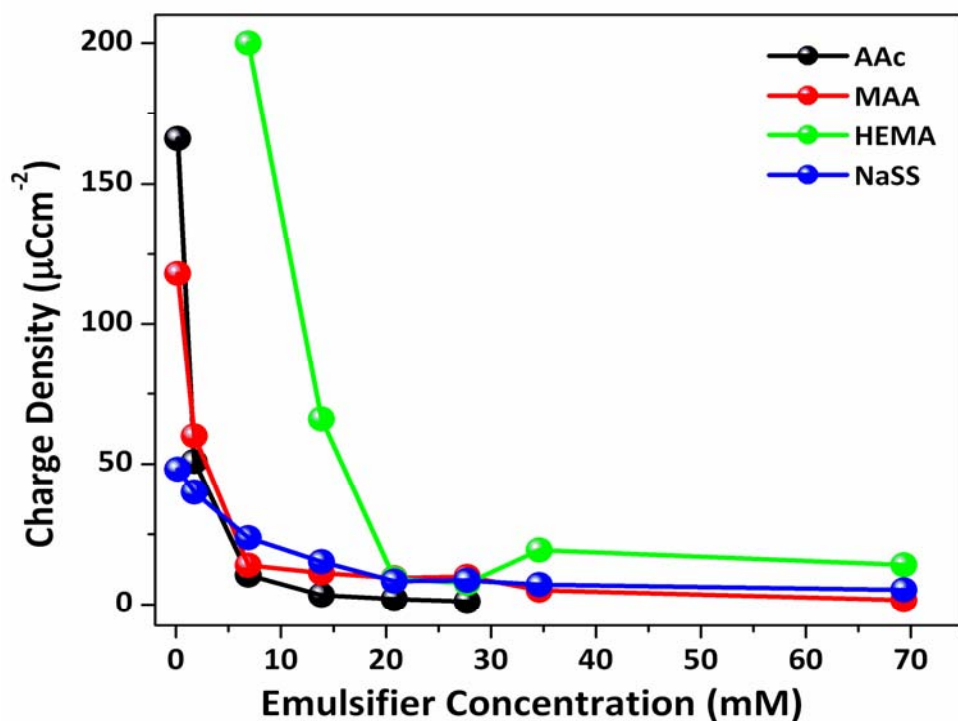


Figure 5.14. A plot of charge density vs. emulsifier concentration

5.3.6. Thermal Studies of Copolymers

5.3.6.1. Thermo gravimetric Analysis

The thermal stability of the copolymer particles was determined using TG-DTA in nitrogen atmosphere. The thermal stability of a polymer is an important characteristic because of the potential application of the material as thermally stable materials in various areas. The TGA thermograms of the copolymers are shown in Fig. 5.15(A). The derivatives of these thermograms are shown in Fig. 5.15(B). HEMA copolymer starts decomposing from 390⁰C and has a less thermal stability than that of the homopolymer (polystyrene). Whereas for AAc, MMA, and NaSS copolymers the onset of decomposition is 400⁰C and all the copolymers decomposes completely at 450⁰C [Figure 5.15(A)]. The close inspection of TGA thermogram and derivative thermograms help us to deduce the descending order of thermal stability as follows: AAc>NaSS>MMA>HEMA. These results provide an insight to copolymer bulk nature and the degree of incorporation. The rigidity of polystyrene is increased by the introduction of acrylic monomers (AAc and MMA) which brings gelly nature or elasticity to the polymer. This allows the polymer to sustain more heat and thermally stable. The effect of monomer structure plays a key role in increasing the thermal stability which can be explained as follows: AAc comonomer incorporation is more compared to MMA which brings gelly nature to the otherwise rigid copolymer. The incorporation of HEMA in the backbone of the HEMA copolymer is less due to its sterical hinderence which decreases the rigidity of the copolymer. For NaSS the crosslinking is not pronounced which is usually the case due to its relatively low incorporation in the polymer backbone. Due to this both NaSS and HEMA copolymers show relatively lesser stability than their counterparts. Thus one can conclude that sterically less hindered and more hydrophilic monomers like AAc and MAA yielded polymers that are more thermally stable.

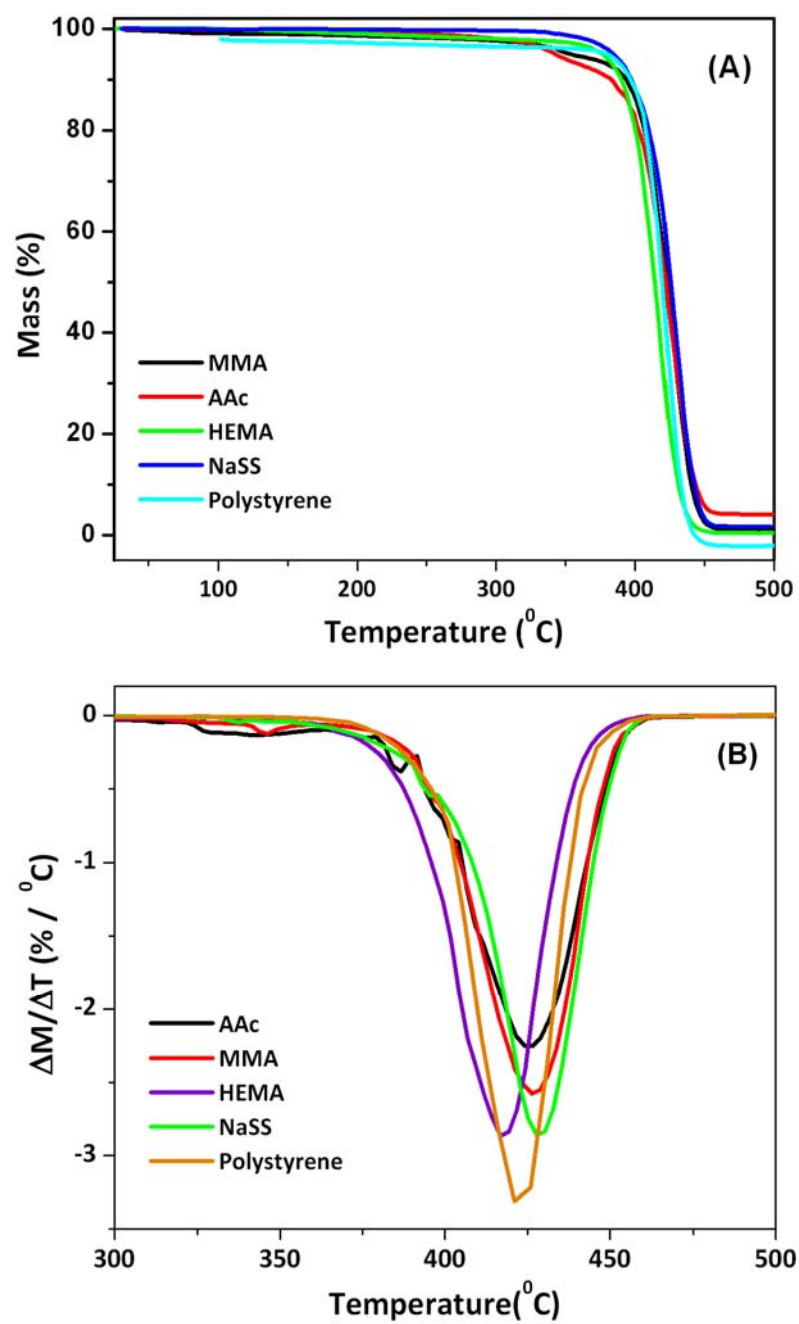


Figure 5.15. (A) TGA Thermogram of copolymers (B) derivative of thermograms

5.3.6.2. Differential scanning calorimeter studies

The glass transition temperature (T_g) of all the copolymer samples were determined using DSC. Figure 5.16 shows representative DSC thermograms of various copolymer samples. The measured T_g of 100% (100/0) polystyrene is 104°C. For AAc copolymer T_g is smaller (100°C). AAc brings gel nature to the copolymer that may be the reason for its smaller T_g . Introduction of aliphatic group in the side chain increases the polymer glass transition temperature which is visible in case of MMA and HEMA²³. NaSS shows a slight increase in T_g due to a very small incorporation of NaSS and relatively small amount of cross linking. It has been shown that NaSS incorporation in the backbone increases the glass transition temperature. Thus the monomeric structure also controls the thermal properties (glass transition temperature and thermal decomposition temperature) of the polystyrene copolymer.

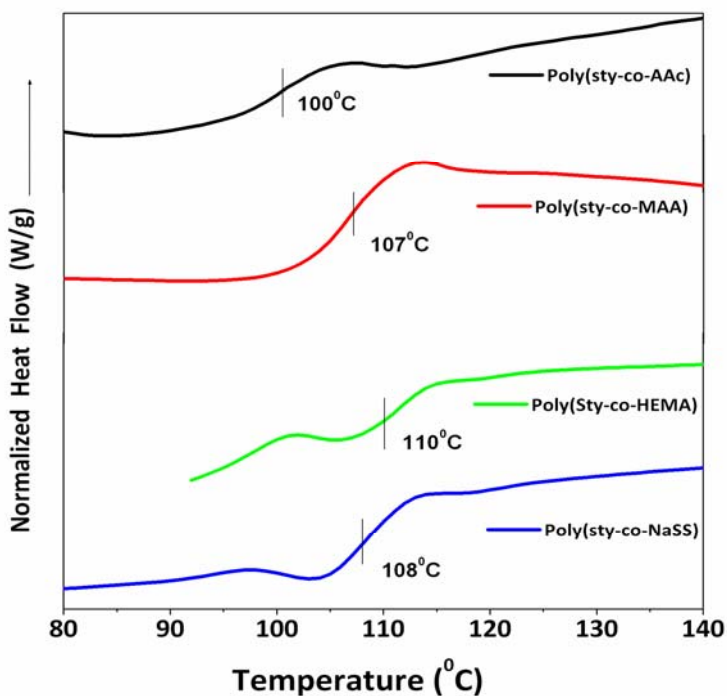


Figure 5.16. DSC thermograms of copolymers of polystyrene obtained from different ionic comonomers.

5.3.7. Diffraction studies of self-assembled latexes

All the highly charged monodisperse particles have similar size and hence similar charges. Therefore they tend to self assemble into non-close packed structures to minimize the electrostatic repulsion force. These arrays are commonly known as crystalline colloidal arrays (CCA)²¹⁻³⁰. High surface charge of particles, high dielectric constant of medium and low concentration of ionic impurities are the driving forces for the formation of crystalline colloidal crystals at low volume fractions of particles. AAc, MAA, HEMA and NaSS copolymer particles readily self assemble into different non close packed patterns on a glass slide upon vertical deposition of colloidal solution. Figure 5.17 shows the AFM images of poly (styrene-co-MAA) copolymer particles sedimented on glass slides which exhibit the hexagonal close packed structures. Similarly all other copolymers also exhibit close packed structures. Reflectance spectra of all the copolymer colloids are recorded from the sedimented samples on glass slides and presented in Figure 5.18. All the copolymer particles exhibit very sharp diffraction. The reflectance spectra peak position varies from monomer to monomer. These copolymer particles self assembled and produced CCAs which can be utilized in photonic band gap materials^{61, 62} and PCCA smart sensing materials²¹⁻²⁸.

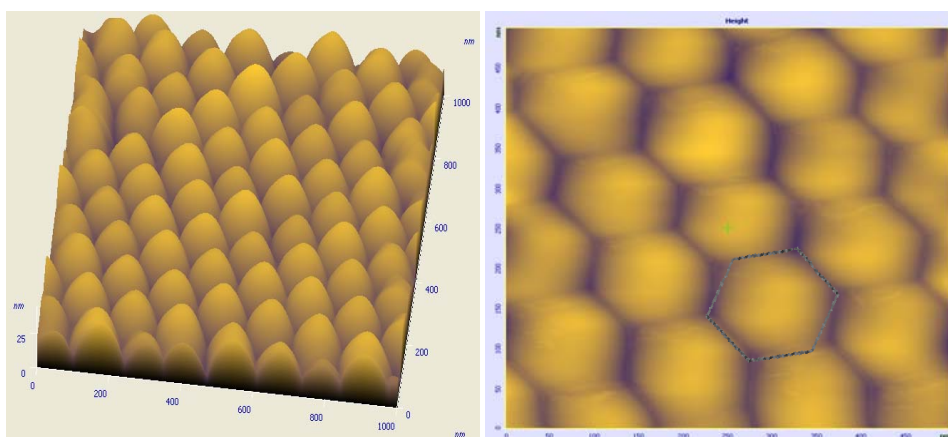


Figure 5.17. AFM micrograph showing poly(S-co-MAA) copolymer hexagonal close packed self assembled structures.

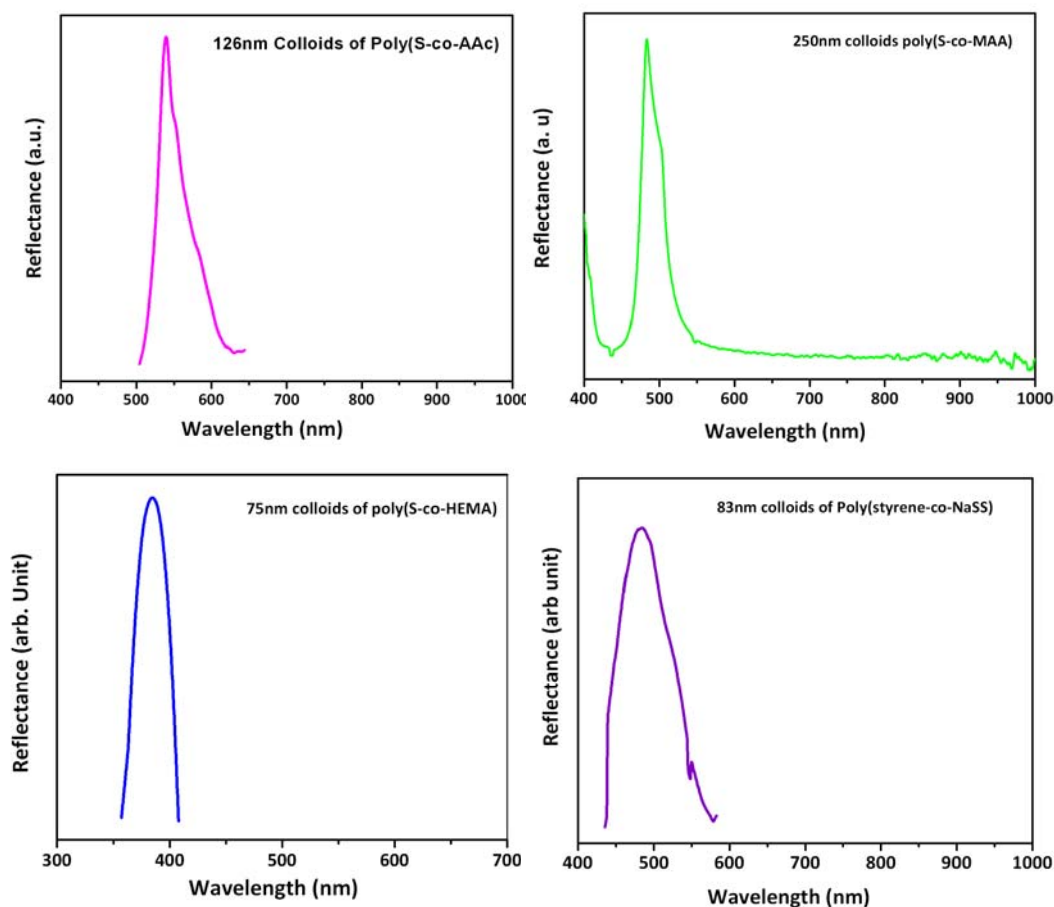


Figure 5.18. Reflectance spectra of CCA obtained by sedimentation of various polystyrene copolymer colloidal particles. Respective particle sizes of colloids from which the CCA is developed is given in the figure.

5.4. Conclusion

A series of emulsion copolymerizations of styrene with variety of ionic comonomers like AAc, MAA, HEMA and NaSS have been carried out by altering the surfactant concentration. The effect ionic comonomer structure on copolymerization kinetics and copolymer properties are studied. All the four copolymers (S-AAc, S-MAA, S-HEMA and S-NaSS) kinetics increase with increasing surfactant

concentration. The kinetics is rather slow below the CMC whereas above CMC it is rapid for all the cases except NaSS because of gel effect which contributes to the kinetics irrespective of below and above CMC regions. However at a fixed surfactant concentration below CMC, AAc copolymerization with styrene is faster followed by MMA, NaSS and HEMA copolymerizations with styrene due to ease of incorporation hydrophilic acrylic monomers. In all the cases particle size increases sharply below CMC and slowly above CMC. The dependence of particle size against surfactant in below CMC regions: AA> MAA> HEMA~ NaSS. Whereas the order is reversed in above CMC region as NaSS>HEMA>AA>MAA. The more hydrophilic acrylic acid shows the higher solubility which results in fair amount of incorporation resulting lower critical length needed to precipitate and hence delays the precipitation time which results in less number of precursor particles which lead to bigger sized particles. Whereas HEMA due to its hydrophobicity character, the oligomeric chain which precipitates rapidly to yield large number of particles which matures as smaller sized particles. Above CMC the trend of dependency of particle size on emulsifier is more for NaSS followed by HEMA, AA and MAA. The hydrophobicity and the crosslinking enhance the chances of NaSS-Styrene oligomeric radical to diffuse the hydrophobic core of the swollen micelle readily and decreases the chances of secondary radical formation or shift in locus of polymerization. This results in bigger size copolymer particle. Acrylic oligomers tend to polymerize either in aqueous medium or surface and less proportion diffuses inside micelle. Number of particles increases with increasing surfactant concentration and comonomer structure plays a vital role since the dependence of number of particle on emulsifier is more in case of MAA followed by HEMA, NaSS and AAc in above CMC region. AAc copolymer show good thermal stability upto 400⁰C followed by MMA, NaSS and HEMA. T_g of HEMA copolymer is more followed by NaSS and MAA. T_g of AAc copolymer smaller than polystyrene homopolymer which may be due to the gelly nature it brings to the polymer. All the copolymer colloidal particles sedimented on a glass slide form robust close packed structures which diffract visible light and potentially can be used in PCCA sensing materials and photonic crystal devices.

References

1. Fitch, R. M. *Polymer Colloids*; Academic Press: San Diego, 1997.
2. Urban, D.; Takamura K. (Ed.,) *Polymer Dispersions and Their Industrial Applications*; Wiley –VCH: Weinheim, Germany, 2002.
3. Kawaguchi, H. in Tsuruta, T.; Hayashi, T.; Kataoka, K.; Ishihara, K.; Kimura, Y. (Eds.,) *Biomedical applications of polymeric materials*; CRC press: Boca Raton, FL, 1993, pp 299–324.
4. Rembaum, A.; Yen, S. P. S.; Molday, R. S. *J. Macromol. Sci-Chem.* **1979**, *A13*, 603.
5. Lee, C. F.; Young, T. H.; Huang, Y. H.; Chiu, W. Y. *Polymer* **2000**, *41*, 8565
6. Tamilvanan, S.; Sa, B. *J. Microencapsul.* **1999**, *16*, 411.
7. Tamai, H.; Hamamoto, S.; Nishiyama, F.; Yasuda, H. *J. Colloid Interface Sci.* **1995**, *171*, 250.
8. Himm, R. E.; Foldes, R. G.; Hand, D. W. *Contraception.* **1985**, *32*, 267.
9. Zeitlin, L.; Whaley, K. J.; Hegarty, T. A.; Moench, T. R.; Cone, R. A. *Contraception.* **1997**, *56*, 329.
10. Kim, J. H.; El-Aasser, M. S.; Klein, A.; Vanderhoff, J. W. *J. Appl. Polym. Sci.* **1988**, *35*, 2117.
11. Djinić, V. M.; Antić, V. V.; Džonlagic, J.; Govedarica, M. N. *React. Funct. Polym.* **2000**, *44*, 299.
12. Hong, L.; Chen, N. *J. Polym. Sci. Polym. Phys.* **2000**, *38*, 1530.
13. Chen, S. L.; Krishnan, L.; Srinivasan, S.; Benziger, J.; Bocarsly, A. B. *J. Membr. Sci.* **2004**, *243*, 327.
14. Malini, K. A.; Anantharaman, M. R.; Sindhu, S.; Chinnasamy, C. N.; Ponpandian, N.; Narayanasamy, A.; Balachandran, M.; Pillai, V. N. S. *J. Mater. Sci.* **2001**, *36*, 821.
15. Alfrey, T. Jr.; Bradford, E. B.; Vanderhoff, J. W., *J. Opt. Soc. Am.* **1954**, *44*, 603.

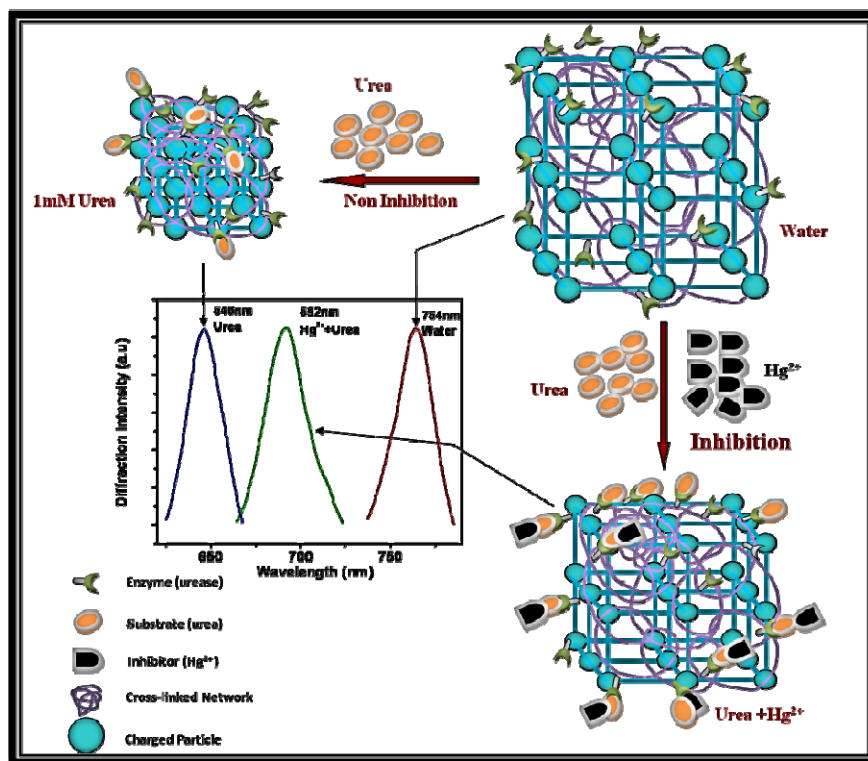
16. Krieger, I. M.; O'Neill, F. M.; *J. Am. Chem. Soc.* **1968**, *90*, 3114.
17. Hiltner, P. A.; Krieger, I. M. *J. Phys. Chem.* **1969**, *73*, 2386.
18. Luck, W.; Klier, M.; Wesslau, H.; *Ber. Bunsenges. Phys. Chem.* **1963**, *67*, 75.
19. Carlson, R. J.; Asher, S. A. *Appl. Spectrosc.* **1984**, *38*, 297.
20. Runquist, P. A.; Photinos, P.; Jagannathan, S.; Asher, S. A. *J. Chem. Phys.* **1989**, *91*, 4932.
21. Holtz, J. H.; Asher, S. A. *Nature* **1997**, *389*, 829.
22. Holtz, J. H.; Holtz, J. S. W.; Munro, C.; Asher, S. A. *Anal. Chem.* **1998**, *70*, 780.
23. Lee, K.; Asher, S. A. *J. Am. Chem. Soc.* **2000**, *122*, 9534.
24. Alexeev, V. L.; Sharma, A. C.; Goponenko, A. V.; Das, S.; Lednev, I. K.; Wilcox, C. S.; Finegold, D. N.; Asher, S. A. *Anal. Chem.*, **2003**, *75*, 2316.
25. Sharma, A.; Jana, T.; Kesavamoorthy, R.; Shi, L.; Virji, M.; Finegold D.; Asher, S.A. *J. Am. Chem. Soc.*, **2004**, *126*, 2971.
26. Asher, S.A.; Sharma, A.C.; Goponenko A.V.; Ward, M.M. *Anal. Chem.*, **2003**, *75*, 1676.
27. Asher, S.A.; Peteu, S.; Reese, C.; Lin M.; Finegold, D. *Anal. and Bioanal. Chem.*, **2002**, *373*, 632.
28. Kimble, K. W.; Walker, J. P.; Finegold, D.N.; Asher, S. A. *Anal Bioanal Chem* **2000** *385*, 678.
29. Reese, C.E.; Guerrero, C.D.; Weissman, J.M.; Lee, K.; Asher, S. A. *J. Colloid and Interface Science*, **2000**, *232*, 76.
30. Reese C.E.; Asher, S. A. *J. Colloid Interface Science*, **2002**, *248*, 41.
31. Okubo, M.; Konishi, Y.; Minami, H.; *Colloid Polym. Sci.*, **2000**, *278*, 659.
32. Bai, F.; Yang, X.; Huang, W. *Macromolecules* **2004**, *37*, 9746.
33. Lee, J.; Ha, J. U.; Choe, S. Lee, C.S.; Shim, S. E. *J. Colloid and Interface Science* **2006**, *298*, 663.
34. Smith, W. V. *J. Am. Chem. Soc.* **1949**, *71*, 4077.
35. Harkins, W. D. *J. Am. Chem. Soc.* **1947**, *69*, 1428.

36. Odian. G, *Principles of polymerization*, 4th edition; Wiley- Interscience: New York , 2004, Chapter 4.
37. Evans, D. F.; Wennerstrom, H. *The Colloidal Domain; Where Physics, Chemistry, Biology, and Technology Meet*, 2nd Ed., Wiley-VCH: Newyork, 1999.
38. Arunbabu, D.; Sannigrahi, A.; Jana, T. *J. Appl. Polym. Sci.* **2008**, 108, 2718.
39. Arunbabu, D.; Hazrika, M.; Jana, T. *Bull. Mater. Sci.* **2010**, 32, 633.
40. Wang, S.T.; Poehlein, G. W. *J. Appl. Polym. Sci.* **1993**, 50, 2173.
41. Slawinski, M.; Meuldijk, J.; Van Herk, A. M.; German, A.L. *J. Appl. Polym. Sci.* **2000** 78, 875.
42. Polpanich, D.; Tangboriboonrat, P.; Elaissari, A. *Colloid Polym. Sci.* **2005**, 284, 183.
43. Arunbabu, D.; Sanga, Z.; Seenimeera K. M.; Jana, T. *Polym. Int.* **2009**, 58, 88.
44. Musyanovych, A.; Rossmanith, R.; Tontsch, C.; Landfester, K.; *Langmuir* **2007**, 23, 5367.
45. Wang, P.H.; Pan, C.Y. *Colloid Polym. Sci.* **2001**, 279, 98.
46. Wang, P.H.; Pan, C.Y. *Colloid Polym. Sci.* **2002**, 280, 152.
47. Kobayashi, H.; Chaiyasat, A.; Oshima, Y.; Suzuki, T.; Okubo M. *Langmuir*, **2009**, 25, 101.
48. Lv, H.; Lin, Q.; Zhang, K.; Yu, K.; Yao, T.; Zhang, X.; Zhang, J.; Yang B. *Langmuir* **2008**, 24, 13736.
49. Lebduk, J.; Nuparek Jr., J.S. Kaspar, K.; Cermak, V. *Journal of Polym. Sci.: Part A Polym. Chem.* **1986**, 24, 777.
50. Chen, S. A.; Chang H. S. *J. Polym. Sci. Part A: Polym. Chem.* **1990**, 28, 2547.
51. Xu, X. J.; Siow, K. S.; Wong, M. K.; Gan, L. M. *J. Polym. Sci. Part A: Polym. Chem.* **2001**, 39, 1634.
52. Juang, M. S. D.; Krieger, I. M.; *J. Polym. Sci.: Polym. Chem. Ed.* **1976**, 14, 2089.

53. Weiss, R. A.; Lundberg, R. D.; Turner, S. R. *J. Polym. Sci. Polym. Chem. Ed.* **1985**, *23*, 549.
54. Kim, J. H.; Chainey, M.; El-Aasser, M. S.; Vanderhoff, J. W. *J. Polym. Sci. Part A: Polym. Chem.* **1992**, *30*, 171.
55. Sunkara, H. B.; Jethmalani J. M.; Ford, W. T. *J. Polym. Sci. Part A: Polym. Chem.* **1994**, *32*, 1431.
56. Brijmohan, S.B.; Swier, S.; Weiss, R.A.; Shaw, M.T. *Ind. Eng. Chem. Res.* **2005**, *44*, 8039.
57. Roberts, J. M.; Linse, P.; Osteryoung, J. G. *Langmuir* **1998**, *14*, 204.
58. Fitch, R. M.; Tsai, C. H. *J. Polym. Sci. Part B: Polym. Lett.* **1970**, *8*, 703
59. I. Pirmaa, (Ed), *Emulsion polymerization*, Academic press: New York, 1982.
60. Downey, J. S.; Frank, R. S.; Li, W. H.; Stolver, H. D. *Macromolecules* **1999**, *32*, 2838.
61. El-aasser, M. S.; Lovell, P.A. (Eds.,) *Emulsion polymerization and Emulsion Polymers*; John Wiley and Sons: Sussex, UK, 1997.
62. Xia Y. N; Gates, B; Yin Y.D.; Lu, Y. *Adv. Mater.* **2000**, *12*, 693.

Chapter 6

Photonic Crystal Hydrogel Material for the Sensing of Toxic Mercury Ion (Hg^{+2}) in Water



A novel polymer hydrogel based photonic crystal sensor material has been developed for the determination of toxic mercury ion (Hg^{+2}) concentration in water. This sensor material diffracts visible light and the shifts the diffraction wavelength owing to the volume phase transitions experienced by the polymer hydrogel upon exposure to the different mercury ion concentrations.

6.1. Introduction

Heavy metals that are accumulated in the natural resources and bio-converted to toxic chemicals like methylmercury in living organisms especially in the marine organisms cause adverse effects to living creatures and environment. Heavy metal toxicity is not only due to the developments in the field of science and technology but also because of the centuries old practices which have left huge amount of mercury in landfills, mines, industrial sites, soils and sediments¹⁻³. Among all the heavy metal cations mercury is a well known biotoxicant, non biodegradable, accumulates readily in the environment and exhibits toxic effects even at very low concentration. Mercury ion (Hg^{2+}) enters into the food chain in the form of methylmercury in aqueous medium. Methylmercury causes numerous disorders including sensory and neurological damages in human body. The human heart, kidney, stomach, and intestines can also be severely damaged by the mercury pollution. Hence the toxicity of mercury ion on environment is of serious concern and has drawn huge attention over the last century⁴⁻¹⁰.

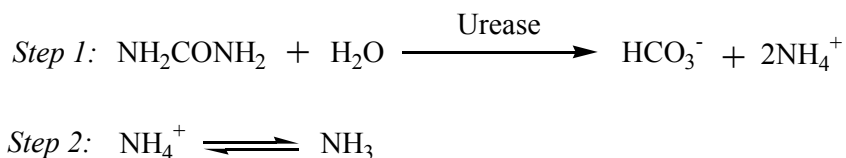
Concerns over the toxicity of mercury have motivated the search of rapid, precise and reliable methods for monitoring, sensing and quantification of traces amount of mercury ion in the natural resources like water, soil, and air and bio products. The current techniques which are utilized for the quantification of mercury ion (Hg^{2+}) include atomic absorption spectrometry,¹¹ X-ray fluorescence spectroscopy,¹² inductive coupled plasma mass spectroscopy (ICPMS),¹³ high performance liquid chromatography,¹⁴ and cold vapor atomic fluorescence spectrometry etc¹⁵. All these techniques involve expensive equipment, complicated time consuming experiments, high levels of operator's skill and in addition they are user unfriendly. Therefore to overcome these drawbacks, large numbers of efforts have been discovered in recent years to obtain simple, inexpensive and on-the-spot method that allows real time detection of Hg^{2+} in aqueous medium. Numerous sensors have been developed based on gold nanoparticles,¹⁶ polymer-oligonucleotide composites,¹⁷ proteins,¹⁸ organic fluorophores or chromophores,¹⁹ DNazymes,²⁰ and semiconductor nanocrystals.²¹ The detection methodologies of these sensors rely on the changes in the fluorescence

intensity, color and hence sensing can be carried out visually with the naked eye as well as with simple fluorometer and UV-Visible spectrometer. However, many of these sensors have number of limitations which include poor selectivity due to the coexistence of other metal ions, irreversibility, slow response, incompatibility with aqueous solution, complicated synthetic routes, tedious reaction conditions and not cost effective. The environmental protection agency (EPA), USA has recommended and set 2 ppb (or 2 $\mu\text{g} / \text{L}$) Hg^{2+} concentration in the drinking water as the maximum contaminant level (MCL)⁴. Often, the detection limit of the Hg^{2+} ion sensors reported in the literature are higher than the MCL suggested by EPA, USA. Therefore, a sensor which rectifies all the above issues is of great demand and development of this still remains a bigger challenge for the chemists.

In this chapter, we report a novel reusable sensor which addresses all the problems discussed above, for the determination of Hg^{2+} ion in aqueous medium. The sensing motif is based on polymerized crystalline colloidal array (PCCA) technology.²²⁻²⁷ It was demonstrated that PCCA sensing technology can be utilized to develop numerous chemical sensors for the sensing of various analytes such as glucose, metal cations, creatinine, pH, ionic strength etc. The PCCA consists of polymer hydrogel and array of colloidal particles, which is known as crystalline colloidal array (CCA). This CCA and hence the PCCA diffract light in the visible range. The wavelength of the diffracted light can be varied by changing the hydrogel volume which alters the lattice spacing of embedded CCA. The volume of the hydrogel can be tuned as a function of analyte concentration by appropriate chemical or physical modification of hydrogel. Therefore, the concentration of analyte can be determined from the wavelength of the diffracted light by the PCCA. This novel sensing technology brings many advantages in the sensing technology which includes low cost, require no instrument or very low tech instrument, operates in aqueous medium and user friendly.²²⁻²⁸ Therefore, we believe that development of Hg^{2+} ion sensor based on the PCCA technology will be an important breakthrough in the areas of Hg^{2+} ion sensing.

Heavy metals are known to inhibit the enzymes and reduce the catalytic efficiency in the important enzymatic reactions²⁹. In the literature large numbers of

conventional biosensors are designed by immobilizing or coating the enzymes on pH electrodes and the change in pH was measured as a function of analytes concentration which undergoes catalytic reaction with enzyme and changes the pH.^{30,31} Urease enzyme from jack beans has high specificity, proficiency and stability which make it an ideal candidate in the designing and usage of biosensor. The enzyme urease hydrolyses urea to ammonium (NH_4^+) and bicarbonate (HCO_3^-) ions (Scheme 6.1)³². Principal inhibitors of urease are Hg^{2+} , Cu^{2+} and Ag^+ ions³³. These inhibitors interfere the urea hydrolysis and hence the production of NH_4^+ and HCO_3^- ions suppresses. The use of heavy metal inhibition on urea hydrolysis has been explored for sensing of heavy metal ions.³⁴ Zeng et. al. reported urea sensing based on urea reaction with urease.³⁵ A holographic sensor for urea has been developed in which urease coupled holograms were used to detect and quantify urea³⁶.



Scheme 6.1. Hydrolysis of urea by urease yields bicarbonate and ammonium ions.

This chapter deals with urease immobilized PCCA (UPCCA) based sensing material for the determination of Hg^{2+} in aqueous medium. When the UPCCA exposed to the urea solution, the immobilized urease enzyme hydrolyzes the urea and produces NH_4^+ and HCO_3^- ions within the hydrogel. These ions result in the charge-screening between the carboxylate groups of the polyacrylamide backbone which triggers the shrinkage of gel. Therefore, the UPCCA displays blue shift in the diffraction. Instead of only urea when UPCCA is exposed to the solution of urea and Hg^{2+} , then the Hg^{2+} inhibits the urea hydrolysis and suppresses the production of NH_4^+ and HCO_3^- ions within the hydrogel. This result in the less blue shift of UPCCA. Therefore the blue shift of UPCCA diffraction can be monitored as a function of Hg^{2+} concentration for a fixed urea concentration. A schematic representation of UPCCA sensing motif is represented in Figure 6.1. We have studied in detail enzyme (urease)-substrate (urea) kinetic and

their inhibition in the solution states (where urease is in the free form) and as well as in the hydrogel state (where urease is immobilized in the hydrogel). This in depth kinetic study reveals the reason behind the very high specificity of the UPCCA sensor towards Hg^{2+} .

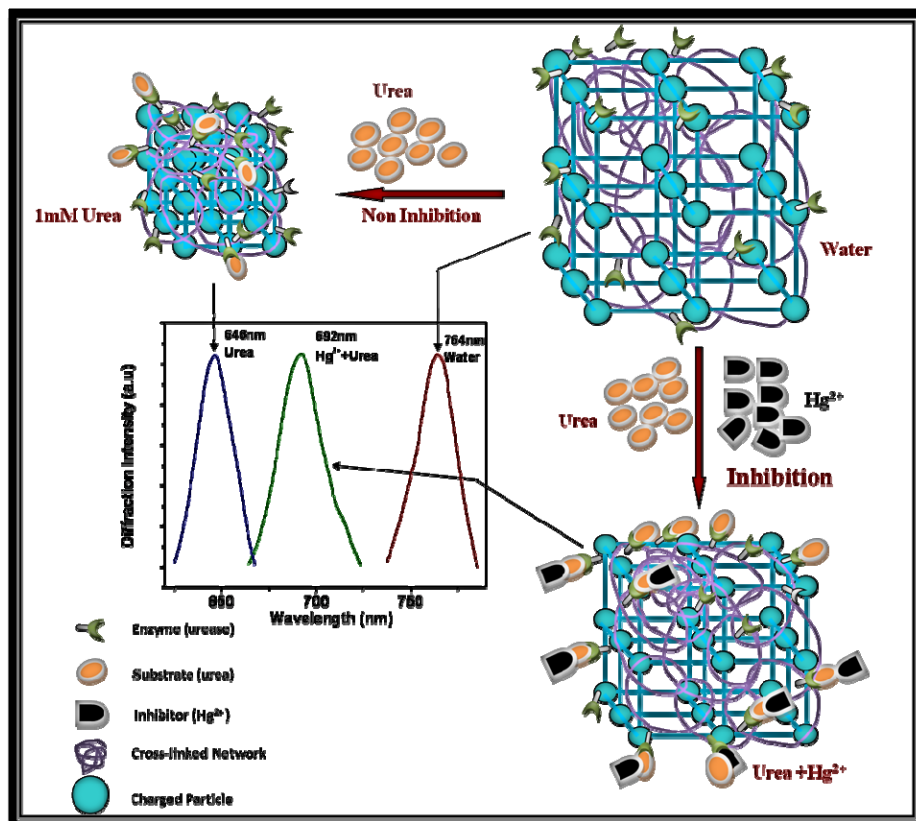
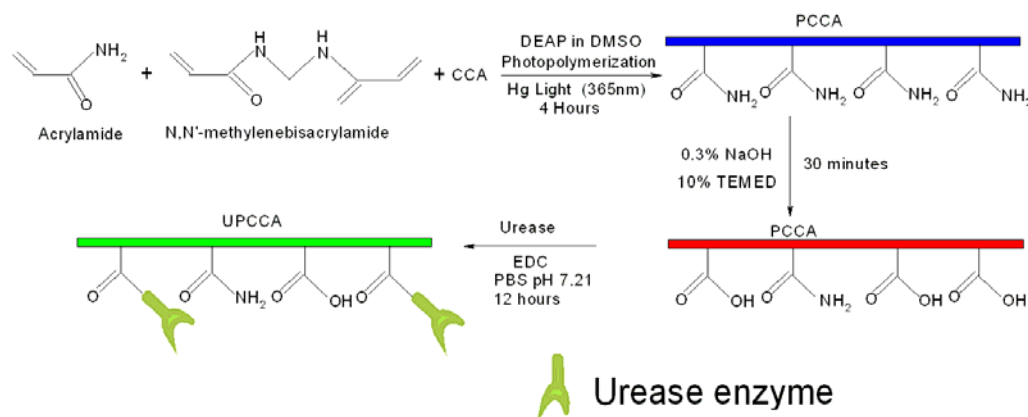


Figure 6.1. Schematic representation of UPCCA sensor concept in which sensing motif is relied on two steps coupled spontaneous processes.

6.2. Experimental Section

The preparation of PCCA based light diffracting sensor material for the sensing of mercury involves three major steps as follows and these steps are summarized in

Scheme 6.2. The steps involved are: (1) preparation of PCCA, (2) preparation of ions responsive PCCA (carboxylated PCCA), and (3) preparation of urease coupled (UPCCA) sensor for mercury.



Scheme 6.2. Preparation of urease coupled polymerized crystalline colloidal array (UPCCA) for the sensing of mercury ion (Hg^{2+}).

6.2.1. Preparation of PCCA

Acrylamide (AA, 0.100 g, 1.40 mmol, Sigma Aldrich), N,N'-methylenebisacrylamide (0.005 g, 0.01951 mmol), CCA (2.00 g, 8 wt %, 102 nm diameter crosslinked polystyrene particles prepared from previously reported recipe (chapter 2)³⁷, and AG 501-X8 ion-exchange resin (0.10 g, 20-50 mesh, mixed bed, Bio-Rad) were mixed together in a 10 ml screwcap glass vial by shaking in vortex mixer. 10% v/v diethoxyacetophenone (DEAP 7.7 μ L, 3.84 mol, Aldrich) in dimethyl sulfoxide (DMSO, Fisher) was added in to the above reaction mixture and mixed with the help of vortex mixer. This reaction solution (polymerization mixture) is nitrogen bubbled thoroughly to remove the any dissolved oxygen. The polymerization mixture was withdrawn from the vial using thin needle to avoid ion exchange resin and injected into a polymerization cell consisting of two quartz disks, separated by a 127 μ m thick parafilm spacer. The polymerization cell was placed under mercury (Black Ray) lamp

operating at 365 nm for 4 hours. After the completion of the reaction the quartz cell was opened in millipore water, and the obtained PCCA was washed thoroughly with millipore water several times.

6.2.2. Preparation of ionic strength responsive PCCA (carboxylated PCCA)

The hydrolysis of PCCA makes the PCCA ions responsive. Partial hydrolysis of amide groups of polyacrylamide backbone of PCCA yield carboxylate groups. These covalently attached carboxylate groups carries counter ions inside the hydrogel and the hydrogel (PCCA) swells owing to the osmotic pressure. Therefore, the PCCA becomes ionic strength responsive. The hydrolysis of PCCA was carried out as follows: a small piece of PCCA was treated with 25 mL of aqueous hydrolysis solution containing 0.3N NaOH (Merck) with 10% v/v *N,N,N',N'*-tetramethylethylenediamine (TEMED, Sigma-Aldrich) for 1.5 hour. The hydrolyzed PCCA was washed thoroughly several times with Millipore water.

6.2.3. Preparation of urease coupled PCCA (UPCCA) sensor for mercury

0.005g of urease (Jack Bean, 0.005g, MW 480 kDa SRL, India) and 0.005g of solid ethyl-(3-dimethylaminopropyl) carbodiimide hydrochloride (EDC, 0.005g, 0.026mmol, Aldrich) were dissolved in 1ml 0.1mM phosphate buffered saline (PBS) at pH 7.21. The urease-EDC solution was placed on top of the hydrolyzed PCCA for 12 hours. After 12 hours the resulting UPCCA mercury sensor was washed extensively with Millipore water.

6.2.4. Preparation of CCA free urease coupled hydrogel

CCA free hydrogel (blank hydrogel) was prepared using the similar recipe as described above (preparation of PCCA). In this case water (2g) was used instead of CCA. This blank hydrogel was hydrolyzed and urease coupled using the exactly identical experimental condition as described above for the determination of attached

enzyme, free carboxylate concentrations and studies of enzyme-substrate-inhibition kinetics.

6.2.5. Determination of coupled enzyme concentration and free carboxylate concentrations

An UV-Visible spectrophotometer (Cary 100Bio, Varian) was used to record the absorption spectra of urease coupled blank hydrogel, urease solution in buffer and to study the urease-urea- inhibitor kinetics. An auto titrator (702 SM Titrino, Metrohm) was used for the determination of free carboxylate concentration in the blank hydrogel. The hydrogel was titrated against the standard 0.1N NaOH.

6.2.6. Measurement of UPCCA mercury sensor response

All the diffraction measurements were carried out in reflection mode with Ocean Optics (USB4000-UV-VIS-NIR) spectrophotometer. The sensing experiments of the UPCCA sensor were carried out as follows: A small piece of UPCCA was fixed in a petridish (made of polystyrene, Hi-Glass, India) and the diffraction was recorded in water. Then the UPCCA was exposed to the different concentrations of urea solution in water and their diffraction spectra were collected. A gradual blue shift was observed with increasing urea concentration. Then the UPCCA was washed thoroughly with water and the original diffraction in water was obtained. Then the UPCCA was exposed to the 1mM urea solution in water which contains Hg^{2+} ion and the diffraction was recorded. Again the UPCCA was washed with water and got back the original diffraction in water. Then the UPCCA was exposed to the next higher Hg^{2+} concentration along with 1mM urea solution. After every exposure the UPCCA was washed with water and obtained the original diffraction in water.

6.2.7. Enzyme kinetics studies

The well known Berthelot reaction^{38, 39} was used to study the urease-urea hydrolysis kinetics and the inhibition of this hydrolysis by various heavy metal ions such as Hg^{2+} , Cu^{2+} and Ag^+ . Briefly the method is as follows: Two reagents; reagent A [phenol (5 g, 53 mmol, Merck- India) and sodium nitroprusside (25mg, 0.084mmol, Merck-India) were dissolved in 500 ml of water] and reagent B [NaOH (2.5g, 0.0625mmol, Merck-India) and NaOCl contains 5% active chlorine (4.2 mL, Merck)] were prepared. A small piece of UPCCA (blank hydrogel) was taken in a disposable plastic cuvette. Reagent A (1.5 ml), urea solution of known concentration and reagent B (1.5 ml) were added to the cuvette subsequently. The production of indophenols blue dye started immediately after the addition of reagent B. The progress of the reaction was monitored with time by recording the absorption spectra of indophenols dye using a UV-Vis spectrophotometer (Cary100 Bio, Varian). The values of absorption correspond to the dye concentration which is equal to the produced ammonia concentration due to the urea-urease hydrolysis.^{38, 39} The experiment was carried out with various urea concentrations for the studies of inhibition kinetics in the presence of inhibitors (Hg^{2+} , Cu^{2+} , and Ag^+). We have also carried out the urease-urea hydrolysis kinetics experiments by varying the inhibitor concentrations. The similar urea-urease hydrolysis and inhibition kinetics were done using free urease in the solution.

6.3. Results and Discussion

The polymer hydrogel in the PCCA can readily undergo volume change in response to the various environmental stimuli such as change in pH and ionic strength.^{24, 40,41} It was demonstrated that the net change in the total free energy of the hydrogel is the driving force for the volume change of the hydrogel and the sensing capabilities of these PCCA based sensors relied on the hydrogel volume change^{22-28, 42, 43}. The total free energy of the hydrogel is the combination of three different free

energies; namely ionic free energy (ΔG_{ionic}), free energy of mixing (ΔG_{mix}) and free energy due to elastic restoring forces ($\Delta G_{\text{elastic}}$). Any change in one of these free energies alters the total free energy and caused the volume change (swelling or shrinking) of the hydrogel.

Our aim is to develop a PCCA based light diffracting sensing material which detects ultra low concentration of mercury ion (Hg^{2+}) in the water. Since mercury ion (Hg^{2+}) is a very toxic element present in the polluted water; therefore the efficient, very specific and a colorimetric sensor which operates in water is absolutely needed. PCCA based sensor is the ideal choice for this goal. Optical color readout from the mercury sensing material which can be visually determined by matching the color observed with a color chart is the most desirable. To achieve the above mentioned goal, we have developed a PCCA based sensor which detects mercury in water very selectively using enzymatic hydrolysis of the substrate and its inhibition by the mercury (Hg^{2+}) ion. Our sensor mechanism is the combination of enzyme-substrate reaction and its inhibition by the inhibitor. We have made a sensor which respond to the substrate concentration and this response can be interfered quantitatively by the suitable inhibitor of the enzyme. Hence the interference of the sensor response by the inhibitor to the fixed substrate concentration can be quantified as an inhibitor concentration. Hence, our sensing motif is relied on two step coupled simultaneous processes.

We have utilized urease (enzyme) – urea (substrate) reaction (Scheme 6.1) and followed by the inhibition by the mercury ion (Hg^{2+}) to achieve the PCCA based sensing motif for the detection of toxic mercury ion (Hg^{2+}) in the water. Urea specific enzyme urease is coupled to the ions responsive PCCA (carboxyated) as described in the experimental section. This urease coupled PCCA (UPCCA) hydrolyzes the urea and produces NH_4^+ and HCO_3^- ions within the UPCCA hydrogel over that outside. The production of ions within hydrogel induces the charge-screening between the carboxylate groups of the polyacrylamide backbone. As this occurs, the carboxylates experience less electrostatic repulsion between themselves and the polyacrylamide backbone relaxes, causing the hydrogel to shrink. As a result the UPCCA shows diffraction blue shifting. Hence the diffraction blue shift can be monitored as a function

of urea concentration. When an inhibitor (such as mercury ion) is introduced into the solution, it binds to the urease and deactivates the enzyme functionality by inhibiting the enzyme –substrate reaction. This inhibition process intervenes the production of ions and hence the hydrogel shrinking suppresses. This suppression results the further diffraction red shifting of UPPCA from the blue shifted UPCCA when it was exposed to the urea only. Therefore the suppression of hydrogel shrinking can be controlled as a function of inhibitor concentration (mercury here) for a fixed concentration of substrate (urea here). Hence the net change in the diffraction wavelength shift (red shift) from the initial blue shift with the fixed urea concentration can be quantitatively monitored as a function of inhibitor concentration. Figure 6.1 represents the sensing motif of our sensor.

6.3.1. Coupling of urease in the ionic strength responsive PCCA

The ionic strength responsive PCCA is prepared by creating carboxylate groups on to the polymer backbone through the hydrolysis of amide functionality using sodium hydroxide. The urease coupled PCCA (UPCCA) is prepared using the coupling reagents as described in the experimental section. We have estimated the amount of urease coupled in the PCCA by monitoring the absorbance of urease at 278 nm in the blank gel (gel made in the identical condition as PCCA without CCA). The absorption spectrum of the urease, plot for the calculation of molar extinction coefficient of urease and the absorption spectrum of urease coupled blank gels are presented in the Figure 6.2, 6.3 and 6.4 respectively. We have calculated that $360 \mu\text{mol}/\text{cm}^3$ urease is loaded on to the PCCA. We have also tested and estimated the amount of free carboxylate ions present in the UPCCA after the urease coupling by titrating the free carboxyl with 0.1 N NaOH solutions. Our calculated value for free carboxylate is $0.3 \mu\text{mol}/\text{cm}^3$. Hence our UPCCA contains both urease enzyme, which hydrolyses the urea results the production of ions within the hydrogel, and free carboxylates which response to the ions generated inside the hydrogel.

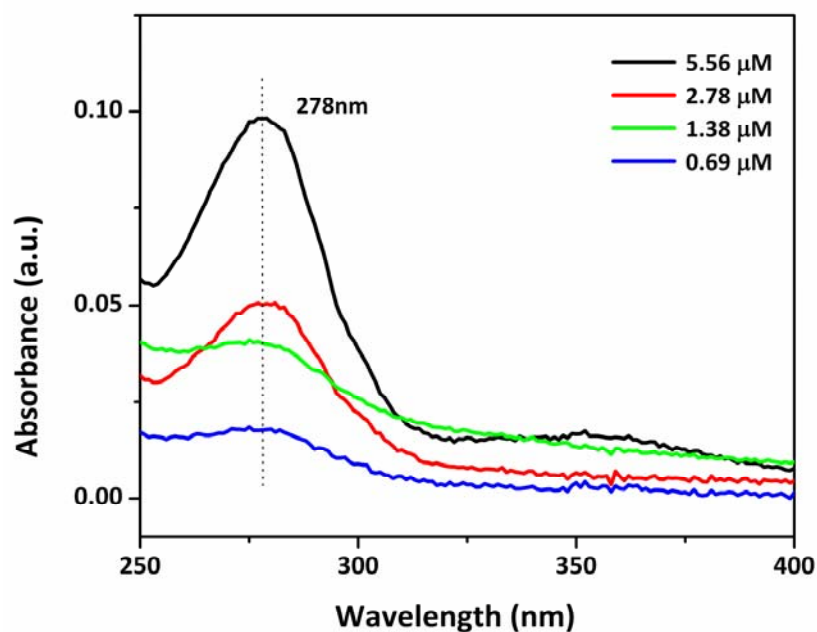


Figure 6.2. Absorption spectra of urease enzyme in phosphate buffered saline (PBS) medium.

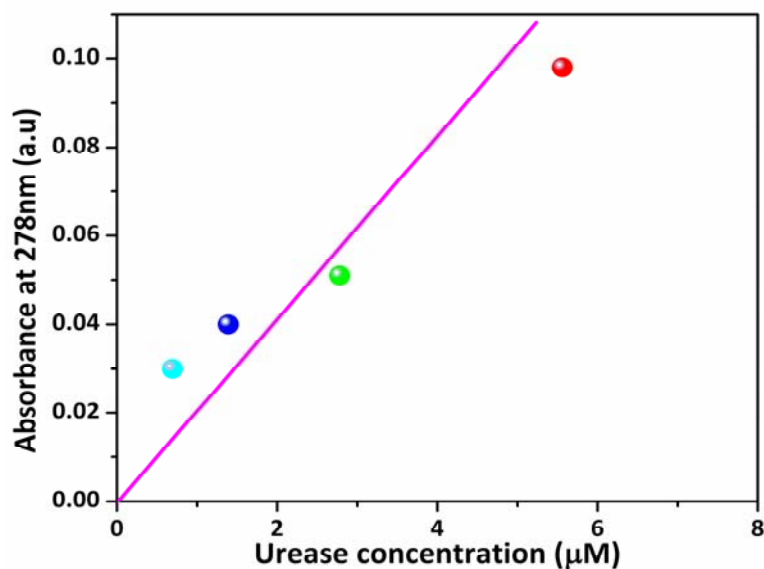


Figure 6.3. Plot for the calculation of molar extinction coefficient (ϵ) of urease in aqueous (PBS) medium. From the slope molar extinction coefficient was estimated to be $20800 \text{ M}^{-1} \text{ cm}^{-1}$

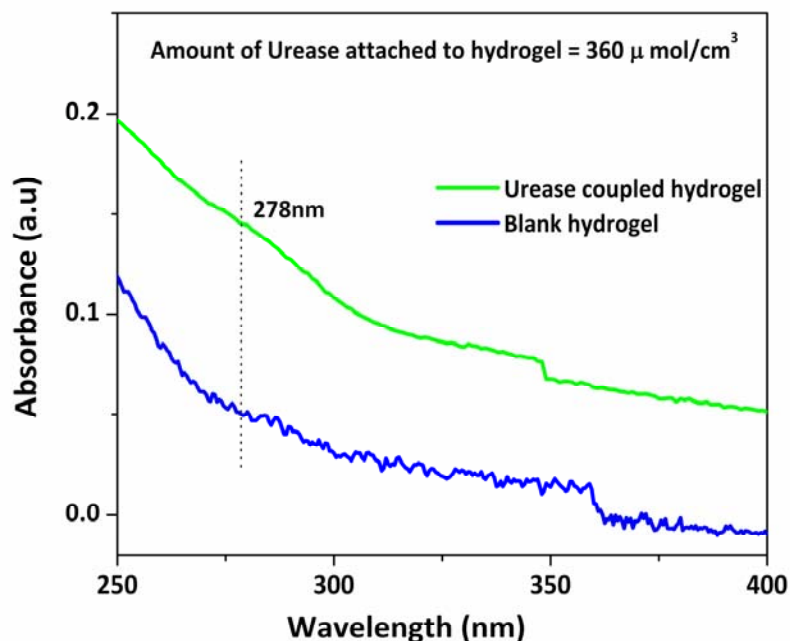


Figure 6.4. Absorption spectra of blank hydrogel, urease coupled blank hydrogel (hydrogel made in the identical condition as PCCA without CCA) for the determination of urease loading in the hydrogel.

6.3.2. Dependence of UPCCA diffraction on urea concentration

Our UPCCA can be utilized as a urea sensor. Figure 6.5 shows the dependence of UPCCA diffraction on the urea concentration in the water solution. Inset of the Figure 6.5 represents the diffraction spectra of the UPCCA in response to various urea concentrations. Our UPCCA consists of both free carboxylate ions and urease. The urease loaded in UPCCA hydrolyzes the urea and yields the bicarbonate and the ammonium ions within the hydrogel as shown in the Scheme 6.1. These ions within the UPCCA trigger the charge –screening of the carboxylates by decreasing the electrostatic repulsion between themselves, resulting the shrinkage of the UPCCA. As a result of this

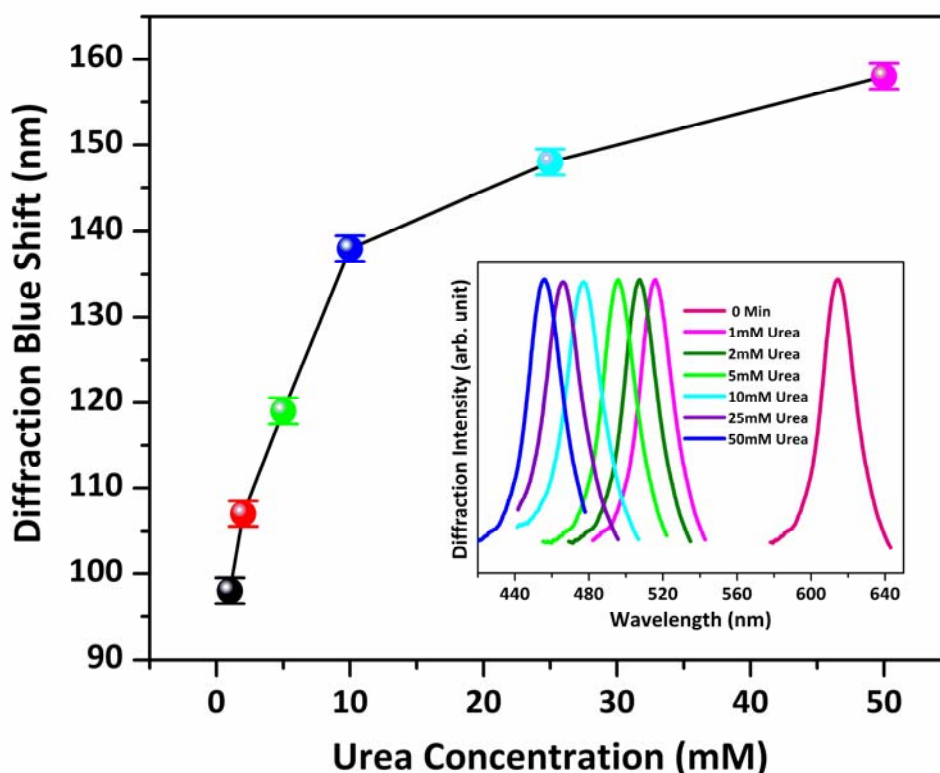


Figure 6.5. *Dependence of UPCCA diffraction as a function of urea concentration in water. Inset: Diffraction spectra of UPCCA in response to various urea concentrations.*

volume shrinkage the diffraction blue shift is observed as a function of the urea concentration (Figure 6.5). As the urea concentration in the exterior solution increases, UPCCA diffraction shifts more towards blue. It is evident from the Figure 6.5 that the UPCCA diffraction blue shifts with increasing urea concentration. Initially the diffraction blue shift is quite faster and then it begins to saturate at 25mM urea concentration. The response of the UPCCA is completely reversible in nature. After exposing the UPCCA with various urea concentrations; a thorough washing of the UPCCA with water brings back the original diffraction from its blue shifted diffraction. A control experiment was carried out with a urease free ion responsive PCCA (carboxylated) to realize the necessity of the urease enzyme in the PCCA for the sensing of urea. This urease free PCCA does not respond to the urea. This attributes the fact

that the enzyme (urease)-substrate (urea) reaction and the production of the ions is absolutely necessary for this sensing motif.

6.3.3. Dependence of UPCCA diffraction on mercury concentration

Mercury acts as an inhibitor for the urease – urea hydrolysis reaction. Hence it interferes the hydrolysis of urea and restricts the production of NH_4^+ and HCO_3^- ions. The hydrogel volume and consequently the UPCCA diffraction shift is a function concentration of NH_4^+ and HCO_3^- ions within the hydrogel. Therefore, the mercury concentration which suppresses the production of these ions can be quantified by monitoring the diffraction shift of the UPCCA. We have examined our UPCCA response to the various mercury concentrations in presence of 1 mM urea solution. The maximum contaminant level (MCL) of mercury set by the Environmental Protection Agency (EPA), USA in the drinking water is 2 $\mu\text{g/L}$ (2 ppb).⁴ Hence the detection of mercury in water below and above MCL is essential to affirm whether the tested water is safe to drink or not. We have tested our UPCCA response with mercury concentration in the range of 1 $\mu\text{g/L}$ or 1 ppb (below MCL) to 40 $\mu\text{g/L}$ or 40 ppb (above MCL). First UPCCA is exposed to 1 mM urea and a blue shift (~ 118 nm) from 764 nm (in water) to 646 nm (in 1 mM urea) is observed (Figure 6.6) due to the production ions inside the UPCCA owing to the urease-urea reaction (Scheme 6.1). This production of ions decreases the electrostatic repulsion between the carboxylates due to the charge-screening and hence the polyacrylamide backbone relaxes, resulting the UPCCA diffraction blue shift. Subsequently we washed the UPCCA with water and the diffraction comes back to its original position 764 nm. After washing with water we exposed our UPCCA to a mercury concentration (1 ppb) along with 1 mM urea solution and blue shift (~ 98 nm) from 764 nm (in water) to 666 nm (in 1 ppb mercury + 1 mM urea) is observed (Figure 6.6). We have repeated the similar washing and testing of with higher mercury concentration along with the 1 mM urea. The net diffraction blue shift decreases and moves towards the original position 764 nm with increasing mercury concentration in the 1 mM urea solution (Figure 6.6).

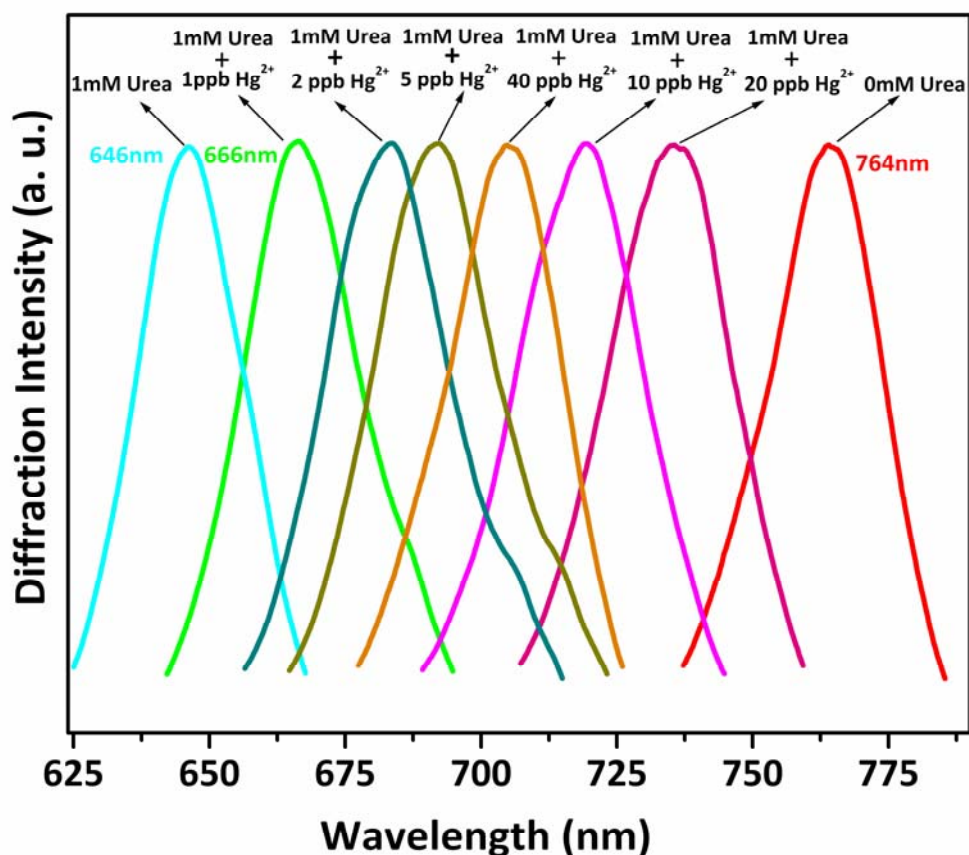


Figure 6.6. Diffraction spectra of UPCCA in response to various mercury ion (Hg^{2+}) concentrations in presence of 1mM urea in water.

We analyze and represent the results as follows: the UPCCA diffraction in response to the 1 mM urea 646 nm is set as a zero mercury concentration and hence other UPCCA diffractions in response to the higher mercury concentrations presented in Figure 6.6 are treated as red shifted relative to the 1 mM urea (or zero mercury concentration). Figure 6.7 represents the diffraction red shift of UPCCA as a function of mercury concentration. The diffraction monotonically red shifts with increasing mercury concentration and starts to decrease at ~ 40 ppb. This red shift with increasing mercury concentration is observed because of the inhibition of urease – urea reaction by

mercury. This inhibition suppresses the production of NH_4^+ and HCO_3^- ions which results from the urease – urea hydrolysis. As a result of this suppression the hydrogel shrinkage is reduced compare to the 1 mM urea and red shifts are observed in presence of mercury. The decrease of red shift after the 40 ppb mercury concentration (Figure 6.7) is due to the fact that the ionic strength owing to the mercury salt (mercuric chloride) is overshadowed the suppression of ions production by the mercury inhibitor. The sensing of higher concentration (>40 ppb) of Hg^{+2} requires wider diffraction wavelength shift which can be achieved in number of ways viz. using higher urea concentration, decreasing the cross-linking of the gel and reducing the thickness of the PCCA.

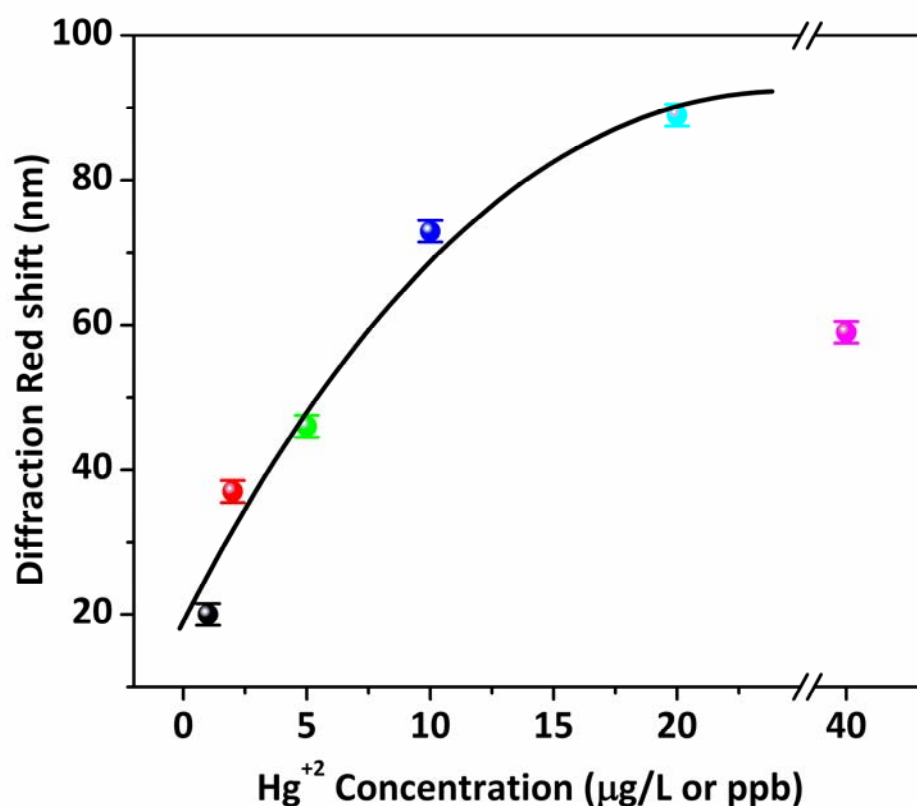


Figure 6.7. Diffraction red shift of UPCCA as a function of mercury ion (Hg^{2+}) concentration in water in presence of 1mM urea. The solid line is a guiding line for the points.

Our UPCCA sensing response and the data presented in Figure 6.6 and 6.7 are completely reversible, reproducible. The UPCCA sample shows excellent mechanical stability and hence same piece of sample can be used repeatedly without compromising the detection limit for the sensing of mercury concentration in water. In the previous section, in control experiment we have showed that the urease free ions responsive PCCA (carboxylated) does not response to the urea concentration since urea does not produce any ions because of the unavailability of the urease enzyme in the PCCA. Similarly this urease free PCCA does not response to the mercury concentrations. This is due to the fact that these mercury concentrations (1 ppb to 40 ppb) produce very low ionic strength in the order of nano molar which is not enough for the ions responsive PCCA to response. Therefore the above control experiments clearly demonstrate that both the enzyme urease and the ions responsive PCCA (carboxylated) are required and need to be coupled together for the successful sensing of the mercury concentration in the water. Besides mercury (Hg^{+2}), copper (Cu^{+2}) and silver (Ag^{+}) ions are the known inhibitors for the urease and urea hydrolysis reaction but they have much lower inhibitive efficiency compared to mercury ion.²⁹ The UPCCA yielded negligible diffraction shifts when it was exposed to the wide range of copper and silver ions concentrations. This observation implies that the current UPCCA sensor is exclusively responsive to the mercury ion. The high specificity of the UPCCA towards mercury is due to the strong inhibiting capacity of mercury ion compared to the others. Detailed comparative analysis of the inhibiting efficiencies is discussed in the following section.

6.3.4. Studies of inhibition mechanism

It is worthwhile to note that we have washed the UPCCA with water after every exposure to the mercury concentration and got back the UPCCA original diffraction in water. Only after this we exposed the UPCCA to the next higher mercury concentration. It must be noted that unless we follow this repeated washing methods as mentioned above, UPCCA does not response as presented in Figure 6.6 and 6.7; instead response saturates after the first mercury exposure. Another important experimental step for the

sensing is that, we are adding the substrate and inhibitor together. These unusual experimental conditions (repeated washing, addition of substrate and inhibitor together) as well as very strong specificity of UPCCA towards mercury ion compared to other inhibitors promoted us to study and analyze the inhibition kinetics of the urease-urea (enzyme-substrate) hydrolysis in the PCCA. We have studied the urease-urea hydrolysis reaction kinetics both in solution (free enzyme in aqueous medium) and in blank hydrogel (CCA free hydrogel, here enzyme is covalently attached to the polymer backbone through amide linkage in the hydrogel) states as described in the experimental procedure using well known Berthelot reaction^{38, 39}. The studies are carried out in absence of inhibitors as well as in presence of various inhibitors viz. mercury (Hg^{+2}), copper (Cu^{+2}) and silver (Ag^{+}) ions. The kinetic study allows us to find out the type of inhibition takes place with the above mentioned inhibitors and as well as their relative inhibitive efficiency both in solution and in hydrogel state.

The progression curves of urease-urea hydrolysis with the wide range of substrate (urea) concentrations for a fixed enzyme concentration in both solution ($0.011\mu\text{mol}/\text{cm}^3$) and hydrogel states ($360\mu\text{mol}/\text{cm}^3$) are shown in the Figure 6.8. In both the cases the rate of hydrolysis is greatly enhanced with the increasing urea concentration and hence gives us opportunity to study the reaction kinetics in depth. The rate of hydrolysis both in solution and hydrogel states for a fixed enzyme and urea concentrations can be easily altered by the addition of mercury ions as evident from the progression curves in Figure 6.9.

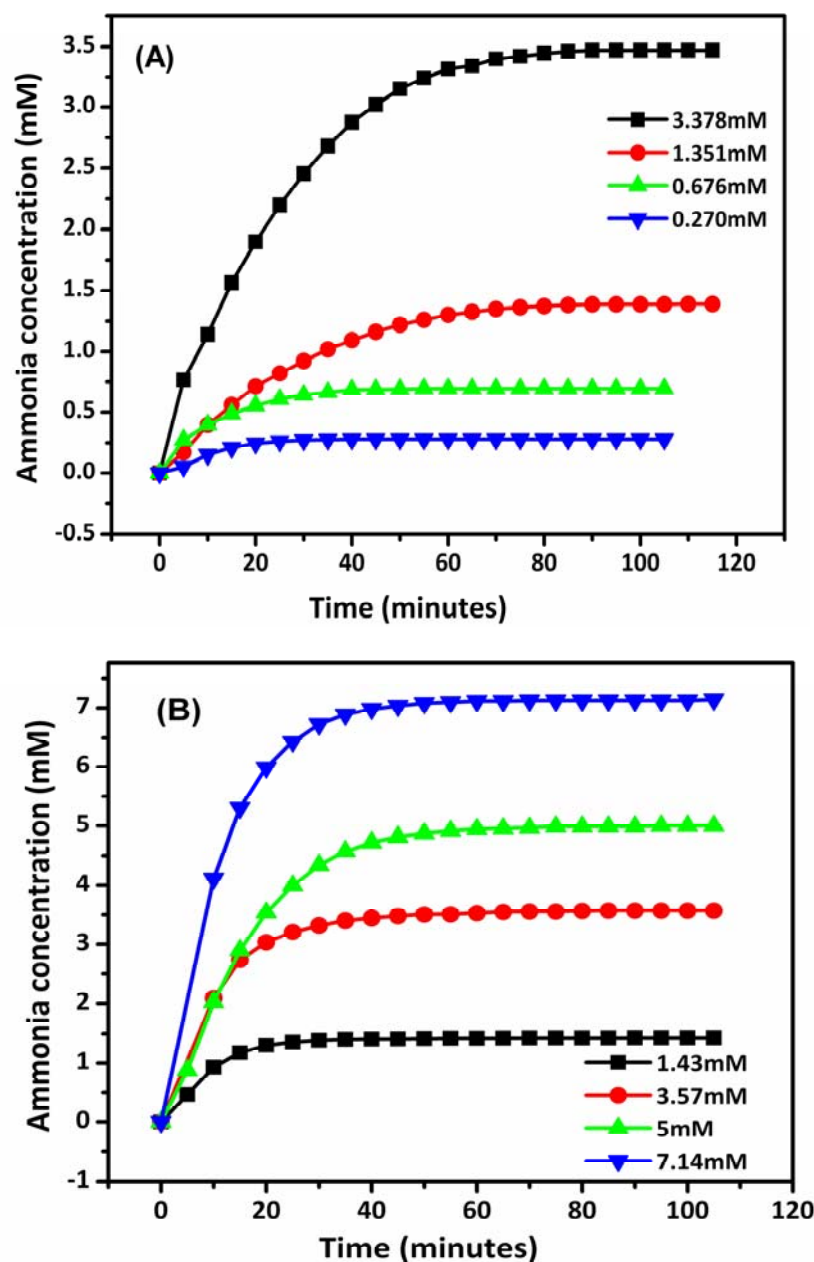


Figure 6.8. Progressive curves for urease-urea hydrolysis for various urea concentrations (indicated in the figure) for a fixed enzyme concentration. The hydrolysis is monitored by UV-Vis spectroscopy using Berthelot method. (A) solution state; enzyme concentration = $0.011 \mu\text{mol}/\text{cm}^3$ (B) hydrogel state; enzyme concentration = $360 \mu\text{mol}/\text{cm}^3$.

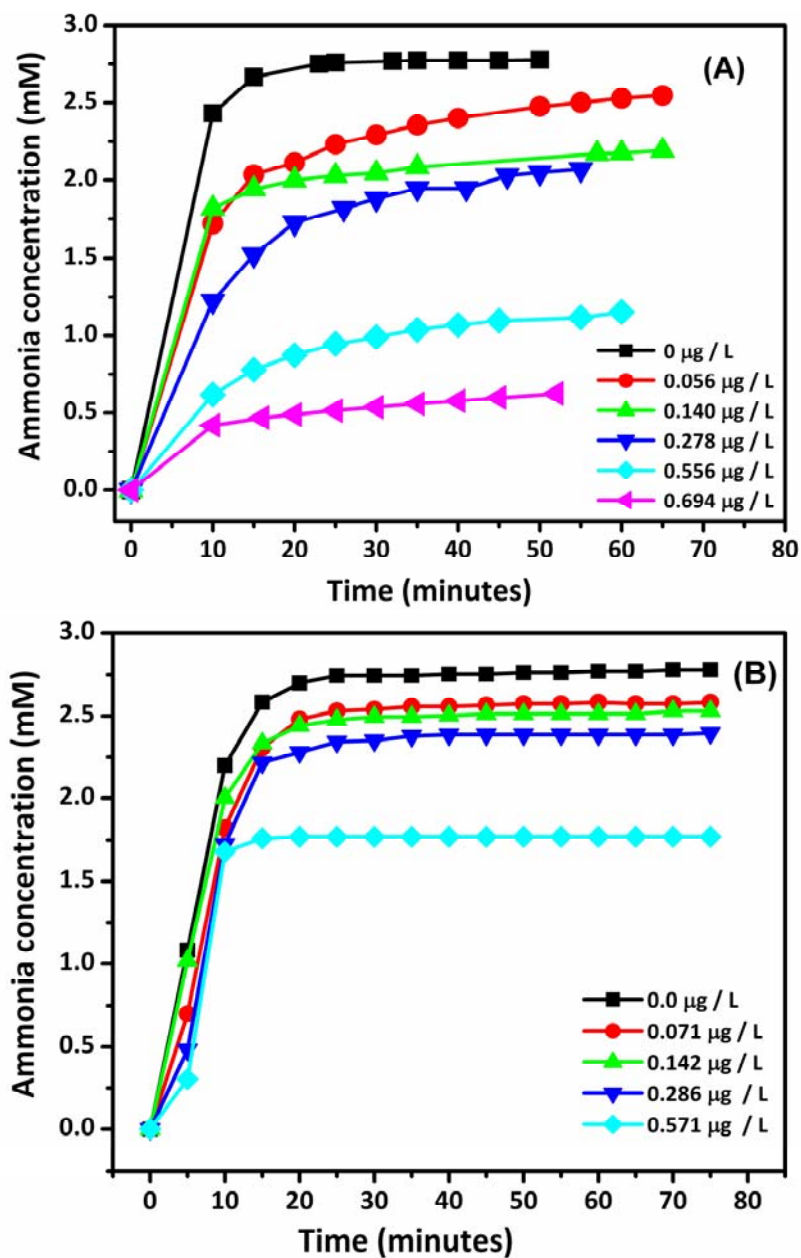


Figure 6.9. Progressive curves for urease-urea hydrolysis for various Hg^{2+} concentrations (indicated in the figures) for a fixed enzyme and substrate (2.78mM, urea) concentration. The hydrolysis is monitored using UV-Visible spectroscopy by Berthelot method. (A) solution state; enzyme concentration= $0.011 \mu mol / cm^3$ (B) hydrogel state; enzyme concentration= $360 \mu mol / cm^3$.

The hydrolysis rate decreases with increasing mercury ion concentration proves that the mercury ion inhibits the urease-urea hydrolysis. In all the kinetics studies the enzyme concentrations and the inhibitor concentrations are kept constant. The progression curves of these kinetics studies involving Hg^{2+} , Cu^{2+} , and Ag^+ inhibitor are presented in Figure 6.10, 6.11 and 6.12 respectively. The Lineweaver-Burk (L-B)⁴⁴ plots obtained from these above progression curves for all the inhibitors both in solution and gel states are presented in Figure 6.13. The sub-figures in the left and right rows of the L-B plots are the results obtained in the solution and the hydrogel states, respectively. The slopes and intercepts of all the subfigures of the Figure 6.13 are tabulated in Table 6.1. In all the inhibitors cases the nature of the L-B plots in case of solution state are different than the hydrogel state. The data obtained from Figure 6.13 and Table 6.1 clearly show that in case of solution state the slopes and intercepts of L-B plots with and without inhibitors are different where as in case of hydrogel state only the intercepts are different but their slopes are identical. These observations are true for all the inhibitors cases. The above observations imply that the inhibition mechanism in solution state is noncompetitive type where as it is uncompetitive in nature when the urease is attached to the polymer backbone in hydrogel (hydrogel state).⁴⁴ The noncompetitive inhibition mechanism of urease enzyme is known in the literature.⁴⁵ The noncompetitive inhibition nature in the solution state indicates that when the urease enzyme (E) is free in the aqueous solution then the inhibitor (I) can bind directly to the substrate active sites of the free enzyme (E) by forming the enzyme-inhibitor complex (EI) and as well as can bind to the enzyme-substrate (ES) complex producing enzyme-substrate-inhibitor (ESI) complex (Scheme 6.3).⁴⁴ In contrast, if the enzyme is immobilized in the hydrogel matrix (hydrogel state) as it is in the UPCCA, then the inhibitor binds only to the ES complex resulting ESI complex and hence the uncompetitive inhibitive mechanism is obtained. Therefore, the above results and discussion clearly attribute that the enzyme urease behaves entirely in different manners towards the inhibitors in hydrogel state compared to the solution state.

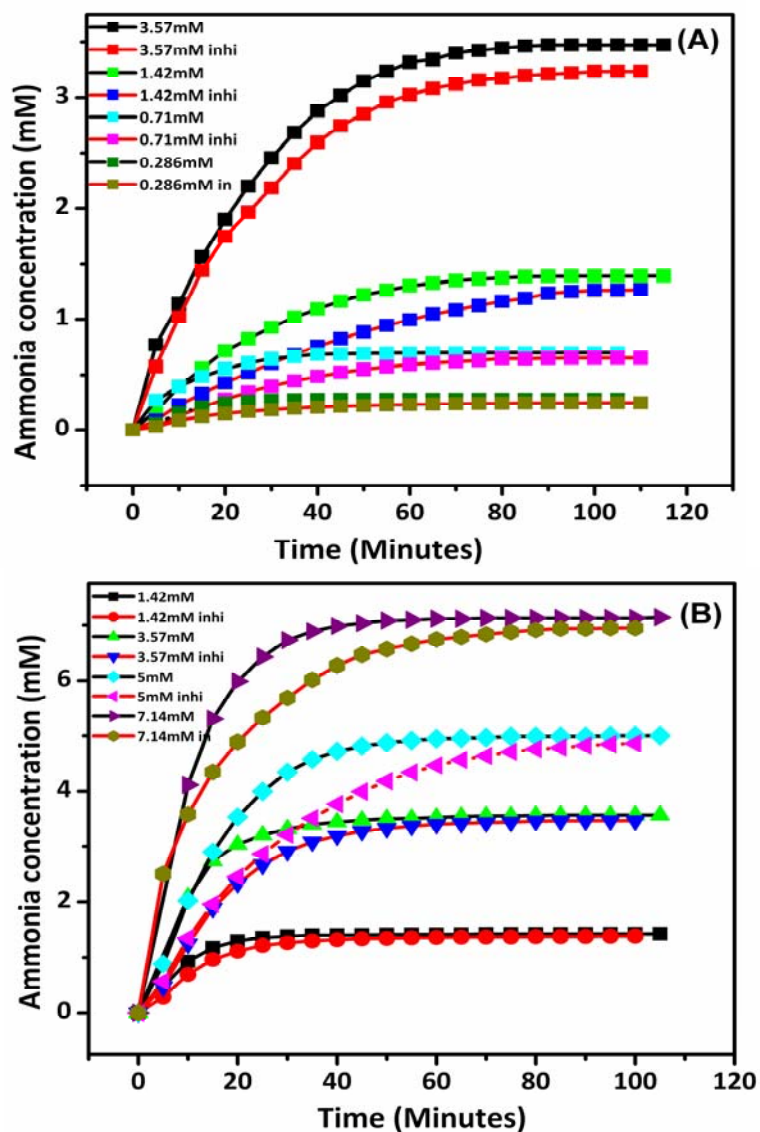


Figure 6.10. Progression curves of urease-urea hydrolysis monitored by Berthelot method with and without inhibitor (Hg^{2+}) both in solution and hydrogel states. In all the cases urease enzyme and inhibitor (Hg^{2+}) concentration are kept constant. (A) solution state; enzyme concentration = $0.011 \mu\text{mol}/\text{cm}^3$ and inhibitor concentration = 0.556 ppb (B) hydrogel state; enzyme concentration = $360 \mu\text{mol}/\text{cm}^3$ and inhibitor concentration = 0.571 ppb . Black lines are non inhibition processes and red lines are inhibition processes. Urea concentrations are mentioned in the figures.

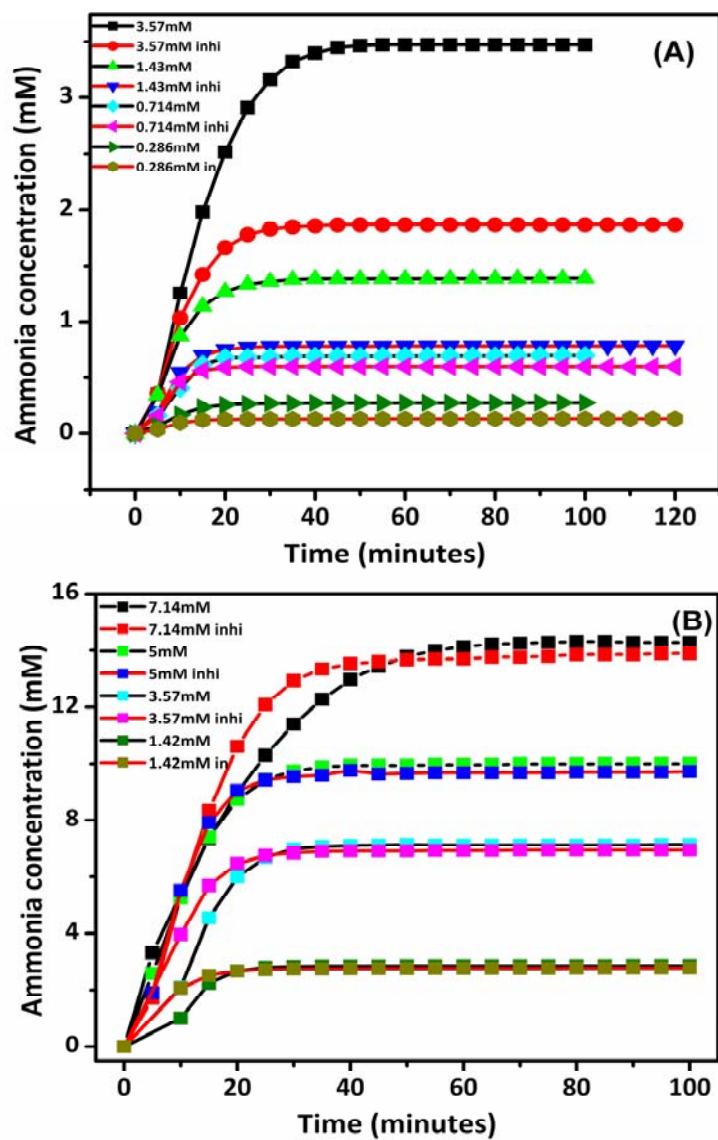


Figure 6.11. Progression curves of urease-urea hydrolysis monitored by Berthelot method with and without inhibitor (Cu^{2+}) both in solution and hydrogel states. In all the cases urease enzyme and inhibitor (Cu^{2+}) concentration are kept constant. (A) solution state; enzyme concentration = $0.011 \mu\text{mol}/\text{cm}^3$ and inhibitor concentration = 0.556 ppb (B) hydrogel state; enzyme concentration = $360 \mu\text{mol}/\text{cm}^3$ and inhibitor concentration = 0.571 ppb . Black lines are non inhibition processes and red lines are inhibition processes. Urea concentrations are mentioned in the figures.

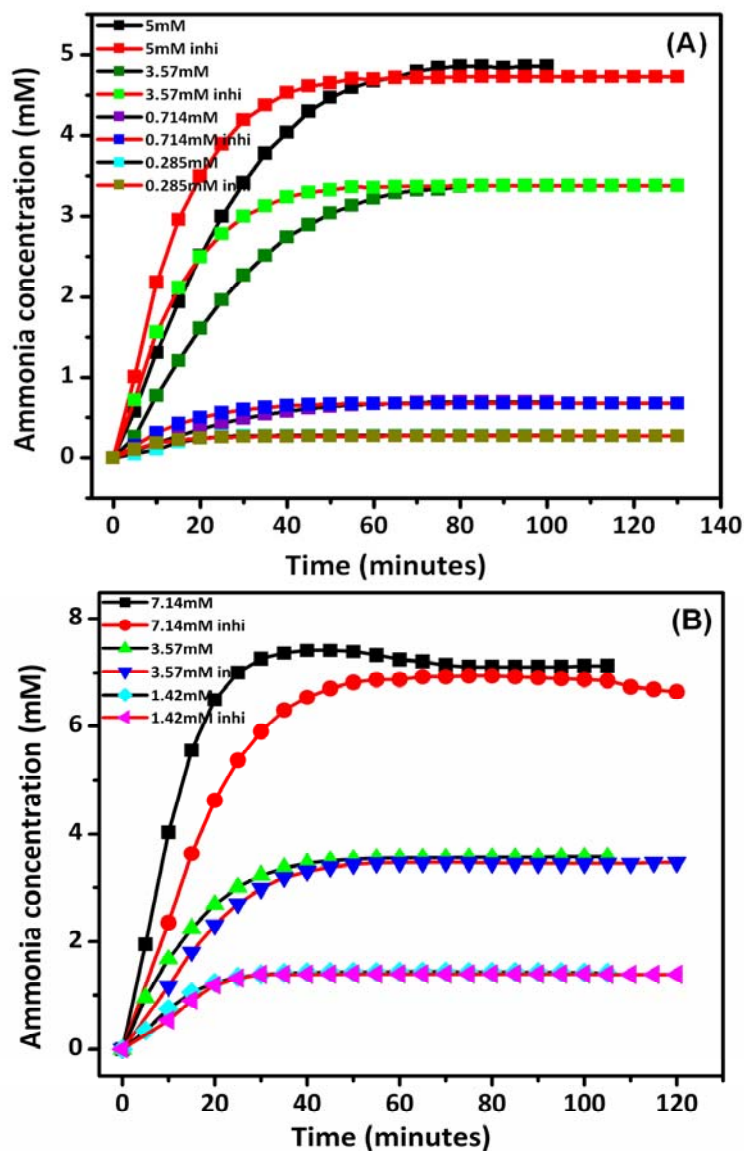


Figure 6.12. Progression curves of urease-urea hydrolysis monitored by Berthelot method with and without inhibitor (Ag^+) both in solution and hydrogel states. In all the cases urease enzyme and inhibitor (Ag^+) concentration are kept constant. (A) solution state; enzyme concentration = $0.011 \mu\text{mol}/\text{cm}^3$ and inhibitor concentration = 0.556 ppb (B) hydrogel state; enzyme concentration = $360 \mu\text{mol}/\text{cm}^3$ and inhibitor concentration = 0.571 ppb . Black lines = non inhibition processes; red lines = inhibition processes. Urea concentrations are mentioned in the figures.

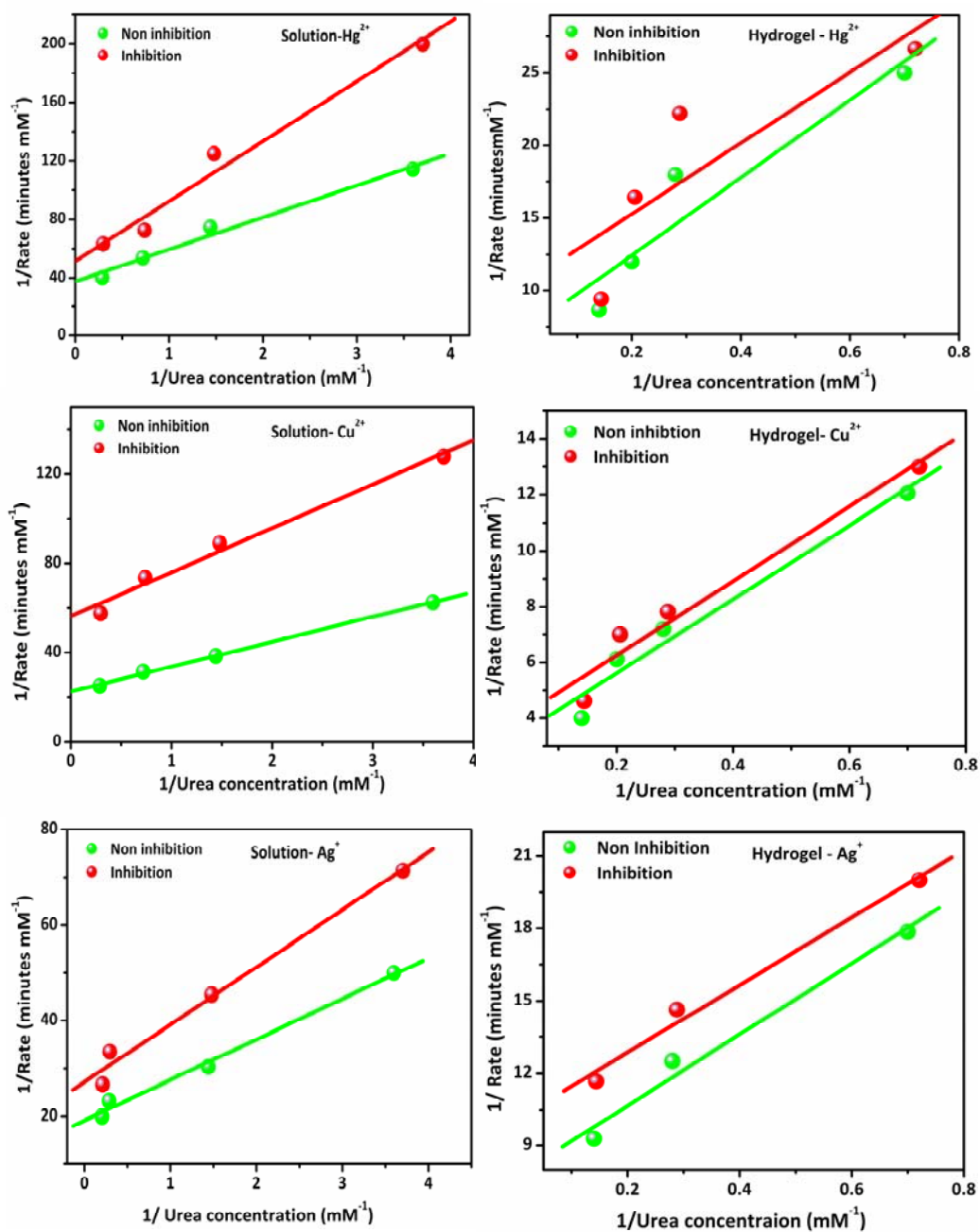
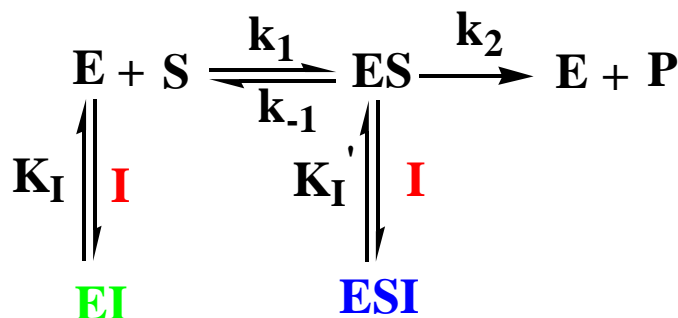


Figure 6.13. Lineweaver-Burk (L-B) plots obtained from the progression curves (Figures 6.10-6.12) of urease-urea hydrolysis in presence and absence of inhibitors. The left and right rows subfigures are for the solution and hydrogel states, respectively. Lines in the figures are the best linear fit lines obtained from the data points.

Table 6.1: The slopes and intercepts obtained from the L-B Plots presented in Figure 6.13.

Hydrogel State						
	<i>Without</i> Hg^{2+}	<i>With</i> Hg^{2+}	<i>Without</i> Cu^{2+}	<i>With</i> Cu^{2+}	<i>Without</i> Ag^+	<i>With</i> Ag^+
Slope	26.73	24.05	13.22	13.31	14.73	13.98
Intercept	7.1	10.41	2.98	3.59	7.72	10.07
Solution State						
	<i>Without</i> Hg^{2+}	<i>With</i> Hg^{2+}	<i>Without</i> Cu^{2+}	<i>With</i> Cu^{2+}	<i>Without</i> Ag^+	<i>With</i> Ag^+
Slope	21.86	40.98	11.14	19.72	8.47	12.01
Intercept	37.69	51.47	22.52	56.25	19.17	27.19

The uncompetitive nature of the inhibition explains why we have chosen such an unusual experimental conditions, for example addition of substrate (urea) and inhibitor together to the UPCCA and washing the UPCCA with water after every exposure to the inhibitor solution. The separate addition of inhibitor (I) prior to the ES complex formation can not be done since the uncompetitive nature of the inhibition process requires the ES complex for the inhibitor to produce ESI complex. The next obvious question is : will it be OK if inhibitor is added after ES complex formation or other wards is it possible to add inhibitor after the addition of substrate (urea) to the UPCCA? This is also not possible because if this is done then ES will breaks down to the product owing to its instability and faster reaction rate (higher rate constant) before it produces the ESI. Therefore the uncompetitive inhibition mechanism clearly demands that inhibitor and substrate need to be added together to the UPCCA. The washing of UPCCA is required after every exposure to the inhibitor since the formation of ESI complex in the uncompetitive type inhibition process is in dynamic equilibrium with the product formation from the ES complex (Scheme 6.3). If the washing is not carried out then inhibitor does not have chance to suppress the raise of ions (NH_4^+ and HCO_3^-) concentration within the hydrogel due to the urea hydrolysis.



Scheme 6.3. Enzyme (urease) - substrate (urea) reaction and the inhibition process by the inhibitors.

6.3.5. Responses towards various inhibitors

We have tested our UPCCA with all the three inhibitors (Hg^{+2} , Cu^{+2} and Ag^{+}) and obtained responses only with the Hg^{+2} . The Cu^{+2} and Ag^{+} ions exhibit negligible responses. To understand the relative inhibitive strengths of these inhibitors we have calculated the stability constants (K_I and K'_I , Scheme 6.3) for the inhibition processes both in solution and hydrogel states using the slopes and intercepts from Figure 6.13 which were tabulated in Table 6.1 with the help of Lineweaver-Burk (L-B) equations⁴⁴ (equation 6.1 and 6.2).

$$\frac{1}{v} = \frac{1}{v_{\max}} + \frac{K_M}{v_{\max}} \frac{1}{[S]} \quad (6.1)$$

Equation 1 is the L-B equation of enzyme-substrate reaction in the absence of inhibitors where v , v_{\max} , K_M and $[S]$ are the rate of the reaction, maximal rate, Michaelis constant and substrate concentration, respectively. In presence of inhibitor the L-B equation of enzyme-substrate reaction is represented as

$$\frac{1}{v} = \frac{\alpha'}{v_{\max}} + \frac{\alpha K_M}{v_{\max}} \frac{1}{[S]} \quad (6.2)$$

$$\text{Where; } \alpha = 1 + \frac{[I]}{K_I} \text{ and } K_I = \frac{[E][I]}{[EI]} \quad \alpha' = 1 + \frac{[I]}{K_I'} \quad K_I' = \frac{[ES][I]}{[ESI]}$$

Table 6.2 represents the stability constants values for all the three inhibitors both in solution and hydrogel states. In the previous section we have shown that the inhibition is uncompetitive in nature in hydrogel state and hence only one type of stability constant (K_I') for ESI complex formation is obtained for the hydrogel state. However, since in solution the inhibition is noncompetitive type and hence both K_I and K_I' are obtained. The smaller value of the stability constant implies the stronger inhibition. The values of the stability constants in solution state are in well agreement with the literature and exhibit inhibitors strength is $Hg^{+2} > Cu^{+2} > Ag^{+1}$ (Table 6.2). Table 6.2 shows that in the hydrogel state the inhibition strength is lower compared to the solution state and the mercury exhibits the strongest inhibition strength among these three. In the hydrogel state the order of the inhibition strength is: $Hg^{+2} \gg Cu^{+2} \approx Ag^{+1}$ (Table 6.2). This order clearly explains the UPCCA response behavior. UPCCA does not response to the copper and silver owing to their very weak inhibitive strength in the hydrogel state. Hence our UPCCA can exclusively detect the mercury in the aqueous medium.

Table 6.2. Stability constants (K_I and K_I') for the inhibition process both in solution and hydrogel states calculated using equation 6.1 and 6. 2 from the kinetics data.

	Solution State			Hydrogel State		
	Hg^{2+}	Cu^{2+}	Ag^{+}	Hg^{2+}	Cu^{2+}	Ag^{+}
K_I (nM)	0.12	3.06	8.04	-	-	-
K_I' (nM)	0.16	1.58	8.07	4.49	11.46	11.24

6.3.6. Reversible nature of the UPCCA sensor

The inhibition of urease enzyme with the mercury is known to be an irreversible in nature in the literature. It has been shown that urease losses its catalytic efficiency once it is exposed to mercury ion. The catalytic efficiency of the urease can be restored only after incubating the enzyme–inhibitor mixture with the strong chelating agents like EDTA (ethylenediaminetetraacetic acid), which strongly bind the mercury ion and thereby urease becomes free from the inhibitor.^{30, 31} Hence, the development of reusable and reversible mercury sensor based on the urease-urea reaction followed by the mercury inhibition has been a great challenge. Interestingly, our UPCCA sensor shows reversibility without compromising the sensing sensitivity. We have used a single piece of UPCCA repeatedly after washing with large quantity of water and obtained the identical response behavior. To strengthen our claim we have carried out the reversibility test with a urease coupled blank hydrogel (CCA free hydrogel which is identical with the UPCCA). Figure 6.14 represents the urease-urea hydrolysis progression curves carried out with the urease coupled blank gel. It is clearly visible from the Figure 6.14 that progression curve suppresses after exposure to the mercury from its original position and the curve goes back to its original position after washing with water. We have observed this behavior repeatedly with various mercury concentrations. Hence the above result demonstrates the reversible nature of our UPCCA. The reason behind this reversibility of our UPCCA and the irreversibility in the solution state is owing to the fact that the inhibition in the hydrogel state is uncompetitive type whereas it is noncompetitive type in the solution state. Hence, the inhibitors form ESI complex in the hydrogel state whereas it form both ES and ESI complexes in the solution. It must be noted that the ESI complex formed in the hydrogel state is not a very strong complex (stability constant, $K_I' = 4.49$ nM, Table 6.2) compared to the solution state ESI complex ($K_I' = 0.16$ nM, Table 6.2). Therefore, washing with large quantity of water repeatedly reactivates the urease readily and we observed the reversibility in case of urease coupled hydrogel. The reversible nature of the current UPCCA sensor has remarkable importance in the actual application of this

sensor. A single piece of UPCCA can be utilized repeatedly to quantify the Hg^{+2} in water without loosing the sensitivity of the sensor.

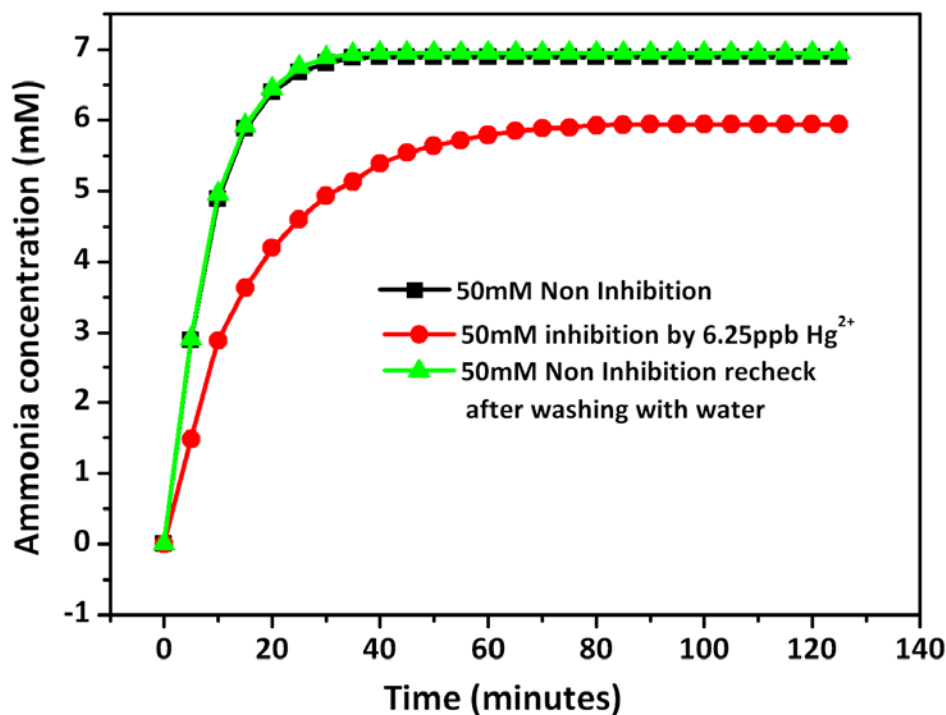


Figure 6.14. *Urease-urea hydrolysis progression curves carried out with urease coupled blank gel (identical with UPCCA but CCA free). The gel is exposed to Hg^{2+} ($6.25\mu\text{g/L}$ or ppb) concentration and the suppression is observed. After washing in the water we have obtained identical progressive curves with urea (50 mM) as it was before the exposure with Hg^{2+} .*

6.4. Conclusion

A novel polymer hydrogel based photonic crystal sensor material has been developed for the determination of toxic mercury ion (Hg^{+2}) concentration in water. This UPCCA sensor material diffracts visible light and the shifts the diffraction wavelength owing to the volume phase transitions experienced by the polymer hydrogel

upon exposure to the different mercury ion concentrations. Our UPCCA consists of urease and carboxylate groups, and therefore responsive to any variation in the ions concentration within the hydrogel due to the enzymatic reactions of the urease. The sensing motif relies on the two consecutive enzymatic pathways, namely hydrolysis of urea by the urease and the inhibition of urea hydrolysis by the mercury ion. The urea hydrolysis by the urease attached to the UPCCA produces ions (NH_4^+ and HCO_3^-) inside the hydrogel over the outside which causes the blue shifting of diffraction carboxylated UPCCA. However in presence of mercury ion the urea hydrolysis is perturbed due to the inhibitive character of the mercury and therefore the net blue shifting of diffraction decreases or in other words red shifts is observed. The most notably the UPCCA is very selective to the mercury ion and the sensor response is reversible in nature. Systematic kinetics studies of urease-urea hydrolysis and the inhibition processes reveal that the selectivity and reversibility of the sensor is due to the uncompetitive inhibition nature of the urease when it is covalently attached to the polymer backbone as it is in the UPCCA. The sensor detection limit is 1 ppb ($1\mu\text{g/liter}$), which is well below the maximum contaminant level (2 ppb) recommended by the EPA, USA for the safe drinking of water.

References

1. Patnaik, P. In *A Comprehensive Guide to the Hazardous properties of Chemical Substances*; Wiley: New York, 1999, PP 614-625.
2. Ireland, M. P.; Dillon, H. K.; Ho, M. H. In *Biological Monitoring of Heavy Metals*; Elsevier: North Holland, 1991.
3. (a) Stern, A. H. *Environ. Res.* **2005**, *98*, 133-142. (b) Campbell, L. M.; Dixon, D. G.; Hecky, R. E. *J. Toxicol. Environ. Health B* **2003**, *6*, 325-356. (c) Morel, F. M. M.; Kraepiel, A. M.L.; Amyot, M. *Annu. Rev. Ecol. Syst.* **1998**, *29*, 543-566.
4. Websites of the Environmental Protection Agency, USA (<http://www.epa.gov>).
5. Morita, M.; Yoshinaga, J.; Edmonds, J. S. *Pure Appl. Chem.* **1998**, *70*, 1585.
6. Harris, H. H.; Pickering, I.; George, G. N. *Science* **2003**, *301*, 1203.
7. Renzoni, A.; Zino, F.; Franchi, E. *Environ. Res. Sect A* **1998**, *77*, 68-72.
8. Boening, D. W. *Chemosphere* **2000**, *40*, 1335-1351.
9. Baughman, T. A. *Environ. Health Perspect.* **2006**, *114*, 147-152.
10. Chiang, C. K.; Huang, C. C.; Liu, C. W.; Chang, H. T. *Anal. Chem.* **2008**, *80*, 3716-3721.
11. Bulter, O. T.; Cook, J. M.; Harrington, C. F.; Hill, S. J.; Rieuwerts, J.; Miles, D. L. *J. Anal. At. Spectrom.* **2006**, *21*, 217-243.
12. Bennun, L.; Gomez, J. *Spectrochim. Acta B: At. Spectrosc.* **1997**, *52*, 1195-1200.
13. Li, Y.; Chen, C.; Li, B.; Sun, J.; Wang, J.; Gao, Y.; Zhao, Y.; Chai, Z. *J. Anal. At. Spectrom.* **2006**, *21*, 94-96.
14. Yen-Sun, H.; Uden, P. C. *J. Chromatogr. A* **1994**, *688*, 107-116.
15. Leermakers, M.; Baeyens, W.; Quevauviller, P.; Horvat, M. *Trends Anal. Chem.* **2005**, *24*, 383-393.
16. (a) Huang, C-C.; Chang, H-T. *Anal. Chem.* **2006**, *78*, 8332-8338. (b) Yu, C-J.; Tseng, W-L.; *Langmuir* **2008**, *24*, 12717-12722. (c) Si, S.; Kotal, A.; Mandal, T. K. *J. Phys. Chem. C* **2007**, *111*, 1248-1255. (d) Lee, J. S.; Mirkin, C. A. *Anal. Chem.* **2008**, *80*, 6805-6808. (e) Xue, X.; Wang, F.; Liu, X. *J. Am. Chem. Soc.* **2008**, *130*,

- 3244-3245. (f) Liu, C. W.; Hsieh, Y. T.; Huang, C. C.; Lin, Z. H.; Chang, H. T. *Chem. Commun.* **2008**, 2242-2244.
17. (a) Liu, X.; Tang, Y.; Wang, L.; Zhang, J.; Song, S.; Fan, C.; Wang, S. *Adv. Mater.* **2007**, *19*, 1471-1474. (b) Ren, X.; Xu, Q-H. *Langmuir* **2009**, *25*, 29-31.
18. Chen, P.; He, C. *J. Am. Chem. Soc.* **2004**, *126*, 728-729.
19. (a) Coronado, E.; Galan-Mascaros, J. R.; Marti-Gastaldo, C.; Palomares, E.; Durrant, J.R.; Vilar, R.; Gratzel, M.; Nazeeruddin, M. K. *J. Am. Chem. Soc.* **2005**, *127*, 12351-12356. (b) Nolan, E.M.; Lippard, S.J. *J. Am. Chem. Soc.* **2003**, *125*, 14270-14271. (c) Nolan, E.M.; Racine, M.E.; Lippard, S. J. *Inorg. Chem.* **2006**, *45*, 2742-2749. (d) Nolan, E. M.; Lippard, S.J. *J. Am. Chem. Soc.*, **2007**, *129*, 5910-5918. (e) Brulmmer, O.; La Clair, J.J.; Janda, K. D. *Org. Lett.* **1999**, *1*, 415-418. (f) Prodi, L.; Bargossi, C.; Montalti, M.; Zaccheroni, N.; Su, N.; Bradshaw, J. S.; Izatt, R.M.; Savage, P. B. *J. Am. Chem. Soc.* **2000**, *122*, 6769-6770.
20. (a) Li, T.; Dong S.; Wang, E. *Anal. Chem.* **2009**, *81*, 2145. (b) Liu, J.; Lu, Y. *Angew. Chem., Int. Ed.* **2007**, *46*, 7587-7590.
21. (a) Chen, B.; Yu, Y.; Zhou, Z.; Zhong, P. *Chem. Lett.* **2004**, *33*, 1608-1609. (b) Zhu, C.; Li, L.; Fang, F.; Chen, J.; Wu, Y. *Chem. Lett.* **2005**, *34*, 898-899.
22. Holtz, J. H.; Asher, S. A. *Nature* **1997**, *389*, 829-832.
23. Holtz, J. H.; Holtz J. S. W.; Munro, C. H.; Asher, S. A. *Anal. Chem.* **1998**, *70*, 780-791.
24. Lee, K.; Asher, S. A. *J. Am. Chem. Soc.* **2000**, *122*, 9534-9537.
25. Sharma, A.; Jana, T.; Kesavamoorthy, R.; Shi, L.; Virji, M.; Finegold, D.; Asher, S.A. *J. Am. Chem. Soc.*, **2004**, *126*, 2971-2977.
26. Muscatello, M. M.; Asher, S. A. *Adv. Func. Mater.* **2008**, *18*, 1186-1193.
27. Xu, X.; Goponeko, A.V.; Asher, S. A. *J. Am. Chem. Soc.* **2008**, *130*, 3113-3119.
28. Maurer, M. K; Gould, S. E.; Scott, P. J. *Sensors and Actuators B* **2008**, *134*, 736-742.
29. (a) Preininger, C.; Wolfbeis O. S. *Biosen. Bioelectron.* **1996**, *11*, 981-990. (b) Zaborska, W.; Krajewska, B.; Olech, Z. *J. Enzyme. Inhib. Med. Chem.* **2004**, *19*, 65-69.

30. Krawczyk, T.K.V.; Moszczyńska, M.; Trojanowicz, M. *Biosen. Bioelectron.* **2000**, *15*, 681–691.
31. Yang, Y.; Wang, Z.; Yang, M.; Guoa M.; Wu, Z.; Shen, G.; Yu, R. *Sens. Actuators, B* **2006**, *114*, 1–8.
32. Qin, Y.; Cabral, J.M.S. *Biocatal. Biotransform.* **2002**, *20*, 1–14.
33. Zhylyak, G.A.; Dzyadevich, S.V.; Korpan, Y.I.; Soldatkin, A.P.; El'skaya, A.V. *Sens. Actuators B* **1995**, *24-25*, 145-148.
34. (a) Krajewska, B.; Zaborska, W.; Chudy, M. *J. Inorg. Biochem.* **2004**, *98*, 1160–1168. (b) Volotovskiy, V.; Jung Nam, Y.; Kim, N. *Sens. Actuators, B* **1997**, *42*, 233–237. (c) Preininger, C. *Mikrochim. Acta* 1999, *130*, 209-214.
35. Zeng, F.; Wu, S.; Sun, Z.; Xi H.; Li, R.; Hou, Z. *Sens. Actuators, B* **2002**, *81*, 273 – 276.
36. Marshall, A. J.; Young, D. S.; Blyth, J.; Kabilan S.; Lowe C. R. *Anal. Chem.* **2004**, *76*, 1518 – 1523.
37. Arunbabu, D.; Sannigrahi, A.; Jana, T. *J. App.Polym. Sci.*, **2008**, *108*, 2718–2725.
38. Berthelot, M. *Repert. Chem. Applique* **1859**, *1*, 284.
39. Patton, C. J.; Crouch S. R. *Anal. Chem.* **1977**, *49*, 464.
40. Tanaka, T. *Sci. Am.*, **1981**, *244*, 124.
41. Takeoka, Y.; Berker, A. N.; Du, R.; Enoki, T.; Grosberg, A.; Kardar, M.; Oya, T.; Tanaka, K.; Wang, G.; Yu, X.; Tanaka, T. *Phys. Rev. Lett.*, **1999**, *82*, 4863.
42. Asher, S. A. in *Nanoparticles: Building Blocks for Nanotechnology*; Rotello, V. M. (ed.); Kluwer: New York, 2004.
43. (a). Kamenjicki, M.; Lednev I. K.; Asher, S. A. *J. Phys. Chem B*, **2004**, *108*, 12637; Kamenjicki M.; Asher, S. A. *Sens. Actuators B*, **2005**, *106*, 373.
44. Atkins, P.; Paula, J-D. *Atkins' Physical Chemistry*, 7th Edition., Oxford University Press: New York, 2002.
45. (a).Qin, Y.; Cabral, J. M. S. *Appl. Biochem. Biotech.*, 1994, **49**, 217; (b). Fidaleo M.; Lavecchia, R.; *Chem. Biochem. Eng.*, 2003, **17**, 311.

Chapter 7

Summary & Conclusions

7.1 Summary

Thesis entitled “*Synthesis of Charged Polystyrene Colloids and Polymer Hydrogel Photonic Crystal Mercury Sensor*” covers various aspects of emulsion copolymerization especially focuses on synthesis and utilization of highly monodisperse polystyrene copolymer particles and their use in urease coupled polymerized crystalline colloidal array (polymer hydrogel photonic crystal) smart sensing material for the sensing of toxic mercury ion (Hg^{2+}) in water. Thesis contains seven chapters which includes an introductory chapter, five working chapters, and a concluding chapter. The summary of the contents of each chapter is given below chapterwise.

Chapter 1

Brief introduction of various topics related to thesis contents, the scope and aim of the thesis has been discussed. A detail insight about colloids, monodisperse colloids and polymer colloids has been discussed. A brief picture of emulsion polymerization and its unique features has been illustrated. Different classes of hydrogels and characteristic expansion and contraction behavior of hydrogels are discussed. A detailed description of versatile classes of PCCA smart sensing materials and their functioning are presented. Enzymes, enzymatic reaction and their various types of inhibition processes are discussed.

Chapter 2

This chapter deals with synthesis of charged spherical colloidal particles of poly [styrene-(co-2-propene sulfonic acid)] crosslinked with divinylbenzene by emulsion polymerization. The effects of concentration of both the emulsifier and initiator on the polymerization kinetics, particle size, and charge density are studied. The particle size is found to be dependent on both the emulsifier and initiator concentration and their power dependencies are different. Below critical micelle concentration (CMC), the particle size varies significantly within a small range of emulsifier concentration. In contrast,

particle size decrease is not very pronounced at the heterogeneous (micellar) particle nucleation regime where the emulsifier concentration is well above of the CMC. The power dependencies of the number of particles on surfactant concentration are explained in the light of conversion–time profile of the polymerization. The surface charge density of the colloidal particles also varies with both the emulsifier and initiator concentration. Both the particle size and charge density show an inverse relation with the molecular weight of the polymer.

Chapter 3

In this chapter, we have synthesized highly charged, crosslinked poly (styrene-co-divinylbenzene-co-sulfopropyl methacrylate) copolymer colloidal particles using emulsion polymerization. The effects of concentration of the emulsifier and the initiator on the particle size and the charge density of the colloidal particles are studied. Colloidal particle size is highly dependent upon the concentration of the emulsifier and the initiator. The colloidal particle diameter decreases with increasing concentration of the emulsifier and increases with increasing concentration of the initiator in the polymerization mixture. Number of particles, surface charge density and charges per particle are also functions of both the emulsifier and the initiator concentration. The surface charge density and the number of charges per sphere increase with increasing particle diameter. These copolymer colloid particles self assemble readily and diffract visible light. Polymer hydrogel imbibed with these colloids shows the light diffraction.

Chapter 4

A series of poly(S-co-NaSS) copolymers containing various NaSS loadings have been synthesized using emulsion polymerization. The copolymerization kinetics are significantly influenced by the monomer feed ratio and are greatly enhanced with increasing NaSS content in the reaction. The gel effect, the shift of particle nucleation locus and the increase in the number of particles are found to be the driving force for the enhancement of the polymerization kinetics. FTIR studies demonstrate the occurrence

of association of the polymer chains due to $-\text{SO}_3\text{H}$ groups which results in the gel effect. NMR spectroscopy has been used to determine the monomer composition in the copolymers and the monomer reactivity ratios. Styrene monomer reactivity ratio is less than unity, whereas that of NaSS is very high. The monomer reactivity ratio values suggest that the NaSS selectively adds to NaSS rather than styrene, whereas styrene prefers to react with NaSS over its own monomer. Monomer reactivity ratios demonstrated that the styrene copolymerization is nearly twice as fast as the homopolymerization, whereas NaSS homopolymerization is nearly ten times faster than copolymerization with styrene. The particle size varies with the NaSS content in the copolymer. The variations of particle size have been explained in the light of the particle nucleation mechanism. TGA studies showed that the thermal stability increases markedly for higher NaSS content. The glass transition temperature depends upon the copolymer composition.

Chapter 5

Emulsion copolymerization of styrene with comonomers viz acrylic acid (AA), methacrylic acid (MAA), 2-Hydroxyethyl methacrylate (HEMA) and sodium styrene sulphonate (NaSS) are carried out by varying emulsifier (SDS) concentration. The effect of comonomers on copolymerization kinetics, particle size, thermal properties and their self-assembly are studied. A steady increment in kinetics in all the copolymers are observed with surfactant excepts NaSS where gel effect accelerated the copolymer kinetics even nullifying the critical micellar concentration (CMC) factor. Below the CMC polymerization kinetics is slower and increases tremendously in all the copolymer cases (AAc, MMA, and HEMA). The particle size increases sharply with decreasing surfactant concentration below CMC and it decreases slowly with the increase in surfactant concentration above CMC for all the copolymer systems. The trend of particle size variation with surfactant concentration is different for different copolymer systems. The increasing order of dependency of particle size on surfactant concentration is as follows $\text{AAc} > \text{MMA} > \text{NaSS} > \text{HEMA}$ in below CMC region whereas the increasing order of dependency is reversed as follows $\text{NaSS} > \text{HEMA} > \text{AAc} > \text{MAA}$. Hydrophobic

HEMA rapidly precipitates and forms more precursor oligomers which matures into large number of smaller sized particles. Hydrophilic acrylic acid produces less number of precursor particles due to its slow rate of precipitation which yields bigger particles. Number of particle increases with increasing surfactant and it follows the order MAA>HEMA>NaSS>AAc below CMC; whereas the order above CMC is NaSS>HEMA>AAc>MAA. AAc copolymers showed good thermal stability followed by MMA, NaSS and HEMA. Highly charged colloidal particles are sedimented on glass slide self assembled into close packed structures which bragg diffract the visible light and have the potential to be used in photonic crystal devices.

Chapter 6

This chapter demonstrates development of a new photonic crystal hydrogel for the sensing of highly toxic mercury ion (Hg^{2+}) in water. This new sensing material optically reports the Hg^{2+} concentration in water via diffraction of visible light from polymerized crystalline colloidal array (PCCA). The PCCA consists of light diffracting crystalline colloidal array (CCA) of monodisperse, highly charged polystyrene particles, which are polymerized within the polyacrylamide hydrogel. The changes in hydrogel surroundings trigger the volume change of hydrogel, which alters the lattice spacing of CCA and hence shifts the diffraction wavelength of light. The ions responsive urease coupled PCCA (UPCCA) hydrolyzes the urea and produces the HCO_3^- and NH_4^+ ions inside the hydrogel. These ions induce the charge-screening of the polyacrylamide carboxylates by decreasing the electrostatic repulsion between carboxylates and the polyacrylamide backbone relaxes, causing the shrinkage of hydrogel. Hence the UPCCA exhibits the blue shift of the diffracted wavelength. Hg^{2+} being the principal inhibitor of the urease-urea hydrolysis perturbs the urea hydrolysis by the UPCCA when UPCCA is exposed to Hg^{2+} along with urea and hence suppresses the production of ions. This intervenes the shrinkage of hydrogel and does not allow the hydrogel to shrink as it shrinks in absence of Hg^{2+} . Therefore the PCCA net blue shift decreases in presence of Hg^{2+} along with urea compared to only urea. The extent of this hydrogel volume change is a function of Hg^{2+} concentrations. This UPCCA photonic crystal

sensor detects ultra low (1 ppb) concentration of Hg^{2+} in water, exhibits reversibility and displays very high selectivity towards Hg^{2+} . The uncompetitive inhibition nature of urease enzyme, when it is covalently attached in the polymer hydrogel backbone, is the driving force for the very high selectivity and reversibility of the UPCCA sensor.

7.2. Conclusions

Chapter 2

1. A series of charged spherical poly [styrene-(co-2-propene sulfonic acid)] particles crosslinked with divinylbenzene of different sizes have been synthesized by emulsion polymerization and characterized.
2. The decrease in particles size with increasing emulsifier concentration in the below CMC regime is sharper whereas the decrease in particle size is dull in the above CMC regime. The particle formation mechanism above CMC is micellar nucleation whereas particles are formed through homogeneous nucleation below CMC.
3. The exponent for particle size dependence in case of emulsifier variation is bigger (-0.43) compared to initiator variation (0.053), which implies that the variation of the emulsifier concentration would be the better way to prepare particles of different sizes.
4. The surface charge density of the particles depends upon both the emulsifier concentration and the initiator concentration. The optimization of the surface charge density of the colloidal particles can be done more efficiently by varying the emulsifier concentration rather than the initiator concentration.

Chapter 3

1. A series of recipes have been developed for the synthesis of 24–102 nm sized highly charged, crosslinked particles using emulsion polymerization.

2. The particle diameter of poly (S-co-DVB-co-SPM) copolymer colloidal particles decreases with increasing concentration of emulsifier and increases with increasing concentration of initiator in the reaction mixture.
3. Number of particles (N_p) increases with the increase in emulsifier concentration whereas N_p decreases with increasing initiator concentration and N_p has an inverse correlation with the particle size. The synthesized particles diffract visible light.

Chapter 4

1. A series of poly(S-co-NaSS) copolymers containing various NaSS loadings have been synthesized using emulsion polymerization by varying the compositions of styrene and NaSS.
2. The enhanced gel effect, the shift of particle nucleation locus and the increase in the number of particles caused by increasing NaSS content are found to be the driving force for the enhancement of the polymerization kinetics.
3. NMR spectroscopy has been employed to determine the monomer composition of the copolymers which were applied in Fineman-Ross and Kelen-Tüdös equation to calculate the monomer reactivity ratios.
4. Monomer reactivity ratio values showed that NaSS homopolymerization is ≈ 10 times faster than its copolymerization with styrene and styrene copolymerization with NaSS is only ~ 2 times faster than its homopolymerization.

Chapter 5

1. A series of emulsion copolymerizations of styrene with variety of ionic comonomers AAc, MAA, HEMA and NaSS have been carried out by varying the surfactant concentration and the effect monomeric structure on copolymerization kinetics and copolymer properties are studied.

2. The dependence of particle size variation with SDS concentration below CMC follows the order as AAc (0.4460)>MAA (0.3956)> NaSS (0.2524)> HEMA (0.2408) whereas the dependency is almost reversed in the above the CMC region as NaSS (0.61472) > HEMA (0.2281) >AAc (0.2062) >NaSS (0.172).
3. For a fixed emulsifier concentration below CMC (0.1734mM) kinetics of the polymerization follows the order as NaSS>AAc>MAA> HEMA. In the above CMC emulsifier (27.04mM) concentration region the kinetic of AAc, MAA and NaSS are comparable but HEMA conversion is quite slow compared to others.
4. All the copolymer particles produced are highly charged and monodisperse. They self assemble upon sedimentation and diffract visible light obeying Bragg's law. These copolymer particles can be successfully utilized to prepare PCCA sensing materials and other photonic crystal devices.

Chapter 6

1. A novel polymer hydrogel based photonic crystal sensor material has been developed for the determination of toxic mercury ion (Hg^{+2}) concentration in water.
2. UPCCA sensor can sense Hg^{2+} as low as 1ppb Hg^{2+} which is below the maximum contamination limit (2ppb) for Hg^{2+} recommended by environmental protection agency (EPA) of USA.
3. UPCCA “smart” sensor is reversible in nature, functions in aqueous medium, very much cheap and field usable.
4. The urease enzyme behaves remarkably differently towards the inhibition when it is attached to hydrogel compared to the solution state.

7.3. Scope of Future Work

Thesis addressed various issues of emulsion polymerization such as effect of emulsifier, initiator and ionic comonomer concentration and structure on particle size, polymerization kinetics, number of particles, charge density, reactivity ratio of monomers in a copolymer systems, locus of polymerization, and self assembly. An embedding of self-assembled colloids inside the hydrogel matrix, functionalization of hydrogel moieties and coupling with urease enzyme to generate UPCCA are studied. Urease coupled polymerized crystalline colloidal array is found to be smart sensing material for the sensing of toxic mercury ion (Hg^{2+}) in water as low as 1ppb. Enzymatic kinetics using urease coupled hydrogel gave us an insight to utilize hydrogel as a template to bind enzyme and do their enzymatic kinetics. Throughout the study we have experienced many issues which need to be addressed and more importantly the thesis work inspired us to think in new directions. Overall the thesis has following outcome and the potential which need to be addressed by the researchers in future.

1. Emulsion copolymerization recipes to readily prepare highly charged monodispersed copolymer particles employing various ionic comonomer systems such as COPS-1, AAc, MAA, HEMA and NaSS can be developed varying SDS and other parameters.
2. More hydrophilic and hydrophobic monomer pairs can be handpicked to study the various aspects of emulsion polymerization which includes particle size copolymer kinetics and locus of polymerization.
3. A study on number of functional groups present in hydrogel before and after coupling of ligands or enzymes can be launched.
4. Self assembled AAc, MAA, HEMA, and NaSS copolymer structures can be utilized as templates to develop hollow and core shell nanostructures. Photonic band gap materials can also be developed by choosing appropriate metal nano particles and coating them.

5. Urease coupled PCCA can be utilized as a quantitative tool to determine urea in blood and human serum.
6. Every enzyme has their own inhibitor(s); so designing and development of enzymatic PCCA sensors for the sensing of their inhibitor counterparts may be good research prospect and challenge.
7. It has been proved that immobilized enzyme is more efficient compared to free enzyme. So polymer hydrogel materials should be used as a near perfect supports to couple or bind enzymes and enzyme coupled hydrogels can be utilized to study their enzymatic kinetics more efficiently.

Publications

&

Presentations

Publications

1. Tuning the Particle Size and Charge Density of Cross linked Polystyrene Particles, **Dhamodaran Arunbabu**, Arindam Sannigrahi, Tushar Jana, *J. App. Polym. Sci.* **2008**, *108*, 2718-2725.
2. Synthesis of Crosslinked Poly (styrene-*co*divinylbenzene-*co*-Sulfopropyl methacrylate) Nanoparticles by Emulsion Polymerization: Tuning the Particle Size and the Surface Charge Density. **Dhamodaran Arunbabu**, Mousumi Hazarika, Somsankar Naik and Tushar Jana, *Bull. Mater. Sci.* **2009**, *32*, 633-641.
3. Emulsion copolymerization of styrene and sodium styrene sulphonate: Kinetics investigation, Determination of monomer reactivity ratios and co-polymer properties. **Dhamodaran Arunbabu**, Zomuan sanga, Kamal mohamed Seeni meera and Tushar Jana, *Polym. Int.* **2008**, *58*, 88–96.
4. Emulsion Copolymerization of Styrene: Effect of Ionic Comonomer Structure. **Dhamodaran Arunbabu** and Tushar Jana (Communicated to *Journal of colloid and interface science*)
5. Photonic Crystal Hydrogel Material for the Sensing of Toxic Mercury Ion (Hg^{+2}) in Water, **Dhamodaran Arunbabu**, Arindam Sannigrahi, Tushar Jana, (communicated to *Soft Matter*)
6. Blends of Polybenzimidazole and Poly (vinylidene fluoride) for Use in Fuel Cell. **Dhamodaran Arunbabu**, Arindam Sannigrahi, Tushar Jana, *J. Phys. Chem. B* **2008**, *112*, 5305-5310.
7. Thermoreversible Gelation of Polybenzimidazole in Phosphoric Acid, Arindam Sannigrahi, **Dhamodaran Arunbabu**, Tushar Jana, *Macromol. Rapid. Commun.* **2006**, *27*, 1962-1967.

8. Aggregation Behavior of Polybenzimidazole in Aprotic Polar Solvent, **Arindam Sannigrahi**, Dhamodaran Arunbabu, R. Murali Sankar, Tushar Jana, *Macromolecules*. **2007**, *40*, 2844-2851.
9. Tuning the Molecular Properties of Polybenzimidazole by Copolymerization, **Arindam Sannigrahi**, Dhamodaran Arunbabu, R. Murali Sankar, Tushar Jana, *J. Phys. Chem. B*. **2007**, *111*, 12124-12132.
10. Formation of core (polystyrene)–shell (polybenzimidazole) nanoparticles using sulfonated polystyrene as template, Mousumi Hazarika, **Dhamodaran Arunbabu**, Tushar Jana, *J. Colloid and Interface Sci.* **2010**, *351*, 374–383.

Note: Publications 1-5 are included in this thesis as chapters 2-6, respectively.

Conference Presentations

1. Poster presented on **“Synthesis of Monodisperse Polystyrene Colloidal Particles”** in *3rd annual in-house symposium CHEMFEST-2006* of the School of Chemistry, University of Hyderabad, Hyderabad, India.
2. Poster presented on **“Synthesis of Charged Crosslinked Polystyrene Colloidal Particles: Effect of Emulsifier and Initiator Concentration.”** In *4th annual in-house symposium CHEMFEST-2007* of the School of Chemistry, University of Hyderabad, Hyderabad, India.
3. Poster presented on **“Synthesis of Charged Crosslinked Polystyrene Colloidal Particles and its application in the Generation of Mercury(Hg^{2+}) Sensor”** in *Poly 2008: International Conference on Advances in Polymer Science and Technology*, during January 28-31, **2008**, at Indian Institute of Technology, New Delhi, India. **[Received best poster award]**
4. Poster presented on **“Emulsion Copolymerization of Styrene and Sodium Styrene Sulfonate: Kinetics, Monomer Reactivity Ratios and Copolymer Properties”** in *5th annual in-house symposium CHEMFEST 2008* of the School of Chemistry, University of Hyderabad, Hyderabad, India.
5. Poster presented on **“Charged Polystyrene Colloids: Synthesis and Applications”** in *6th annual in-house symposium CHEMFEST 2009* of the School of Chemistry, University of Hyderabad, Hyderabad, India.
6. Oral talk and poster Presented on **“Smart enzymatic biosensor for the sensing and determination of Mercury (Hg^{2+})”** in *7th annual in-house symposium CHEMFEST 2010* of the School of Chemistry, University of Hyderabad, Hyderabad, India.